CUKUROVA UNIVERSITY
INSTITUTE OF NATURAL AND APPLIED SCIENCES

PhD THESIS

Surface Coating Application and Characterization of Polymer Structures Produced by Additive Manufacturing

İsmail AKTİTİZ

Mechanical Engineering Department

November, 2024

CUKUROVA UNIVERSITY
INSTITUTE OF NATURAL AND APPLIED SCIENCES

PhD THESIS APPROVAL

Surface Coating Application and Characterization of Polymer Structures Produced by Additive Manufacturing

İsmail AKTİTİZ

Mechanical Engineering Department

This Doctorate Thesis was evaluated by the following Jury Members on 27/11/2024 and was approved by unanimity ~~/ majority of votes.~~

Jury	: Prof. Dr. Kadir AYDIN	(Advisor)	…………………..……
	: Prof. Dr. Abdul Kadir EKŞİ		…………………..……
	: Prof. Dr. Gökhan TÜCCAR		………………….….
	: Assoc. Prof. Dr. Hasan SERİN		……………....…….
	: Assoc. Prof. Dr. Erinç ULUDAMAR		………..…………

This Thesis was written in the Department of Mechanical Engineering, Institute of Natural and Applied Sciences.

Thesis Number:

Prof. Dr. Sadık DİNÇER
Director
Institute of Natural and Applied Sciences

This work was supported by the the Scientific Research Office of Çukurova University.
Project ID: FDK-2021-14089

CONTENTS

CUKUROVA UNIVERSITY
INSTITUTE OF NATURAL AND APPLIED SCIENCES

PhD THESIS

Surface Coating Application and Characterization of Polymer Structures Produced by Additive Manufacturing

İsmail AKTİTİZ

Advisor: Prof. Dr. Kadir AYDIN

Department of Mechanical Engineering

ABSTRACT

The metallization process, which involves the coating of the surfaces of 3D (three-dimensional) printed polymer structures with a metallic thin film, represents a convergence of the advantages inherent to additive manufacturing technology, metals and polymers. Consequently, the final product is a potential material for a range of structural applications. The metallization process enhances the characteristics of polymer structures that are unfavourable, including low electrical conductivity, poor mechanical properties, degradation under various environmental conditions, such as ultraviolet (UV) radiation and moisture, and poor thermal properties. Therefore, more functional polymer structures are produced. Recently, researchers have focused their efforts on the metallization of 3D-printed polymer structures with the objective of enhancing their functionality. In this thesis, 3D polymer structures were fabricated using polylactic acid (PLA) filament and fused deposition modelling (FDM) technology. Prior to metallization, five distinct surface treatments were employed to ensure optimal surface conditions. These included as-printed, dipping, vapour, plasma, and abrasion. Subsequently, the polymer structures were metallised through the deposition of aluminium and copper metallic thin films. The morphological, structural, optical, and electrical properties of these structures were examined through the utilisation of a scanning electron microscope (SEM), energy dispersive spectrum (EDS) analysis, atomic force microscopy (AFM), X-ray diffraction (XRD), Fourier transform infrared spectroscopy (FT-IR) analysis, ultraviolet-visible light and near infrared (UV-VIS-NIR) analysis, contact angle measurement, ellipsometry analysis, and electrical resistance measurement. The results of the EDS and XRD analyses confirm the presence of aluminium and copper in the polymer structure. The contact angles for aluminium and copper coatings vary up to 91.728° and 88.309°, respectively. The electrical conductivity values of $6.6x10^5$ S/m for aluminium and $7.87x10^5$ S/m for copper at 1000 nm were obtained.

Keywords: Surface Coating, Metallization, Additive Manufacturing, Sputtering, Thin Film.

ÇUKUROVA ÜNİVERSİTESİ
FEN BİLİMLERİ ENSTİTÜSÜ

DOKTORA TEZİ

Eklemeli İmalat ile Üretilen Polimer Yapılara Yüzey Kaplama Uygulaması ve Karakterizasyonu

İsmail AKTİTİZ

Danışman: Prof. Dr. Kadir AYDIN

Makine Mühendisliği Anabilim Dalı

ÖZ

3B (Üç boyutlu) basılan polimer yapıların yüzeylerinin metalik ince film ile kaplanarak metalizasyon işleminin gerçekleştirilmesi, eklemeli imalat teknolojisinin, metallerin ve polimerlerin sahip olduğu avantajları bir araya getirerek nihai ürünü farklı yapısal uygulamalar için aday malzeme haline getirmektedir. Metalizasyon işlemi polimer yapıların, düşük elektrik iletkenliği, arzu edilmeyen mekanik özellikleri, ultraviole (UV) radyasyon ve nem gibi farklı çevre koşullarında bozunma ve zayıf termal stabilite dezavantajlarını ortadan kaldırarak daha işlevsel polimer yapıların elde edilmesine olanak sağlamaktadır. Bu sebeple son yıllarda araştırmacılar, 3B basılan polimer yapıları daha fonksiyonel hale getirmek için, polimerlerin metalizasyonu üzerine çalışmalarını yoğunlaştırmışlardır. Bu tez çalışmasında polilaktik asit (PLA) filament ve eriyik yığma modeli (FDM) teknolojisi kullanılarak 3B polimer yapıların üretimi gerçekleştirilmiştir. Metalizasyon öncesi yüzey optimizasyonunu sağlamak amacı ile beş farklı (basıldığı gibi, daldırma, buhar, plazma ve aşındırma) yüzey işlemi uygulanmıştır. Sonrasında üretilen polimer yapıların yüzeyleri alüminyum ve bakır metalik ince film ile kaplanarak metalize edilmiştir. Bu yapıların morfolojik, yapısal, optiksel ve elektriksel özelliklerini incelemek amacıyla taramalı elektron mikroskobu (SEM), enerji dispersiv spektrum (EDS) analizi, atomik kuvvet mikroskobu (AFM), X-ışını kırınımı (XRD) analizi, fourier dönüşümlü kızılötesi spektroskopisi (FT-IR) analizi, ultraviyole, görünür ışık ve yakın kızılötesi (UV-VIS-NIR) analizi, temas açısı ölçümü, elipsometri analizi ve elektriksel direnç ölçümü yapılmıştır. EDS ve XRD analiz sonuçları, polimer yapısında alüminyum ve bakırın varlığını doğrulanmaktadır. Alüminyum ve bakır kaplamalar için temas açıları sırasıyla 91,728° ve 88.309°'ye kadar artmıştır. 1000 nm kalınlıkta alüminyum için $6.6x10^5$ S/m ve bakır için $7.87x10^5$ S/m elektriksel iletkenlik değerleri elde edilmiştir.

Anahtar Kelimeler: Yüzey Kaplama, Metalizasyon, Eklemeli İmalat, Saçtırma, İnce Film.

GENİŞLETİLMİŞ ÖZET

Eklemeli imalat yani diğer isimleri ile hızlı prototipleme veya üç boyutlu (3B) baskı, her türlü karmaşıklıkta polimer, seramik, metal veya kompozit malzemelerin üretilmesine olanak sağlayarak kullanıcılara büyük bir üretim esnekliği oluşturmaktadır. Bu üretim teknolojisi günümüzde, elektronik, uzay, havacılık, tıp, otomotiv, enerji, mimari ve askeri alanlar gibi çok yaygın uyglama alanlarına sahiptir. Eklemeli imalat yönteminde üretim yapabilmek için öncelikle bilgisayar destekli tasarım (CAD) programı ile 3B model tasarlanması gerekmektedir. Tasarlanan bu 3B katı model stl formatında yazıyıca aktarılır ve katman katman nihai ürünün üretimi gerçekleştirilmektedir. Eriyik yığma modeli (FDM), doğrudan metal lazer sinterleme (DMLS), seçici lazer sinterleme (SLS), Stereolitografi (SLA) ve malzeme jeti gibi teknikler eklemeli imalat endüstrisinde sıklıkla kullanılan teknolojilerdir.

Erimiş filament üretimi (FFF) olarak da bilinen ekstrüzyon tabanlı FDM, basit imalat süreci, güvenilirliği, boyutsal kararlılığı, düşük bakım maliyeti ve yüksek çözünürlüklü nesneler üretmedeki maliyet etkinliği gibi avantajlarından dolayı, araştırmacılar, akademisyenler tasarımcılar için eklemeli imalat teknikleri arasında en çok tercih edilen teknik haline gelmiştir. FDM tekonolojisi ile üretim yapmak için farklı filament malzemeleri kullanılmaktadır. Bu malzemeler arasında polilaktik asit (PLA), akrilonitril bütadien stiren (ABS), polikarbonat (PC), poliamidler (PA), polistiren (PS) gibi polimerler bulunmaktadır. FDM prosesinde, malzeme katmanlarını oluşturarak nihai ürünü elde etmek için, bir makara yoluyla sürekli bir termoplastik polimer filament kaynağı kullanılmaktadır. Baskı için yeterli polimer filament temin edildikten sonra, bu filament esktrüzyon başlığının içindeki ısıtma elemanı tarafından yarı sıvı bir faza ısıtılmaktadır. Bu yarı sıvı termoplastik polimer, baskı platformu üzerindeki ekstrüzyon nozulundan ekstrüde edilmesiyle üretimi tamalanmaktadır.

FDM yöntemi ile hazırlanan polimer yapılar, düşük yüzey sertliğine, çekme dayanımına ve elastite modülüne, yüksek elektriksel dirence, düşük termal ve erozyon direncine sahip olmasının yanısıra ultraviyole (UV) hasarlara karşıda oldukça hassastır. Polimer yapıların yüzeyinde metalik bir kaplamanın yapıldığı polimer metalizasyonu adı verilen bir proses, bu dezavantajları minimize etmektedir. Dolayısıyla 3B basılan polimer yapıların uygulanabilirliğini artırmaktadır. Polimer yüzeylerin metalizasyonu işleminde çeşitli metodlar kullanılmaktadır. Elektriksiz biriktirme, daldırma, stereolitografi, elektrik ark püskürtme ve termal buharlaştırma gibi malzemeleri metalleştirmenin çeşitli teknikleri mevcuttur.

Metalik ince film oluşturmak için kullanılan, fiziksel buhar biriktirme (PVD), tribolojik özelliklerin iyileştirilmesi ve optik özelliklerin geliştirilmesi gibi avantajlarından dolayı metalik kaplamaların oluşturulması için yaygın olarak kullanılan teknolojidir. Ayrıca, bu yöntem, hâlihazırda çeşitli sektörler tarafından kullanılması ile geniş bir uygulama yelpazesine sahiptir. Doğru akım (DC) magnetron püskürtme tekniği ve radyo frekansı (RF) magnetron püskürtme tekniği ile düşük sıcaklıklarda polimer yapıların yüzeyleri başarılı bir şekilde kaplanabildiğinden dolayı, PVD teknolojileri içerisinde polimer yapılara metalik ince film kaplama uygulaması için önde gelen püskürtme yöntemleri arasındadır. Birçok araştırmacı, metallerin ve polimerlerin emsalsiz özelliklerini, 3B baskı ile birleştirerek yeni bir konsept oluşturmak amacıyla 3B polimer yapıların metalizasyonu üzerine çalışmalarını yoğunlaştırmışlardır.

Bu tez çalışmasında, eklemeli imalat ile üretilen polimer yapıların dezavantajlarını geliştirmek, onları farklı yapısal uygulamalar için fonksiyonel aday malzemeler olarak kullanılmasını sağlamak amacıyla, 3B basılan polimer yapıların yüzeyleri alüminyum ve bakır metalik ince film ile kaplanarak metalizasyon işlemi tamamlanmıştır. 3B baskısı yapılan polimer yapıların tasarımları SolidWorks bilgisayar destekli tasarım (CAD) programı ile hazırlanmıştır. Sonrasında sahip olduğu avantajlarından dolayı FDM teknolojisi ve PLA polimer filament kullanılarak 3B yapıların üretimi tamamlanmıştır. Metalizasyon öncesi yüzey optimizasyonunu sağlamak, kaplama malzemesi ve altlık polimer yapı arasındaki arayüzey özelliklerini geliştirmek ve kaplama sonrası malzeme özelliklerini iyileştirmek amacı ile işlem yok, daldırma, buhar, plazma ve aşındırma gibi farklı yüzey işlemleri uygulanmıştır. Yüzey işlemi uygulanan polimer yapılara ilk olarak alüminyum ince film kaplamalar RF püskürtme tekniği kullanılarak tamamlanmıştır. Sonrasında bakır ince film kaplamalar ise DC püskürtme tekniği kullanılarak polimer yapıların yüzeylerinde oluşturulmuştur. Son aşamada ise kaplama öncesi ve sonrası polimer numunelerin morfolojik, yapısal, optik ve elektriksel özelliklerini incelemek için taramalı elektron mikroskobu (SEM), Enerji Dağılım Spektroskopisi (EDS) analiz, atomik kuvvet mikroskobu (AFM), X-ışını kırınım difraktometresi (XRD), fourier dönüşümlü kızılötesi spektrometresi (FT-IR) analizi, ultraviyole, görünür ışık ve yakın kızılötesi (UV-VIS-NIR) analizi, temas açısı ölçümü, elipsometre analizi ve elektriksel direnç ölçümü gibi analizler yapılmıştır.

Alüminyum kaplama yapılan polimer yapılar için analiz sonuçlarını incelediğimizde, SEM görüntüleri, diklorometan dipping ve diklorometan buhar yapılan numunelerde yüzey pürüzlülüğünün önemli ölçüde iyileştiğini göstermektedir. Ayrıca, metalizasyon işlemi sonrası diklorometan buhar yüzey işlemi uygulanan numunelerde termal olarak indüklenen artık gerilimin neden olduğu dalgalanma benzeri bir yüzey morfolojisini gözlemlenmiştir. EDS analiz sonuçları ise polimer yüzeyinde alüminyum elementinin varlığını doğrulamaktadır. AFM sonuçlarına baktığımızda soğuk oksijen plazma yüzey işleminin uygulandığı polimer yapılarda metalizasyon öncesi iğneli bir yüzey yapısı ortaya çıkarmıştır. XRD analiz sonuçlarına göre difraksiyon pikleri 2θ~38.380°, 44.162°, 64.928°, 78.014° ve 82.204°'de ortaya çıkmıştır. Metalizasyon öncesi polimer yapıların FT-IR analiz sonuçları dört ana pikin varlığını göstermektedir. Bu piklerden yaklaşık 1750 cm^{-1} dalga boyuna sahip pik C = O bağına, yaklaşık 1078-1180 cm^{-1} dalga boyuna sahip pik C = O bağına, 1450-1380 cm^{-1} dalga boyuna sahip pik C = O – H bağına ve yaklaşık 3000 cm^{-1} dalga boyuna sahip pik C = H bağlarına karşılık gelmektedir. UV-VIS-NIR analiz sonuçları metalizasyon sonrası soğuk oksijen plazma yüzey işlemi uygulanan polimer yapıların yansıma değerinde önemli artışlar olduğunu göstermektedir.

Bakır kaplama yapılan polimer yapılar için analiz sonuçlarını incelediğimizde SEM görüntüleri, diklorometan buhar yüzey işlemi uygulanan numunelerde pürüzsüz bir yüzey morfolojisine sahip olduğunu göstermektedir. EDS analiz sonuçları polimer yapıdaki bakırın varlığını doğrulamaktadır. Ayrıca DC saçtırma tekniği ile başarılı bir şekilde kaplamaların oluşturulduğunu göstermektedir. AFM analiz sonuçları, işlem olmayan, diklorometan daldırma ve diklorometan buhar yüzey işlemi uygulanan polimer yapıların yüzeylerinde kırışıklar olduğunu ortaya çıkarmıştır. Metalizasyon sonrası XRD analiz sonuçlarına baktığımızda ise, dört baskın karakteristik difraksiyon piki 43.14^o, 50.09^o, 73.93^o ve 89.50^o'de konumlanmıştır. Bu pikler (111), (200), (220) ve (311) kristal düzlemlerine sırasıyla atfedilebilir. UV-VIS-NIR analiz sonuçlarına göre, bakır kaplama sonrası işlem yok, diklorometan buhar ve soğuk oksijen plazma numunelerde yansıma şiddetleri yaklaşık olarak 570 nm dalga boyunda tespit edilmiştir. Diklorometan buhar yüzey işlemi uygulanan numunelerin elektriksel iletkenlik değerleri önemli bir artış göstererek $7.87x10^5$ S/m değerine ulaşmıştır.

Elde edilen bulgular neticesinde, alüminyum ve bakır kaplamaların ile 3B basılan polimer yapılara metalizasyon işleminin uygulanması, bu yapıların yüzey özelliklerinde, optik yansımasında ve elektriksel iletkenlik değerlerinde önemli iyileşmeler sağlamaktadır. Buna ek olarak, karmaşık geometriye sahip ağırlık olarak hafif yapıların üretilmesini de mümkün kılmaktadır. Havacılık, uzay tıp, otomotiv ve elektronik gibi çeşitli alanlardaki yapısal uygulamalar için aday malzemeler olabileceği düşünülmektedir.

ACKNOWLEDGEMENTS

I would like to express my gratitude to my advisor Prof. Dr. Kadir AYDIN to guide me through this journey. Without the help of my advisor Prof. Dr. Kadir AYDIN, I would not be able to finish this journey with great success.

I would like to thank my wife and daughter for their support at each stage of the thesis.

I would like to express my gratitude to my parents, whose contributions have been crucial in enabling me to achieve my current status.

I would like to express my gratitude to the academic staff of Cukurova University Central Research Laboratory for their invaluable assistance throughout the analytical process.

Lastly, I would also acknowledge the financial support of the Scientific ResearchProject Unit of Çukurova University (Project No: FDK-2021-14089).

LIST OF TABLES

LIST OF FIGURES

SYMBOLS AND ABBREVIATIONS

ABS : Acrylonitrile Butadiene Styrene
AFM : Atomic Force Microscopy
Ag : Silver
Al : Aluminium
AM : Additive Manufacturing
ASA : Acrylonitrile Styrene Acrylate
ATO : Antimony Tin Oxide
CAD : Computer-Aided Design
CNF : Carbon Nanofibre
Cr : Chromium
CSC : Cylindrical Simple Cubic
Cu : Copper
DC : Direct Current
DLP : Digital Light Process
DLW : Direct Laser Writing
DMLS : Direct Laser Melting
EBM : Electron Beam Melting
EDS : Energy Dispersive Spectroscopy
EPS : Expanded Polystyrene
FDM : Fused Deposition Modeling
FFF : Fused Filament Fabrication
FSC : Four Square Simple Cubic
FT-IR : Fourier Transform Infrared Spectrometry
HDPE : High-Density Polyethene
HV : Vickers Hardness
LENS : Laser Engineered Net Shaping
LOM : Laminated Object Manufacturing
MHz : Megahertz
Mo : Molybdenum
MSC : Mixed Simple Cubic
N_2 : Nitrogen
OCP : Open-Circuit Potential
PA : Polyamides
PC : Polycarbonate
PE : Polyethylene

PEEK	: Polyetheretherketone
PEI	: Polyethyleneimine
PET	: Polyethylene Terephthalate
PI	: Polyimide
PM	: Polymer metallization
PMMA	: Polymethylmethacrylate
PP	: Polyjet Printing
PPSF	: Polyphenylsulfone
PS	: Polystyrene
PVA	: Polyvinyl Alcohol
PVD	: Physical Vapour Deposition
RF	: Radio Frequency
SBC	: Styrene-Butadiene Copolymer
SEM	: Scanning Electron Microscopy
SLA	: Stereolithography
SLM	: Selective Laser Melting
SLS	: Selective Laser Sintering
sscm	: Standard Cubic Centimetres Per Minute
Ti	: Titanium
TPU	: Thermoplastic Polyurethanes
UV	: Ultraviolet
UVO	: Ultraviolet and Ozone
UV-VIS-NIR	: Ultraviolet Visible Light And Near Infrared
W	: Watt
XRD	: X-Ray Diffraction Diffractometer
3D	: Three-Dimensional
3DP	: 3D Printing
θ^o	: Contact Angle
σ	: Electrical Conductivity
Ω	: Electrical Resistance
ρ	: Specific Electrical Resistance
µm	: Micrometre

1. INTRODUCTION

The term "additive manufacturing" (AM) has been defined as combining materials to create objects from 3D model data, typically layer-by-layer, in contrast to the subtractive manufacturing methodologies that are more commonly used. It is also known as three-dimensional printing and rapid prototyping. This manufacturing method can be applied to all classes of materials, including metals, ceramics, polymers, composites, and biological systems. For over two decades, AM has likely been employed as a material processing tool. However, it has only recently begun to emerge as a significant commercial manufacturing technology (Frazier, 2014; Singh et al., 2017). AM can produce components with highly intricate and challenging geometries, utilizing specialized materials with minimal material waste and post-processing requirements. Therefore, AM allows designers and engineers to create unique products that can be economically manufactured in low volumes (Bikas et al., 2016). AM is currently used in several important industries, including aerospace, biomedical, automotive, energy, electronics, architecture, sports, artistic, and military fields (Ngo et al., 2018). Figure 1.1 illustrates the global usage of additive manufacturing. Among the advantages of additive manufacturing are the following:

- In contrast to conventional manufacturing techniques, which entail the removal of significant quantities of material, AM employs the use of consumables more efficiently, whereby parts are formed in a layered fashion. The produced components can be subjected to recycling and subsequently reused in the production process, should this be desired.
- In traditional manufacturing processes, additional components are required in conjunction with the primary machine tool, including jigs, fixtures, cutting tools, and coolers. However, AM does not require these supplementary parts, enabling researchers to produce the necessary components rapidly. Consequently, there is a notable enhancement in the efficiency of the supply chain.
- Since there is no necessity for supplementary machinery or apparatus in the AM method, components exhibiting complex geometries can be readily manufactured in a single piece. In other words, unlike conventional techniques, there is no loss of functional capacity or ease of production. Furthermore, innovative structures with enhanced mechanical properties can be produced by employing materials with disparate mechanical properties in conjunction. Consequently, this facilitates the fabrication of components exhibiting numerous advantageous characteristics.
- Additive manufacturing (AM) technology does not necessitate expensive installations, making it a favorable option for small-scale production. The characteristics of 3D-printed parts are contingent upon the selected AM process, allowing for

straightforward determination of the optimal production method based on the specific requirements of the researcher or engineer. This technology enables the fabrication of parts with intricate geometries in a single piece, eliminating the necessity for complex production lines (Prakash et al., 2017).

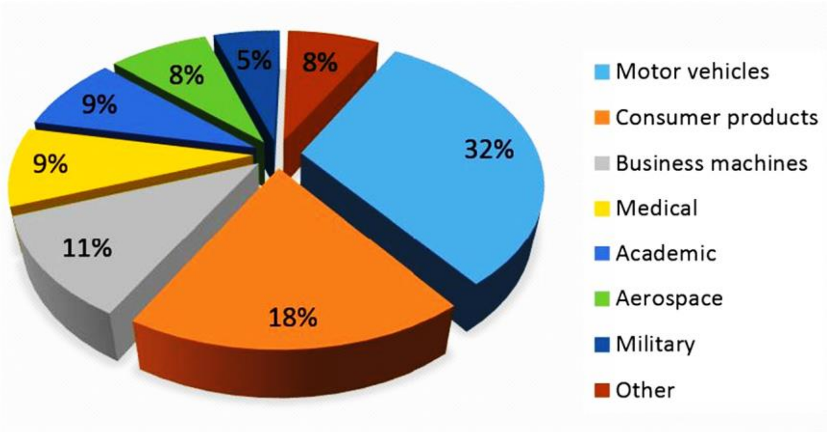

Figure 1.1. The global usage areas of additive manufacturing (Bikas et al., 2016)

In order to produce using any of the three main 3D printing technologies, it is first necessary to create a 3D solid model with the help of computer-aided design (CAD). The prepared 3D model is then converted into the Standard Triangulation Language (.STL) file format and transferred to the 3D printing device. Subsequently, the sample is produced in a series of layers on the 3D printing device. This is a complex procedure, comprising a number of distinct process steps. This is due to the fact that a multitude of process parameters exert an influence on the quality of the manufactured components. The various rapid prototyping technologies employ disparate methodologies for the production of 3D printing. In some cases, metal or polymer powder is sintered using thermal energy from laser or electron beams. In alternative processes, the binder is meticulously dispensed onto the powdered ceramic or polymer. Furthermore, alternative techniques involve the melting of the material and its subsequent production in layers. (Huang et al., 2013; Singh et al. 2017; Blakey-Milner et al. 2021). Fused deposition modeling (FDM), selective laser sintering (SLS), direct laser melting (DMLS), selective laser melting (SLM), electron beam melting (EBM), stereolithography (SLA), digital light process (DLP), 3D printing (3DP), laminated object manufacturing (LOM), polyjet printing (PP), and laser engineered net shaping (LENS) are among the frequently used additive manufacturing methods (Sun et al., 2021; Negi et al., 2013).

In the field of research, FDM has emerged as the most prominent method of 3D printing due to its capacity to produce high-quality, complex products in a safe and controlled manner. FDM is a rapid prototyping technology that enables the production of functional three-dimensional prints using a variety of thermoplastic materials. In the field of FDM technology, the initial step involves the creation of a 3D solid model. Subsequently, the print is produced in a series of layer-by-layer increments. In this process, the thermoplastic material is fed into an extruder that has been heated to a temperature sufficient to melt it. The molten material is then extruded through a nozzle, forming the initial layer of the 3D solid model on the heated plate. Subsequent layers are then deposited on the preceding layer, and the printing process is complete. If necessary, secondary processes may be applied to the printed samples after 3D printing (Dhinakaran et al., 2020). Figure 1.2 illustrates the fundamental operation of the FDM process.

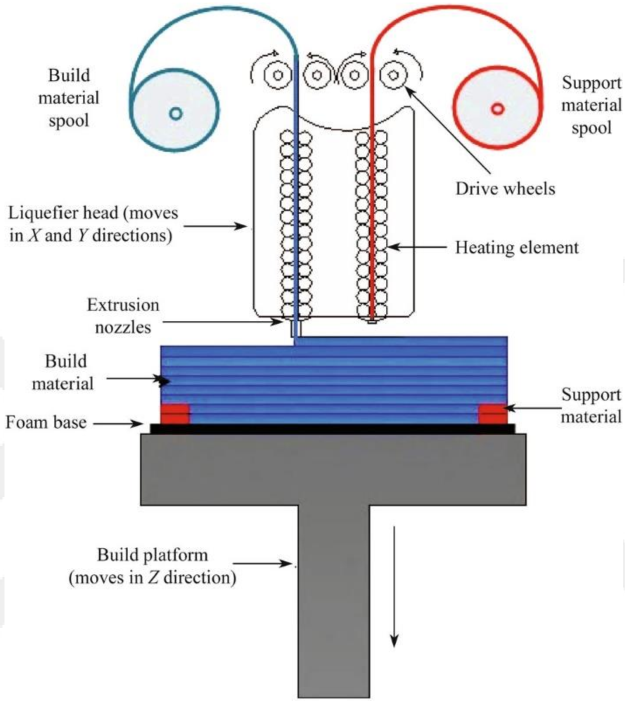

Figure 1.2. The working principle of the FDM process (Mohamed et al., 2015)

The range of thermoplastic filaments available for FDM technology is currently extensive, with applications in a number of diverse fields, including aerospace, medical, and automotive. The most commonly utilised filament materials for the FDM process encompass a range of thermoplastic polymers, including polylactic acid (PLA), acrylonitrile butadiene styrene (ABS), nylon, polycarbonate (PC), polyamides (PA), ULTEM, polystyrene (PS), polyphenylsulfone (PPSF), polypropylene (PP), polyethyleneimine (PEI), thermoplastic polyurethanes (TPU), polyvinyl alcohol (PVA), polyethylene (PE), and polyetheretherketone (PEEK) (Boparai et al., 2015; Rajan et al., 2022). Among the various filaments utilized in FDM rapid prototyping technology, PLA filament is distinguished by its numerous advantageous characteristics. PLA is an aliphatic polyester material produced by the conversion of starch derived from renewable vegetable sources, including corn and potato, into glucose. The glass transition temperature of PLA is 55°C, while its melting point is 180°C. PLA exhibits good biocompatibility and high durability. Furthermore, PLA is completely biodegradable, with the end product after decomposition being water and carbon dioxide. Therefore, it is non-toxic and does not cause environmental pollution. PLA has excellent integral properties and high strength (Joseph et al., 2023).

Polymeric materials are typically not the preferred choice for engineering applications due to their inferior structural properties in comparison to metals. Polymers have low strength and modulus of elasticity, poor electrical conductivity, low thermal and erosion resistance. Furthermore, polymer structures are highly susceptible to ultraviolet (UV) damage. The technique of polymer metallization (PM), which involves the formation of a metallic layer on the surface of polymeric parts, addresses these limitations. This process enhances the functional capabilities of polymer structures, thereby expanding the scope of their applications (Melentiev et al., 2021). In recent years, there has been a notable increase in interest among researchers in the field of metallization, or the use of metal to coat structures. This is due to the fact that it improves the structural and electrical properties of polymer structures produced by additive manufacturing. Furthermore, the ability to obtain final structures with reduced weight and volume has contributed to the growing popularity of this field of study. Various techniques may be utilized for metalizing materials, including electroless deposition, immersion, stereolithography, electric arc spraying, and thermal evaporation (Afshar and Mihut, 2016). Among these methods, physical vapour deposition (PVD) is the most widely used technique for metallization due to a number of advantages. These include the improvement of tribological behaviour, enhancement of optical properties, improvement of decorative properties and a wide range of applications. Furthermore, the advantages of PVD make it suitable for use in many sectors (Baptista et al., 2018).

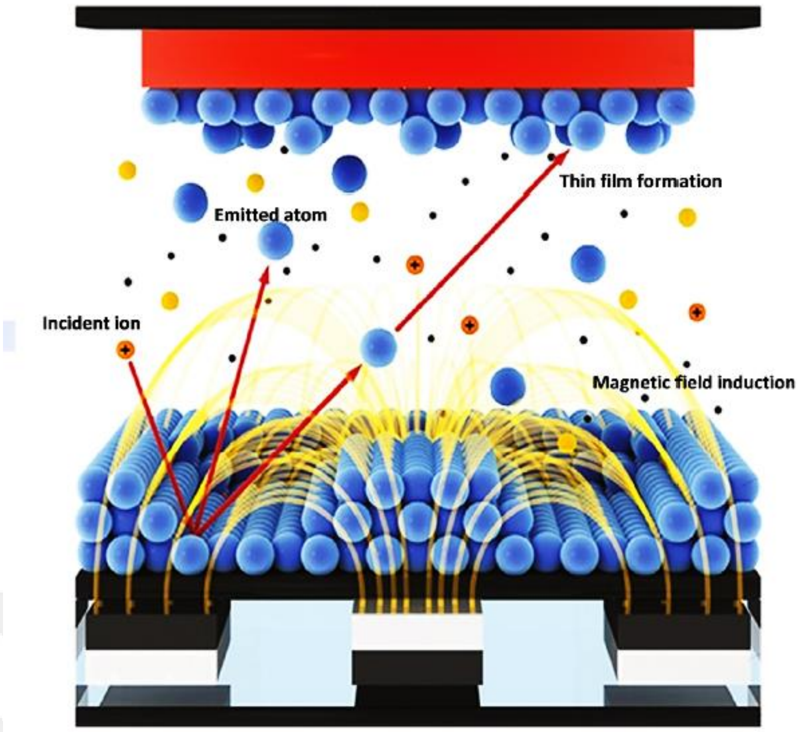

Figure 1.3. The schematic diagram of sputtering technique (Qadir et al., 2019)

The physical vapour deposition processes include sputter deposition, cathodic arc deposition, electron beam physical vapour deposition, evaporative deposition, and pulsed laser deposition (Shahidi et al., 2015). The sputtering technique enables the formation of large-area, smooth coatings at relatively low temperatures. Furthermore, sputtering is the most preferred technology due to its numerous advantages, including the fact that there are almost no limitations on the target material (Deng et al., 2020). The source material or target material is cathodized in the sputtering process. Furthermore, the target material is bombarded with ions produced from an inert gas, and the process is kinetically controlled. In a variety of sectors, primarily utilising argon gas, the generation of positive ions is achieved through the ignition of plasma between the base material, the anode, and the target material, the cathode. As a consequence of the electric field's influence on the target material's surface, electrons are directed away from the cathodic region. This results in the transfer of kinetic energy to the target atoms, leading to the formation of a thin film on the substrate's surface (Mehran et al., 2018). The sputtering technique's schematic diagram is illustrated in Figure 1.3.

The most prevalent sputtering technologies include direct current (DC) magnetron sputtering, radio frequency (RF) magnetron sputtering, DC-RF magnetron sputtering, microwave-enhanced magnetron sputtering, reactive sputtering, ion beam magnetron sputtering, inductively coupled plasma-magnetron sputtering and high power pulsed magnetron sputtering (Behera et al., 2022). The DC magnetron sputtering technique is distinguished by its ability to control the composition and stoichiometry of metallic thin films, facilitate high deposition rates across diverse sectors, and produce thin films of a high degree of purity (Safi, 2000). The RF magnetron sputtering technique offers a number of advantages, including high deposition rates, good adhesion, uniform surface morphology, homogeneity, ease of use and the ability to obtain high-quality thin films that can be economically applied even over large areas at room temperature without the need for melting, as is required in thermal sputtering (Mandal et al., 2021).

The sputtering technique allows for the successful application of a variety of metal coatings, including Al, Cu, Mo, Ti, Ag, and Cr, to polymer substrate materials (Melentiev et al., 2022; Lin et al., 2005). Among the various metal coatings, aluminium (Al) and copper (Cu) have emerged as the focus of research interest in a range of structural applications due to their unique properties. Aluminium films, in particular, have been identified as potential materials for use in the optical, microelectronics, telecommunications, and construction/building industries, given their exceptional characteristics, including high conductivity, low resistivity, high reflectivity, enhanced adhesion, and superior resistance to oxidation and corrosion (Mwema et al., 2018). Copper films (Cu) are employed in a multitude of applications, particularly within the electrical industry. In addition to superior electromigration performance, enhanced thermal, and electrical conductivity, a higher melting point and improved mechanical strength, they also facilitate the formation of high current density copper interconnects. Collectively, these properties render copper thin films a distinctive contender for practical applications (Velicu et al., 2017).

The objective of this thesis is to enhance the functional properties of polymer structures produced by additive manufacturing technology through the metallization process, whereby the surfaces of these structures are coated with metal. The resulting metallised polymer structures are therefore suitable for a range of structural applications. 3D solid model designs were created for the 3D-printed polymer structures using the SolidWorks computer-aided design software. Subsequently, FDM technology and PLA filament were selected for the production of 3D prints, given their advantageous characteristics. Prior to metallization, five different surface treatments were applied to ensure optimal surface conditions. These included as-printed, dipping, vapour, plasma, and abrasion. The objective was to enhance the interfacial properties between the coating material and the underlying polymer structure, as well as to improve the material properties of the structures formed after coating. Prior to metallization, the 3D-printed polymer structures with surface treatment were divided into two groups. The first group was coated with aluminium using the radio frequency (RF) sputtering technique, while the second group was coated with copper using direct current (DC) sputtering. A range of analytical techniques were employed to investigate the morphological, structural, optical, and electrical properties of the metallised polymer structures, including scanning electron microscopy (SEM), energy dispersive spectroscopy (EDS) analysis, atomic force microscopy (AFM), X-ray diffraction diffractometer (XRD), Fourier transform infrared spectrometry (FT-IR) analysis, ultraviolet-visible light and near infrared (UV-VIS-NIR) analysis, contact angle measurement, ellipsometer analysis, and electrical resistance measurement. A graphical summary of this thesis work is shown in Figure 1.4.

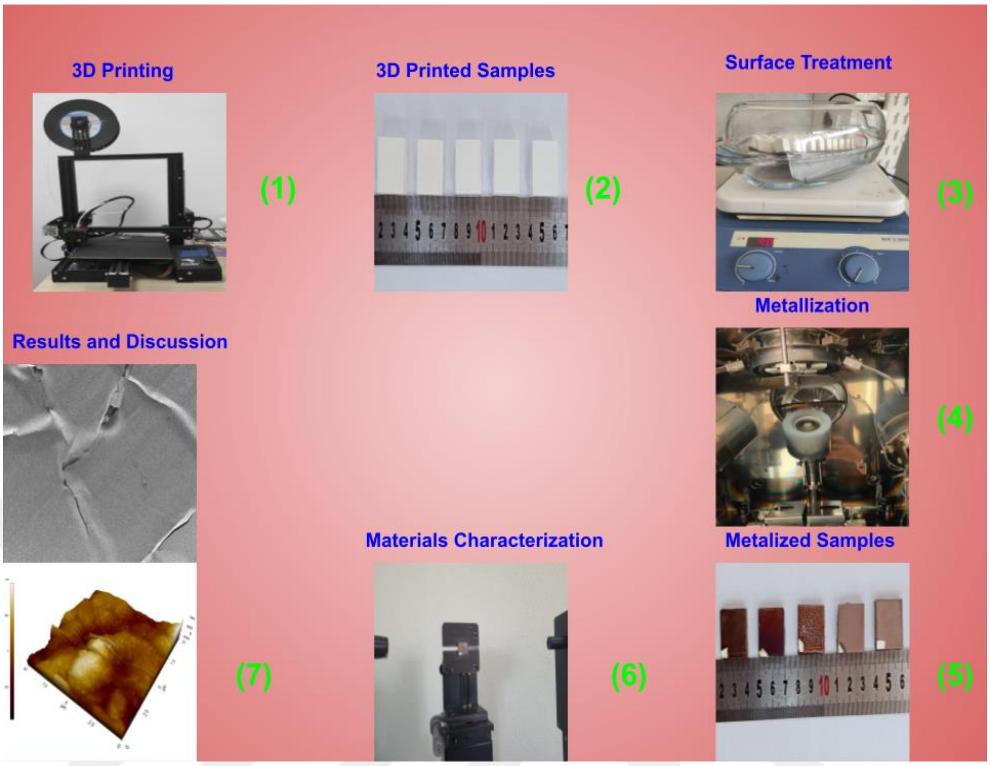

Figure 1.4. The graphical summary of the thesis work

2. LITERATURE REVIEW

In recent years, a significant number of researchers have concentrated their efforts on investigating the potential of polymer structures and parts produced by additive manufacturing as candidate materials for a range of structural applications.

The objective of Wang et al. (2023) was to develop a hybrid rapid prototyping technology that combines a digital light process with a laser-activated electroless coating process for 3D-printed electronic structures. A functional photocurable polymer for selective metallization doped with 3 wt% antimony tin oxide (ATO) and 1 wt% TiO_2 nanoparticles was prepared for use in the DLP. A 3D-printed LED circuit board has been developed to validate the feasibility of this hybrid rapid prototyping technology for the customization of fully functional 3D-printed electronics. The electrical conductivity values of the produced samples were 5.2x10^7 S/m, which is very close to the electrical conductivity value of pure copper. The image of the produced circuits is shown in Figure 2.1.

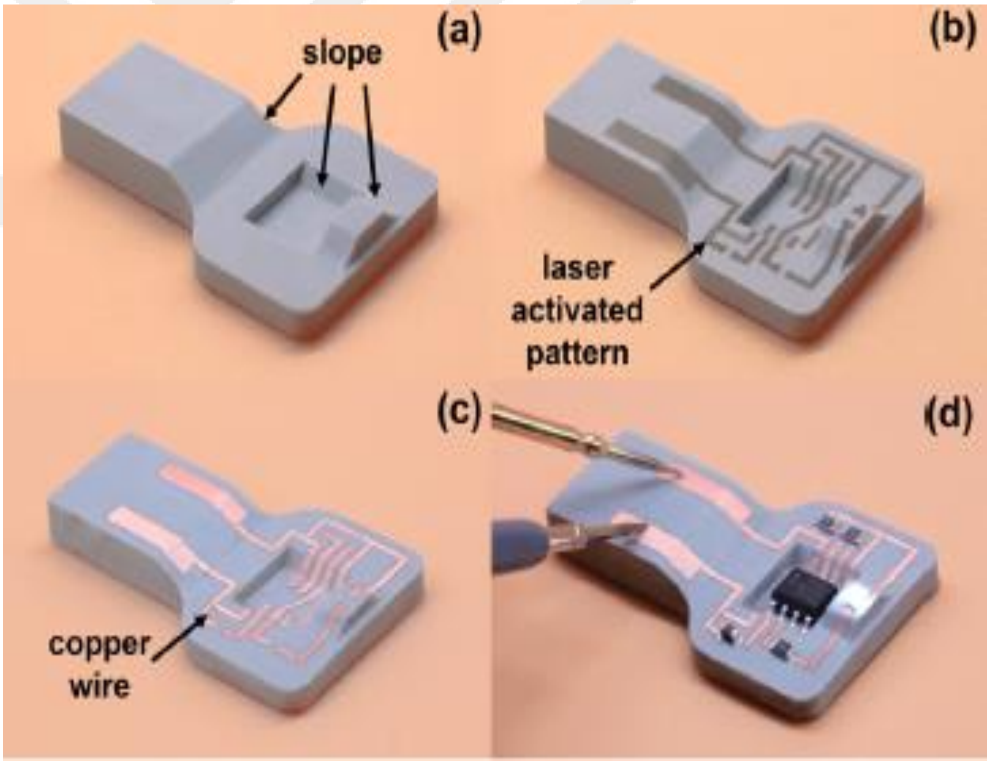

Figure 2.1. 3D printed circuit board image (Wang et al., 2023)

Vásquez-Peralvo et al. (2022) designed, simulated, and fabricated three distinct prototypes of dielectric 3D frequency selective structures operating in the millimetre wave band, employing the technique of VAT photopolymerization. Subsequently, the prepared samples were metallized using metallic dye atomization and electroplating techniques. The results demonstrated that modified and reduced bandpasses were obtained for some structures. In contrast, copper electroplating achieved a reduced loss bandpass for highly intricate structures, such as the torus. Consequently, it can be inferred that inductive 3D frequency selective structures in the millimetre wave band will facilitate the cost-effective production of such structures. The image of the inductive 3D frequency selective structures prepared in the study is presented in Figure 2.2.

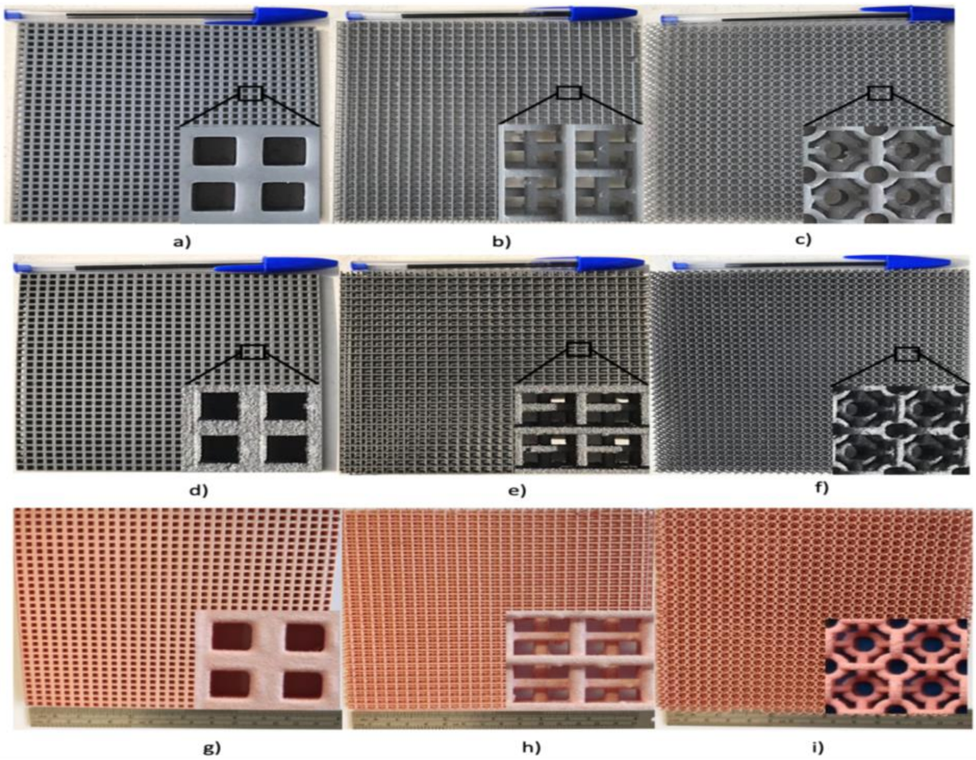

Figure 2.2. Inductive 3D frequency selective structures (Vásquez-Peralvo et al., 2022)

In a recent study, Liu et al. (2022) investigated methods for fabricating structural circuits. The DLP rapid prototyping technique was employed to construct a substrate structure comprising ultraviolet-curable resin and $Cu_2(OH)PO_4$ particles. Subsequently, the substrate structure was metallized through laser activation and electroless plating. The copper layers demonstrated the highest 5B level in the adhesion test, indicating good mechanical adhesion. The authors asserted that the acceptable electrical conductivity value was 7.5×10^{-8} Ω.m. Furthermore, they proposed that their work could be a reference for fabricating bespoke functional electronic products in various industries, including consumer electronics, communication engineering, automotive and aerospace. Figure 2.3 illustrates the polymer structures where the metallization process was performed.

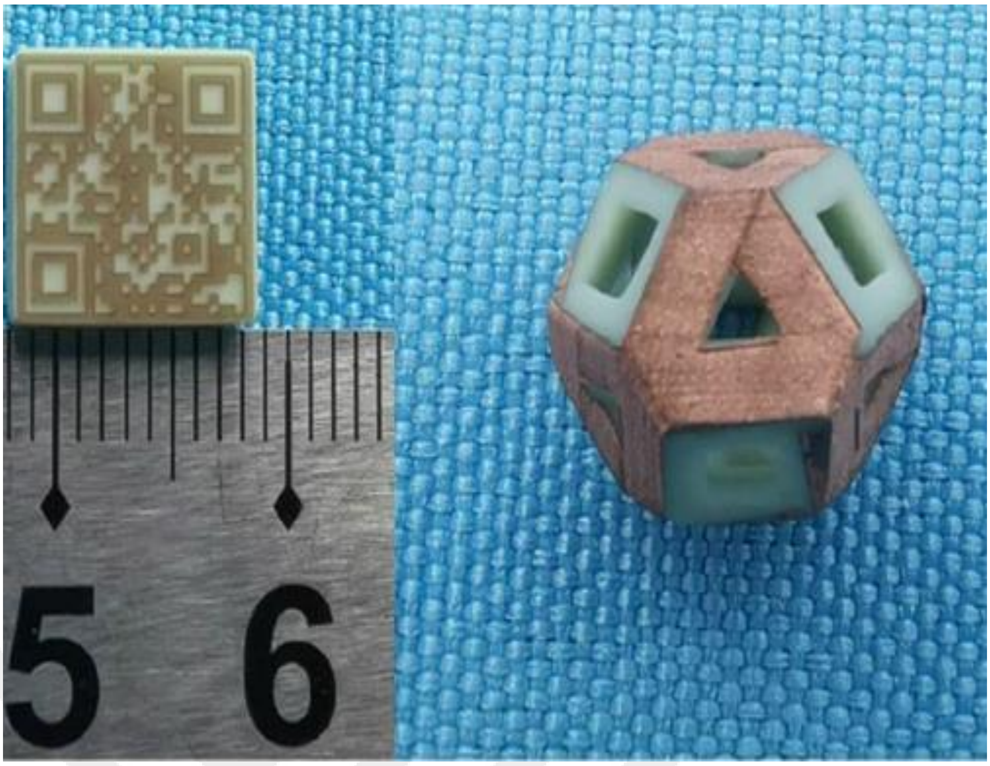

Figure 2.3. Metallized polymer structures (Liu et al., 2022)

Bachiller et al. (2023) studied the 3D printing and metallic film coating of high-frequency devices. In this study, the researchers employed the VAT photopolymerization method and utilized a range of resins. The printed devices were subjected to a two-stage coating process: electroless metallization and galvanic coating. Using scanning electron microscopy, profilometry and contact metrology, and the researchers performed dimensional analyses to evaluate the effect of the coating on the manufacturing process. They reported that the electromagnetic response of the devices they developed was excellent and comparable to that of commercial devices produced by inference techniques. Images of the prototypes produced in the study are shown in Figure 2.4.

Figure 2.4. 3D-printed antenna prototype (Bachiller et al., 2023)

In a study by Xiao et al. (2020), the correlation between the compressive crush strength of 3D-printed composite meshes and the expected stresses of the human mandible was investigated. Furthermore, the lattice gradient porosity distribution was calculated under the lower jaw stress distribution. In order to explore the potential applications of graded lattice prosthesis, they proceeded to complete the production of lower jaw prosthesis by coating these 3D-printed structures with a metallic layer. The titanium-coated polymer structures were produced using the SLA method and subsequently coated using the PVD method. The compression test results indicated a two- to three-fold increase in compressive strength for the titanium-coated samples. The porosity of the maximum and minimum stress regions was 68.3% and 86.3%, respectively, exhibiting a porosity difference of approximately 20%. Figure 2.5 illustrates the metallized structures subjected to the compression test.

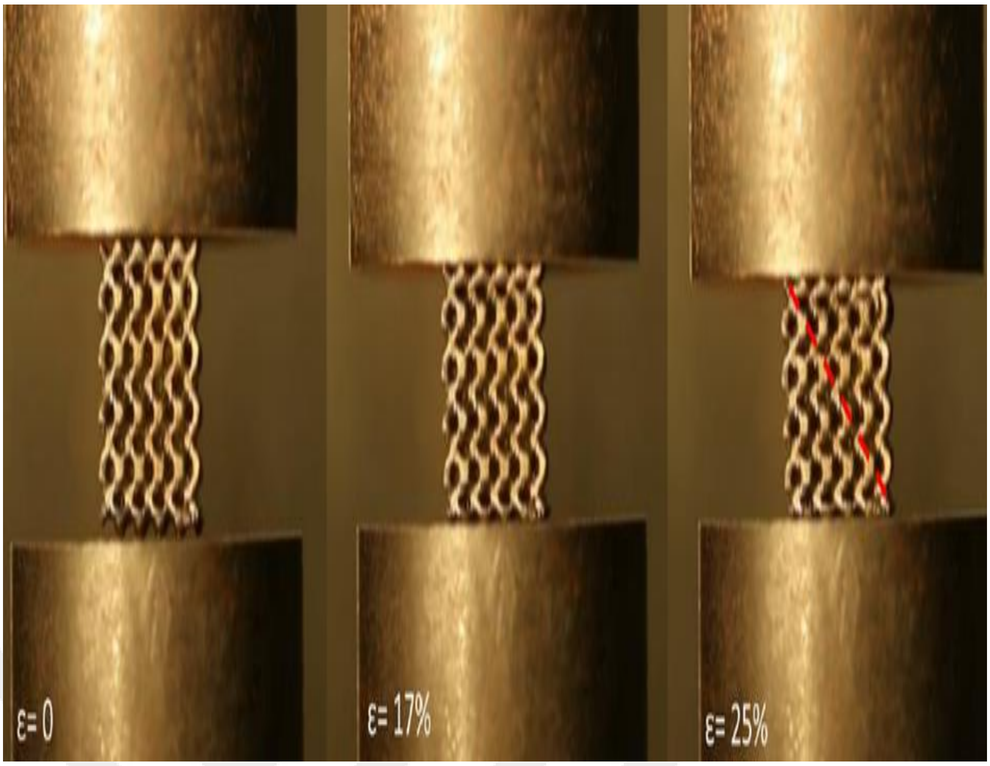

Figure 2.5. The specimens were coated with titanium using the compression testing method (Xiao et al., 2020)

Juarez et al. (2018) conducted an experimental study on the metallization of 3D-printed polymer microlattice structures. In their study, the researchers investigated producing metal-polymer cages by coating epoxy-based micro-lattices with magnetron sputtering. The cage structures were fabricated using a 3D direct laser writing (3D-DLW) process with epoxy-based material. The coating materials selected were aluminium, Inconel 600 and Ti-6Al-4V. Their study employed two different sputtering configurations: fixed and rotary substrate holders. The study concluded that the potential application breadth is extensive, with an unprecedented combination of material properties, including chemical activity, conductivity, and strength. It was also demonstrated that applying metal coatings can alter the deformation mode of materials from node-weighted damage to bond-weighted damage. An SEM image of the coated polymer structures is presented in Figure 2.6.

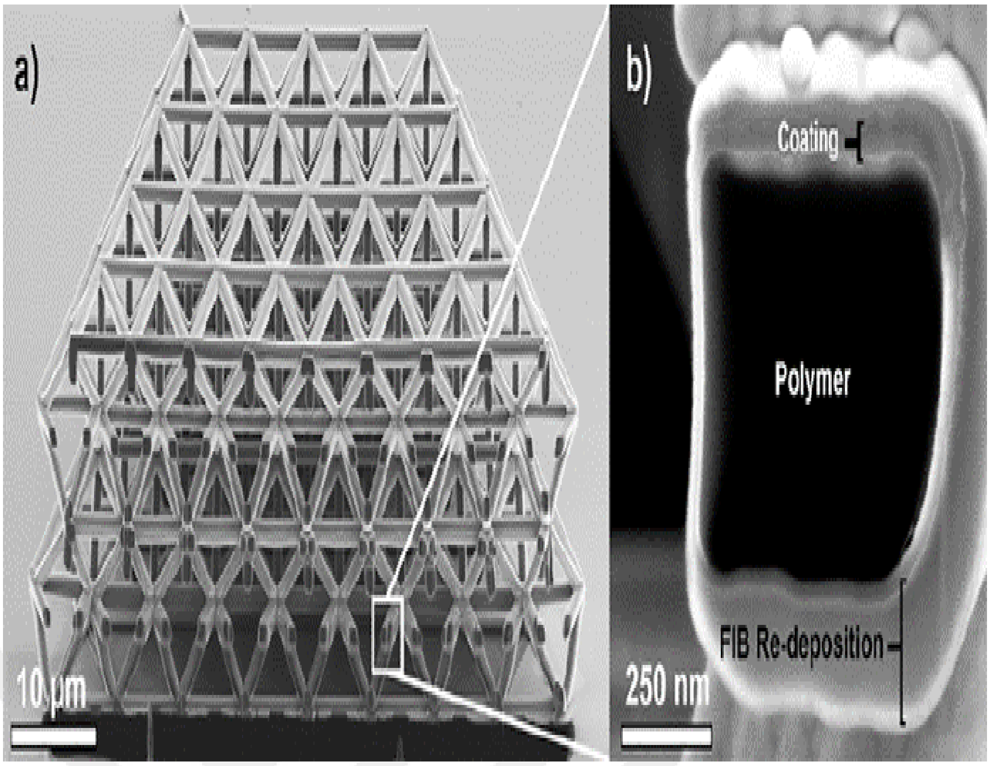

Figure 2.6. SEM image of coated polymer structures (Juarez et al., 2018)

Liu et al. (2016) investigated methods of enhancing the adhesion between the polymer structure and the metal film. To this end, the surfaces of polymethylmethacrylate (PMMA) polymer structures were subjected to UV-ozone surface modification. The researchers observed that the process enhanced the adhesion between the metal film and the PMMA polymer substrate material. They attributed this improvement to the rise in surface wettability and nanoscale surface roughness resulting from generating polar oxygen functional groups. Furthermore, they asserted that metal films in modified PMMA polymer structures exhibited resilience to liquid immersion. The microsensors developed in the study are illustrated in Figure 2.7.

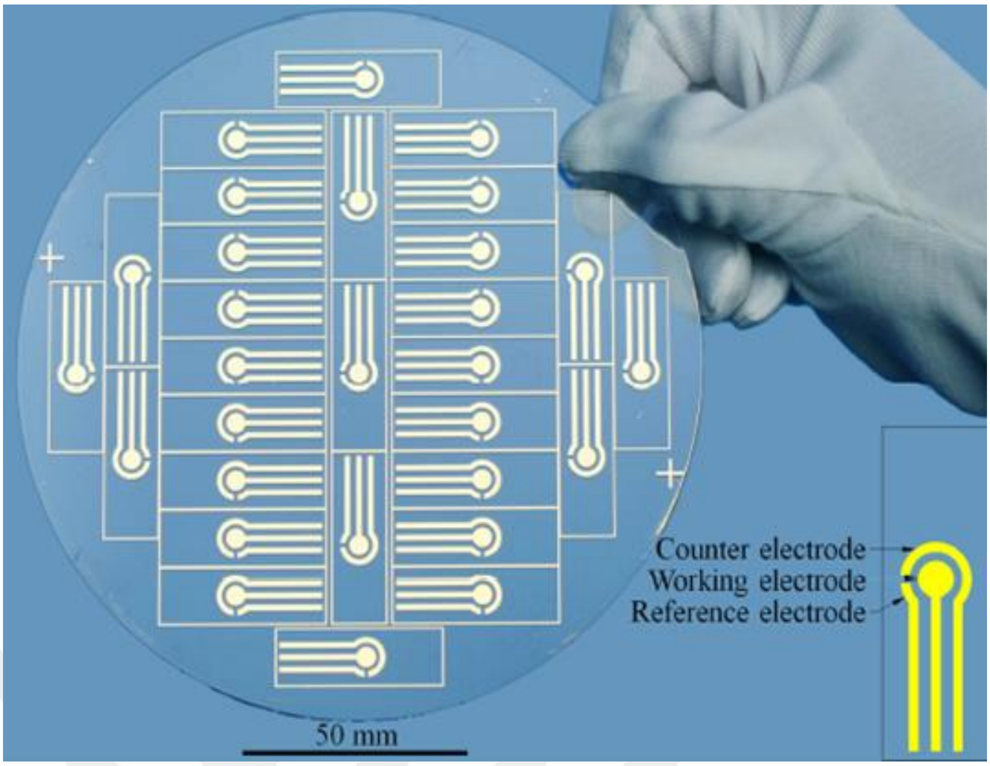

Figure 2.7. Electrochemical microsensors (Liu et al., 2016)

Jiang et al. (2018) fabricated polymer lattice structures, including cylindrical simple cubic (CSC), four square simple cubic (FSC) and mixed simple cubic (MSC), using DLP technology. They then plated copper and nickel using the electroless plating technique to form metal coatings. The compressive strength of the produced polymer structures was investigated experimentally and numerically. It was found that surface metallization can improve mechanical properties. Furthermore, it was demonstrated that Young's modulus increases linearly with the thickness of the metal film. It was concluded that Young's modulus increases from approximately 31 MPa to 96 MPa in copper films and from approximately 31 MPa to 132 MPa in nickel films. The image of copper and nickel-plated lattice structures is given in Figure 2.8.

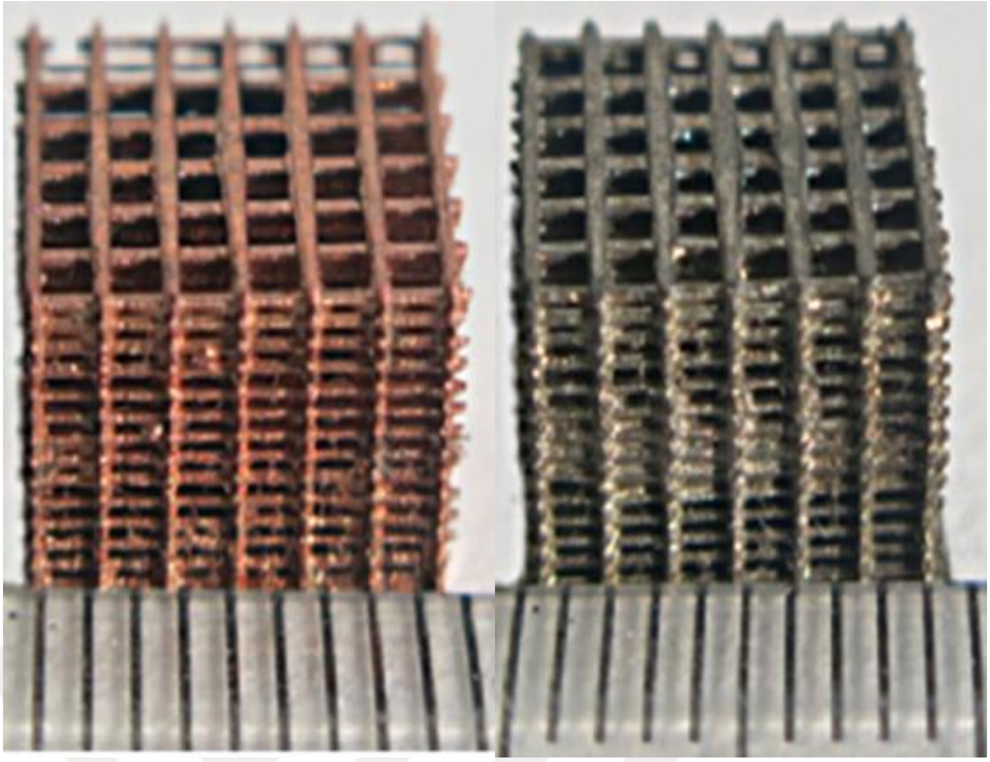

Figure 2.8. Copper and Nickel-plated lattice structures (Jiang et al., 2018)

Xiang et al. (2023) implemented an experimental investigation into the selective metallization of copper phosphate and nickel phosphate as laser-active materials on the polymer surface, utilizing direct activation with laser and electroless plating techniques. Polymer materials PC, ABS, and PEEK were selected for analysis. The copper layers exhibited excellent electrical conductivity and good adhesion strength. Additionally, it was observed that copper patterns demonstrated high selectivity and solubility. The electrical conductivity value of the copper layers was 7.6 μΩ.cm for A thickness of 4.6 μm was observed. The SEM images revealed that the copper particles exhibited continuous growth on the PC polymer structure surfaces, coated without current for 40 minutes, forming large particles on the structure surface. The images of the coatings on different polymer substrates are presented in Figure 2.9.

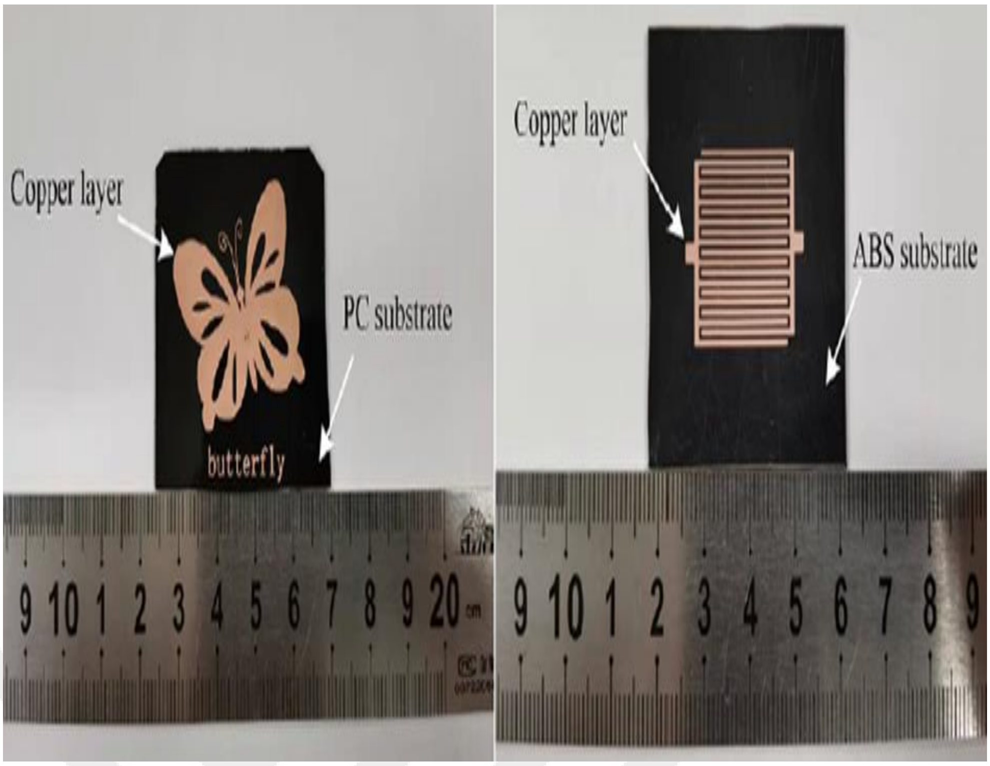

Figure 2.9. Coatings on different polymer substrates (Xiang et al., 2023)

Credi et al. (2023) aimed to fabricate complex-shaped and functional polymer structures directly and cheaply using selective electroless deposition. As an alternative to laser-assisted surface activation, which is very time-consuming and costly, nickel powders were incorporated into the resin from which the polymer structures were fabricated. The 3D polymer structures were then printed in the SLA machine. The composite structures were immersed in an electroless bath at 45ºC for metallization for 20 minutes. It is believed that the structures produced could be candidate materials for multilayer electronic circuits or sensors with magnetic and conductive properties. The conductivity test demonstration of the samples prepared in the study is shown in Figure 2.10.

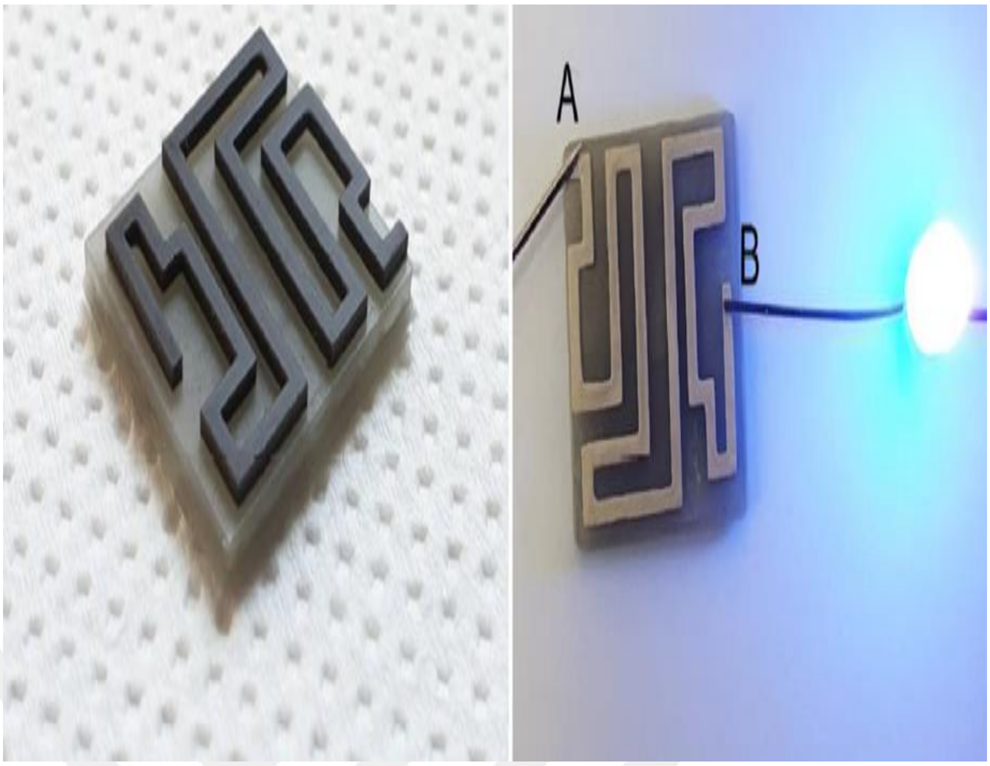

Figure 2.10. The conductivity test demonstration of the samples prepared in the study (Credi et al., 2023)

Romani et al. (2021) researched the metallization of thermoplastic polymer and composite structures by PVD sputtering using the FDM technique. The coating material for metallization was chromium, and the filament material for the production of polymer structures was PLA, acrylonitrile styrene acrylate (ASA), PC-ABS, co-polyester filament, and composite co-polyester filament. The researchers indicated that using different polymer structures would confer significant advantages to the automotive and furniture industries. The prepared PLA and co-polyester filament samples exhibited good homogeneity. The co-polyester filament samples demonstrated the most favourable outcomes in terms of surface roughness following PVD metallization. Consequently, this material is deemed a potential candidate for applications where superior thermal and mechanical properties are sought. Figure 2.11 illustrates the metallization of PLA polymer structures via the PVD method.

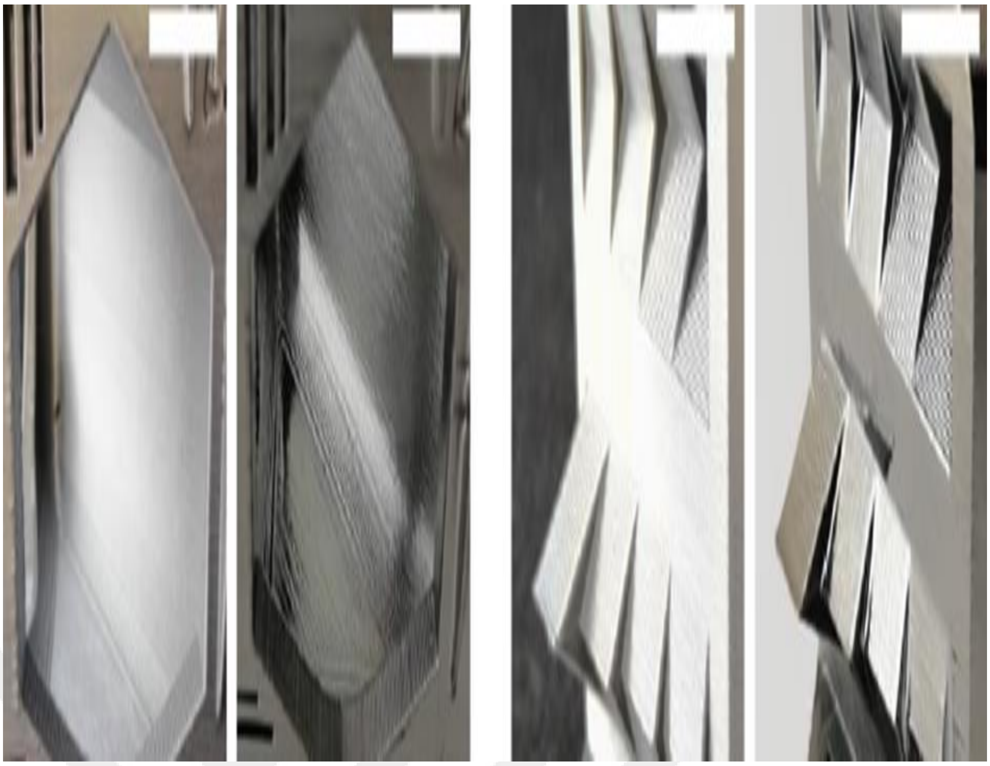

Figure 2.11. The metallization of PLA polymer structures via the PVD method (Romani et al., 2021)

Liao and Kao (2012) developed a novel method for depositing a copper layer on the surface of a polymer substrate. They printed a particle-free silver nitrate ink on the polymer as an activating agent for copper plating. The prepared structures were then subjected to electroless plating, forming highly conductive copper patterns. The prepared copper pods' electrical conductivity was 83, comparable to bulk copper's electrical conductivity value. The adhesion strength of copper in polyethene terephthalate (PET) and polyimide (PI) polymer structures was high. The image of the antenna structures produced by the electroless copper plating technique is presented in Figure 2.12.

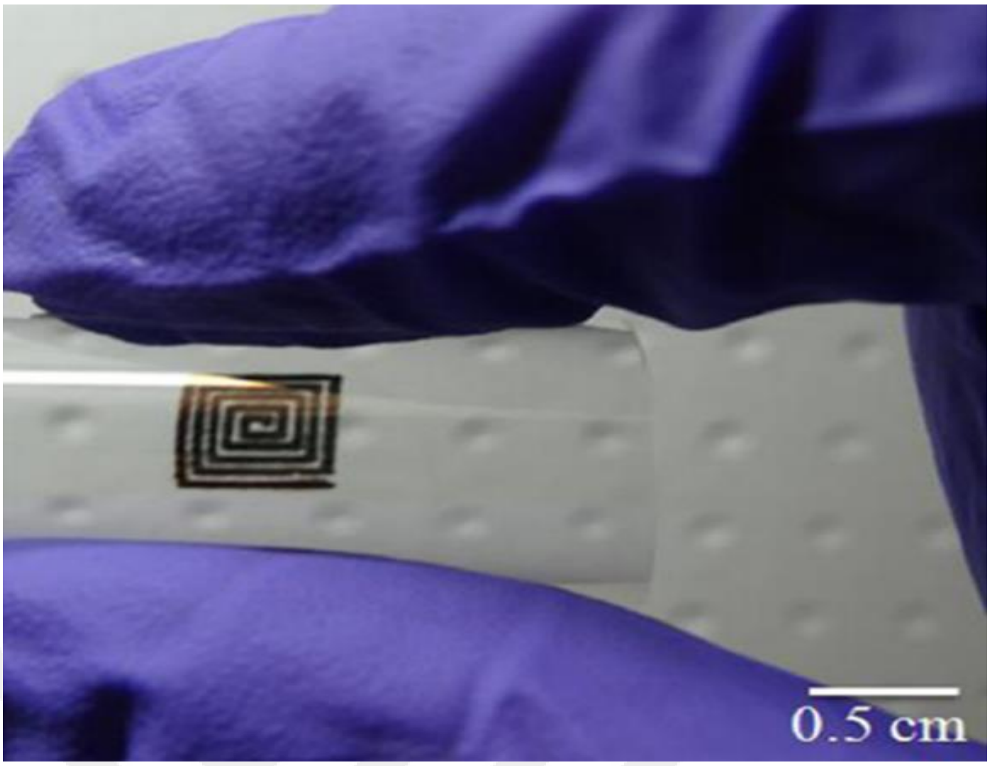

Figure 2.12. Plated copper antenna (Liao and Kao, 2012)

Rani et al. (2017) attempted to enhance the material properties of polyester-silk blend fabrics by applying a copper coating and the plasma sputtering technique. Furthermore, the investigation encompassed the analysis of copper thin film deposition parameters, including assessing gas flow, deposition power, and deposition time. Scanning electron microscopy (SEM) images revealed altered material morphology. At deposition times of 40 minutes, the most significant copper weight percentage was detected. Water contact angles increased with increasing deposition time, reaching 146° for samples deposited for 40 minutes. The results demonstrate that the deposited samples display enhanced hydrophilic behaviour. The electrical resistance value was $7.78 x 10^7$ Ωm for the uncoated sample and $8.13 x 10^3$Ωm for the sample coated for 40 minutes. Furthermore, the copper-coated samples exhibited distinctive antibacterial properties against certain bacterial species. The appearance of the polyester-silk blend before and after coating is illustrated in Figure 2.13.

Figure 2.13. The appearance of the polyester-silk blend before and after coating (Rani et al., 2017)

Srivastava et al. (2023) developed a novel method for coating polymer substrate material with aluminium. Expanded polystyrene (EPS) substrates were coated with aluminium using a new fluid-assisted bottom spray coater technique. The scanning electron microscope (SEM) analysis demonstrated that the coating thickness was approximately 340 µm. Furthermore, the coated samples' dielectric constant was 200 times higher at low frequency than the uncoated samples. The findings suggest that aluminium-coated EPS polymer structures may be suitable for utilization in various applications, including energy storage and electromagnetic interference shielding. An image of the aluminium-coated expanded polystyrene spherical structures produced in the study is presented in Figure 2.14.

Figure 2.14. The aluminium-coated expanded polystyrene spherical structures (Srivastava et al., 2023)

You et al. (2020) evaluated the efficacy of diverse surface roughening techniques on composite structures' surfaces to enhance the surface quality of carbon fibre composite structures. The researchers employed a range of surface treatments, including sand grinding, oxidation, air plasma treatment, and combinations thereof, before electroless copper plating of carbon fibre/cyanate ester structures. Subsequently, electroless copper plating was conducted. The Ra value of the samples subjected to an oxidation process was 0.44 μm, as indicated by the surface roughness results. XRD analysis revealed that the copper coatings exhibited a surface-centred cubic structure. The adhesion test results demonstrated that the oxidation sand grinding process resulted in good adhesion strength, classified as 4B course. Figure 2.15 illustrates the image of the conductive metal patterns.

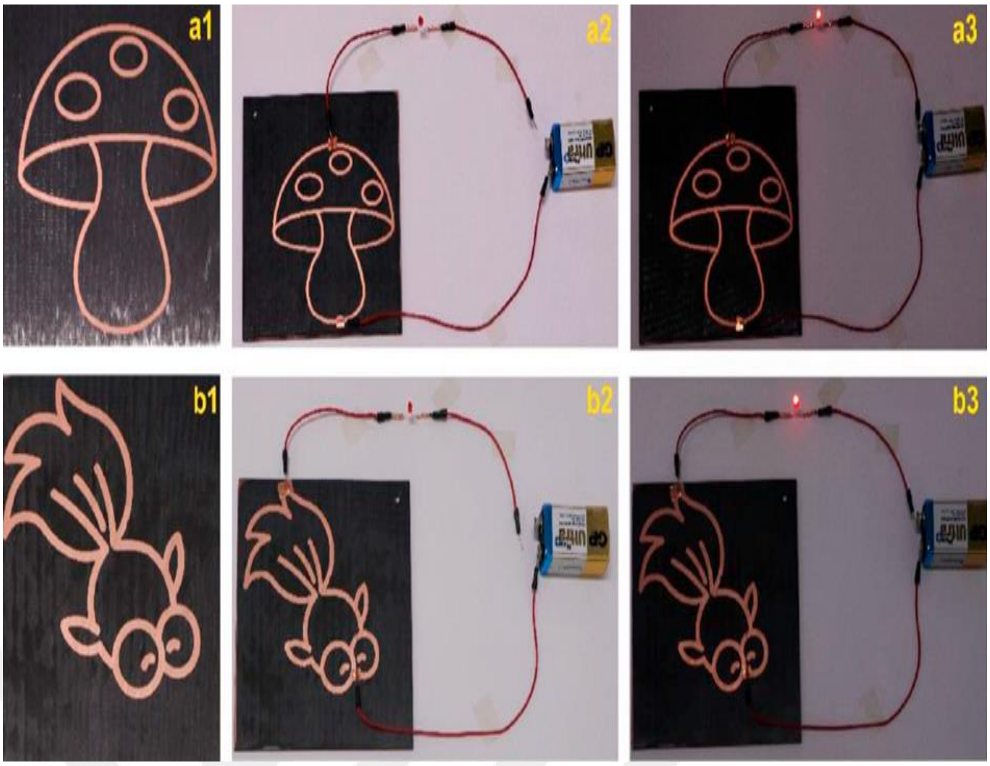

Figure 2.15. The image of conductive metal patterns (You et al., 2020)

Chen et al. (2023) developed a new simple and chromium-free method for electroless copper plating on polyamide-6 (PA6) polymer substrates subjected to UV-induced graft polymerization before metallization. Electrical resistivity measurements showed that the copper coatings reached $3.47x10^{-8}$ Ω.m, approximately 50% of the electrical resistivity of bulk copper. The 3M tape test results show that the adhesion strength between the copper layer and the PA6 polymer base material is excellent, i.e. level 4B. After polyacrylic acid grafting, the water contact angle measurement is 14.1^o, indicating that the structure's hydrophilicity has improved. This study shows that PA6 polymer structures will increase the application areas, especially electronics. The circuit showing the conductivity of the metallized samples is shown in Figure 2.16.

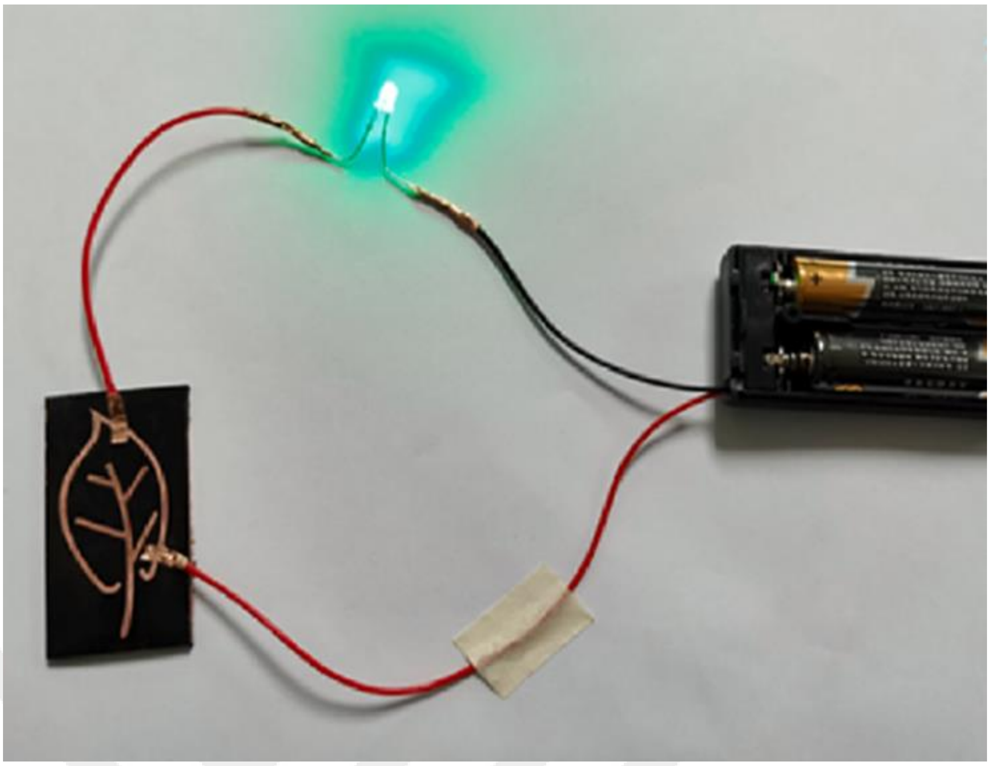

Figure 2.16. The circuit showing the conductivity of the metallized samples (Chen et al., 2023)

Akin et al. (2023) implemented an experimental investigation into the metallization of 3D-printed polymer structures via cold spray-assisted electroless copper plating. The polymer substrates were printed using ABS and PLA filaments. The coating was completed using copper particles with cold spray coating on the printed polymer structures. Subsequently, the metallization process was completed by coating copper on the prepared samples using the electroless plating technique. The electrical conductivity values were 6.47×10^{6} $S.m^{-1}$ for ABS polymer structures and 5.27×10^{6} $S.m^{-1}$ for PLA polymer structures. It was posited that the findings would prove advantageous in many fields, including electronics, energy, and defence. Figure 2.17 illustrates the conductivity of surface-coated polymer structures.

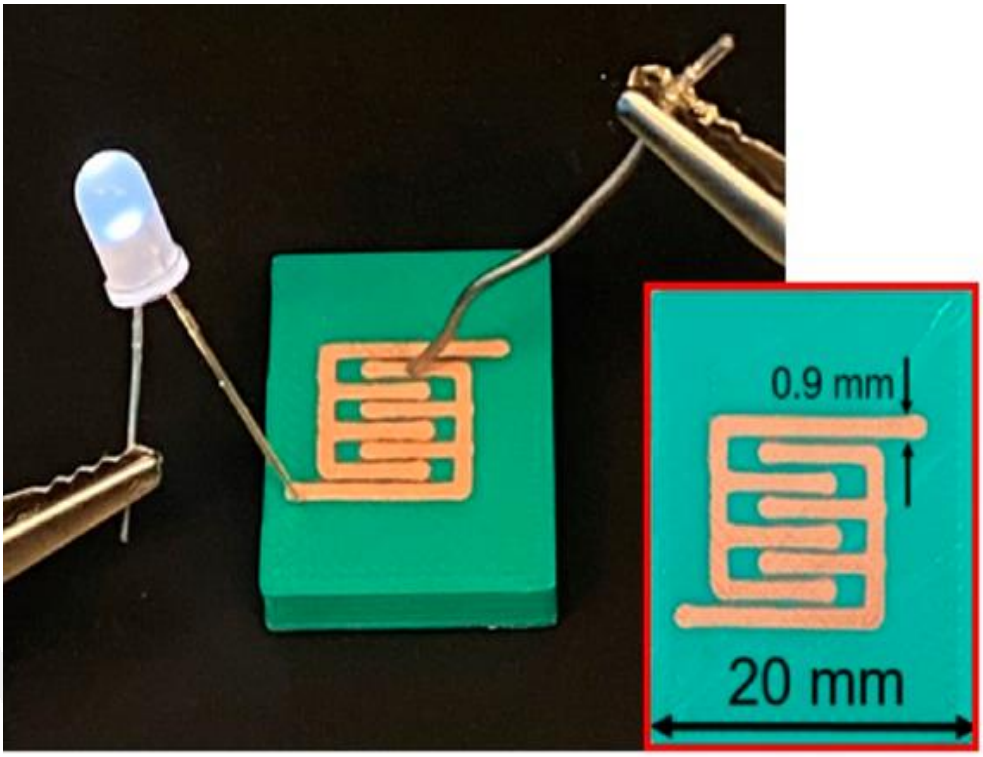

Figure 2.17. The conductivity of surface-coated polymer structures (Akin et al., 2023)

White et al. (2018) completed the metallization process by coating the surfaces of 3D-printed acrylonitrile butadiene styrene (ABS) polymer structures with 1000 nm copper. The researchers selected physical vapour deposition as the coating technique to circumvent the potential damage caused by substances such as toxic chromic acid. Among the processes employed for surface preparation, using solvents proved effective in improving surface roughness. The coated polymer structures were more aesthetically pleasing than the uncoated samples. The researchers also observed that the samples with abrasive surface treatment demonstrated excellent adhesion strength.

Arias and Jaramillo (2020) employed a coating process on the surface of the polycarbonate base material, utilizing aluminium with high reflectivity properties. Before coating, the surface of the polycarbonate sheets was subjected to ultraviolet and ozone treatment for five minutes and ten minutes, respectively. To investigate the impact of this UVO surface treatment, the researchers employed FTIR, water contact angle measurement, and AFM analysis. They posited that the UVO activation effectively resulted in a favourable surface modification of the polymer structure, attributed to the formation of polar groups, including OH and C=O.

In a study conducted by Afshar and Mihut (2020), the durability of 3D-printed polymer structures was investigated in response to exposure to a range of environmental conditions. The surfaces of the 3D-printed polymer structures were initially coated with copper. Subsequently, the prepared samples were subjected to environmental factors, including UV radiation and humidity. It was asserted that if the surface of the 3D-printed polymer is adequately coated, microcracks will not form on the surfaces of the polymer structures due to harsh environmental conditions. Since copper thin film coatings reflect UV radiation in many environmental applications, they were proposed to provide adequate protection. Additionally, it was explained that polymer structures offer protection against corrosion due to surface passivation.

Baligidad et al. (2021) fabricated polyamide 12 (PA12) structures using selective laser sintering. Subsequently, a thin copper layer was deposited on the PA12 substrate at varying deposition powers, specifically 70 W, 100 W and 120 W, via the RF sputtering technique. The researchers observed that copper coatings function as a protective layer in environmental testing, reflecting UV radiation and preventing its penetration. At a deposition power of 120 W, the samples demonstrated satisfactory flexural strength, stiffness, flexibility, electrical conductivity, and good adhesion between the base material and copper.

In a study by Afshar et al. (2019), an epoxy matrix was coated with a protective barrier against ultraviolet radiation using aluminium, copper, titanium, and zirconium. The coatings were applied using the high vacuum DC magnetron sputtering technique. It was demonstrated that metallic coatings can be an effective method of protecting the mechanical properties of epoxy samples that have been exposed to UV radiation. It was stated that ultraviolet radiation is a high-frequency electromagnetic radiation that cannot penetrate deep into metallic layers. Therefore, it was found that thin metallic films are practical barriers against ultraviolet radiation. It was found that specimens coated with aluminium retained their bending strength, elasticity, and durability to a greater extent than those coated with copper, titanium or zirconium.

Mihut et al. (2012) employed the thermal evaporation technique to deposit copper, silver, and aluminium onto high-density polyethene (HDPE) and styrene-butadiene copolymer (SBC) polymer structures containing carbon nanofibre (CNF) to enhance their electromagnetic interference shielding effectiveness. The authors reported that metallic coatings demonstrated good adhesion in undoped SBC structures. They stated that the SE value for copper coatings deposited on 10 wt% CNF/SBC increased to 52 dB at 1300 MHz. This value was 7 dB for only CNF reinforcement and 29 dB for only metallic thin film deposits at 1300 MHz.

In a study conducted by Vasconcelos et al. (2018), an experimental investigation was undertaken into the silver coating of thermoplastic polyurethane materials via the electroless coating technique. The silver coatings demonstrated excellent adhesion and low electrical resistivity. The average film thickness was 12.5 µm, with a resistivity of 8.57 mΩ.cm. The researchers asserted that the coated TPU polymer structures exhibited 400% strain at a 10 mm/min strain rate without compromising electrical conductivity.

Chen and Kang (2017) developed an efficient method to metalize acrylonitrile butadiene styrene (ABS) polymer structures using covalent grafting and spray-assisted layer-by-layer deposition. They investigated the interfacial adhesion between the coating and substrate. They found that the optimized adhesion strength was up to 20 N/cm, a significantly higher value than that achieved in the conventional process.

Jachowicz (2021) conducted a study to enhance industrial helmets' mechanical and physical properties. In this study, the coating materials employed were Cu, Al, TiN, and TiAl. In his research, he employed magnetron sputtering as a coating deposition technique. The base polymer structures selected were acrylonitrile butadiene styrene (ABS), polycarbonate (PC), high-density polyethene (HDPE), and polyamide (PA). The results demonstrated that the TiN coating provided the most effective protection against infrared radiation and scratch resistance. Furthermore, the TiN coatings exhibited the highest surface hardness measurements across all substrates.

In a study conducted by Rezzoug et al. (2016), the experimental investigation of applying metallic coatings to carbon/epoxy polymer composites was undertaken. The surfaces of the structures were coated with zinc using the arc spray technique. A layer of filler particles was applied to the substrate surface before coating to prevent damage to the substrate structure during coating. The results of the erosion test demonstrated that zinc coating enhanced erosion resistance. The surface hardness was also determined to be 25.94 ± 2.72 $HV_{0.1}$, while the average surface roughness for the arc spray coating surface was 10.94 ± 3.5 µm.

Malachowska et al. (2017) employed a metallization process utilizing copper plating on the surface of a polymer polyamide 6 substrate material through the low-pressure cold spray method. The copper powders were subjected to a pre-treatment process in a hydrogen atmosphere to reduce the critical velocity and remove the oxide layer on the surface. The prepared samples' adhesion strength, electrical conductivity, oxygen content, and microstructure were determined. The findings indicated that copper coatings were successfully deposited on the surface of the plastic substrate. Electrical conductivity measurements were 26 µΩ cm. It was stated that the copper plating process on plastic surfaces is related to the powder morphology and oxygen content.

Lackner et al. (2014) attempted to determine the mechanisms underlying the formation of micron-scale surface topography in carbon fibre polymer composite structures. To this end, they employed a magnetron sputtering technique to create Cr-based single and multilayer coatings. The researchers indicated that the film growth conditions, including thermal stresses, generated during magnetron sputtering result in high intrinsic film stress, contributing to diverse surface topographies. In their investigation, they observed that incorporating a multilayer $Cr\text{-}CrN_x$ structure instead of a CrN_x single-layer coating reduced the tendency to fracture due to enhanced plastic deformation and toughness in the layer.

Sugavaneswaran et al. (2019) fabricated three-dimensional structures using ABS polymer material via the fused deposition modelling (FDM) technique. Due to the elevated roughness of these parts in comparison to those produced by conventional methods, they were metallized with electroplating technology, thus meeting the requirements of diverse sectors. The effects of electroplating on the surface roughness and size of the produced parts at various surface angles were analyzed. The experimental results demonstrated minimal surface roughness and dimensional percentage change for 0°, 90°, and 180°.

Maciag et al. (2019) aimed to gather information regarding the surface characteristics of ABS polymer structures produced via the FDM method before and after coating. Additionally, they examined the coating parameters using copper plating with the galvanic technique. Subsequently, the surface of the 3D-printed ABS parts was analyzed following copper plating with an optical profilometer. Before coating, the 3D-printed polymer structures were subjected to acetone vapour treatment for 30, 60, 90, and 120 minutes. The findings indicated that the surface parameters were comparable to those obtained through traditional metal processing methods, suggesting that this process could be an alternative to complex industrial processes.

Pedrosa et al. (2018) deposited a CrN thin film coating on plasma-activated ABS polymer structures, employing reactive magnetron sputtering as the coating technique. The coating process was carried out at varying nitrogen flow rates (0, 2, 3, 4, 6, 8 sccm) and coating times (10, 20, 30, 40, and 60 minutes). Subsequently, a series of analytical techniques were employed to examine the morphological, microstructural, and chemical characteristics of the structures, including X-ray diffraction (XRD), three-dimensional profilometry, open-circuit potential (OCP) measurements, Raman spectroscopy, scanning electron microscopy (SEM), colorimetry, and cross-cut band testing. The results demonstrated that high-quality surface coatings were obtained. At N_2 flow rates of 4, 6, and 8 sccm, the films were susceptible to oxidation in ambient air, failing to meet other end-user requirements such as gloss and reflectance. However, at 2 and 3 sccm N_2 flow rates, the coatings exhibited reduced surface oxidation due to exposure to air, displaying glossy, and reflective surfaces.

Khan et al. (2018) fabricated three-dimensional polymer structures utilizing the FDM method with ABS printing material. Nickel was selected as the coating material due to its low cost and aesthetic appearance. They elected to utilize electroplating as the coating method to complete the metallization process by coating the surfaces of ABS structures, given its ease of process. The findings indicated that the raster angle exerts the most significant influence on the surface roughness and coating thickness of nickel-coated FDM parts, exceeding the impact of the two FDM machine parameters.

The research conducted by Nigam et al. (2018) focused on developing a method for making non-conductive polymer structures conductive, which involved the addition of a conductive layer. A new technique was developed with a high deposition rate and no chemical hazards. An ABS polymer structure was selected as the polymer base material, and copper was chosen as the coating material for metallization. Scanning electron microscope (SEM) images revealed lamellar structures in the copper coatings on the polymer surface. The standard tape test results demonstrated that successful outcomes could be achieved with the selected method for copper coatings on ABS. However, it was observed that the pre-treatment before plating had a significant impact on the plating process.

In a comprehensive experimental study, Vaneckova et al. (2020) investigated the copper plating of 3D-printed composite electrodes. Given the advantages of 3D printing, including speed, cost-effectiveness, and environmental compatibility, the researchers opted for this method over traditional manufacturing techniques. The researchers employed copper-tempered PLA as the filament material. They observed that the electrodes produced by the FDM method exhibited a kinetic barrier for electron transfer. To remove this kinetic barrier, they enhanced the surfaces through copper electroplating. One noteworthy outcome was that the faradaic peak separation value (70-75 mV) surpassed all reported values in the literature for 3D-printed electrodes. Their work has initiated new avenues for the fabrication of 3D-printed electrodes.

Kolczyk et al. (2018) set out to develop a two-step metallization process for polymer structures produced by the stereolithography (SLA) process. The surfaces of these polymer structures were first treated with copper plating by electroless deposition, followed by a second step involving nickel plating on the copper surface through electrodeposition. All prepared samples exhibited excellent tightness and adhesion to the copper substrate. The researchers observed increased nickel plating time resulted in a decoratively shiny structure. XRD results demonstrated that the nickel platings were amorphous, and no nickel oxide was detected in the cathode bed. The researchers attributed this to the successful plating of nickel coatings.

Fontanot et al. (2020) studied the morphological and optical properties of aluminium-coated thermoplastic polymer surfaces. Polymer substrates were obtained via an injection moulding process initiated with polymer granules. The analysis showed that the ABS substrate exhibited a more pronounced surface texture than the PC substrate. While metallic films on the ABS polymer structure demonstrated effective diffusion properties, mirror-like characteristics were observed in PC polymer structures. The findings indicated that an aluminium metallic film with a thickness range of 80-115 nm optimizes surface reflection. Additionally, the protective layer was identified as conferring a significant advantage in terms of resilience to factors such as surface oxidation and mechanical damage while maintaining the desired optical properties.

Dixit et al. (2017) performed copper plating of ABS polymer structures produced using the rapid prototyping technique by electroless plating. For this purpose, they prepared part surfaces in cuboidal, cylindrical, pyramidal, and conical geometries. Two distinct strategies were employed for the surface preparation of the parts. Initially, the ABS polymer structures were coated with aluminium paste. Subsequently, the structures were prepared using chromic acid for etching. It was observed that the conductivity value increased in conjunction with the coating time in all acidic solutions. The results of the adhesion tests indicated that the polymer surfaces coated with aluminium carbon black paste exhibited favourable adhesion properties between the deposited copper coating and the underlying polymer.

In an experimental study on the surface activation of biocomposites for electroless metallization, Rytlewski et al. (2017) produced biocomposites containing PLA, polycaprolactone (PCL), copper(II) oxide, and copper acetylacetonate by the extrusion method. Before coating, the biocomposite structures were irradiated with an excimer laser. The compositions of the composites selected for laser irradiation and electroless metallization were 15% and 5% copper (II) oxide and copper acetylacetonate, respectively. The PCL material was chosen as PLA with 0%, 5%, 10%, and 15% remainder by weight. The general optical evaluation and EDX analysis results indicated that the increase in PCL content positively affected metallization, with more light-coloured copper agglomerates occurring with higher PCL content.

Xie et al. (2024) conducted an experimental study to improve the material properties of polyetherimide (PEI) composite structures, focusing on electromagnetic shielding and electrical conductivity. To this end, Ni/Cu/Ni coatings were deposited on the PEI composite surface using two distinct techniques: electroless and electrodeposition. The findings indicated that an increase in the thickness of the copper interlayer in the surface-centred cubic crystalline structure resulted in enhanced electrical resistance. Furthermore, this interlayer thickness influenced the adhesion strength of coatings on PEI substrates. In samples with a 7.54 μm copper interlayer thickness, microhardness values reached up to 300 $HV_{0.1}$.

Bragaglia et al. (2022) used SLA additive manufacturing technology to fabricate three-dimensional thermosetting polymer structures. The resulting samples were then subjected to silver plating via an electroless plating technique. Subsequently, the samples were treated with three distinct surface treatments, namely acetone, ethanol, and sulphuric acid solution. The findings revealed that the thickness of the silver coatings was approximately 200 nanometres. Additionally, it was reported that the electrical resistance value of the ethanol-treated samples was 4.83 x 10-8 Ωm. The contact angle measurements yielded 81.4°, 79.6°, and 80.3° for the samples treated with acetone, ethanol, and sulfuric acid solutions.

In an experimental study conducted by Siddikali et al. (2022), the electroless metal plating of PETG polymer structures and MWCNT (multi-walled carbon nanotube) reinforced PETG composite structures was investigated. The results indicated that the electroless metal plating process enhanced the polymer composite structures' mechanical, tribological, and surface properties. The composite structures were fabricated using the FDM method and subsequently plated with copper and nickel by electroless plating. The micro Vickers hardness values of the metal-plated composite structures exhibited an increase of 53%, reaching a hardness value of 92 HV. With the augmentation in coating thickness, the water contact angle demonstrated a corresponding increase, reaching a value of 78° in PETG samples. In composite structures, this value was determined to be 88.84°. The researchers posited that the electroless coating technique would enhance the thermal and mechanical properties of the structures.

Spacek et al. (2018) aimed to develop a new tubular daylighting system by metallizing ABS polymer structures to reduce energy consumption. The metallization process of ABS plastic structures was conducted using the PVD method. The adhesion test results demonstrated that the samples coated with a metal film exhibited excellent adhesion strength, specifically grade 5B. The findings indicate that structures coated with aluminium polymers may be a viable alternative to the current silver structures. Additionally, the cost of these candidate materials is estimated to be approximately 50% less.

Zhang et al. (2019) coated the polyester fabric surface with copper by sputtering technique to enhance the characteristics of metal-coated fabrics during synthetic perspiration. The metal-coated samples were then subjected to a supplementary treatment with a benzotriazole solution. The results demonstrated enhanced corrosion resistance by the samples treated with benzotriazole solution. The sheet resistance of the solution-treated samples was 1.15 Ω/sq, nearly identical to the sheet resistance of the copper film. The researchers concluded that the improvements in the material properties of copper-coated fabrics treated with benzotriazole solution would expand the range of potential applications for these materials.

In their experimental study on copper metallization of surface-modified polyamide films, Ji et al. (2008) employed the electroless plating technique for copper plating. Before plating, the structures were modified with a potassium hydroxide (KOH) solution. A silver activation layer was also formed to enhance the adhesion between the polyamide. The FT-IR results indicated the presence of peaks corresponding to the characteristic carbon and oxygen double bond and carbon and nitrogen single bond at 1650 cm-1 and 1370 cm-1, respectively. A notable decline in peak intensity was observed with increased copper coating thickness. The researchers posited that metal-coated polymer films have the potential to be utilized in various applications.

Rytlewski and Zenkiewicz (2013) investigated the physical and chemical changes following the metallization of laser-irradiated thermoset and thermoplastic composite structures. The thermoplastic material was polyamide (PA6), and the thermoset material was polyurethane resin (PU). Furthermore, copper (II) oxide and copper (II) acetylacetonate powders were used as composite structure reinforcement materials. The prepared composite structures were irradiated with laser pulses, and subsequently, copper metallization was conducted via the electroless plating technique. The findings indicated that polyamide composite structures exhibited superior catalytic properties compared to polyurethane resin composite structures. It was observed that laser irradiation increased the amount of copper deposited on the surface across all polymer composite structures.

Rahmatollahpur et al. (2010) coated the surface of biaxially oriented polypropylene plastic material with aluminium and conducted a microstructural analysis of the aluminium layer. The surface of the plastic structures was metallized in a roll-coater system, and the resulting coating thicknesses were found to range from 20 nm to 60 nm. Additionally, the researchers indicated that the aluminium crystal grain size is approximately between 20 and 70 nm. They observed an increase in the intensity of the EDX analysis results of the samples that underwent double coating compared to those that underwent single coating. Upon analyzing the TEM images, the researchers noted the presence of some pinholes, with dimensions ranging from 0.8 to 8 μm.

Moraczewski et al. (2015) subjected the surface of PLA polymer structures to oxygen or nitrogen plasma surface modification before metallization. Subsequently, the surfaces of the samples were coated with autocatalytic copper plating. SEM images revealed the formation of droplets on the surface of the structures following plasma modification. In contrast, AFM images indicated that oxygen surface treatment resulted in more pronounced surface alterations. The applied plasma surface treatments enhanced wettability and surface roughness while also influencing the geometry of the PLA surface. Consequently, surface modification processes are a viable approach for coating PLA structures.

The study conducted by Yu et al. (2016) aimed to create a controlled surface pattern on the surface of polydimethylsiloxane (PDMS) structures. The coatings were produced using direct current (DC) magnetron sputtering technology, with nickel selected as the coating material. Upon analysis of the optical microscope images, it was observed that the thickness of the metal layer impacted the pattern formed. A reduction in coating thickness results in the formation of ripple patterns, whereas an increase in thickness leads to the emergence of cracks. In the case of varying film thicknesses, the water contact angle demonstrated a rise in conjunction with an increase in film thickness, enhancing surface roughness. This phenomenon can be attributed to an augmented hydrophobicity of the metal layer. The materials produced have the potential to be employed in a range of applications, including electronics, optics, and biology.

Equbal et al. (2015) studied the electroless plating of 3D-printed ABS polymer structures using the FDM method. Initially, the surface of the polymer structures was treated with chromic acid to facilitate copper metallic plating. In contrast to the chromic acid surface treatment, sulphuric acid, and hydrogen peroxide were employed. Subsequently, the coating process was conducted in different baths. The optimal electrical resistance of the samples that underwent chromic acid, sulphuric acid, and hydrogen peroxide surface treatment was observed in the samples coated for 48 hours in a sulphuric acid bath. The adhesion test results demonstrated that the coated samples exhibited excellent adhesion strength, reaching the 4B or 5B level.

3. MATERIAL AND METHOD

The thesis study comprises a number of distinct stages, which are illustrated in graphical form in Figure 3.1.

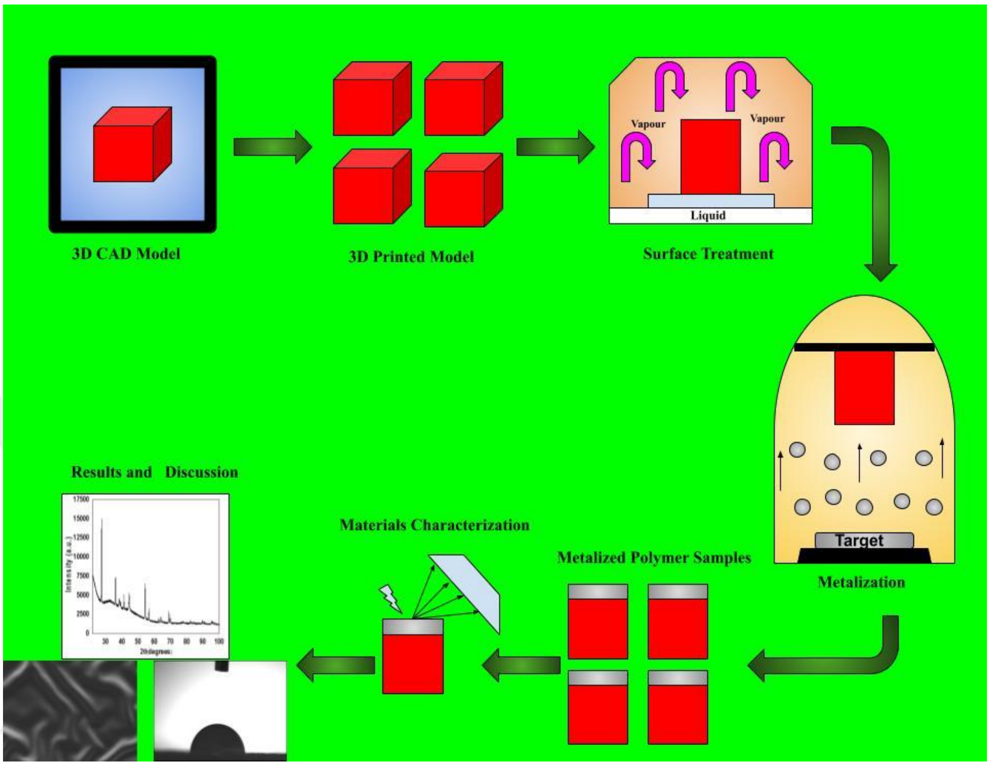

Figure 3.1. Graphical abstract of the experimental steps

3.1. Printing of the Samples with FDM

The 3D desings for the printing of polymer structures were created in the SolidWorks program and transferred to the printer in .stl format. BASF Ultrafuse White PLA filament was used for the printing of 3D polymer structures. The PLA used has a glass transition temperature of 61°C, a melting temperature of 151°C, a Printed Part Density of 1248 kg/m³, and a Melt Volume Rate of 21.2 cm³/10 min. The printing of polymer structures was carried out using the Creality Ender3 Pro 3D printer. Figure 3.2 illustrates the Creality Ender3 Pro 3D printer. The printing parameters used are provided in Table 3.1. The appearance of the completed polymer structures with dimensions of 20x20x10 mm³ is shown in Figure 3.3.

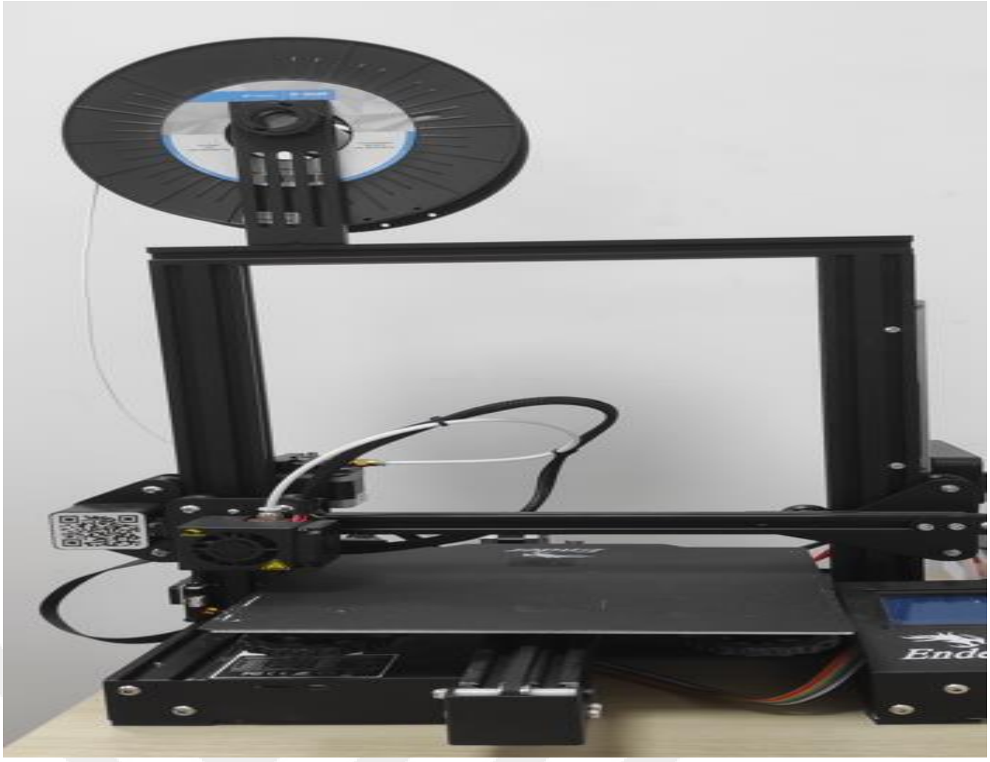

Figure 3.2. Creality Ender3 Pro 3D printer

Table 3.1. Parameters of 3D Printing

Fixed Printing Parameters	
Filament Diameter	1.75 mm
Nozzle Diameter	0.4 mm
Nozzle Temperature	210ºC
Built Platform Temperature	60 ºC
Infill Pattern	Lines
Infill Density	100%
Layer Height	0.2 mm
Print Speed	50mm/s
Wall Line Count	2

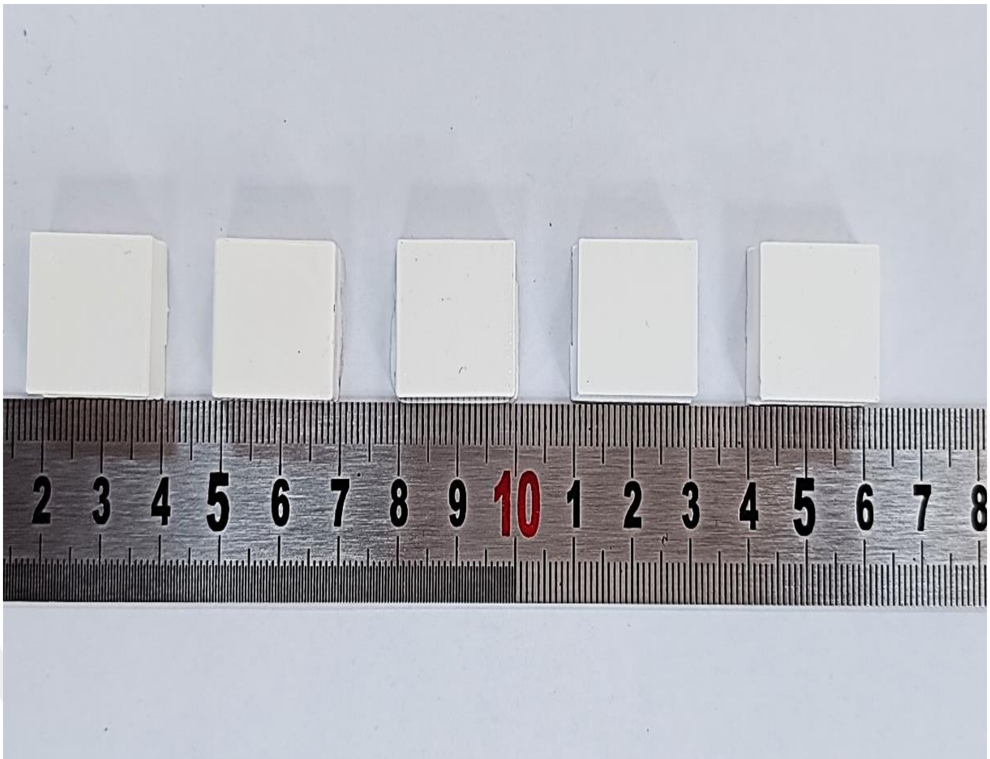

Figure 3.3. 3D printed polymer samples, from left to right; as-printed, dipping, vapour, plasma, abrasion.

3.2. Surface Modification of the Samples

To determine the optimal surface treatment for completed 3D polymer structures, five different surface treatments were applied (As-printed, Dipping, Vapour, Plasma, and Abrasion). Dipping involved immersing the 3D polymer structures in dichloromethane liquid for 60 seconds, followed by air-drying at room temperature (Panda et al., 2020). Vapour treatment exposed the polymer structures to dichloromethane vapour in a closed container at 90°C for 30 minutes, followed by air-drying at room temperature (Jin et al., 2017). Plasma surface treatment was applied using Optosense, OPT-PCO-02, with 100 KHz of radio-frequency energy, flowing oxygen (0.5 L/min), and 2000 W of radio-frequency power for 180 seconds. The oxygen purity was 99.99%. This surface treatment is also referred to as the cold oxygen plasma process (Song et al., 2016). The cold oxygen plasma process is illustrated in Figure 3.4. The final surface treatment involved manually treating the polymer surfaces with 1000-grit sandpaper for 60 seconds (White et al., 2018).

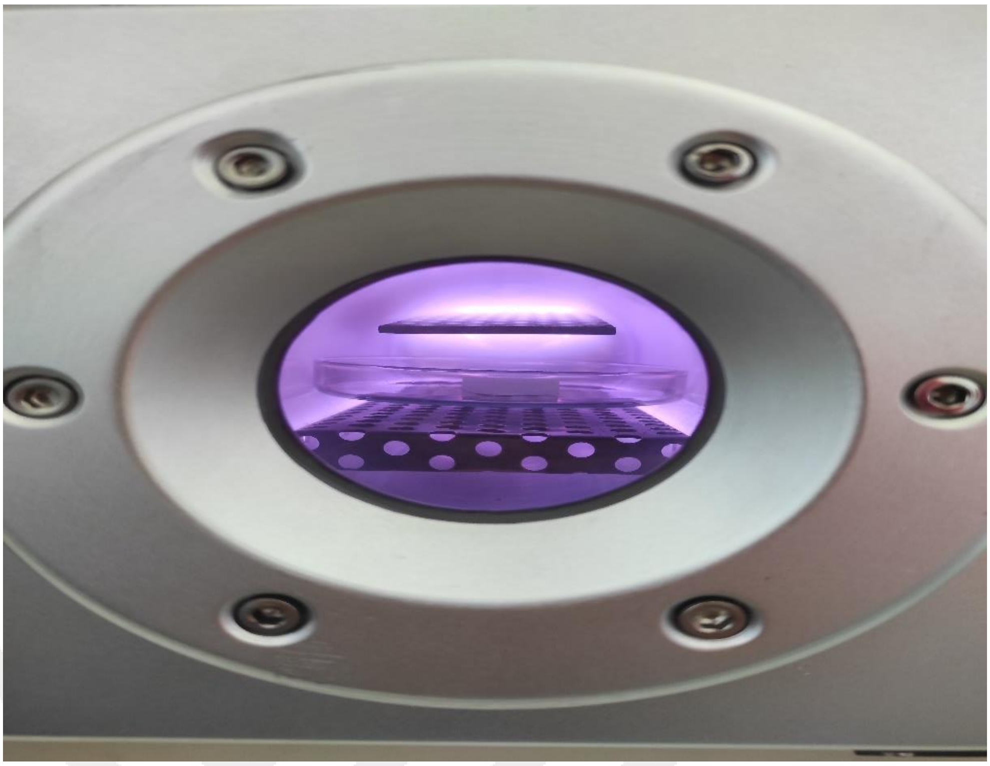

Figure 3.4. The cold oxygen plasma process

3.3. Surface Coating of the Samples

For the metallization of 3D polymer structures, a Box type Physical Vapour Deposition system, based on prismatic/cylindrical vacuum chambers was used, equipped with 2 thermal and/or 1-4 DC-RF sputter sources (NVTS) allowing full co-evaporation (Nanovak NVTS-400). Figure 3.5 and 3.6 illustrates the Physical Vapour Deposition system. The aluminium coating parameters were set as follows: 120-watt RF power, coating pressure of 8 mTorr, base pressure of $2x10^{-6}$ Torr, and a deposition rate of 2.2 Å/s. The coating material used was a 2-inch diameter, 0.250-inch thickness, 99.99% purity aluminium target (purchased from Adesis, Turkey). The appearance of the 3D polymer structures after coating is shown in Figure 3.7.

Figure 3.5. The Physical Vapour Deposition system

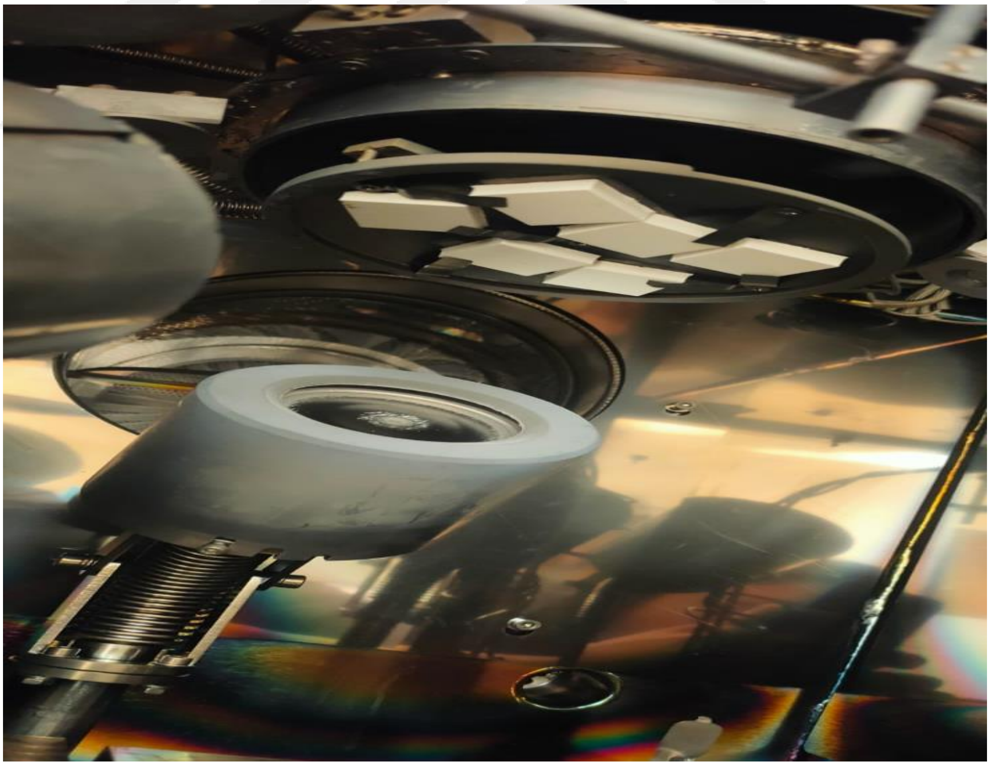

Figure 3.6. The Physical Vapour Deposition system

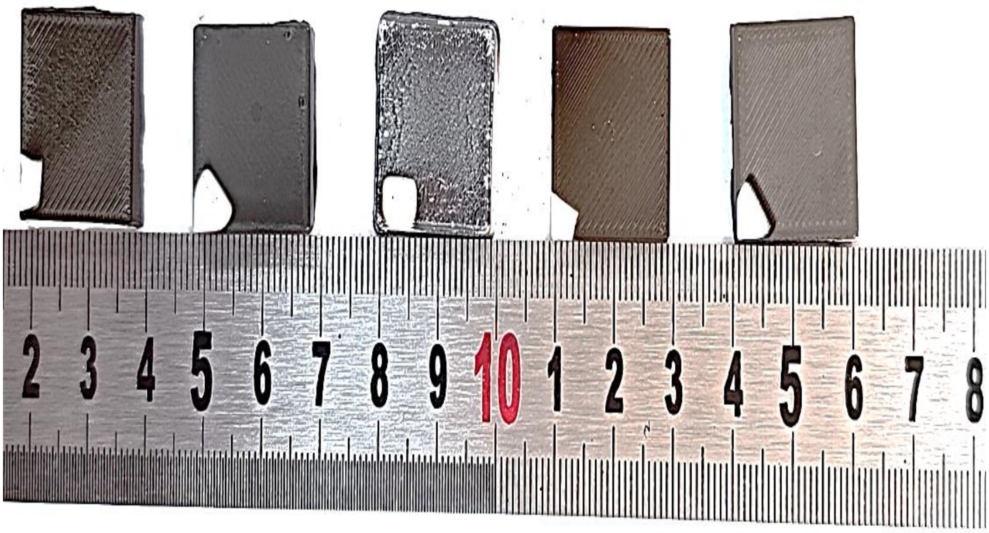

Figure 3.7. The appearance of the 3D polymer structures after aluminium coating

The copper coating parameters were 400 V, 200 mA DC power, 10 mTorr coating pressure, $2x10^{-6}$ Torr base pressure, and a coating rate of 2.5 Å/s. The coating process is shown in Supplementary Figure 3. A 99.99% purity copper target with a diameter of 2 inches and a thickness of 0.250 inches (purchased from Adesis, Turkey) was used as the coating material. The images of the 3D polymer structures after coating are shown in Figure 3.8.

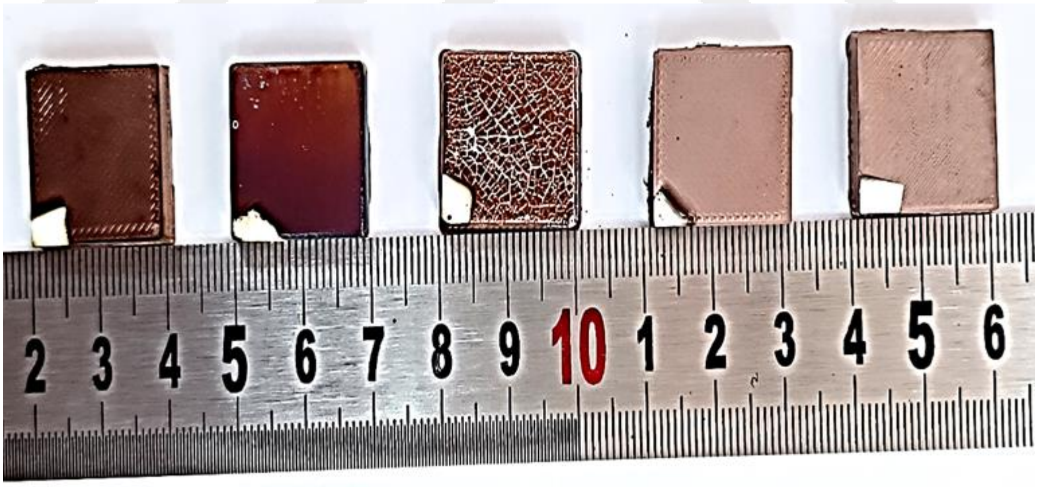

Figure 3.8. The appearance of the 3D polymer structures after copper coating

3.4. Characterization of the Samples

After completing the metallization process on the 3D polymer structures, a comprehensive analysis of their morphological, structural, optical, and electrical properties was conducted. The following techniques and instruments were employed for the analysis. Scanning Electron Microscopy (SEM) and Energy Dispersive Spectroscopy (EDS) analysis: The FEI Quanta 650 Field Emission SEM device was used. Atomic Force Microscopy (AFM): The Park Systems Park

NX10 AFM device was utilized to gain information about surface topography and the 3D structure of the surface. X-ray Diffraction (XRD) analysis: The PANalytical EMPYREAN XRD device was employed to examine the crystal structure of the coated polymer structures. Fourier Transform Infrared Spectroscopy (FT-IR) analysis: The Jasco FT/IR-6700 device was used to investigate the molecular bond structures of the experimental samples. Ultraviolet-Visible-Near Infrared (UV-VIS-NIR) analysis: The Agilent Cary 7000 Universal Measurement Spectrophotometer (UMS) device was utilized for optical property analysis. Ellipsometry analysis: The J.A. Woollam spectroscopic ellipsometer device was employed for ellipsometry analysis, providing information about optical properties. Contact angle measurement: For obtaining information about material properties such as liquid absorption, wettability, liquid retention on the surface, liquid spreading, surface cleanliness, and surface heterogeneity, contact angle measurement on sample surfaces was performed using the Biolin Scientific Attension – Theta Lite. Electrical resistance measurement: The four-point probe method, using the Keithley Source Multimeter device, was employed for electrical resistance measurement.

4. RESULTS AND DISCUSSIONS

4.1. Scanning Electron Microscopy (SEM) and Energy Dispersive Spectroscopy (EDS)

The scanning electron microscope images of 3D-printed polymer structures before metallization and after surface treatment are provided in Figure 4.1-4.5. Upon examination of the images, it is evident that layer lines formed during the production stage of 3D polymer structures are present in as-printed, plasma, and abrasion surface treatments. Additionally, the sample surface treated with sandpaper exhibits an extremely high level of micron-scale surface roughness. In contrast, for dichloromethane dipping and vapour treatments, the existing layer lines disappear, and the surface roughness significantly improves with minimal protrusions observed. Previous literature studies have also indicated the effects of dichloromethane usage on the surface of PLA samples in a similar manner (Jin et al., 2017; Lavecchia et al., 2022; Puerta et al., 2019).

The Scanning Electron Microscopy (SEM) and Energy Dispersive Spectroscopy (EDS) Analysis Results for 3D-printed polymer structures after aluminium coating are shown in Figure 4.6-4.15 and table 4.1-4.5. Figure 4.6-4.15 illustrates that surface morphologies are significantly dependent on the surface preparation technique. Relatively more homogeneous distribution is observed in dichloromethane dipping and vapour treatments. In the sandpaper-treated samples, high roughness and micro-scale cavities resulting from sanding are observed (White et al., 2018). In dichloromethane vapour samples, a morphology resembling fluctuation induced thermally is observed due to residual stress induced thermally. The accumulated thermal stress is believed to originate from both gas atoms striking the growing film and the significant difference in the thermal expansion coefficients between Al and PLA (Pedroni et al., 2021; Slepička et al., 2012). Energy Dispersive Spectroscopy (EDS) Analysis also confirms the presence of a significant amount of carbon (C) element in all metalized samples, indicating the existence of localized polymer regions. Additionally, EDS analysis results confirm the presence of aluminium (Al) elements on the polymer surface (Akin et al., 2023).

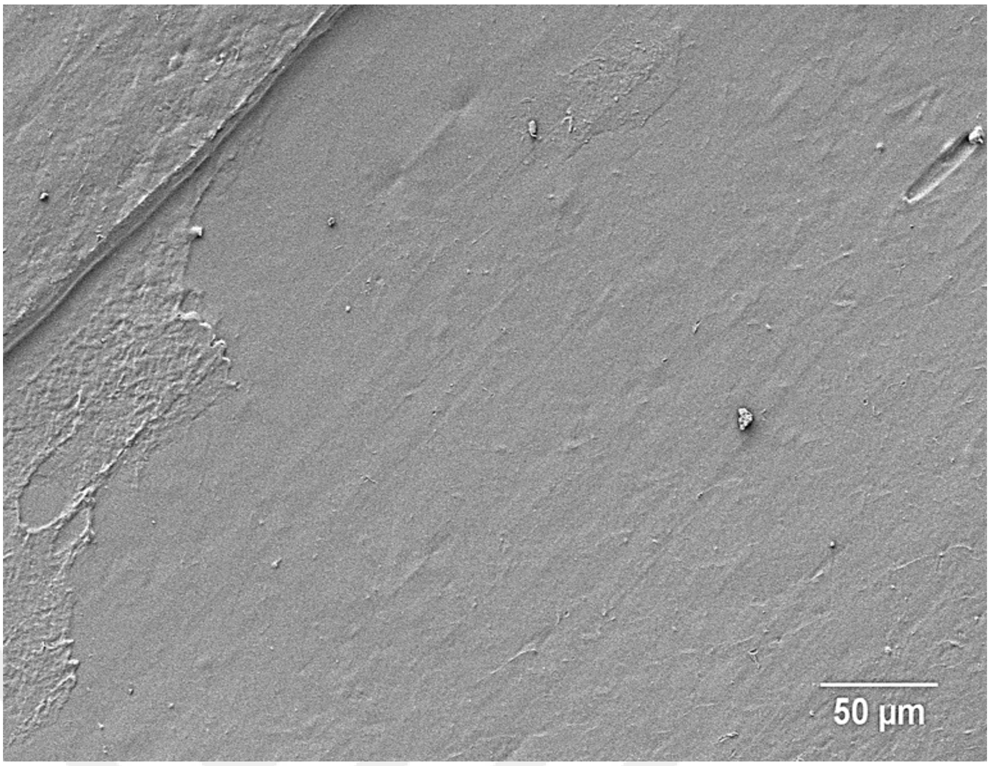

Figure 4.1. SEM image of as-printed samples

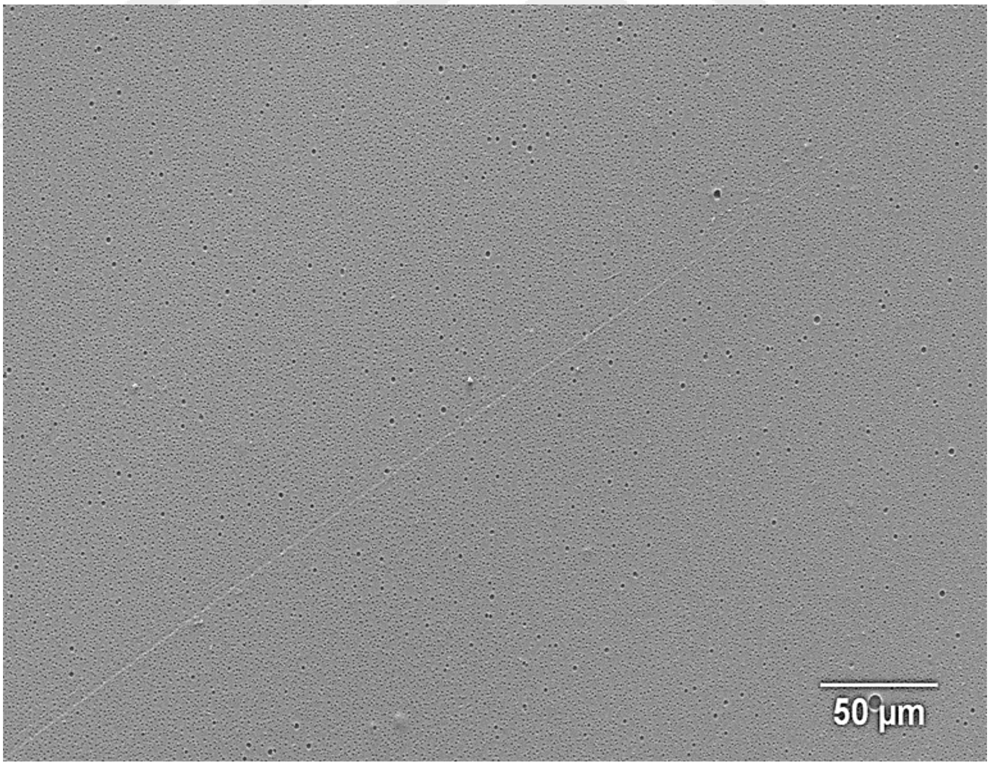

Figure 4.2. SEM image of dipping samples

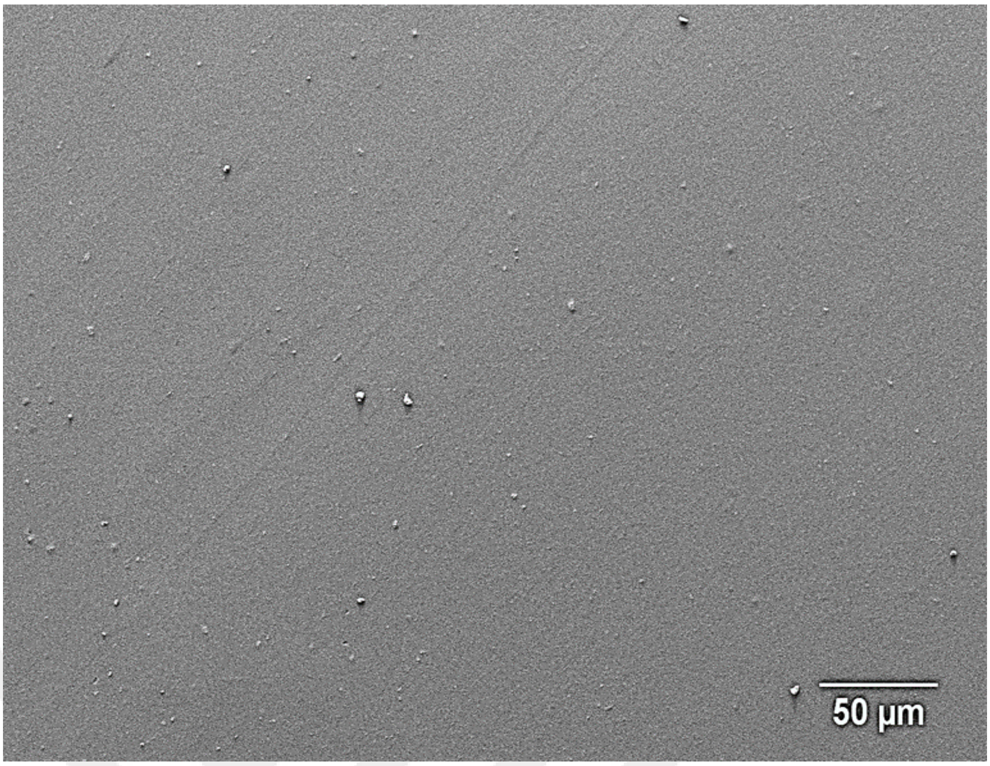

Figure 4.3. SEM image of vapour samples

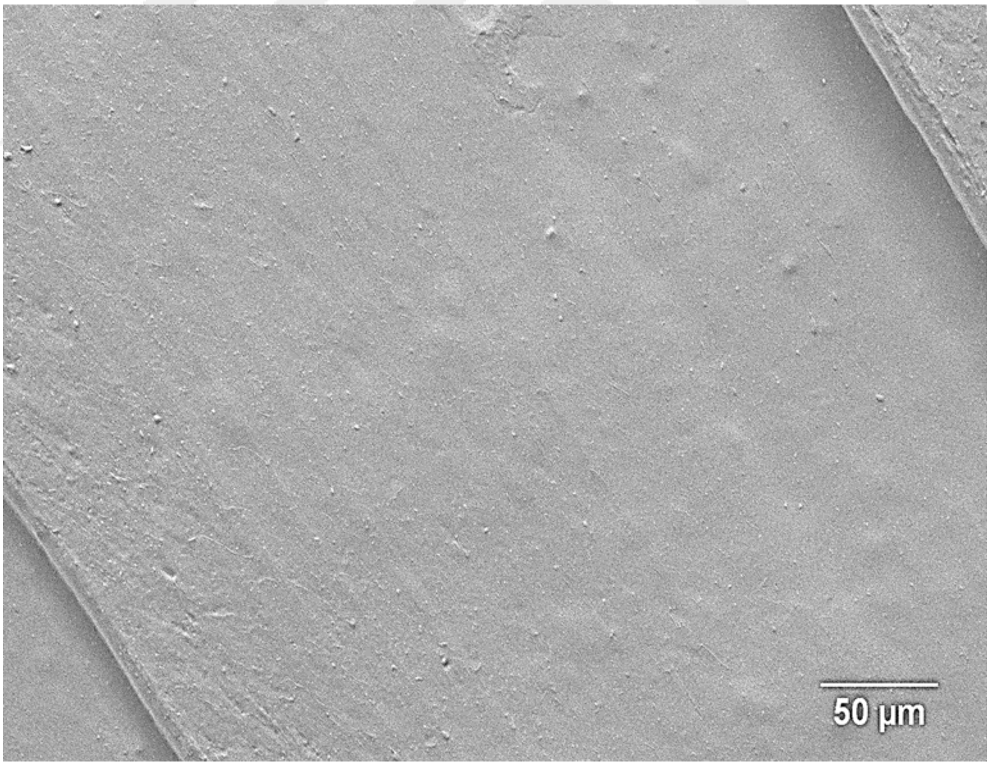

Figure 4.4. SEM image of plasma samples

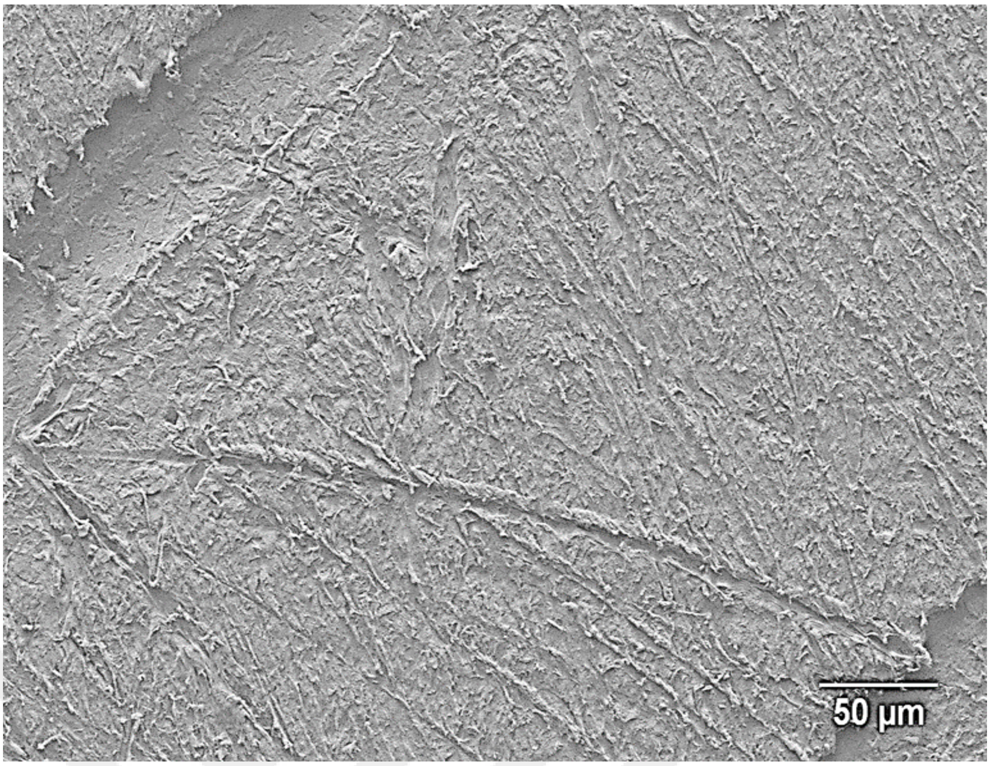

Figure 4.5. SEM image of abrasion samples

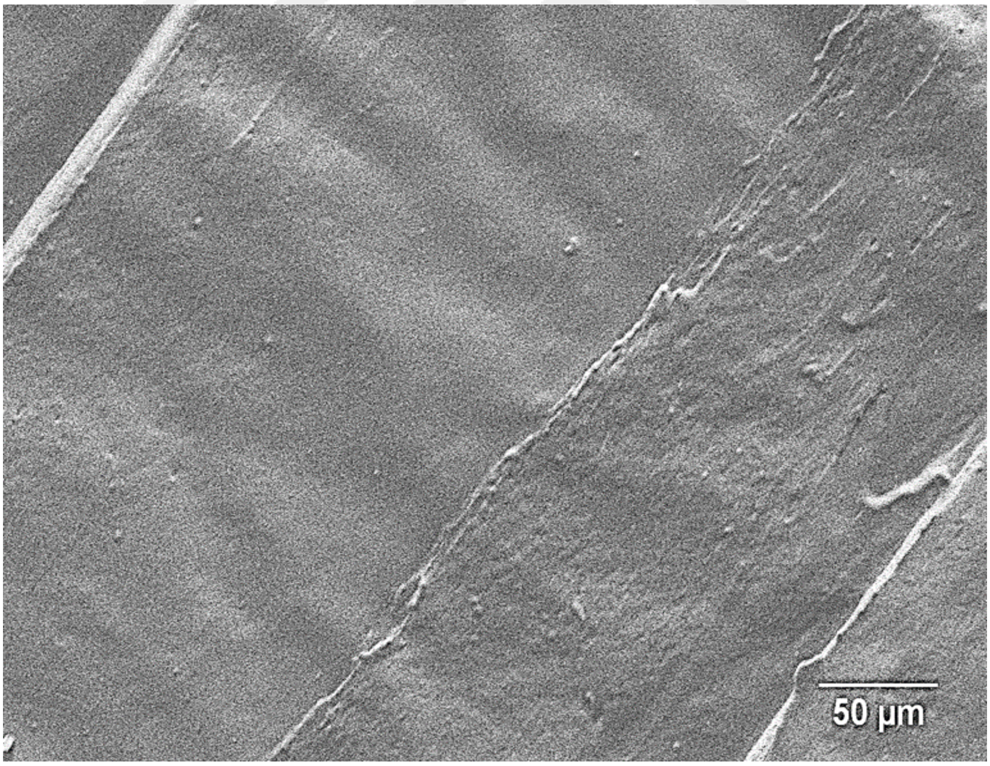

Figure 4.6. SEM image of Al coated as-printed samples

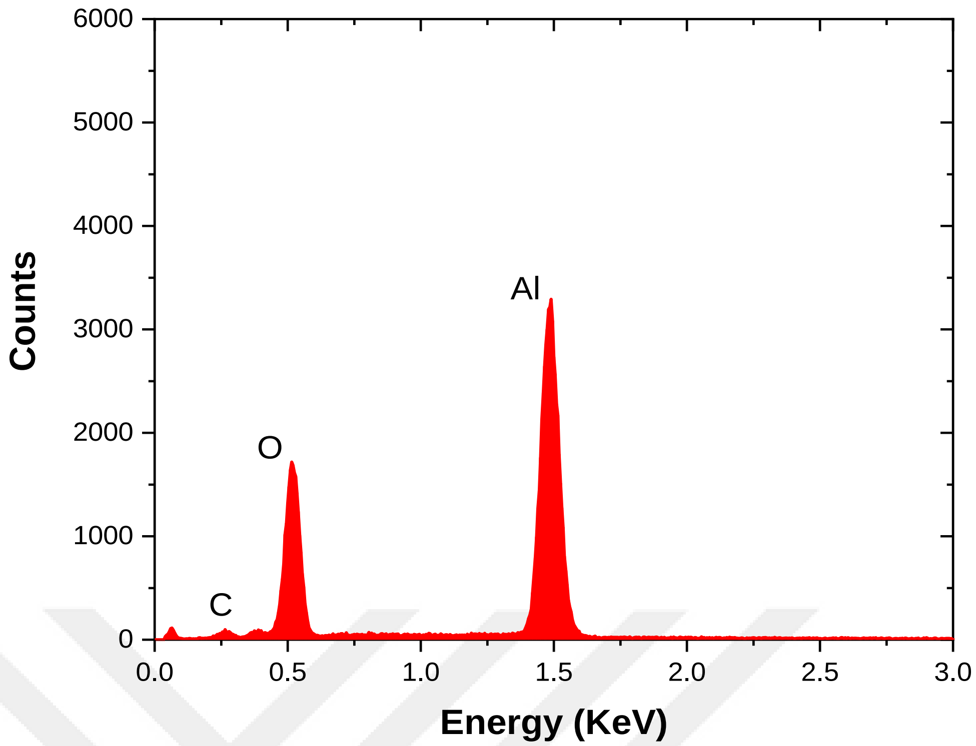

Figure 4.7. EDS analysis of Al coated as-printed samples

Table 4.1. EDS analysis of Al coated as-printed samples

Element	Weight %	Atomic %
C K	5.87	9.98
O K	36.21	46.20
AlK	57.92	43.83

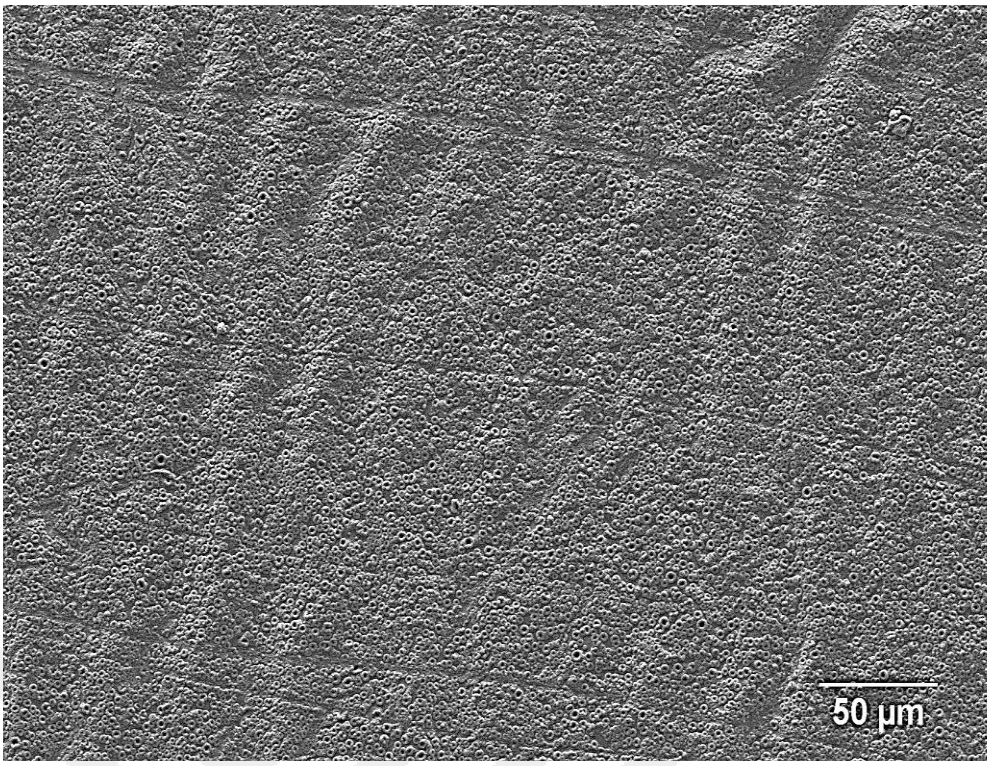

Figure 4.8. SEM image of Al coated dipping samples

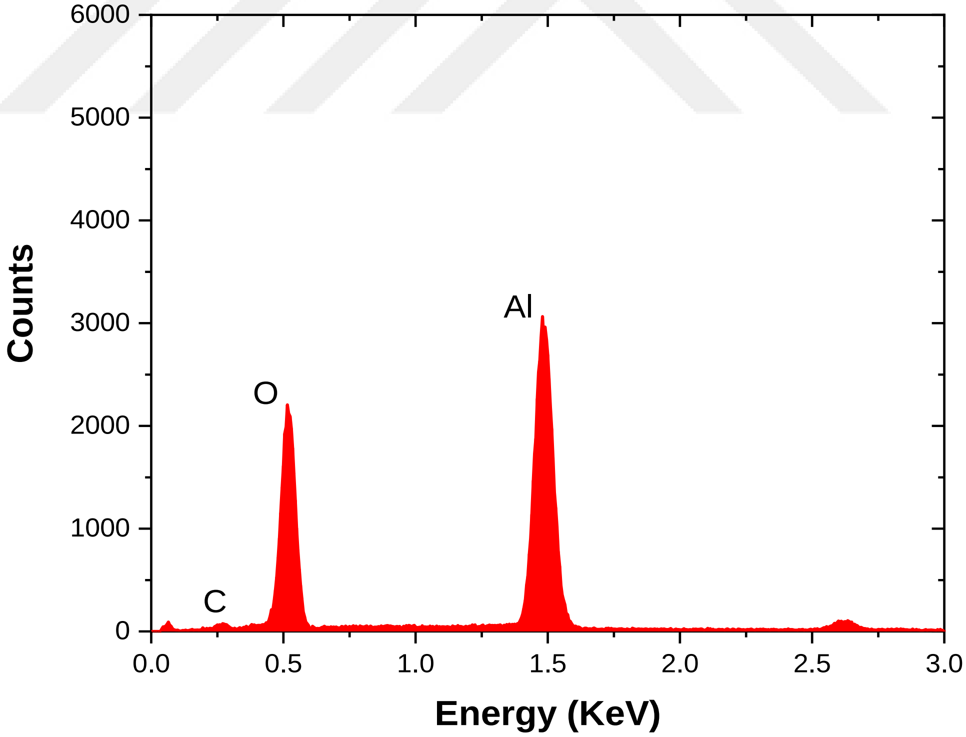

Figure 4.9. EDS analysis of Al coated dipping samples

Table 4.2. EDS analysis of Al coated dipping samples

Element	Weight %	Atomic %
C K	4.62	7.72
O K	41.83	52.46
AlK	53.55	39.83

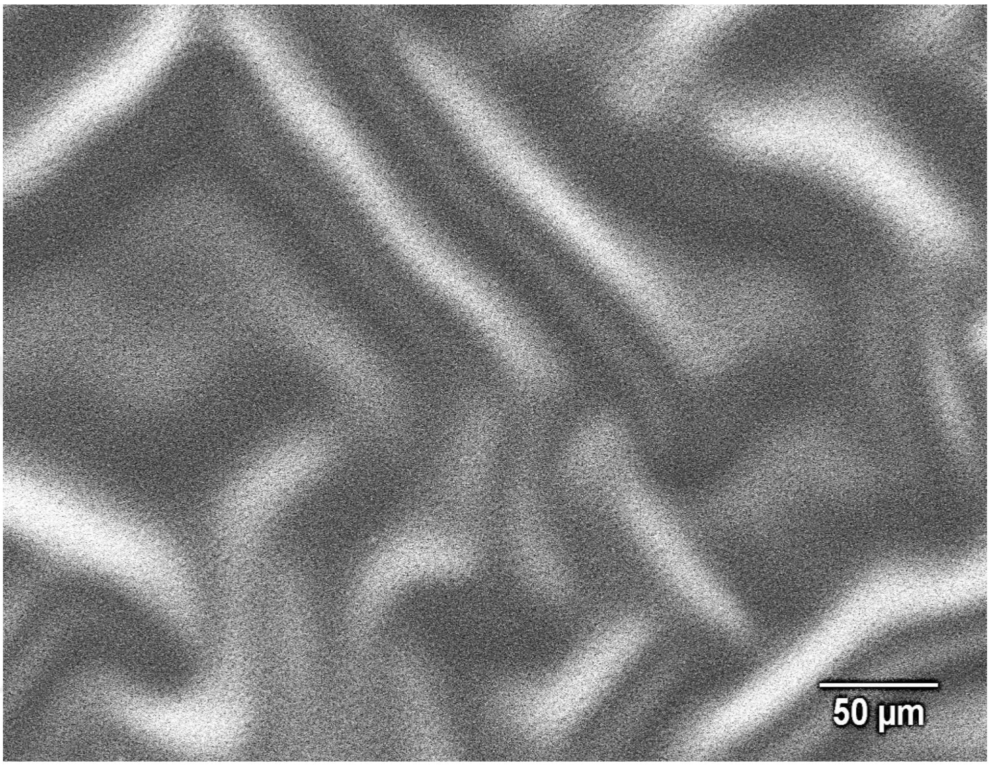

Figure 4.10. SEM image of Al coated vapour samples

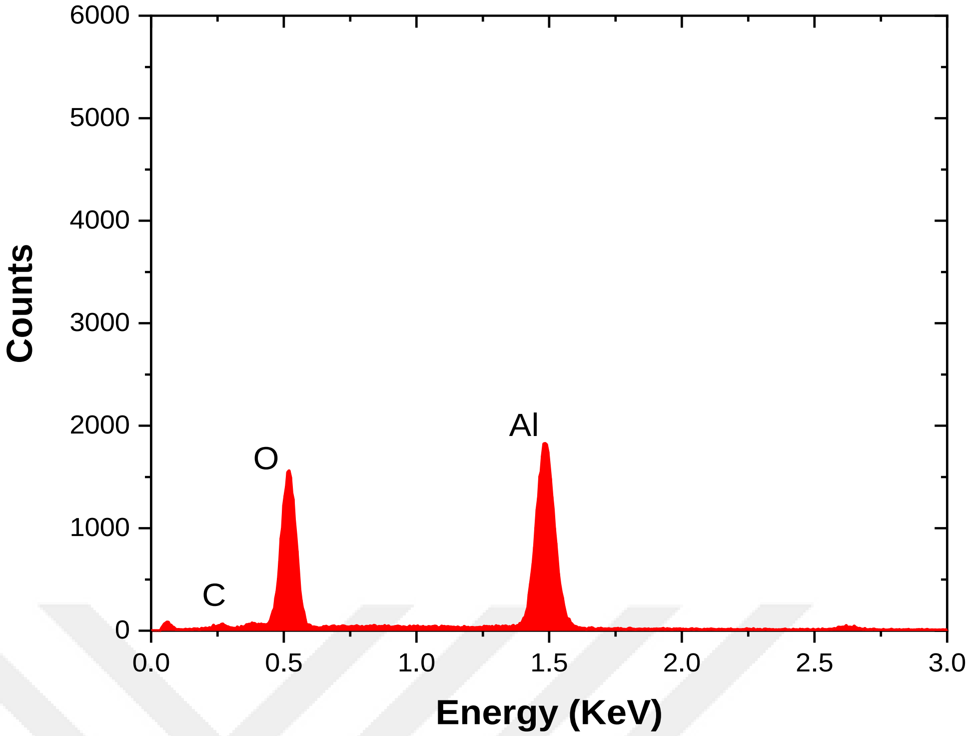

Figure 4.11. EDS analysis of Al coated vapour samples

Table 4.3. EDS analysis of Al coated vapour samples

Element	Weight %	Atomic %
C K	6.44	10.40
O K	45.17	54.80
AlK	48.39	34.80

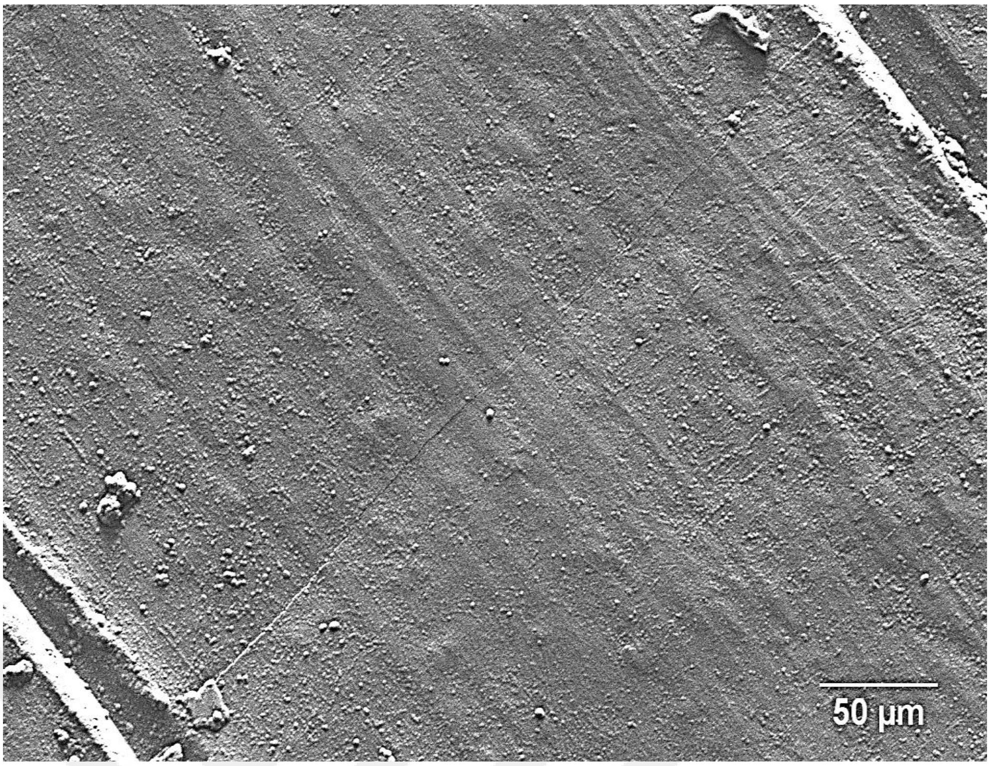

Figure 4.12. SEM image of Al coated plasma samples

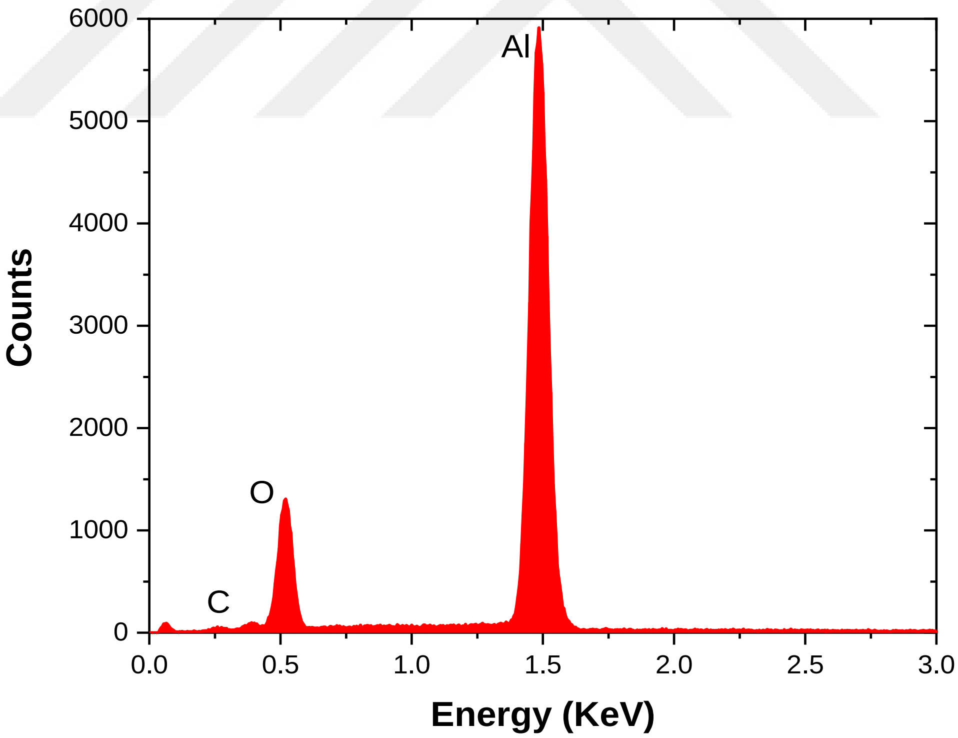

Figure 4.13. EDS analysis of Al coated plasma samples

Table 4.4. EDS analysis of Al coated plasma samples

Element	Weight %	Atomic %
C K	2.60	4.97
O K	21.01	30.11
AlK	76.39	64.92

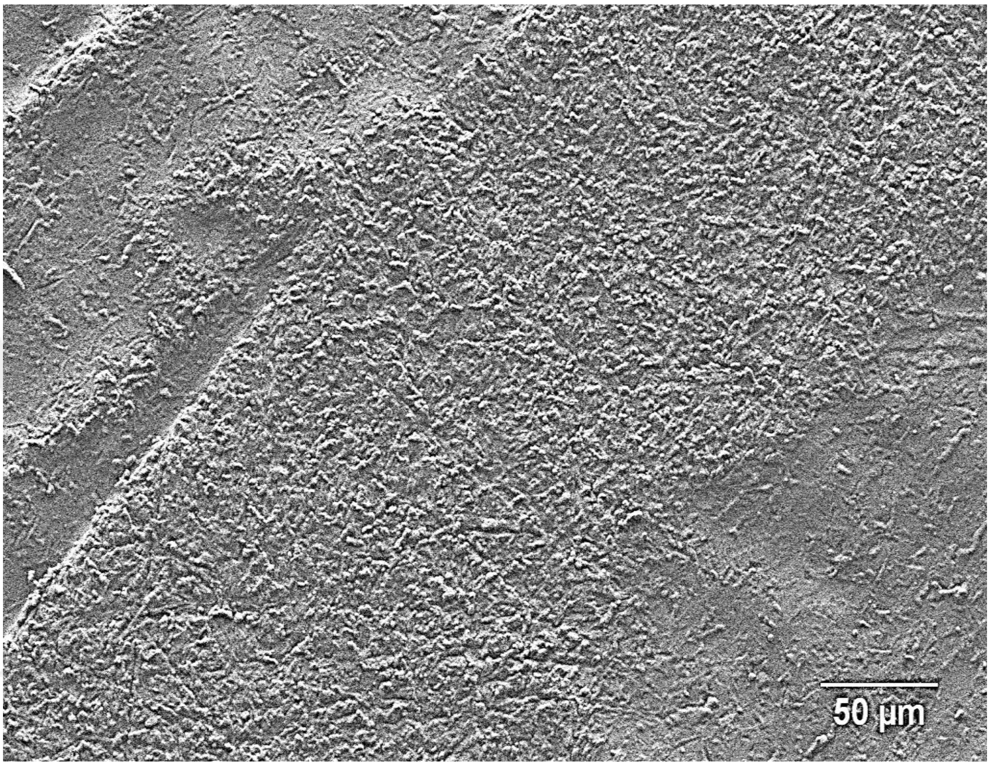

Figure 4.14. SEM image of Al coated abrasion samples

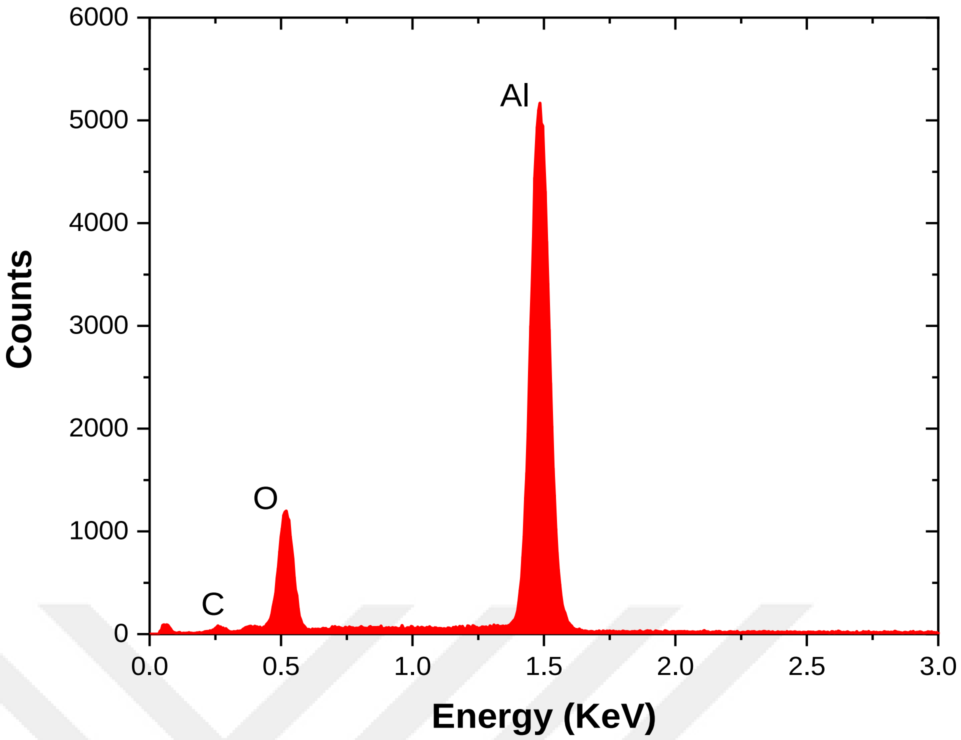

Figure 4.15. EDS analysis of Al coated abrasion samples

Table 4.5. EDS analysis of Al coated abrasion samples

Element	Weight %	Atomic %
C K	3.77	7.09
O K	21.57	30.44
AlK	74.66	62.44

The scanning electron microscopy (SEM) images and Energy Dispersive Spectroscopy (EDS) analysis results of the additively manufactured polymer specimens after copper coating are provided in Figure 4.16-4.25 and Table 4.6-4.10. We observed that the surface of dichloromethane vapour-treated specimens is mostly smooth with occasional delaminations. Similarly, the delaminations are also present in other specimens intermittently. The polymer structures with dichloromethane dipping surface treatment exhibit a micro-porous surface morphology. Similar surface morphologies have been obtained in previous studies on copper coatings (Woskowicz et al., 2020). These delaminations are believed to originate from the cohesive forces between the polymer substrate material and the coating (Lee et al., 2011; Rats et al., 1999). The voids formed during the dichloromethane surface treatment result from the evaporation of residual dichloromethane remaining on the surface after the dipping process (Zerankeshi et al., 2022). Additionally, dichloromethane, as a non-polar solvent, is highly reactive with PLA, causing excessive reaction and crater formation when immersed, potentially resulting in voids formed as a result of excessive etching from the solvent's reaction with the 3D printed surface (Jayakumar et al., 2023). In the mechanical abrasion process, wire-like (strands) pieces were removed from the outer surfaces of 3D printed parts. According to SEM images, the rough surface reveals the strands removed with sanding, showing the outer layers. All sanded surfaces clearly exhibit scratches and protruding particles. These are deformed particles that have not been completely removed (Kariž et al., 2021).

The copper layers were investigated by energy dispersive X-ray (EDX) analysis for further characterization of elemental composition. As shown in Figures 17, 19, 21, 23, and 25, a characteristic L peak belonging to copper appeared at 0.9 keV in the EDX spectrum (Zhang et al., 2016; Zhang et al., 2019). The results demonstrated the pronounced presence of copper within the coating. Therefore, it can be concluded that polymer substrates produced by additive manufacturing were successfully copper-coated via DC sputtering. No foreign substances were observed within the copper coating within the resolution limit of EDX. This indicates that the coating technique used signifies high-purity copper coating. Additionally, substrate elements were observed due to the thickness of the copper coating (Guo et al., 2009). These substrate elements, namely, carbon and oxygen signals detected in the EDX analysis, confirm the presence of other elements such as carbon and oxygen alongside copper on the polymer surface. Thus, it indicates that macromolecules of polymer are still present in the copper areas (Rytlewski et al., 2017; Liao and Kao, 2012). The EDX spectrum of Cu shows a small shoulder alongside the major peak energy of ~1 keV; this is attributed to a small amount of oxygen because of copper's tendency to rapidly oxidize in the air (Bhuiyan et al., 2019).

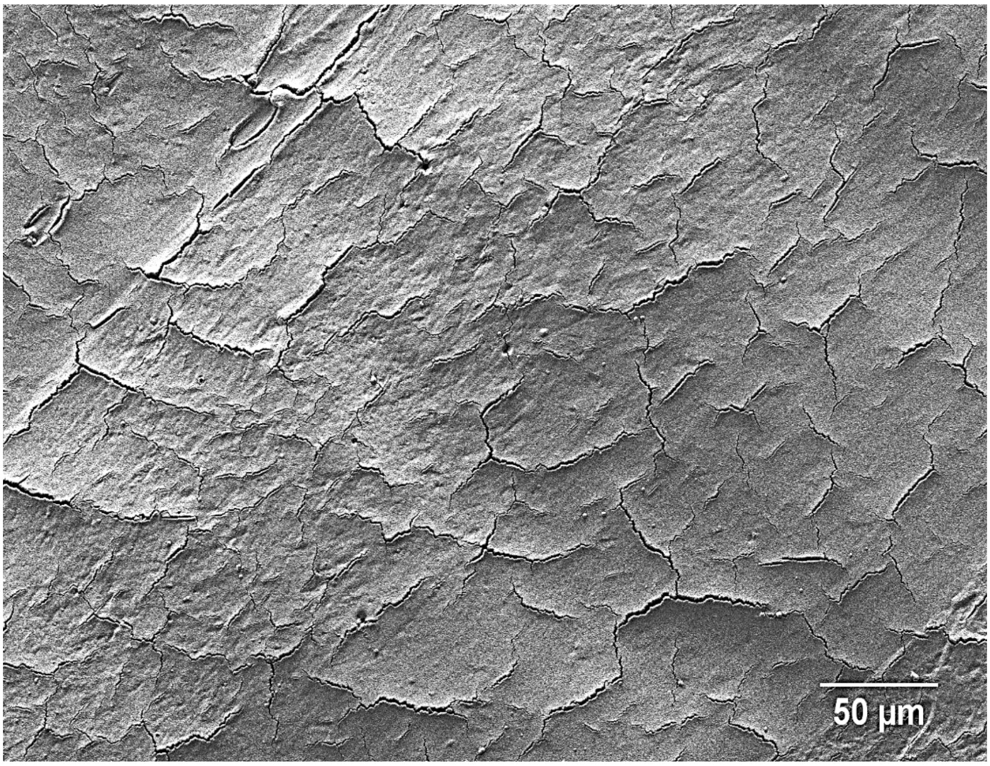

Figure 4.16. SEM image of Cu coated as-printed samples

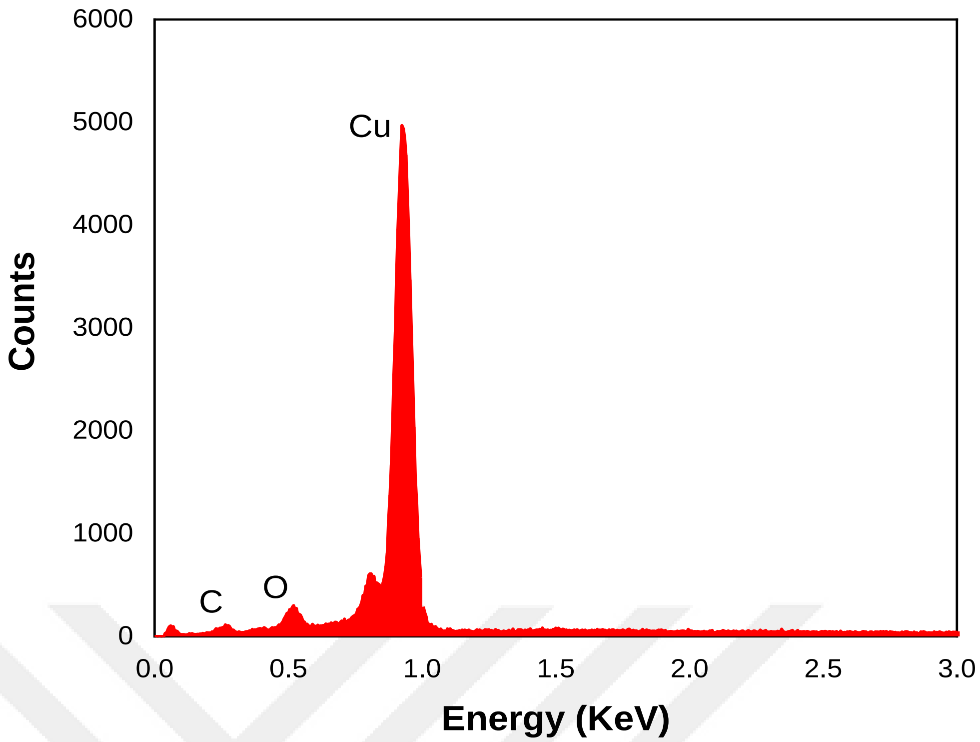

Figure 4.17. EDS analysis of Cu coated as-printed samples

Table 4.6. EDS analysis of Cu coated as-printed samples

Element	Weight %	Atomic %
C K	3.36	14.11
O K	3.89	12.27
CuL	92.74	73.61

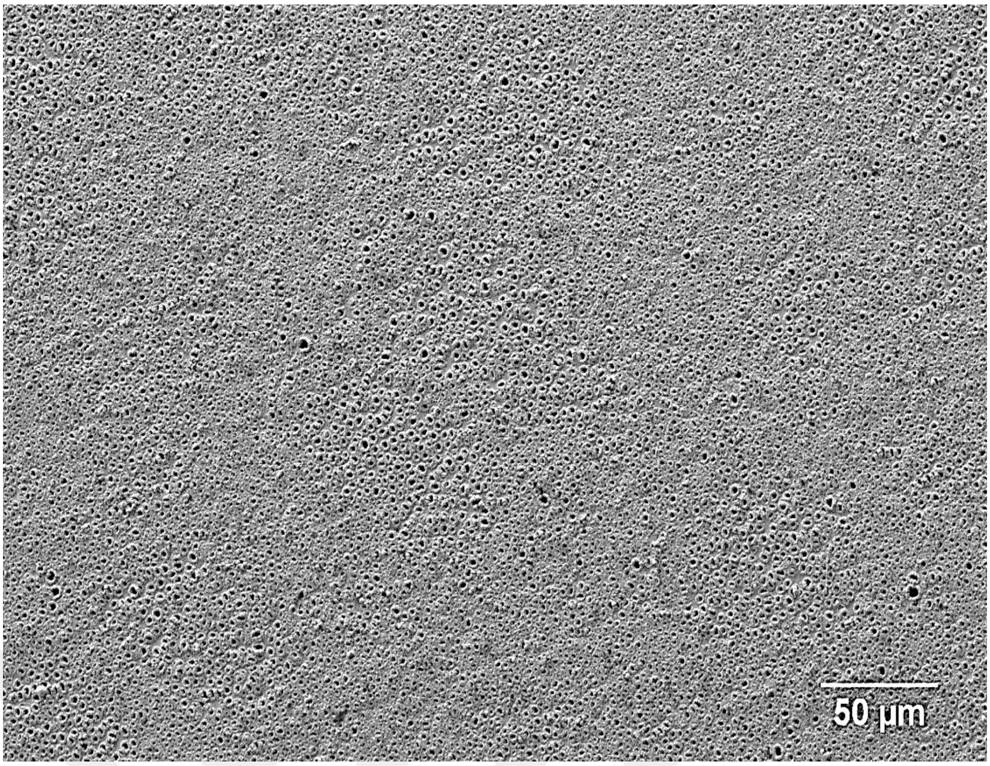

Figure 4.18. SEM image of Cu coated dipping samples

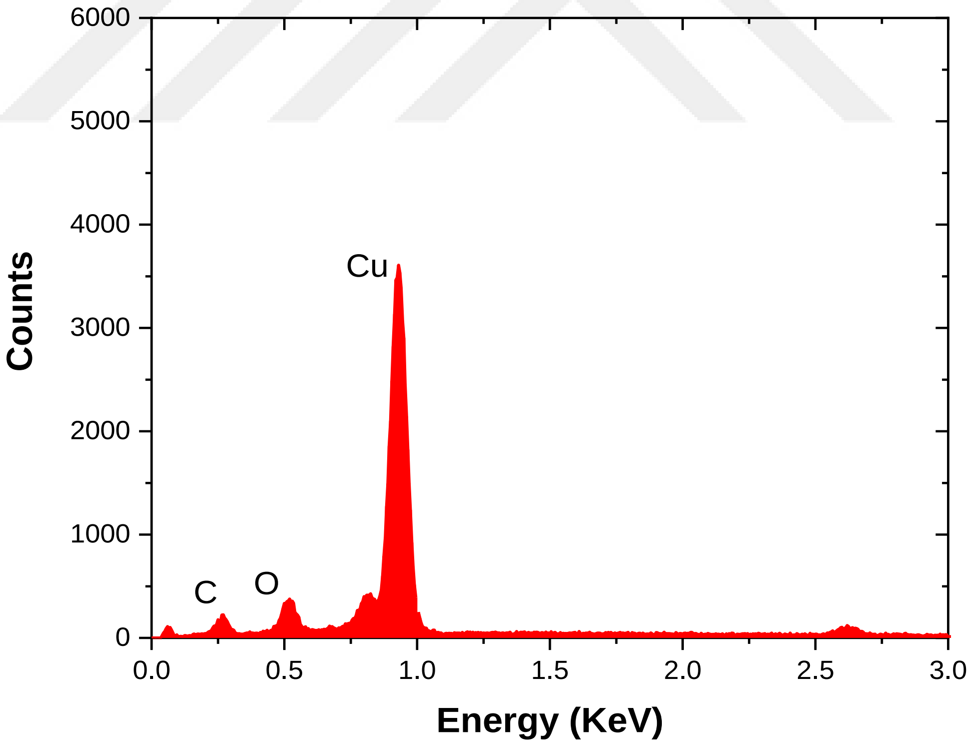

Figure 4.19. EDS analysis of Cu coated dipping samples

Table 4.7. EDS analysis of Cu coated dipping samples

Element	Weight %	Atomic %
C K	8.21	28.06
O K	6.60	16.94
CuL	84.39	54.50

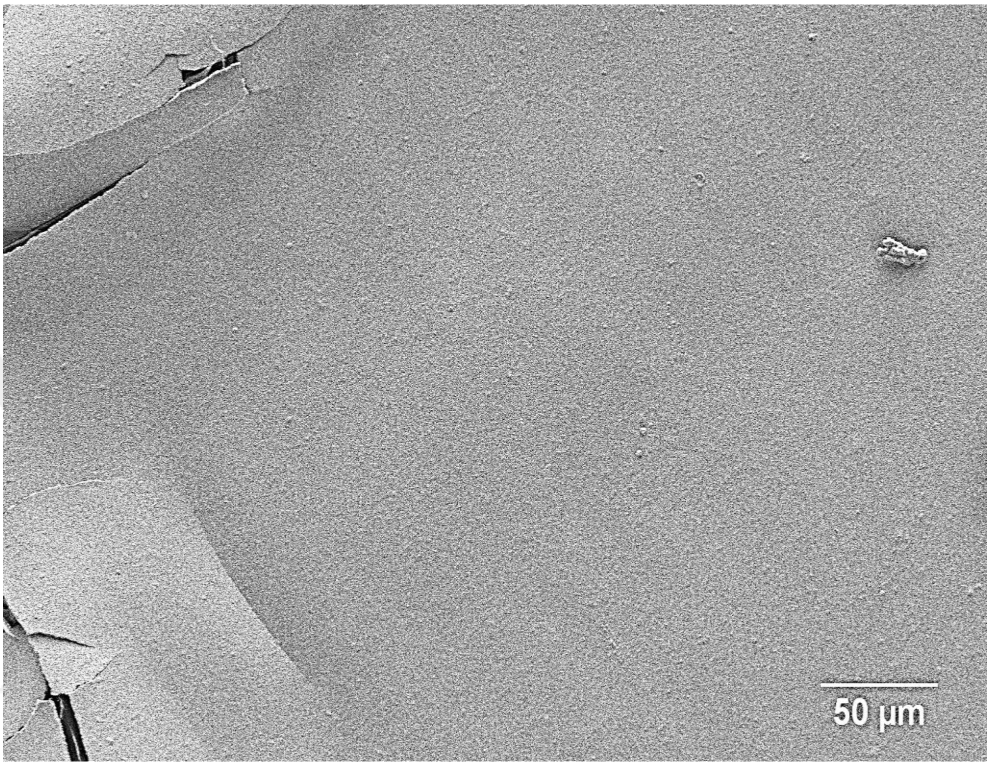

Figure 4.20. SEM image of Cu coated vapour samples

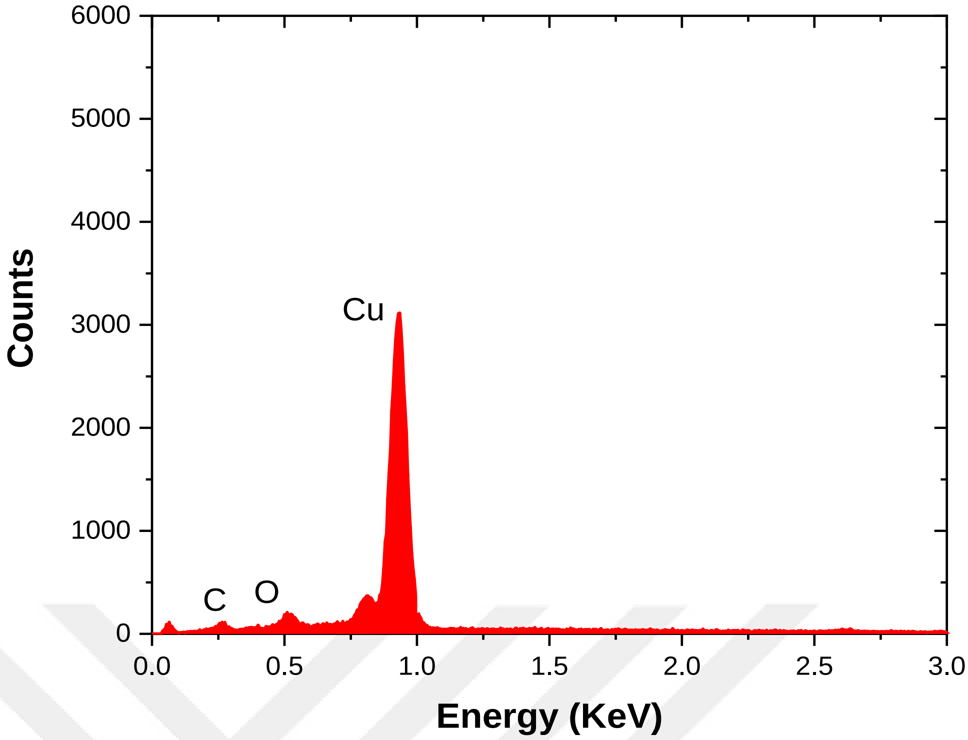

Figure 4.21. EDS analysis of Cu coated vapour samples

Table 4.8. EDS analysis of Cu coated vapour samples

Element	Weight %	Atomic %
C K	5.77	22.01
O K	4.71	13.49
CuL	89.51	64.50

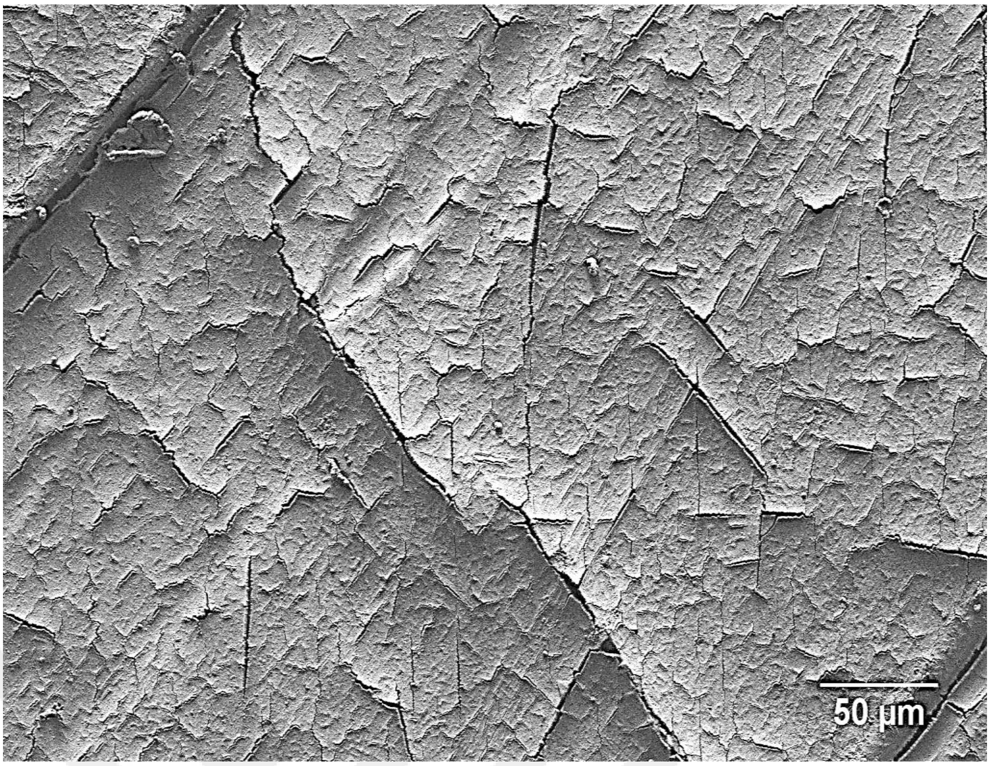

Figure 4.22. SEM image of Cu coated plasma samples

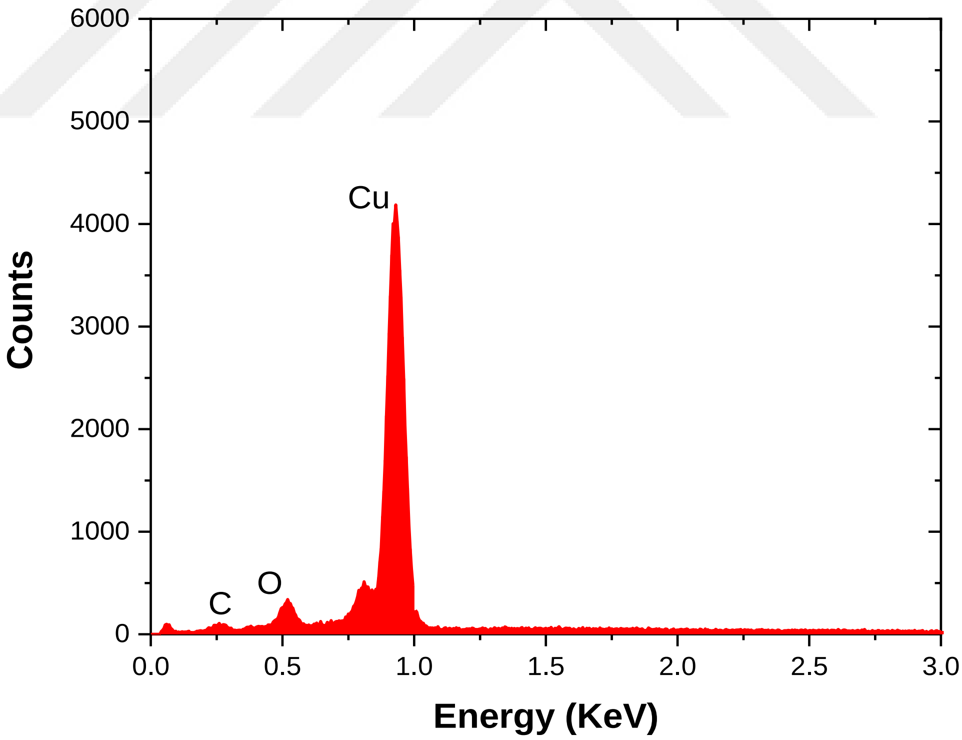

Figure 4.23. EDS analysis of Cu coated plasma samples

Table 4.9. EDS analysis of Cu coated plasma samples

Element	Weight %	Atomic %
C K	4.27	16.87
O K	5.25	15.56
CuL	90.48	67.57

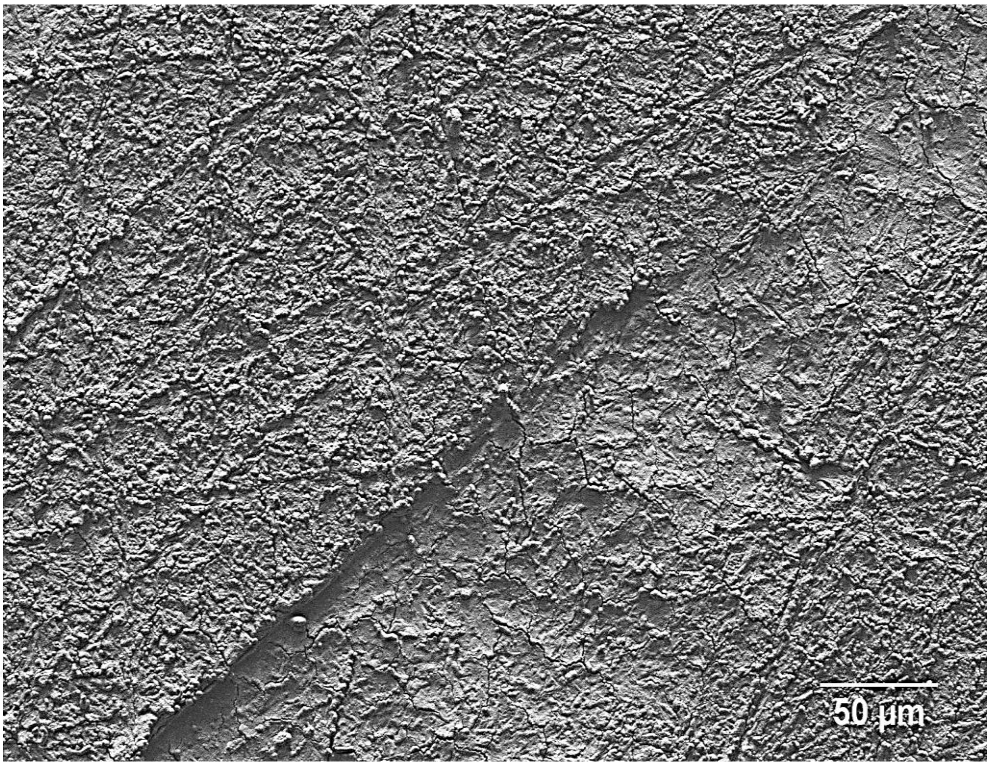

Figure 4.24. SEM image of Cu coated abrasion samples

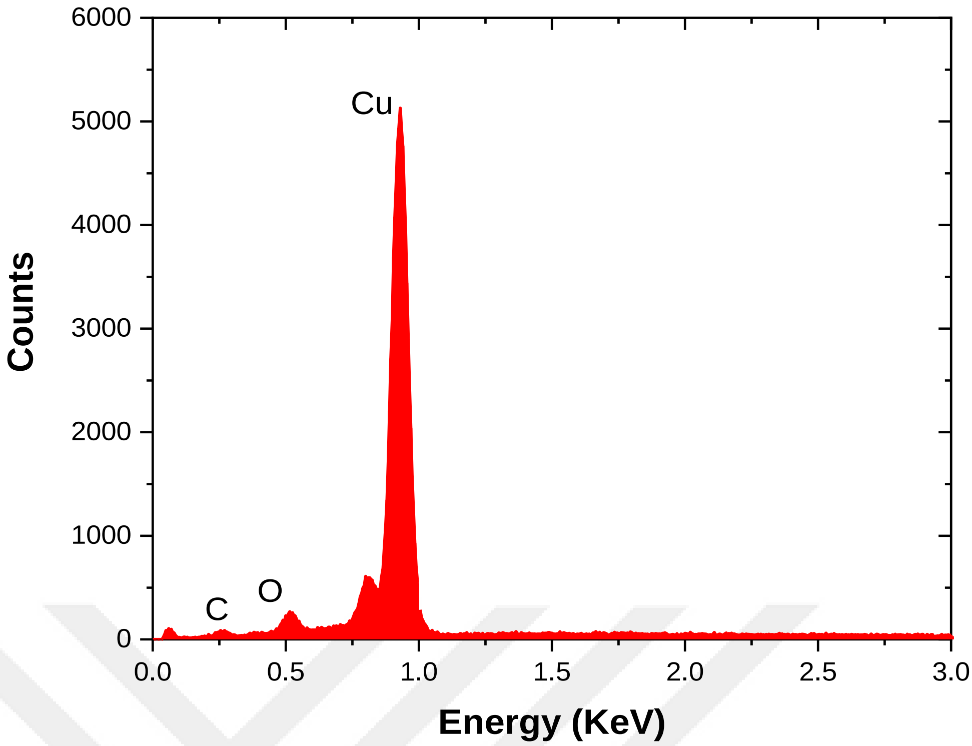

Figure 4.25. EDS analysis of Cu coated abrasion samples

Table 4.10. EDS analysis of Cu coated abrasion samples

Element	Weight %	Atomic %
C K	2.59	11.30
O K	3.44	11.25
CuL	93.97	77.45

4.2. Atomic Force Microscopy (AFM)

The Atomic Force Microscope (AFM) images and surface roughness values of 3D-printed polymer structures before and after metallization are presented in Figures 4.26-4.37. To further characterize surface morphology changes, AFM was performed. When examining the images of the sample before metallization, the needle-like structure of the cold oxygen plasma sample is noteworthy. Similar needle-like structures have been observed in previous studies as well (Wang et al., 2016; Abdulkareem et al., 2021). Surface treatments lead to nanoscale surface roughness on 3D-printed polymer structures due to polymer degradation and associated polymer erosion (Jaidev and Chatterjee, 2019). The most favourable surface roughness was achieved in polymer structures that underwent a dipping surface treatment.

When examining the AFM images after aluminium coating provided in Figures 4.32-4.36, wrinkles were observed in all samples compared to the pre-metallization state. The polymer structures likely exhibit a certain residual stress responsible for the formation of these wrinkles, which is thought to be associated with the production process. The increase in material temperature during the metallization process allows the release of internal stresses. In particular, it is believed that when temperatures exceed 80°C, the sliding or flow of polymer chains may lead to the release of stress. In comparison, the metal coating allows for another stress relief mechanism through wrinkling. Local instabilities arise during coating due to the different thermal expansion coefficients of PLA and aluminium, forcing the rearrangement of the polymer, and resulting in the release of internal stress (Juřík et al., 2017; Ren et al., 2017; Rahmatollahpur et al., 2010). Following metallization, no notable alteration in surface roughness values was recorded for the different surface treatments.

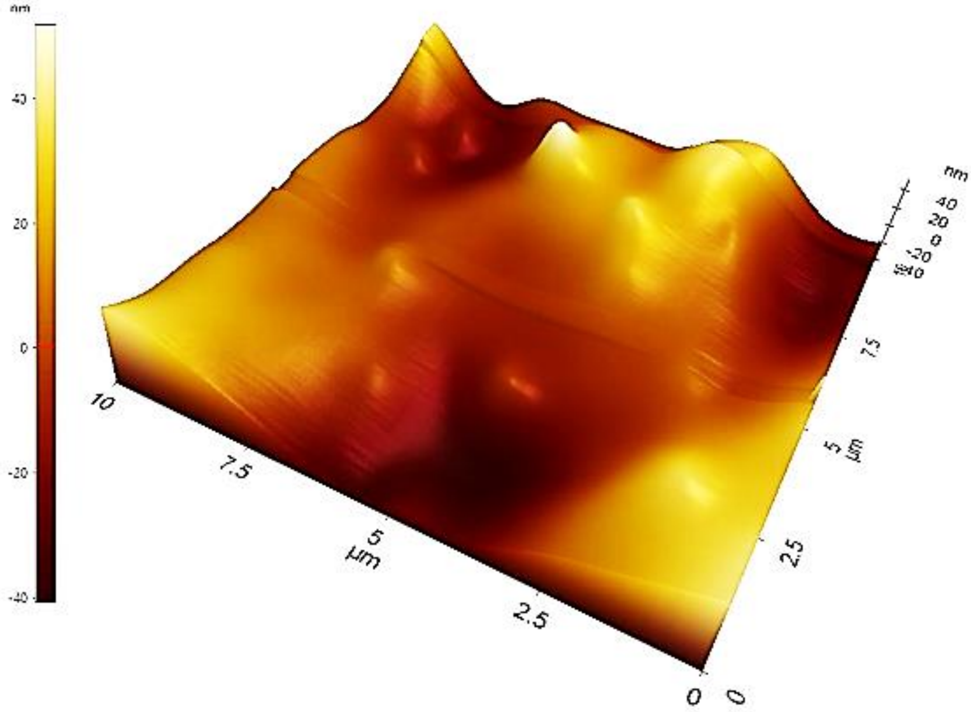

Figure 4.26. AFM image of as-printed samples

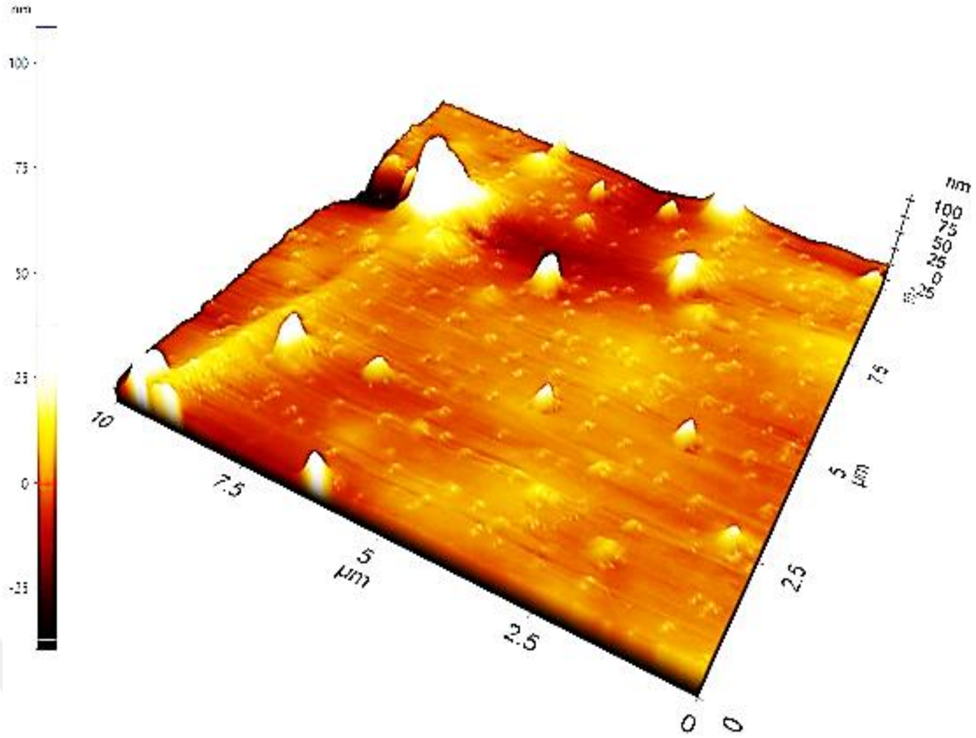

Figure 4.27. AFM image of dipping samples

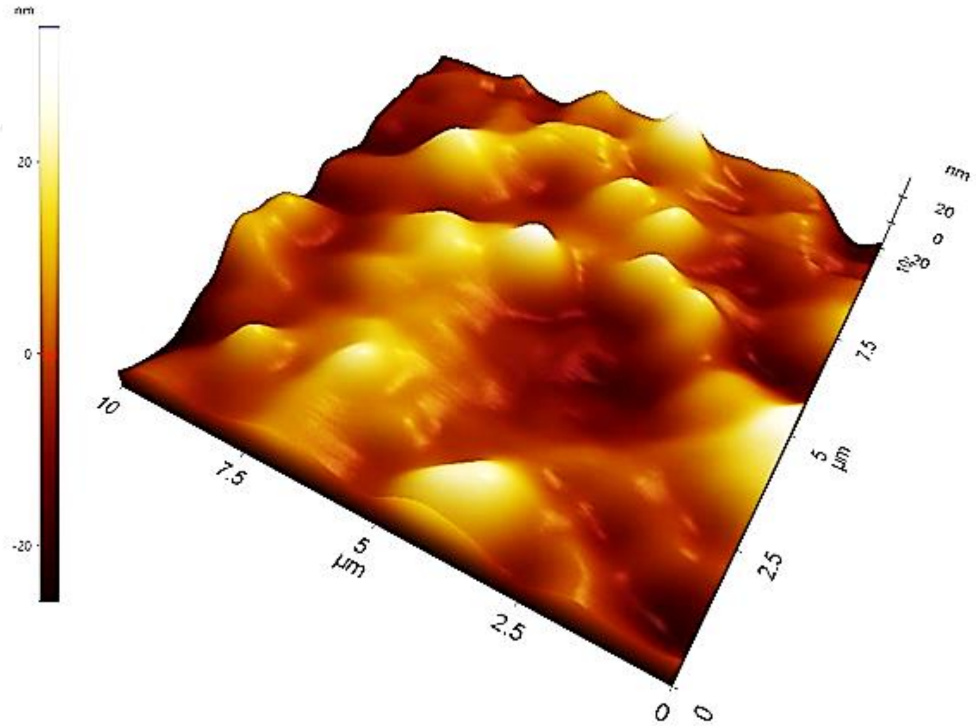

Figure 4.28. AFM image of vapour samples

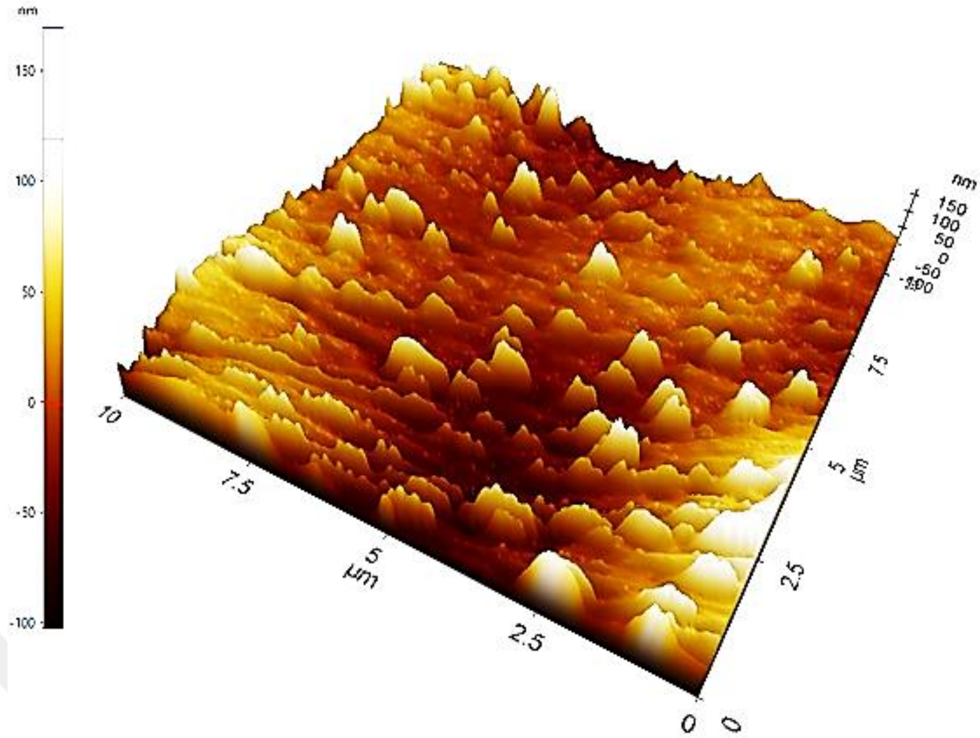

Figure 4.29. AFM images of plasma samples

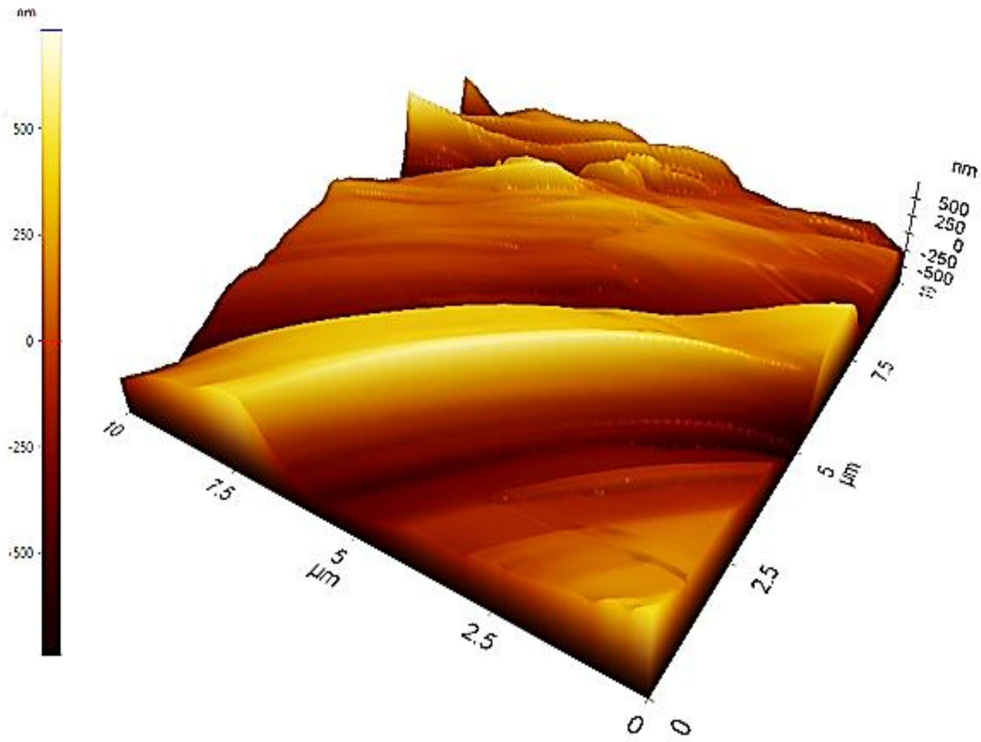

Figure 4.30. AFM images of abrasion samples

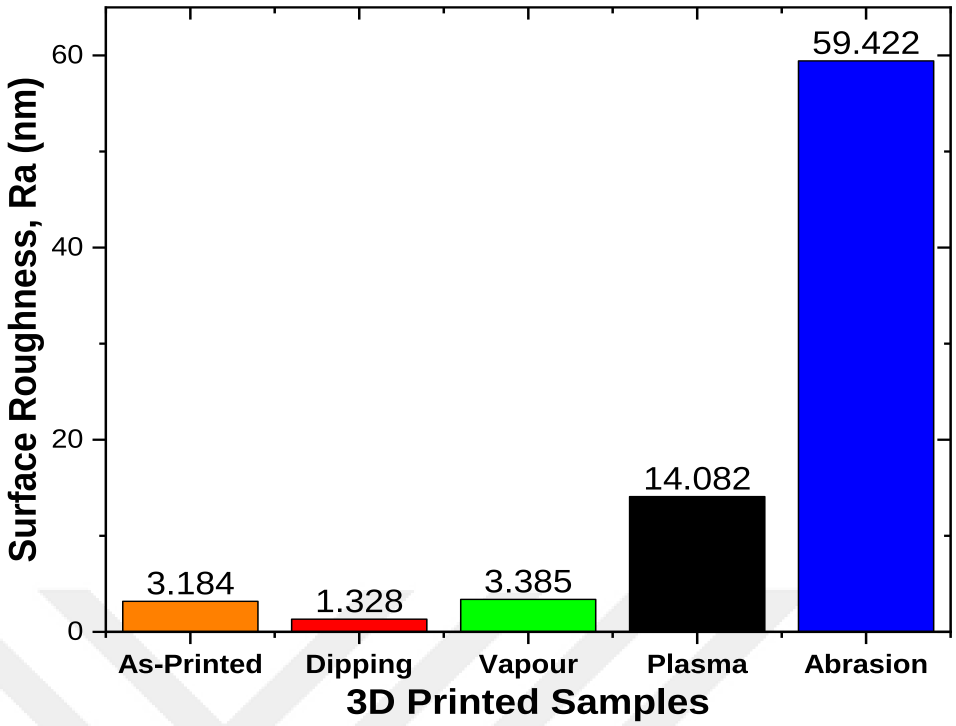

Figure 4.31. Surface roughness values of samples

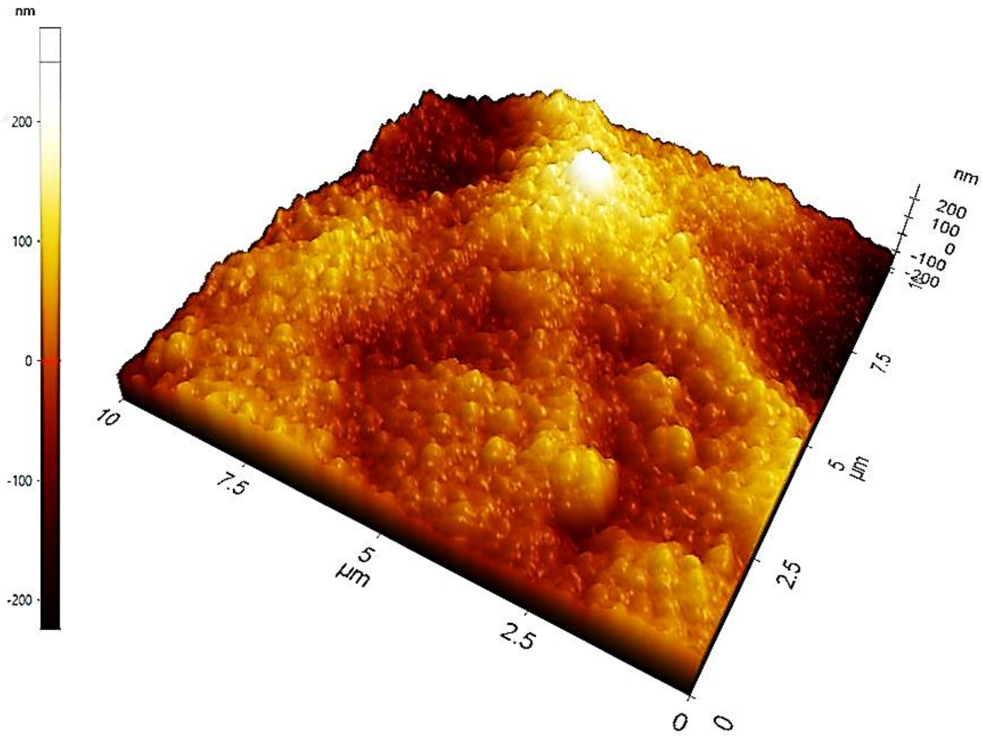

Figure 4.32. AFM image of Al coated as-printed samples

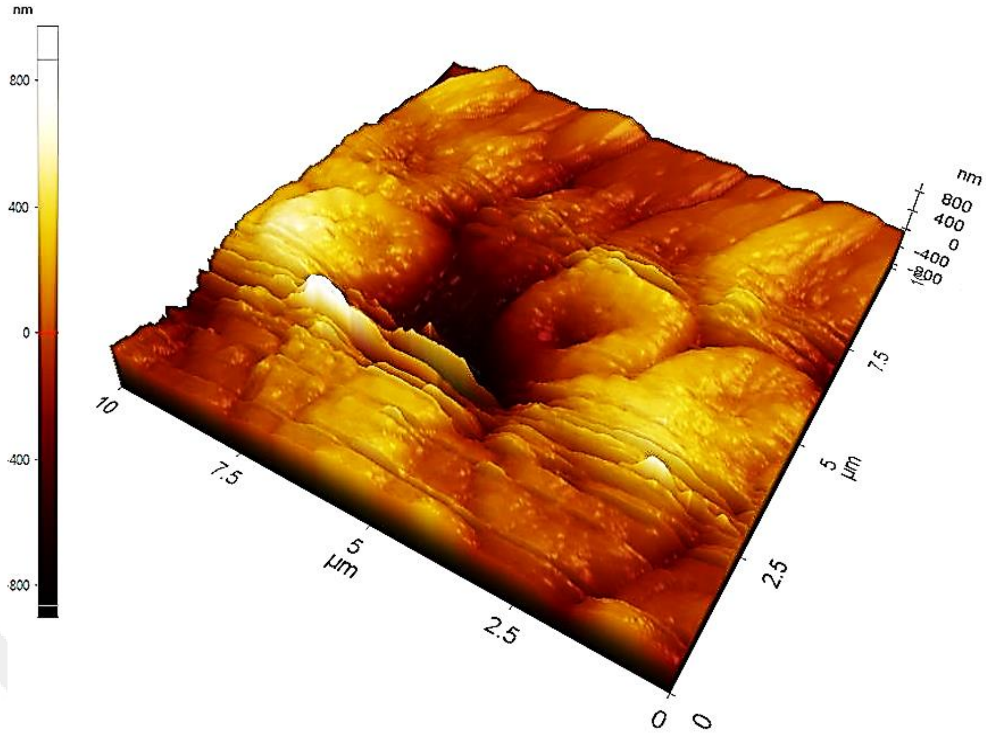

Figure 4.33. AFM image of Al coated dipping samples

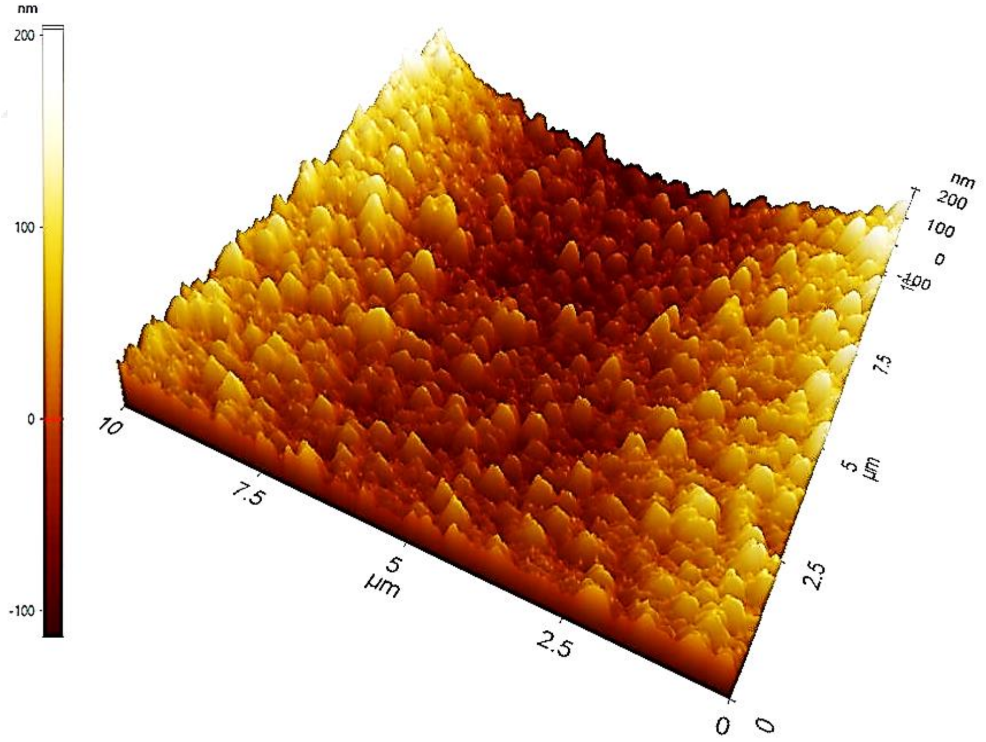

Figure 4.34. AFM image of Al coated vapour samples

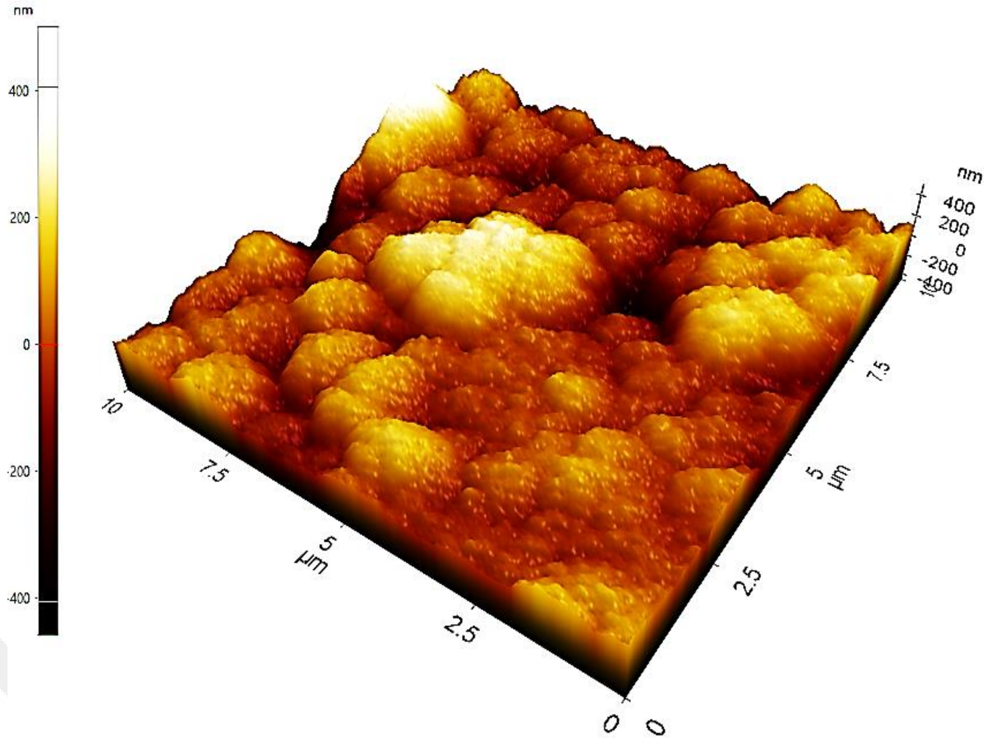

Figure 4.35. AFM image of Al coated plasma samples

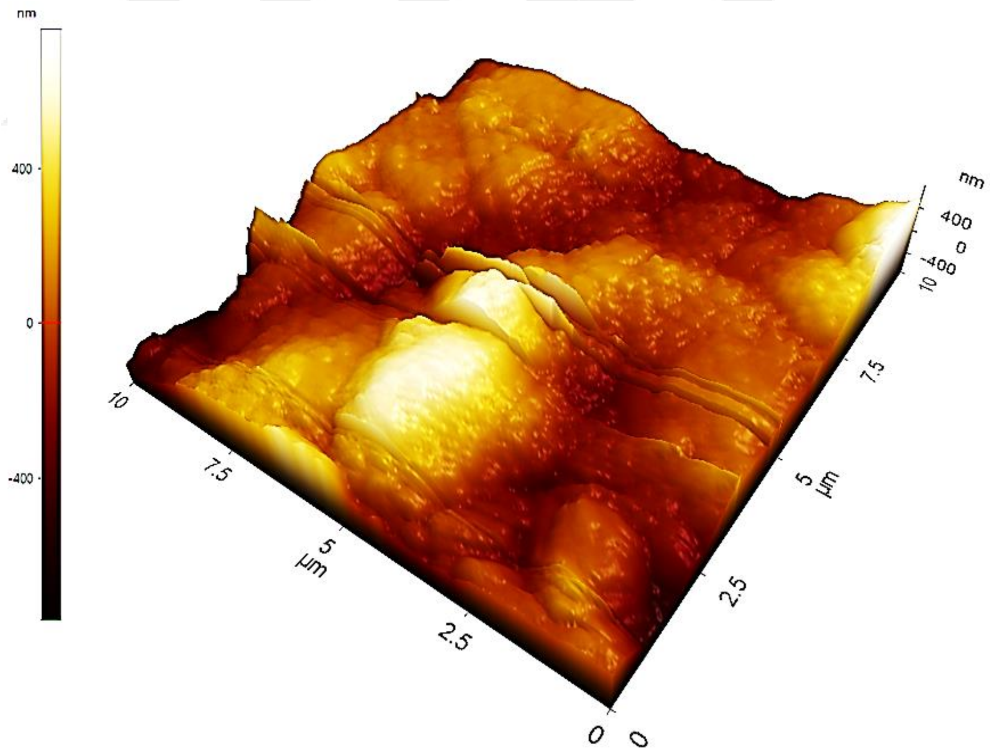

Figure 4.36. AFM image of Al coated abrasion samples

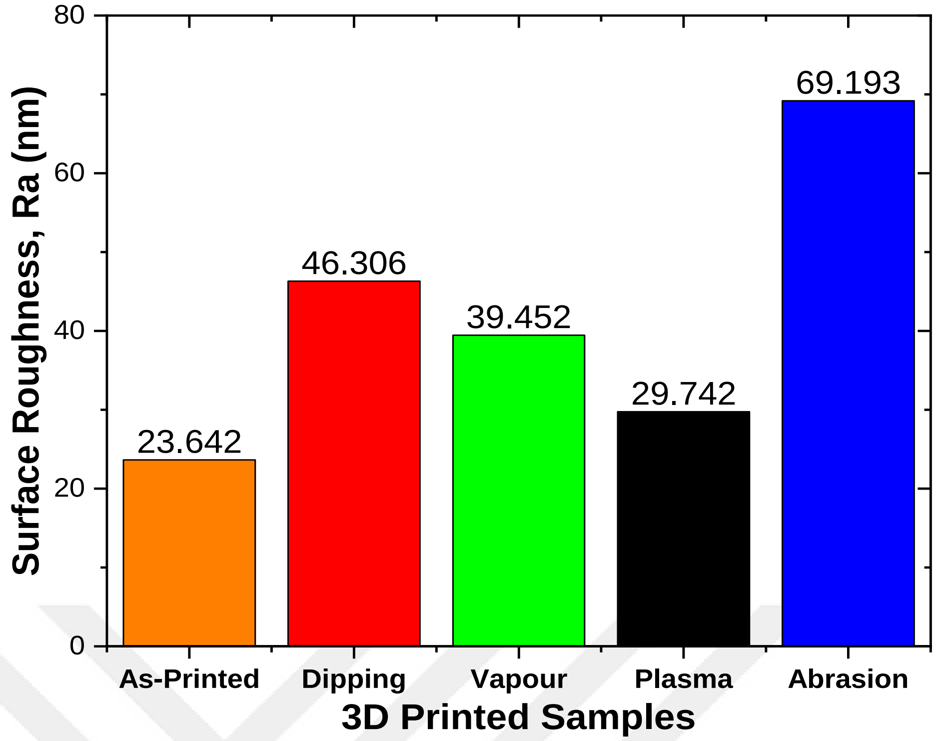

Figure 4.37. Surface roughness values of Al coated samples

The atomic force microscopy (AFM) images and surface roughness values of the copper coated polymer structures are provided in Figure 4.38-4.43. We observed relatively large and high wrinkles with AFM on the surfaces of untreated specimens, dichloromethane dipping treated specimens, and dichloromethane vapour treated specimens. These wrinkles were not visible via SEM and were not present on the surfaces of the cold plasma-treated specimen and mechanically abraded sample. It is believed that such wrinkles result from deformation caused by any force applied to a hard layer deposited on a softer underlying layer (residual stress, thermal expansion, mechanical constraint) (Schweitzer et al., 2023; Rodriguez-Hernandez, 2015; Yu et al., 2016). The coating process is carried out at a constant temperature. However, it has been assessed that the coating wrinkles during cooling due to the different thermal expansion coefficients of copper and polymer (Schweikart and Fery, 2009). The formation of depressions on the polymer surfaces increases the surface area, thus creating a more suitable surface topography for various physical and chemical interactions between the polymer structure and copper (Ge et al., 2003). There is a greater amount of PLA degradation in plastic specimens treated with cold oxygen plasma. These degradations formed as irregularly shaped accumulated large droplets depending on the power and duration of the plasma process. When the specimens are subjected to intense power, degradation of the products begins, resulting in rough structures. The increased roughness is believed to enhance the adhesion area between the metal layer deposited on the polymer surface and the polymer surface itself (Moraczewski et al., 2015; Junkar et al., 2009). It was concluded that the samples that exhibited a vapour surface treatment subsequent to metallization displayed the most favourable surface roughness values.

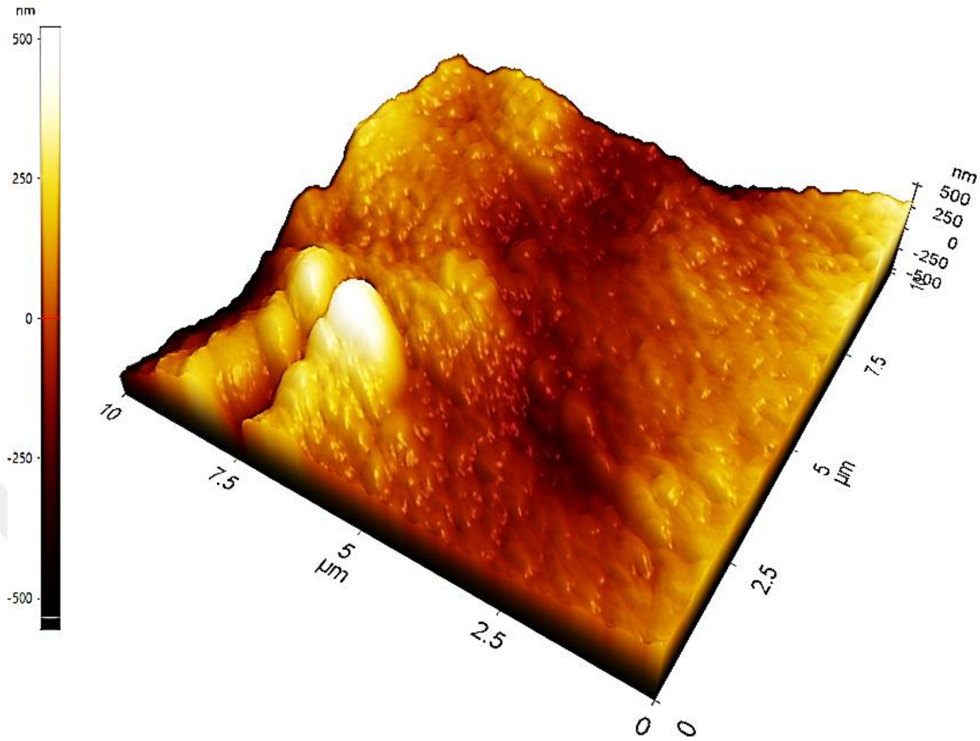

Figure 4.38. AFM image of Cu coated as-printed samples

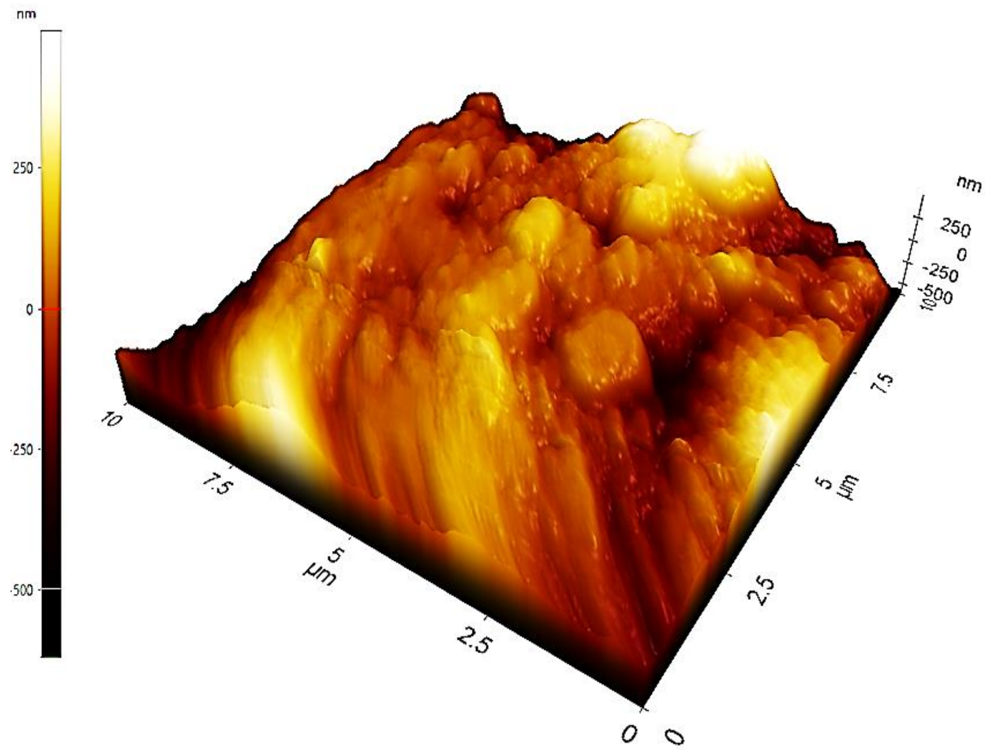

Figure 4.39. AFM image of Cu coated dipping samples

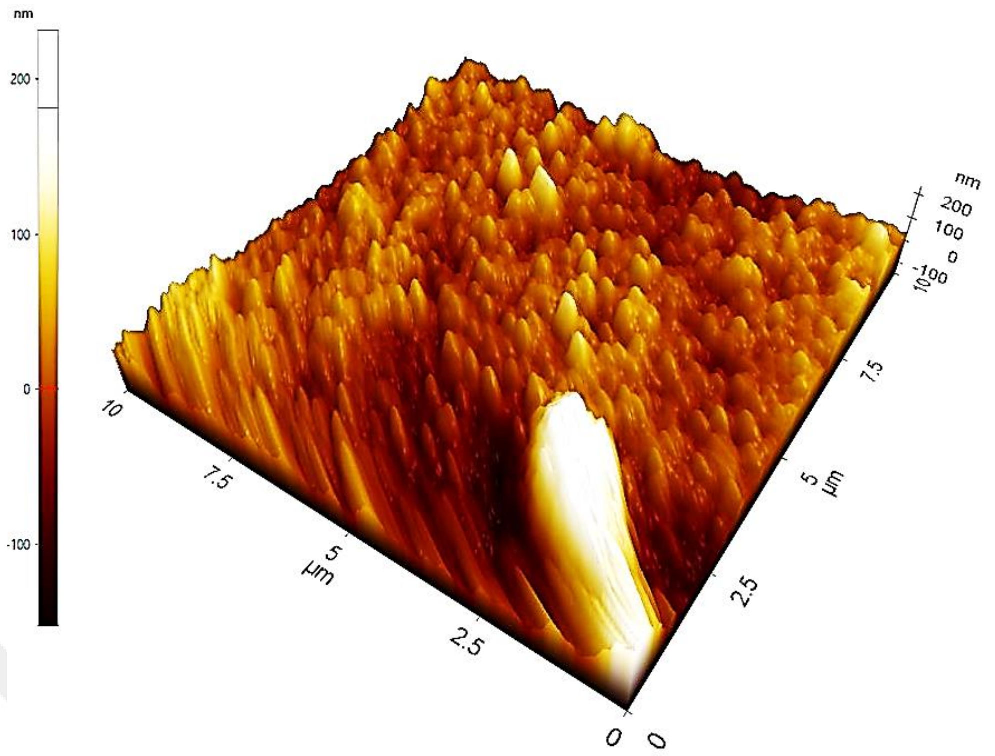

Figure 4.40. AFM image of Cu coated vapour samples

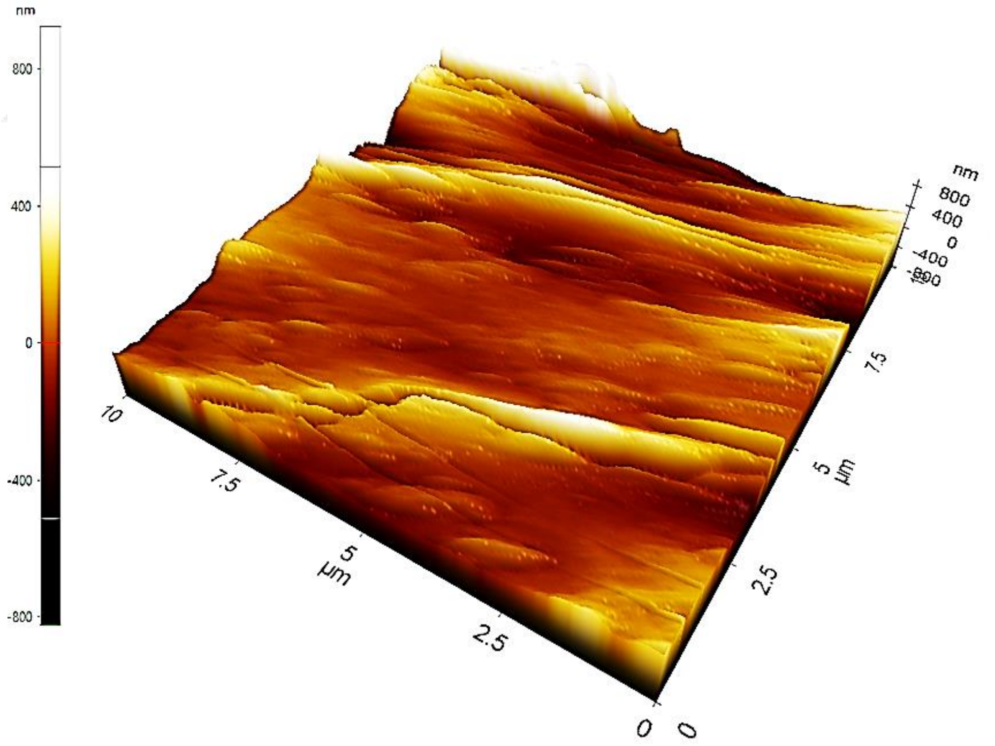

Figure 4.41. AFM image of Cu coated plasma samples

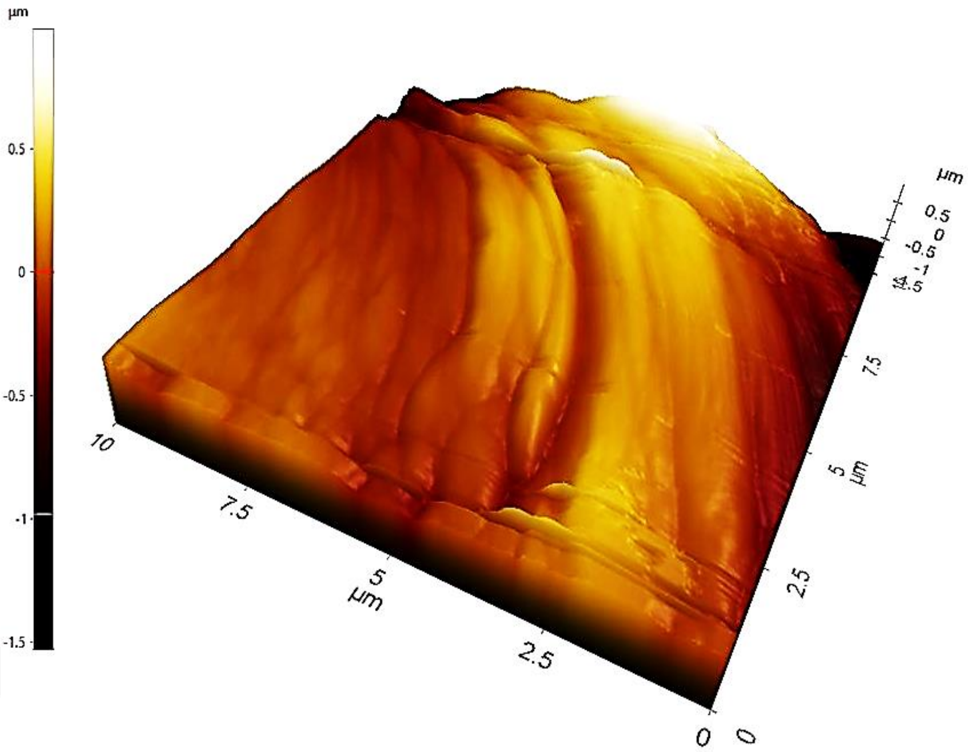

Figure 4.42. AFM image of Cu coated abrasion samples

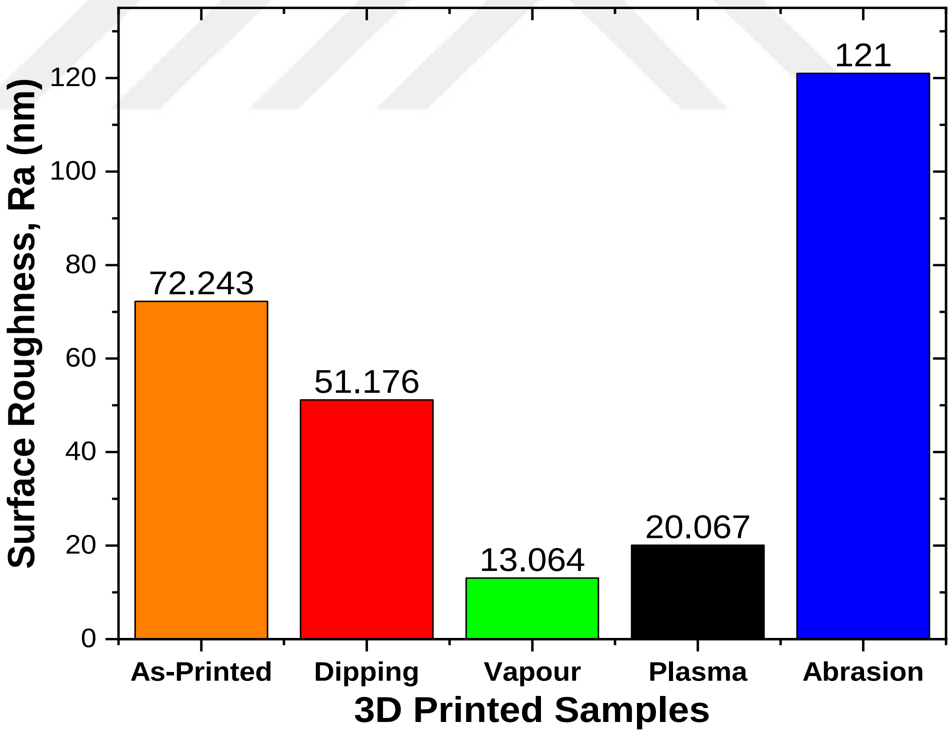

Figure 4.43. Surface roughness values of Cu coated samples

4.3. X-Ray Diffractometry (XRD)

The XRD analysis results of Al coated 3D polymer structures are shown in Figures 4.44-4.48. Diffraction peaks appeared at approximately 38.380°, 44.162°, 64.928°, 78.014°, and 82.204° with corresponding Miller indices of 111, 200, 220, 311, and 222, respectively. These values can be attributed to the International Center of Diffraction Data (ICDD) card number 98-004-3492 for Aluminium. The sharpness of the XRD analysis peaks in the coatings provides information about the crystallinity quality of the coatings. Additionally, oxide structures have been observed within the phase compositions of the coatings. This implies that oxidation has occurred in the metal coating either during or after the coating process. When compared to other surface treatments, polymer structures sanded during the sanding process exhibit higher peak intensity, suggesting higher crystallinity in the sanded samples (Guanhong et al., 2011; Farahmandjou and Nazafarin, 2015).

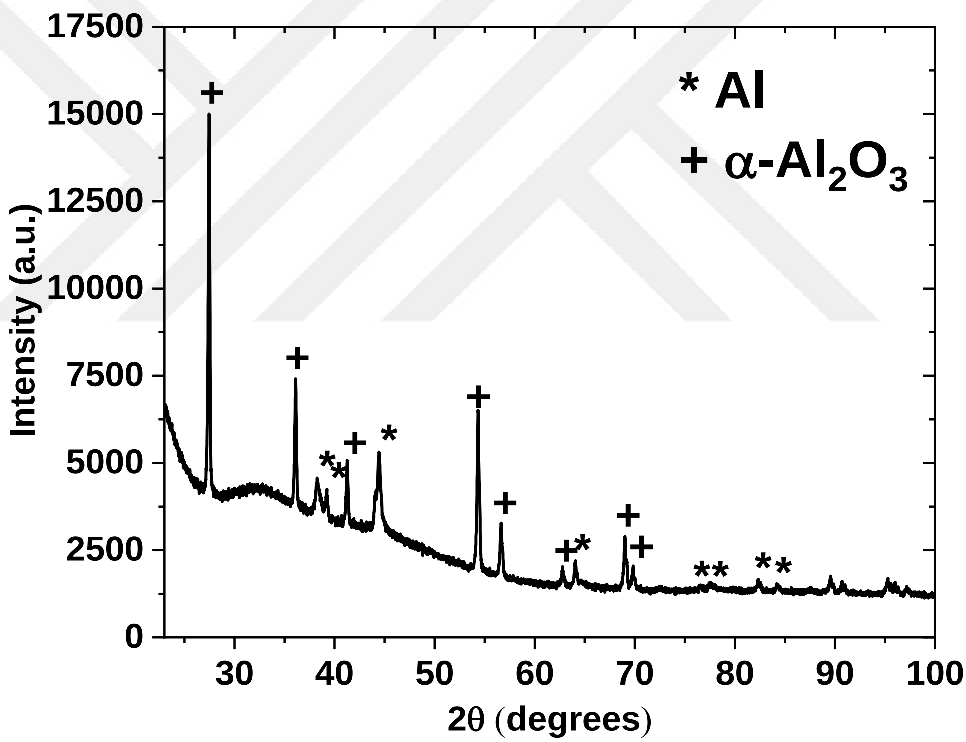

Figure 4.44. XRD analysis of Al coated as-printed samples

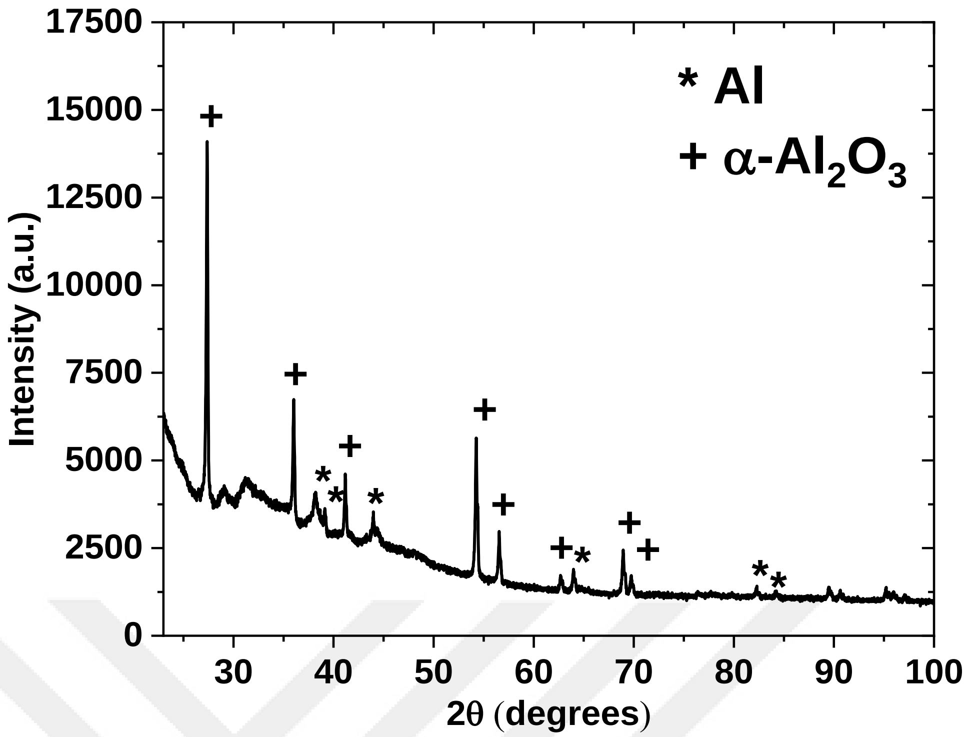

Figure 4.45. XRD analysis of Al coated dipping samples

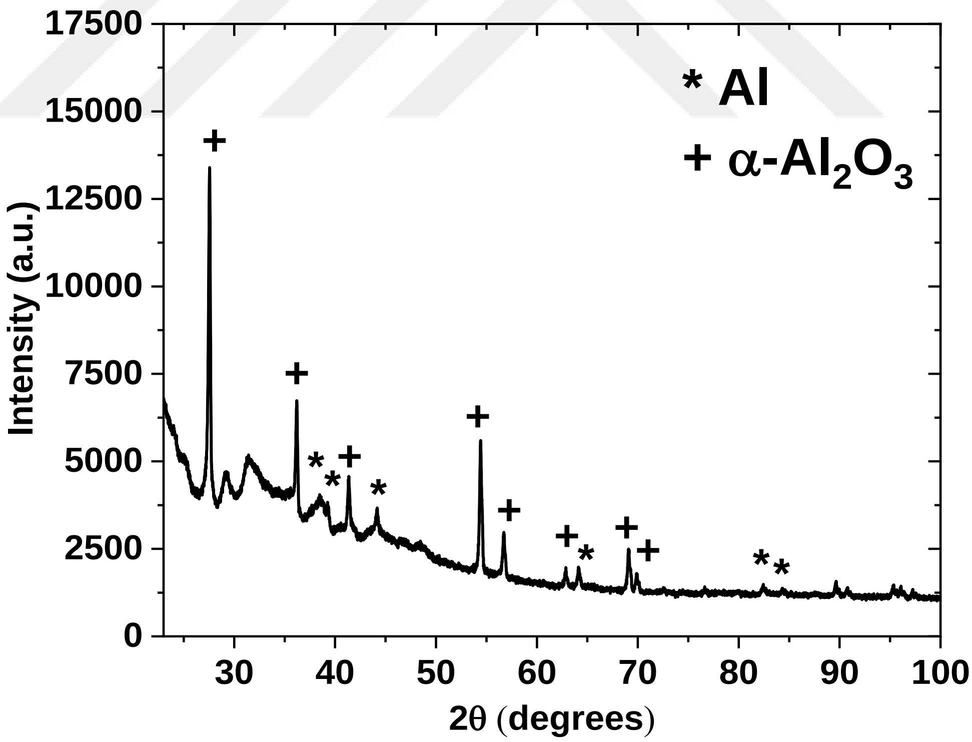

Figure 4.46. XRD analysis of Al coated vapour samples

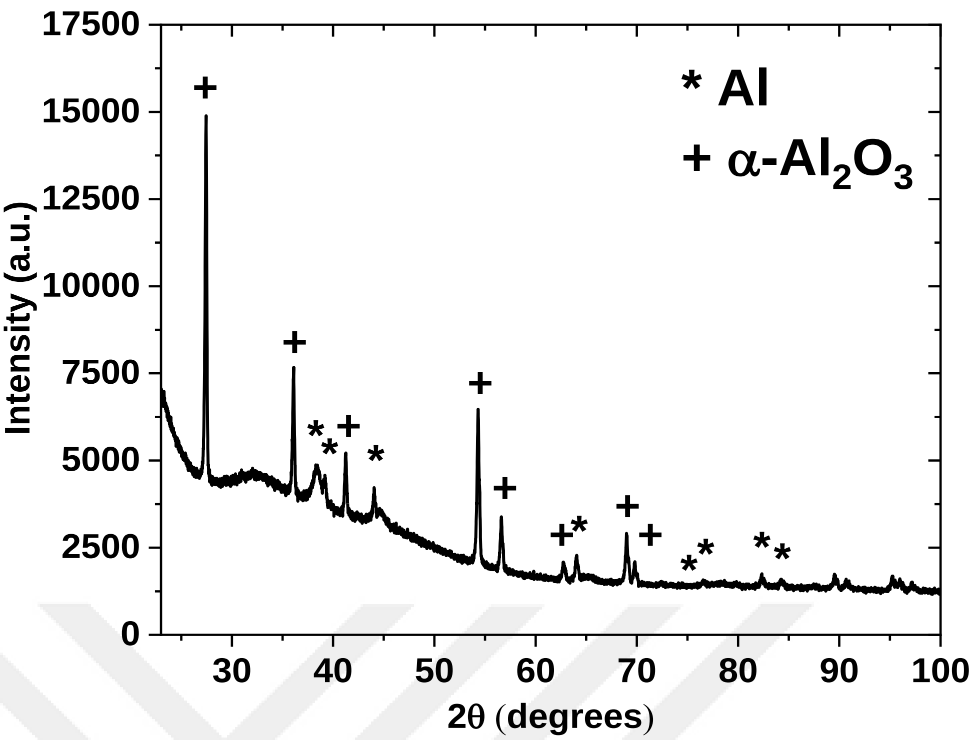

Figure 4.47. XRD analysis of Al coated plasma samples

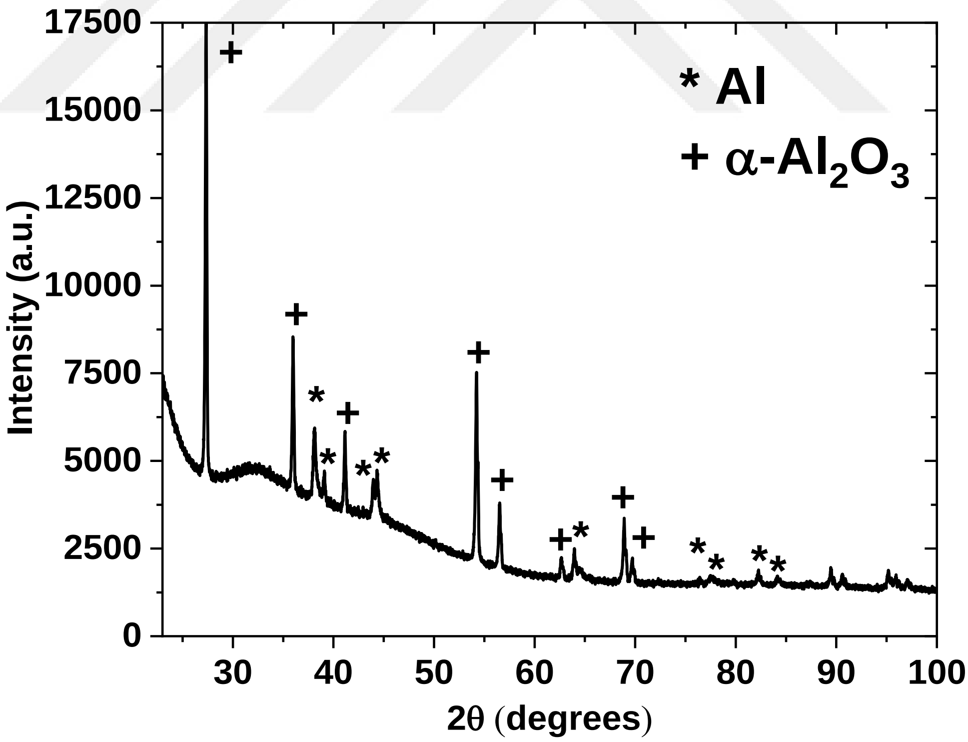

Figure 4.48. XRD analysis of Al coated abrasion samples

The X-ray diffraction (XRD) results of the treated specimen and untreated specimens after Cu coating are provided in Figure 4.49-4.53. XRD analysis provides information about the crystallinity of the coated specimens. Four dominant characteristic diffraction peaks are located at

43.14°, 50.09°, 73.93°, and 89.50°. These peaks can be attributed to the (111), (200), (220), and (311) crystal planes, respectively. All patterns confirm the presence of copper. The XRD patterns indicate that the copper coatings have a face-centered cubic crystalline structure. This suggests that the polymer specimens exhibit excellent conductivity. However, a peak indicating the formation of Cu_2O is observed at an approximate 2θ value of 35. This situation indicates the formation of copper oxide on the surface of the substrate and corresponds to the monoclinic orientation of the Cu_2O phase. This formation is believed to be due to environmental factors. Copper coatings tend to passivate under environmental conditions and exhibit thermodynamically higher resistance. In other words, copper becomes passivated in humid conditions, making the copper layer more resistant to further corrosion. Thus, copper provides good protection to the substrate under humid conditions. As a result, the metallization of polymer structures with copper yields positive results under environmental conditions (Afshar and Mihut, 2016; Guo et al., 2009; Chen et al., 2023; You et al., 2020; Baligidad et al., 2021).

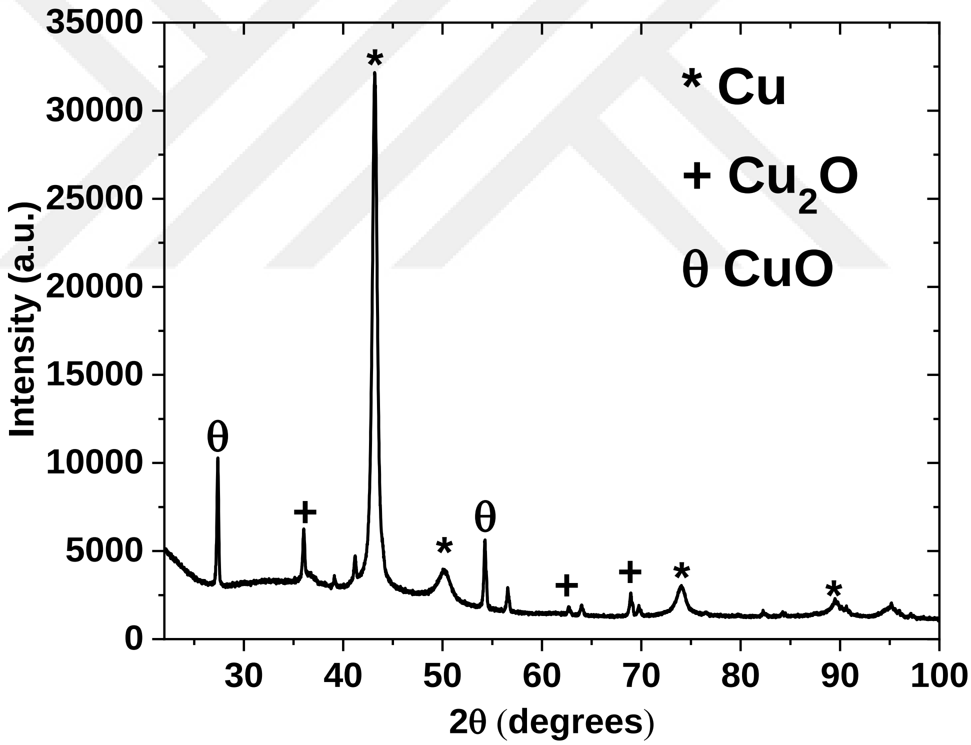

Figure 4.49. XRD analysis of Cu coated as-pinted samples

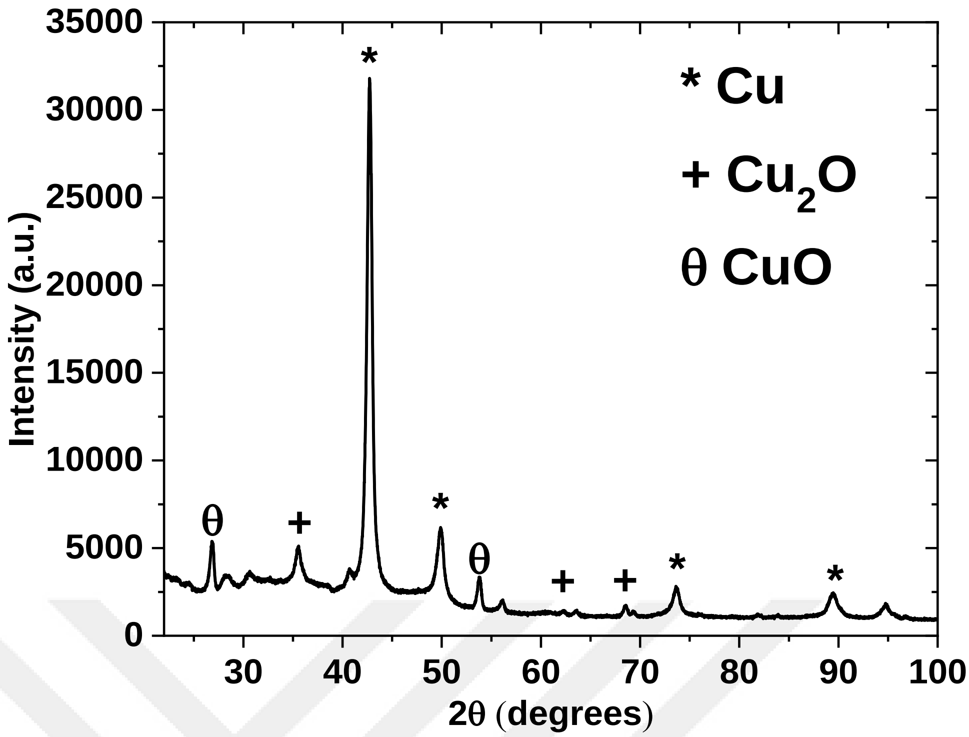

Figure 4.50. XRD analysis of Cu coated dipping samples

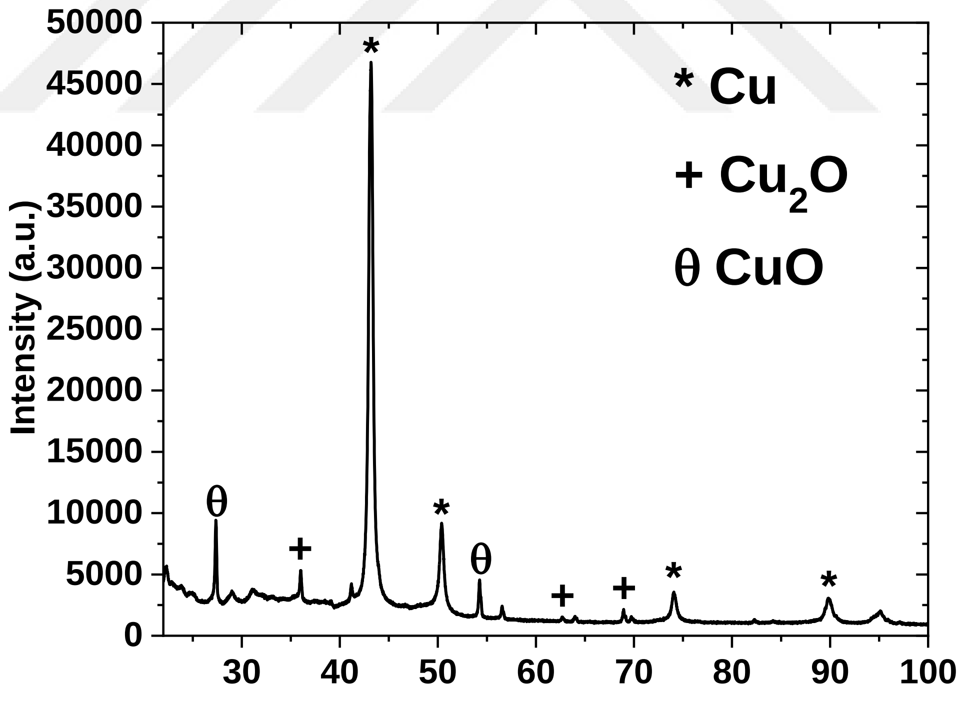

Figure 4.51. XRD analysis of Cu coated vapour samples

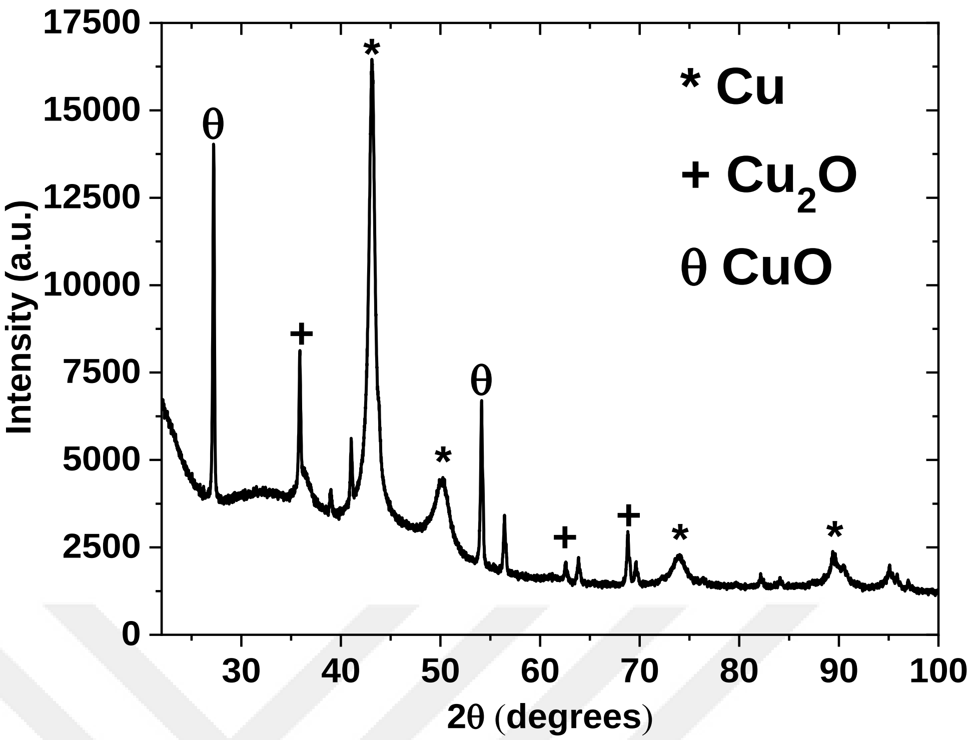

Figure 4.52. XRD analysis of Cu coated plasma samples

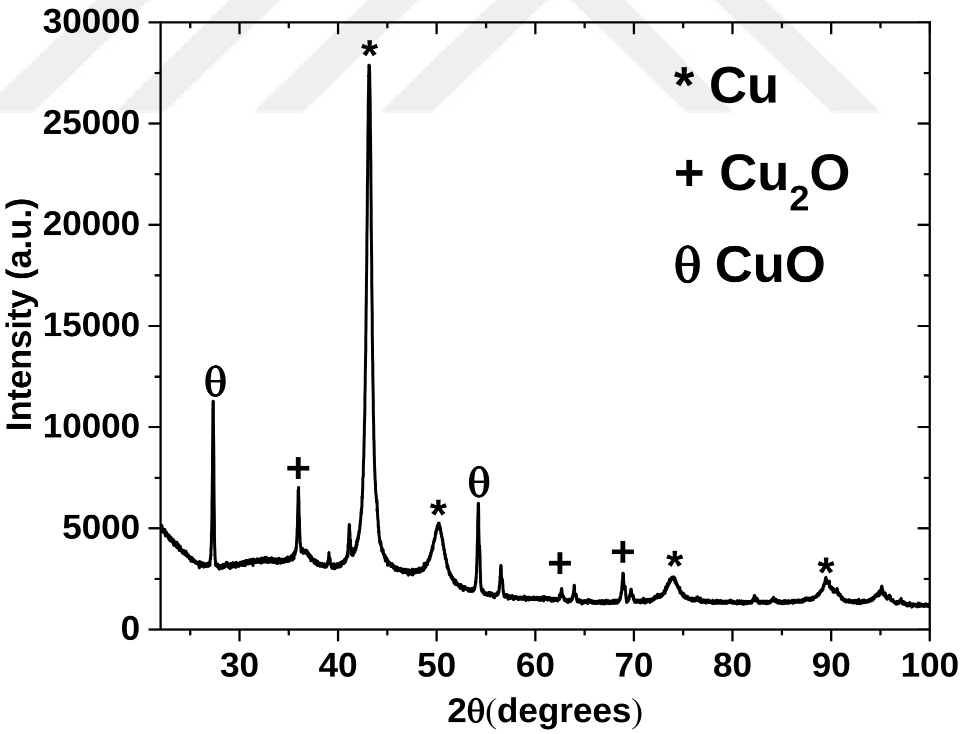

Figure 4.53. XRD analysis of Cu coated abrasion samples

4.4. Fourier Transform Infrared Spectroscopy (FT-IR)

The FT-IR analysis results of 3D-printed polymer structures before and after metallization are presented in Figures 4.54-4.60. Upon examining Figure 10, four main peaks are observed.

These peaks correspond to the C=O bond with a wavelength of approximately 1750 cm^{-1}, the C-O bond with a wavelength of approximately 1078-1180 cm^{-1}, the C-O-H bond with a wavelength of 1450-1380 cm^{-1}, and the C-H bonds with a wavelength of approximately 3000 cm^{-1}. Samples subjected to surface treatment and untreated samples exhibit similar peaks. However, vapour and dipping surface treatments show significant increases in peak intensities. This is believed to represent the density of species related to oxygen, representing surface oxidation resulting from the applied surface treatments (Jordá-Vilaplana et al., 2014; Tengsuthiwat et al., 2019; Xia et al., 2019).

The FT-IR analysis results of 3D-printed polymer structures after metallization are presented in Figure 4.55-4.60. Peaks in the range of 500-600 cm^{-1} can be attributed to stretching vibrations (Amirshaqaqi et al., 2014). Peaks at 510 cm^{-1}, 780 cm^{-1}, and 950 cm^{-1} are associated with Al-O, Al-O, and Al-OH bond vibrations, respectively. The functional groups in polylactic acid facilitate the formation of internal bonds between the polymer and aluminium (Srivastava et al., 2023; Zhu et al., 2010).

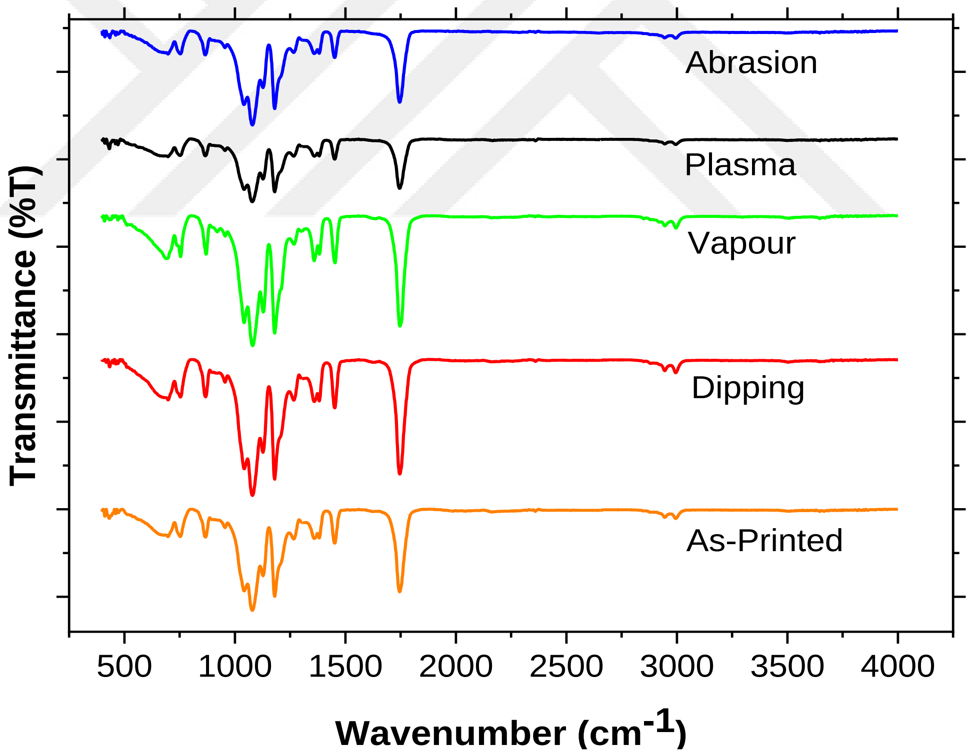

Figure 4.54. FT-IR analysis of samples

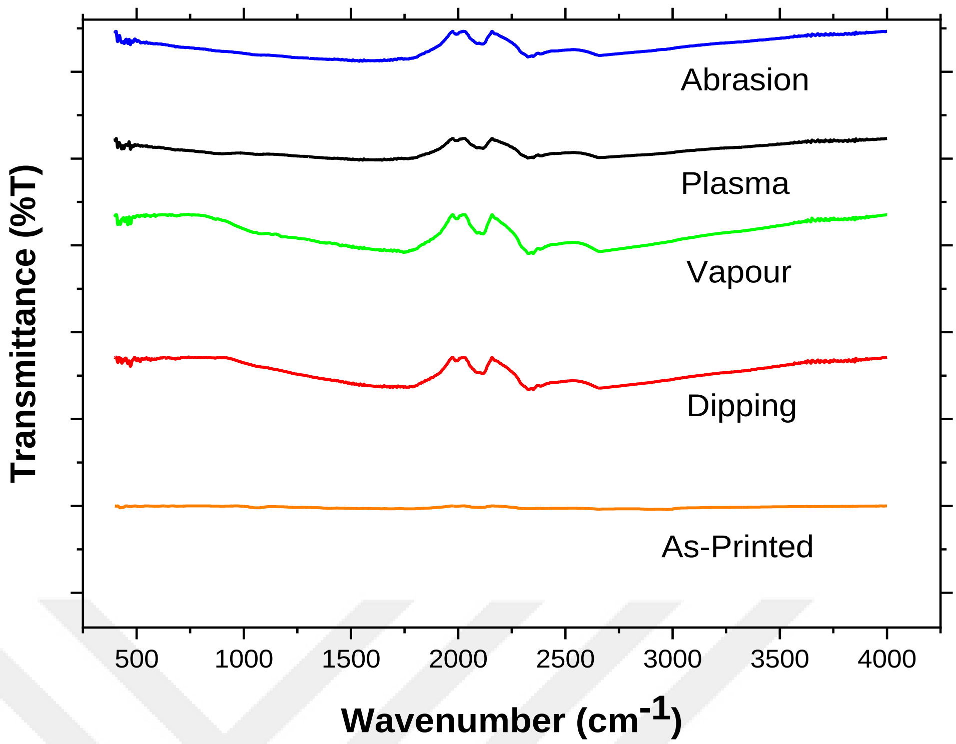

Figure 4.55. FT-IR analysis of Al coated samples

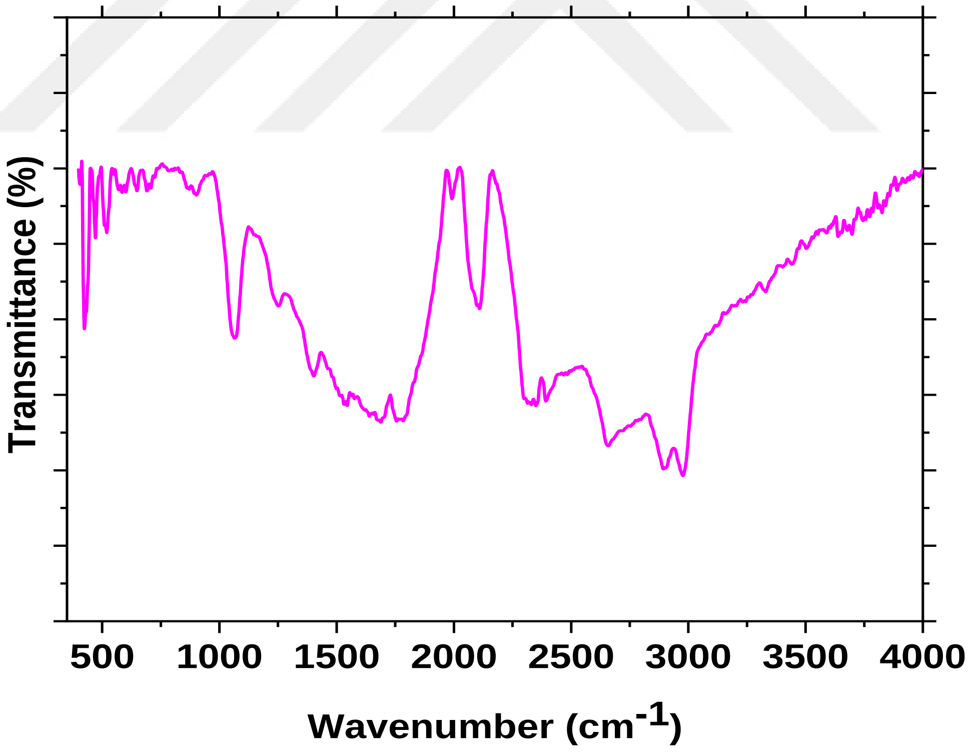

Figure 4.56. FT-IR analysis of Al coated as-printed samples

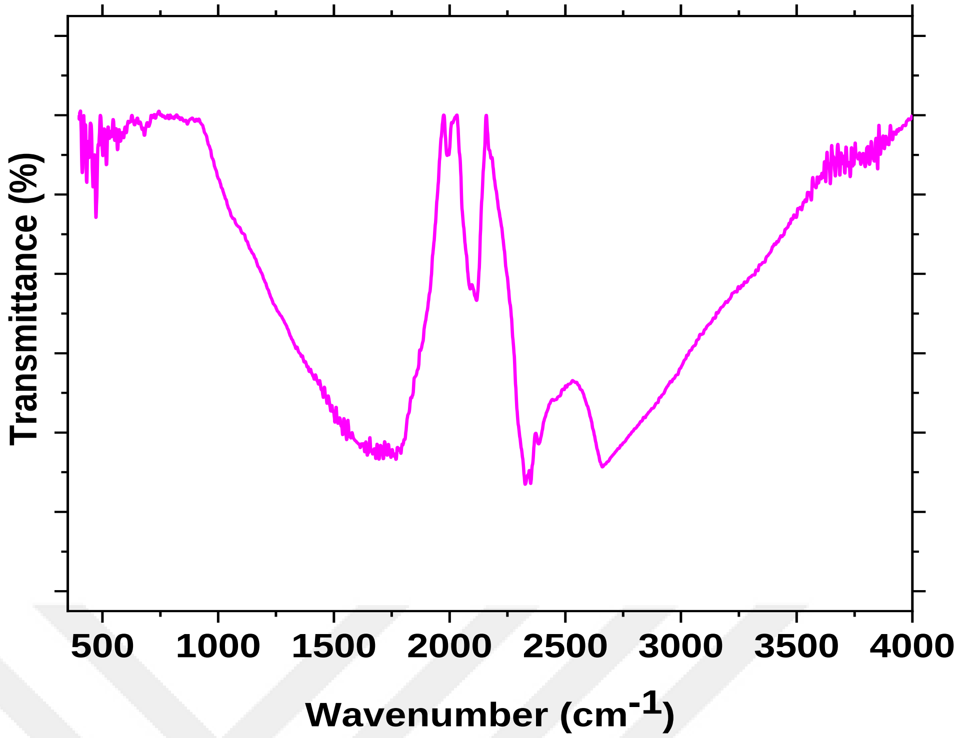

Figure 4.57. FT-IR analysis of Al coated dipping samples

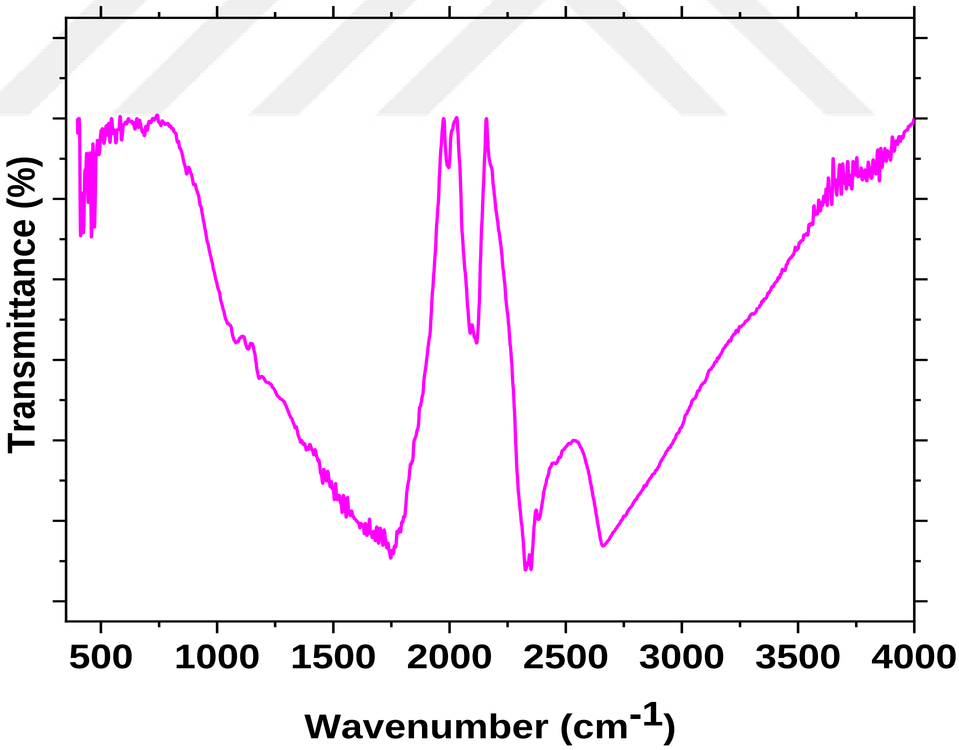

Figure 4.58. FT-IR analysis of Al coated vapour samples

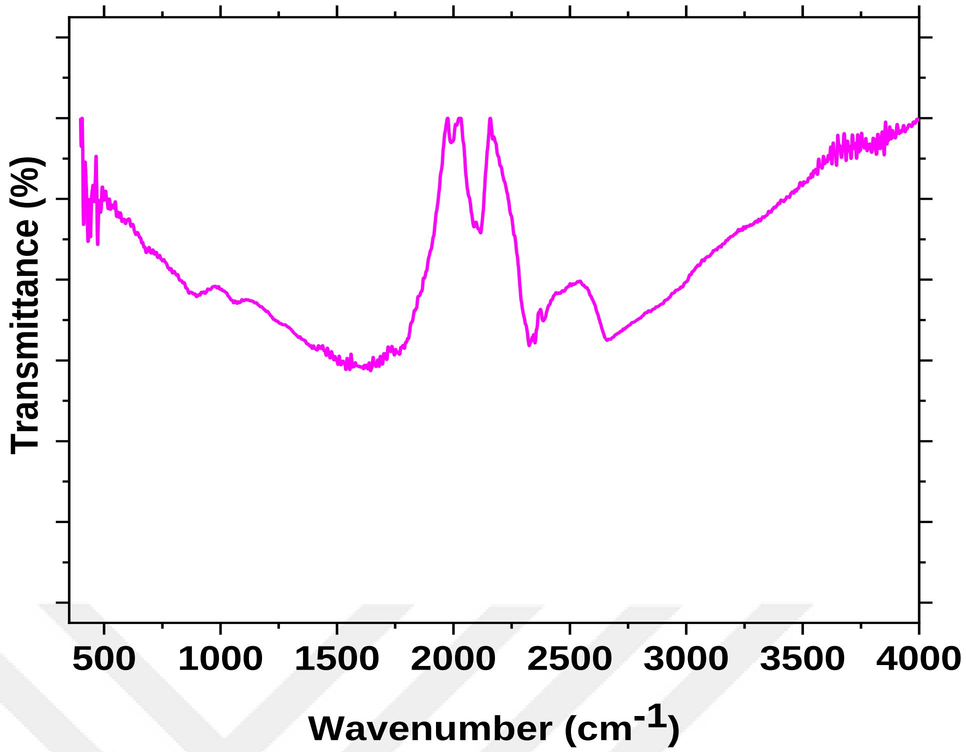

Figure 4.59. FT-IR analysis of Al coated plasma samples

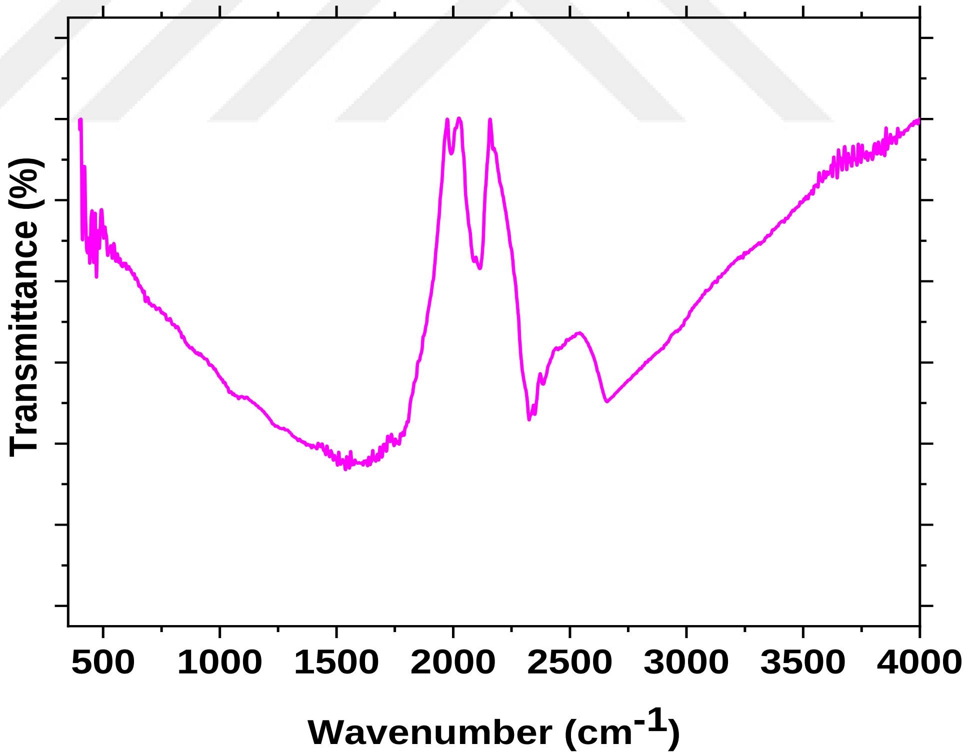

Figure 4.60. FT-IR analysis of Al coated abrasion samples

The Fourier Transform Infrared Spectroscopy (FT-IR) analysis of the polymer specimens before and after copper coating is provided in Figure 4.61-4.67. FT-IR analysis was conducted to evaluate the effect of surface treatments applied to the polymer structures on changes in the chemical structure of the surface. Despite having the same substrate material in all specimens, the FT-IR spectra vary due to chemical changes on the surface of the polymer specimens (Rytlewski and Żenkiewicz, 2013). As previously stated, peak intensities vary depending on different surface treatments. These results indicate successful metallization of the polymer structure surfaces (Ji et al., 2008). As seen in the figure, the surfaces of polymer specimens coated with copper reflect most of the infrared light, hence no significant peak is observed (Zhang et al., 2019). This situation is most likely related to the presence of a very small amount of surface oxides compared to the relatively large metallic mass of these particles (Midander et al., 2009). However, vibrations around 400-900 cm^{-1} can be attributed to metal-oxygen vibration bands (Momeni et al., 2016). Examination of these spectra clearly shows that the peak intensity and peak position slightly shift to different wavelengths. In other words, the copper film forms an outer barrier regarding the penetration of incident radiation into the polymer structure. However, short peaks are observed at certain wavelengths. This result shows that the bond between copper and polymer structure is strong (Rani et al., 2017). FT-IR analysis examines the outer surface layer of the specimens using the ATR technique. Therefore, radiation did not penetrate the polymer specimen due to the thickness of the copper coating (Cucchi et al., 2009).

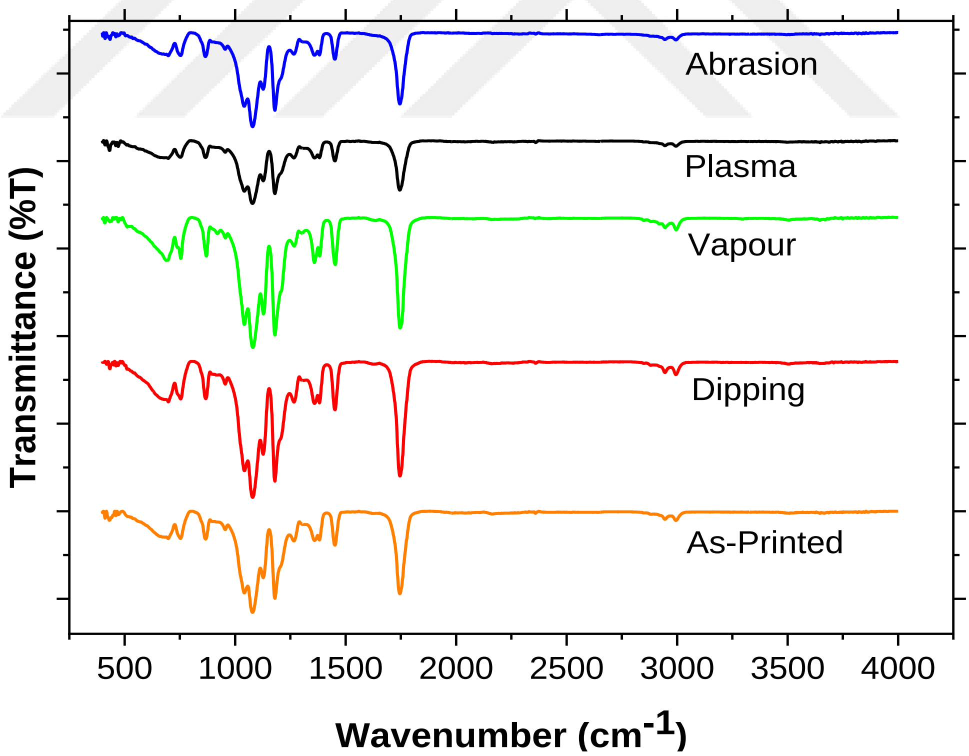

Figure 4.61. FT-IR analysis of samples

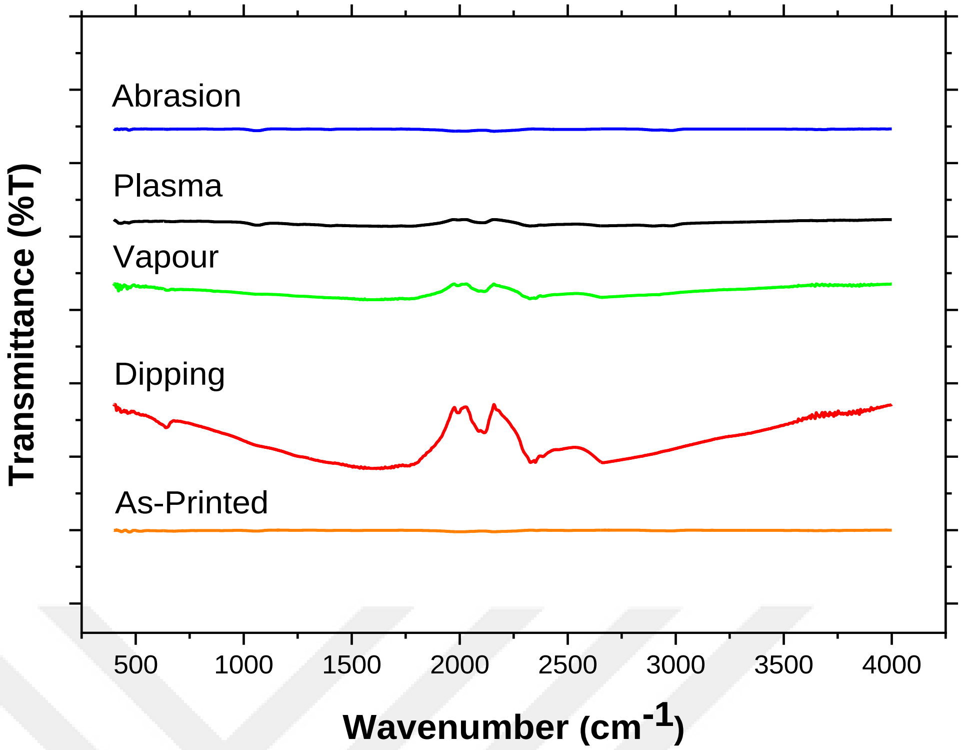

Figure 4.62. FT-IR analysis of Cu coated samples

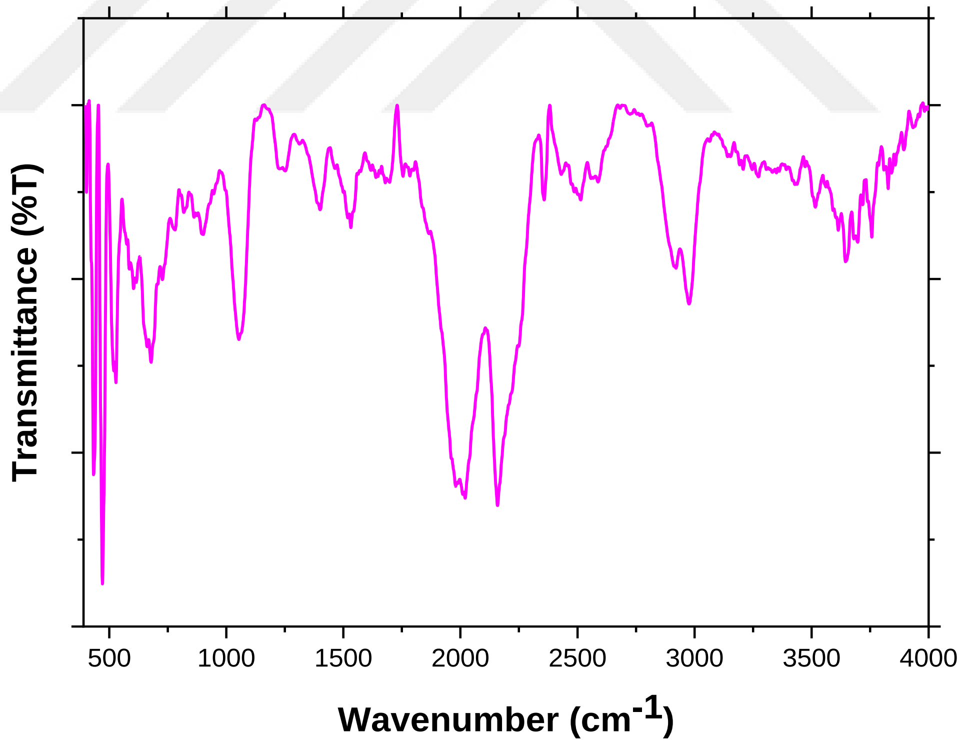

Figure 4.63. FT-IR analysis of Cu coated as-printed samples

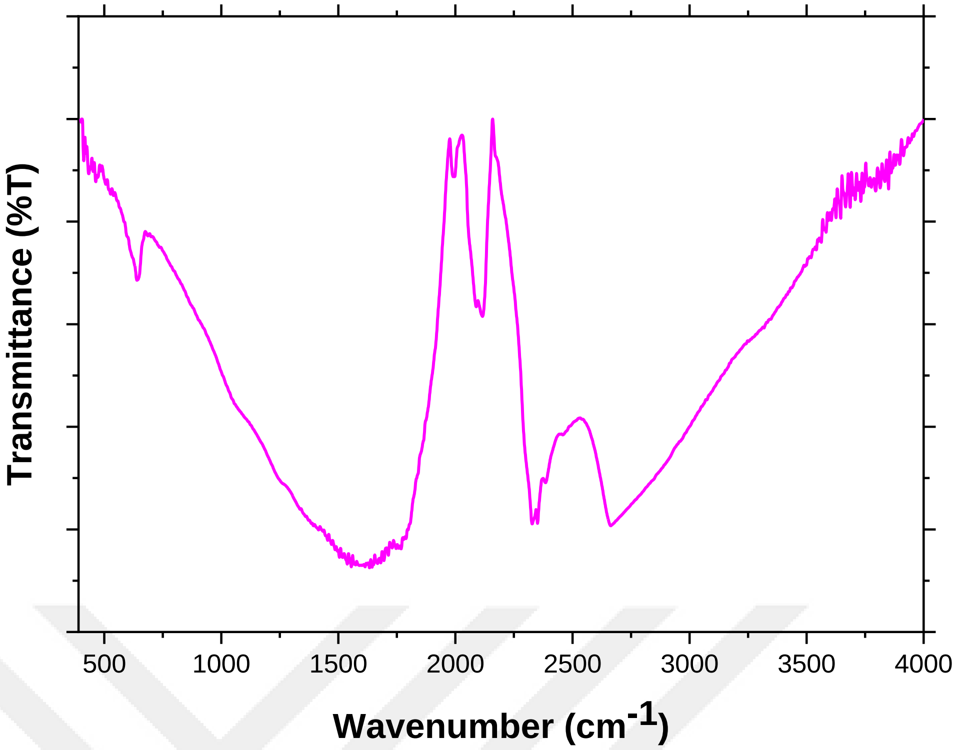

Figure 4.64. FT-IR analysis of Cu coated dipping samples

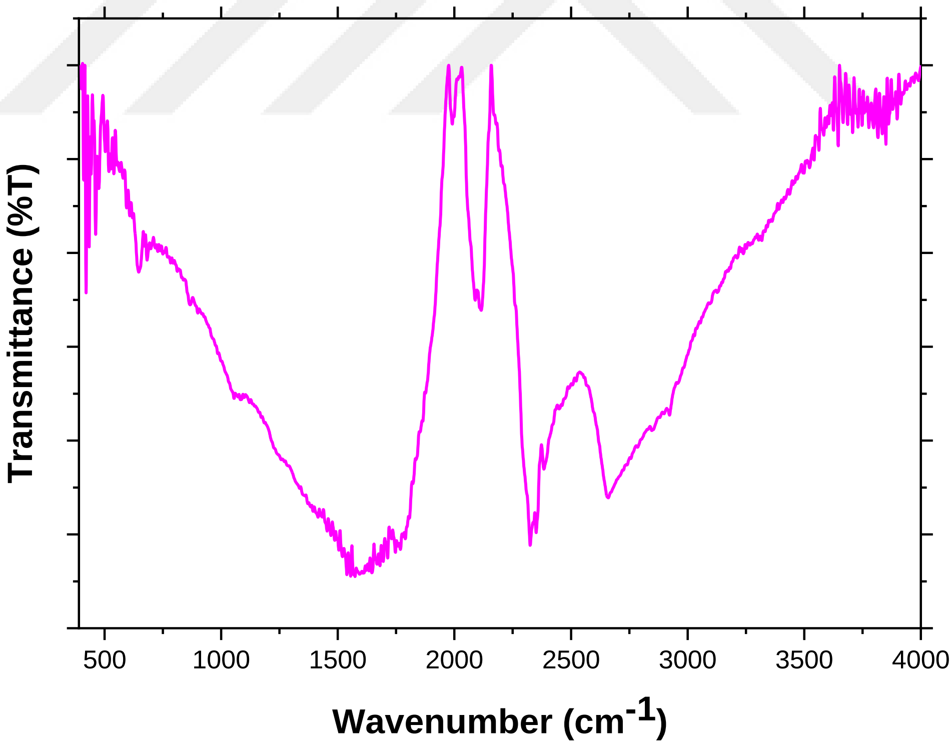

Figure 4.65. FT-IR analysis of Cu coated vapour samples

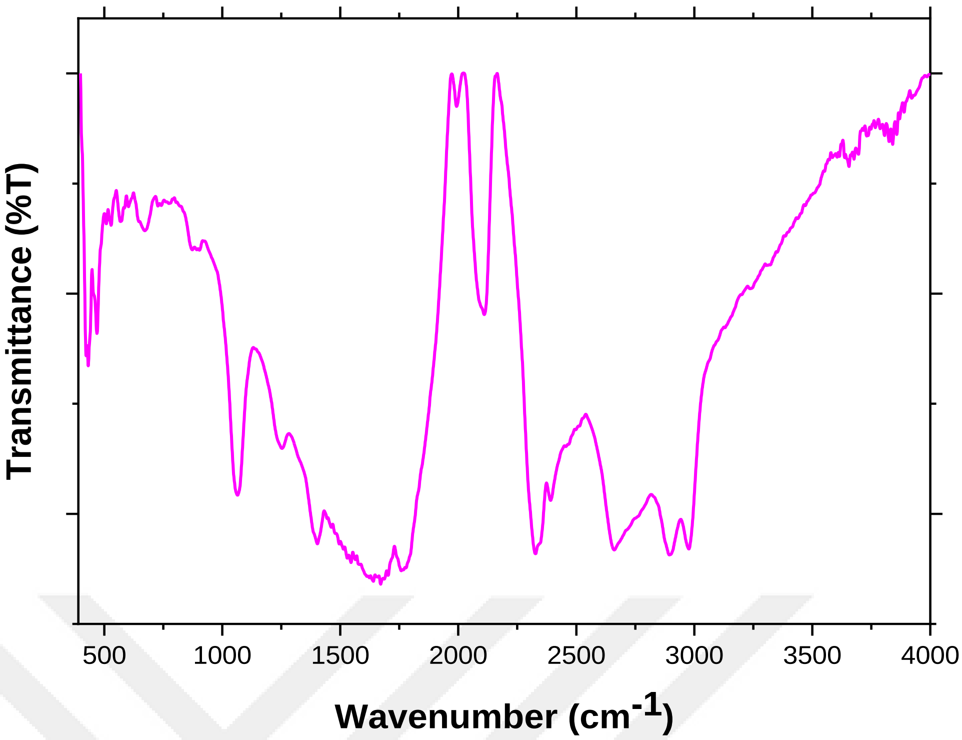

Figure 4.66. FT-IR analysis of Cu coated plasma samples

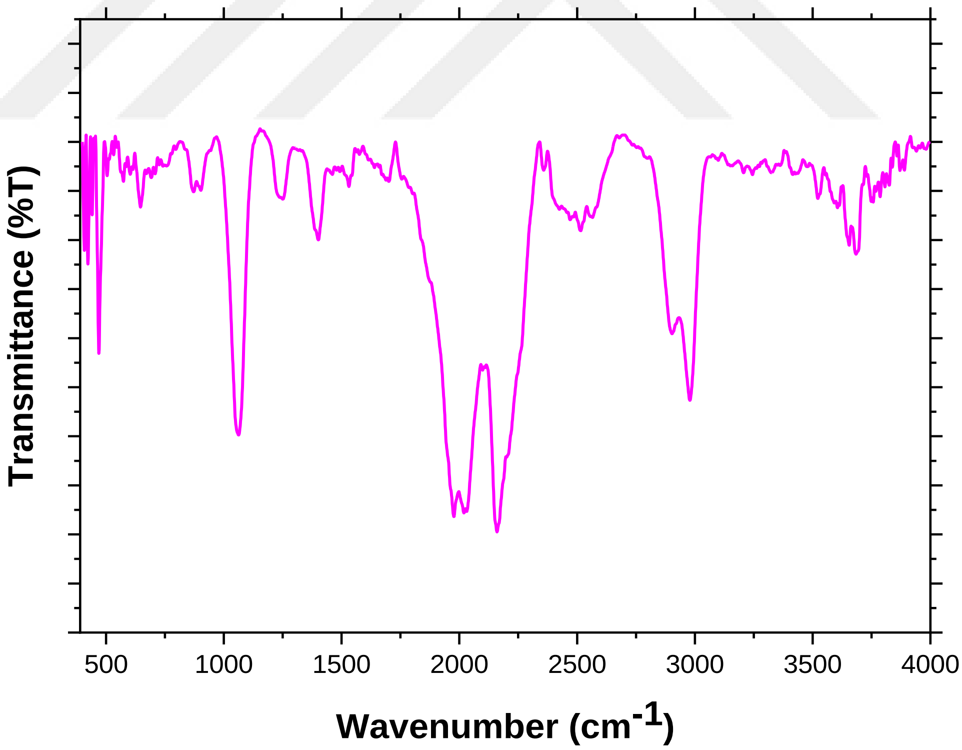

Figure 4.67. FT-IR analysis of Cu coated abrasion samples

4.5. Ultraviolet-Visible-Near Infrared (UV-VIS-NIR)

The ultraviolet, visible light, and near-infrared (UV-Vis-NIR) reflectance analysis of 3D-printed polymer structures before and after Al coating were recorded as a function of wavelength at room temperature, and the results are presented in Figures 4.68-4.69. According to the analysis results, significant improvements in reflectance values were observed in the visible light range (380 nm - 760 nm) and the infrared radiation range (beyond 760 nm) for dichloromethane dipping and dichloromethane vapour surface treatments before metallization. This indicates that reflection occurs in the proposed material across the entire range of radiation, as well as in the infrared and ultraviolet. This is because the polymeric material has almost no heat dissipation, so the entire wavelength of light incident on the surface is reflected and scattered. After metallization, there were substantial increases in reflectance values for polymer structures treated with cold oxygen plasma. Additionally, reflectance values in the ultraviolet radiation range (pre-380 nm) were not at the desired levels. This is characterized by the use of aluminium, which distributes heat in the polymer structure without absorbing it, avoiding heat-induced excitations to the environment (Spacek et al., 2018; Nilsson et al., 2014).

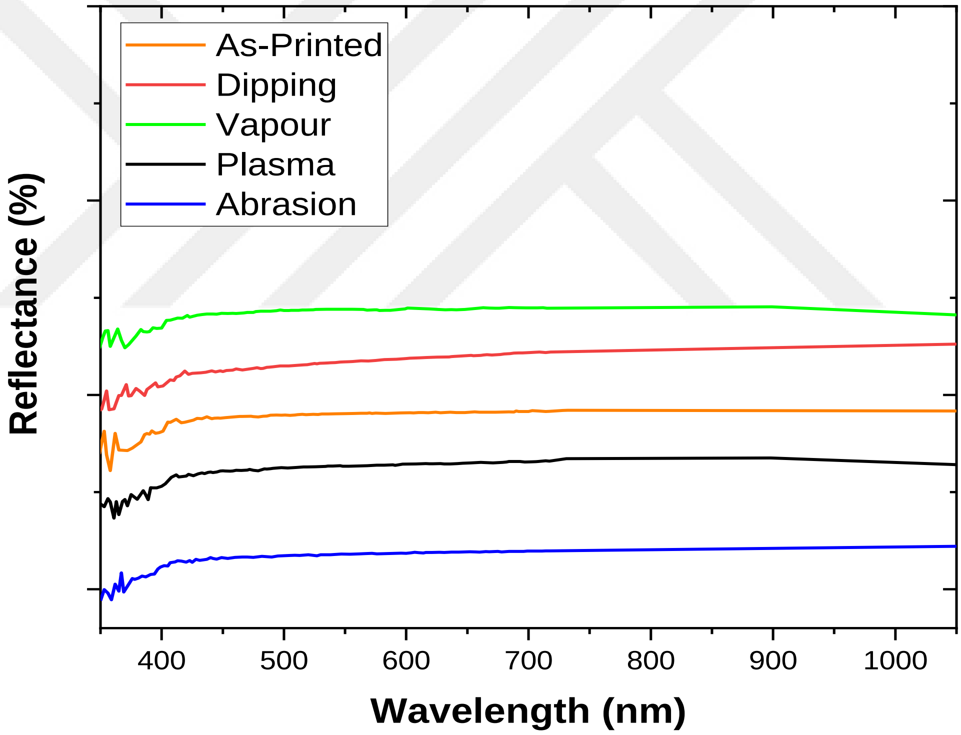

Figure 4.68. UV-VIS-NIR analysis of samples

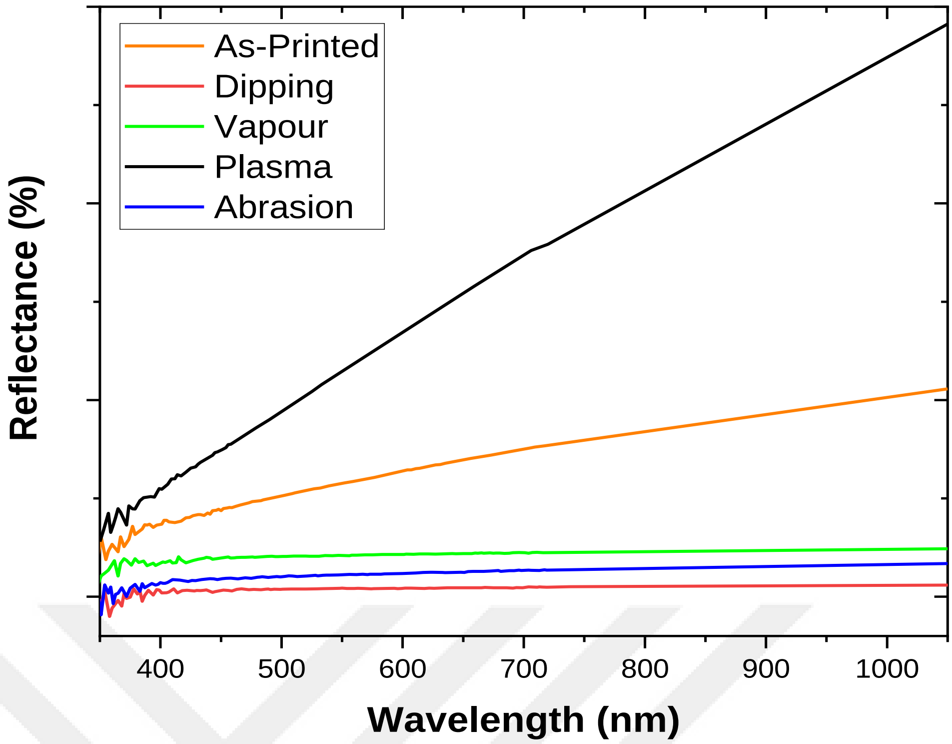

Figure 4.69. UV-VIS-NIR analysis of Al coated samples

UV-VIS-NIR spectroscopy analysis of the treated specimen and untreated specimens after Cu coating are provided in Figure 4.70. UV-VIS-NIR spectroscopy analysis was performed to characterize the localized surface plasmon resonance (LSPR) of the specimens. Different reflectance values were obtained for all specimens in the visible light region. Fringes were observed in the ultraviolet radiation region. Typically, fringes are generated by consistent reflections at the film interfaces. It is believed that the fringes observed in the reflection spectra are indicative of good surface homogeneity and uniformity of enlarged films (Prasanth et al., 2019). Reflection intensities were detected around 570 nm for the as-printed, dichloromethane vapour, and cold oxygen plasma specimens with copper coating. Polymer specimens coated with copper exhibit visible light absorption, making them beneficial for visible light utilization apart from UV light (Sun et al., 2013). The metal oxides present on the polymer surfaces of the as-printed, dichloromethane vapour, and cold oxygen plasma samples cause their reflection intensities to be higher than those of the dichloromethane dipping and mechanical abrasion samples (Xiao et al., 2011). The reflection within the range of 450 to 750 nm, i.e., the useful wavelength range of visible radiation, has been increased. Spectral reflection near the infrared range has increased for all specimens (Alami et al., 2014). Increases in reflectance values have been observed in previous studies with different copper coating methods (Pana et al., 2022).

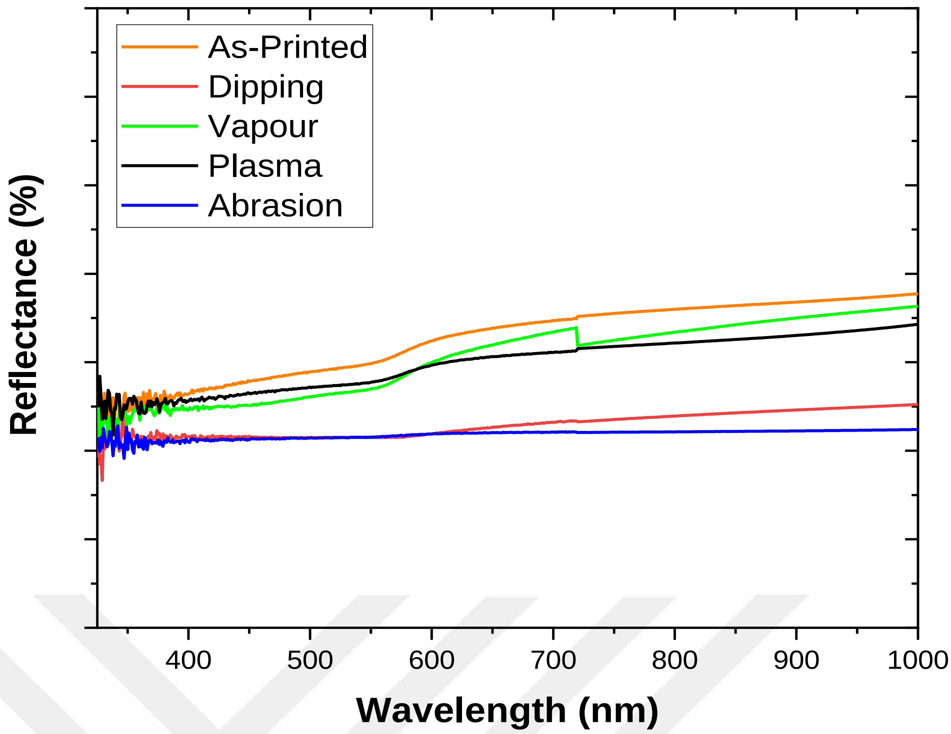

Figure 4.70. UV-VIS-NIR analysis of Cu coated samples

4.6. Contact Angle Measurement

The contact angle measurement images and measured contact angles before and after Al coating of 3D-printed polymer structures are provided in Figures 4.71-4.85. Before metallization, the contact angles of polymer structures; as-pritned and subjected to dichloromethane dipping, dichloromethane vapour, cold oxygen plasma, and sanding were 76.710°, 79.133°, 77.775°, 59.282°, and 87.098°, respectively. After metallization, the contact angles were respectively changed to 87.263°, 68.716°, 78.679°, 91.728°, and 92.446°. The contact angle of 59.282° for polymer structures treated with cold oxygen plasma surface treatment indicates that chemical changes occurred on the polymer surface due to plasma treatment, and these changes made the treated polymer surfaces more hydrophilic compared to their originals (Liu et al., 2016; Cheng et al., 2006; Johansson et al., 2002; Károly et al., 2018). Additionally, a contact angle less than 90° may suggest a moderately hydrophilic behavior. This could be advantageous for multi-layer coating after metallization [Bragaglia et al., 2022]. Generally, there is a significant increase in contact angles after metallization. When adhesive forces exceed cohesive forces, the liquid droplet wets the surface (θ is less than 90°), but when cohesive forces exceed adhesive forces, the surface is only partially wetted. Water is commonly used as a reference liquid; therefore, when the contact angle of a water droplet on a surface is small, the surface is said to be hydrophilic, whereas when contact angles are equal to or greater than 90°, the surface is considered hydrophobic. The contact angle (θ) of a liquid droplet placed on a solid substrate is used to determine the wettability of a specific liquid with a solid surface. The larger the contact angle, the less wettable the surface.

Adhesive forces tend to optimize the solid-liquid contact area depending on the chemistry of the underlying layer and its interaction with the liquid (Siddikali and Sreekanth, 2022; Zhao et al., 2019).

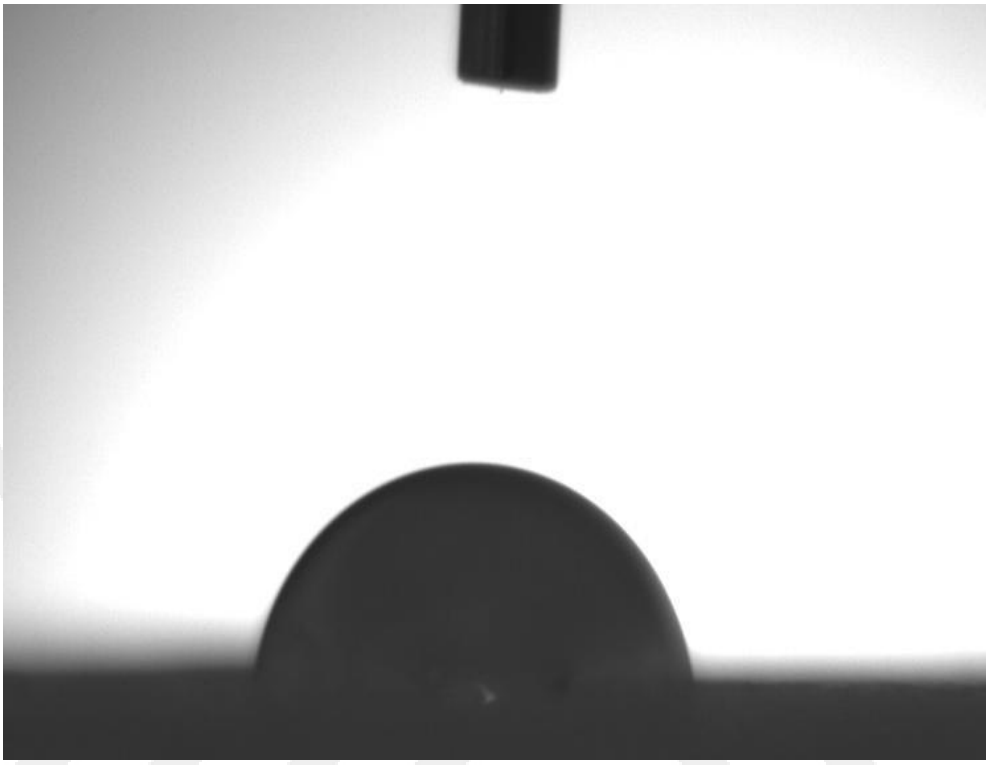

Figure 4.71. Contact angle measurement of as-printed samples

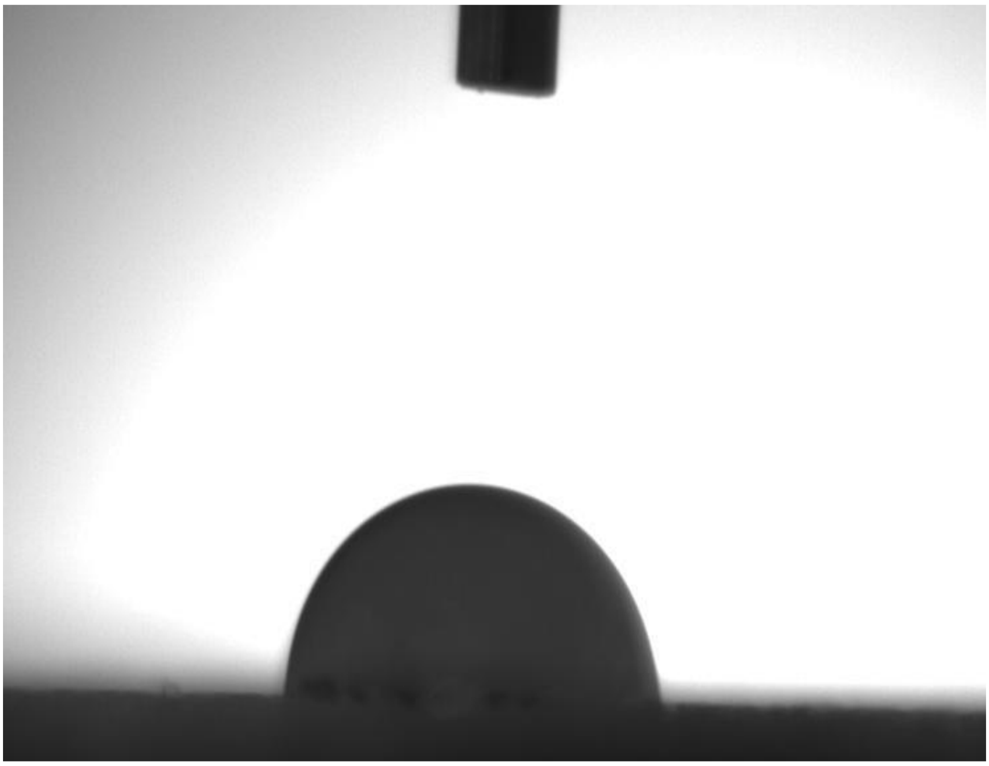

Figure 4.72. Contact angle measurement of Al coated as-printed samples

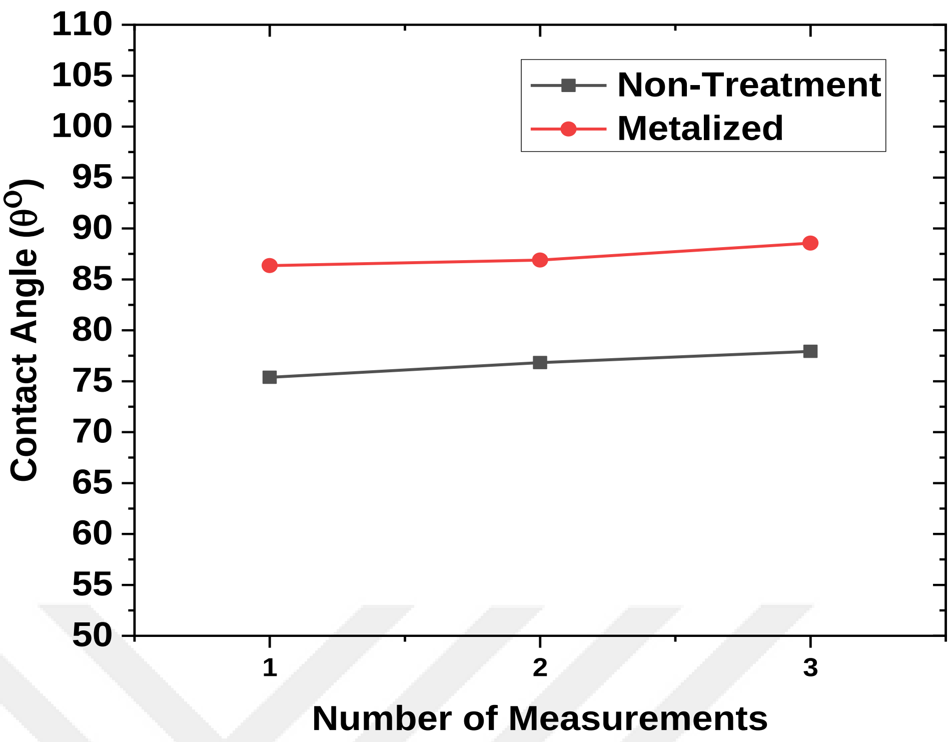

Figure 4.73. Contact angle measurement of as-printed and Al coated as-printed samples

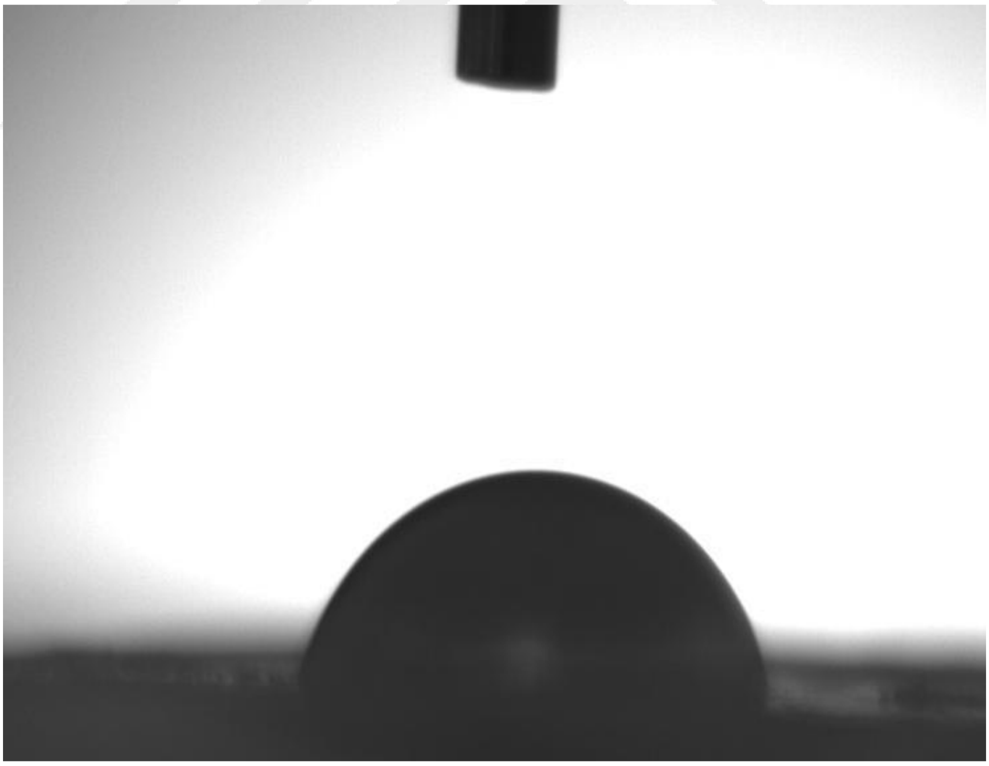

Figure 4.74. Contact angle measurement of dipping samples

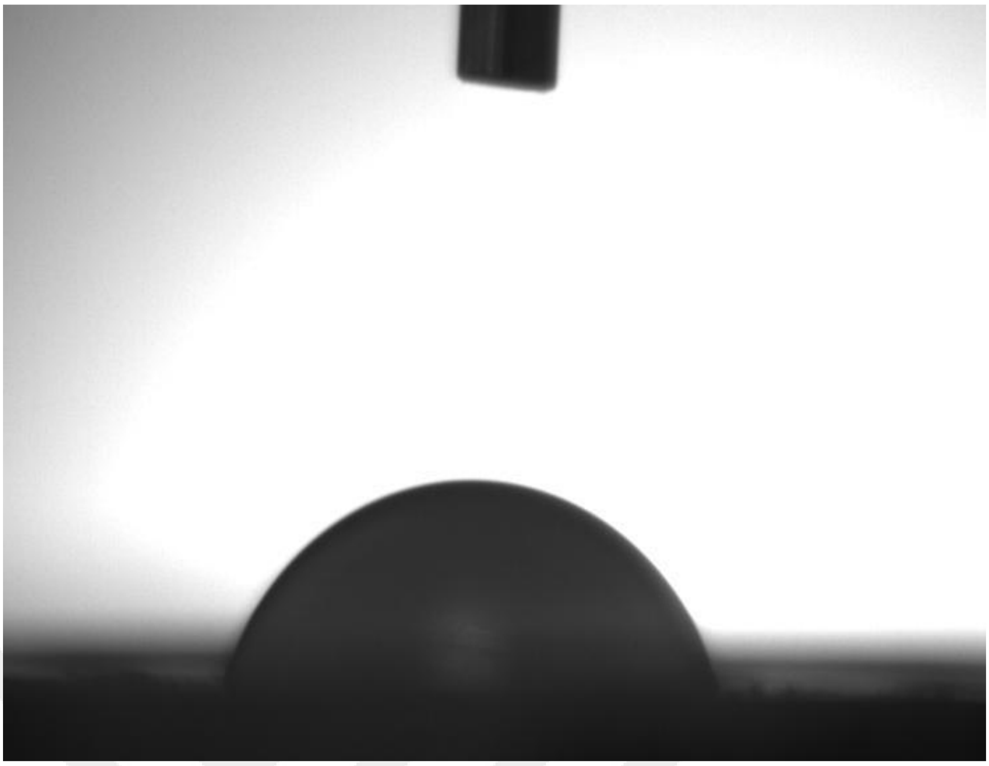

Figure 4.75. Contact angle measurement of Al coated dipping samples

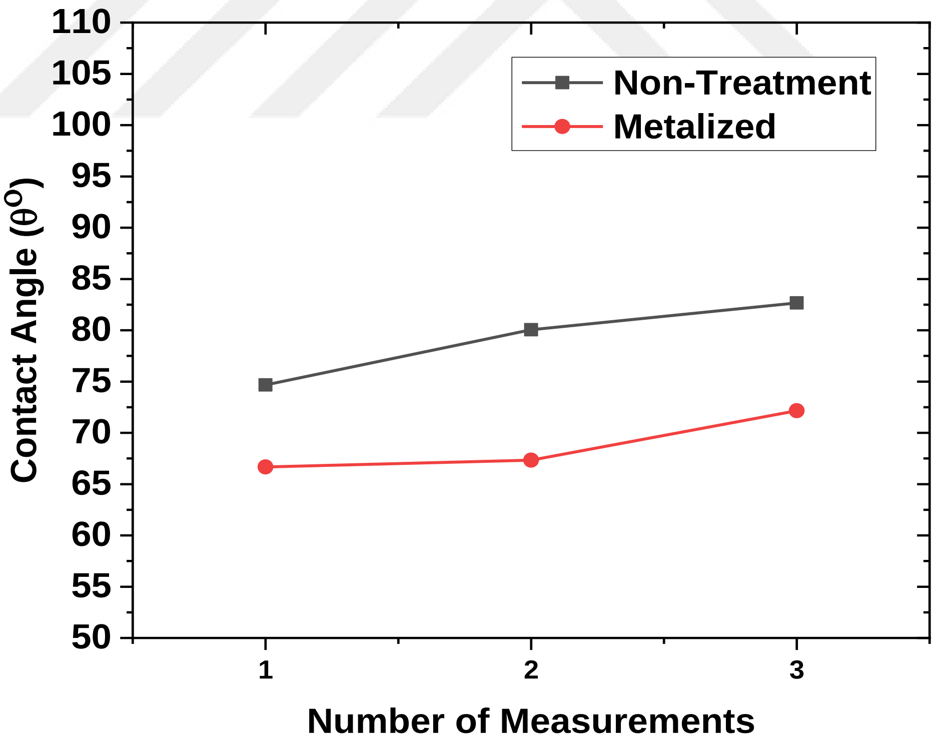

Figure 4.76. Contact angle measurement of dipping and Al coated dipping samples

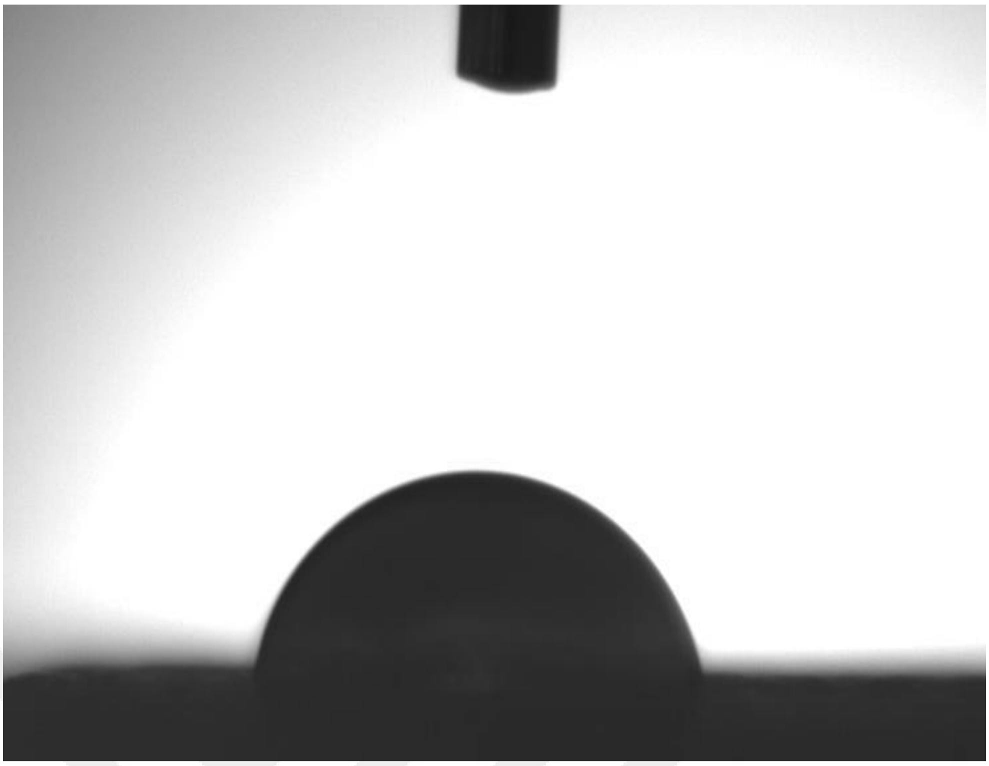

Figure 4.77. Contact angle measurement of vapour samples

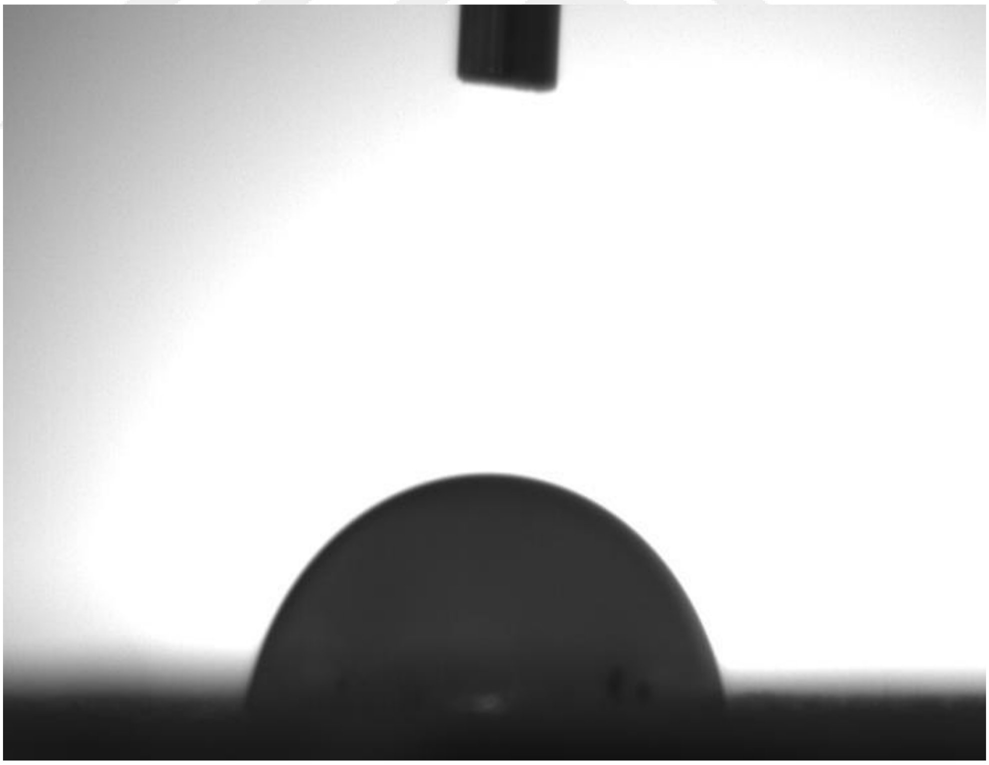

Figure 4.78. Contact angle measurement of Al coated vapour samples

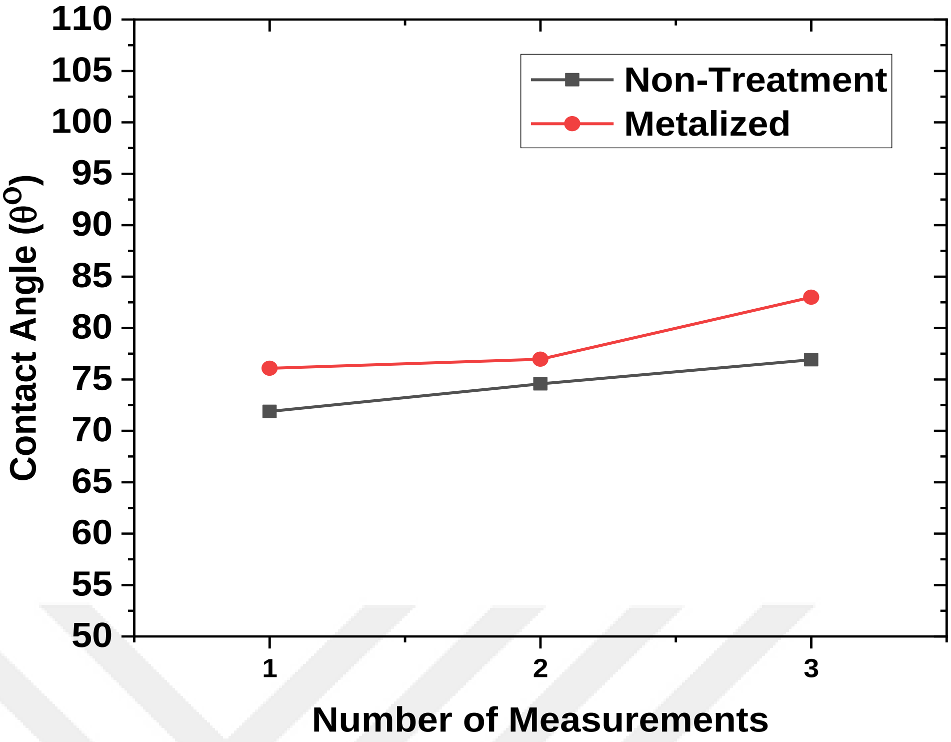

Figure 4.79. Contact angle measurement of vapour and Al coated vapour samples

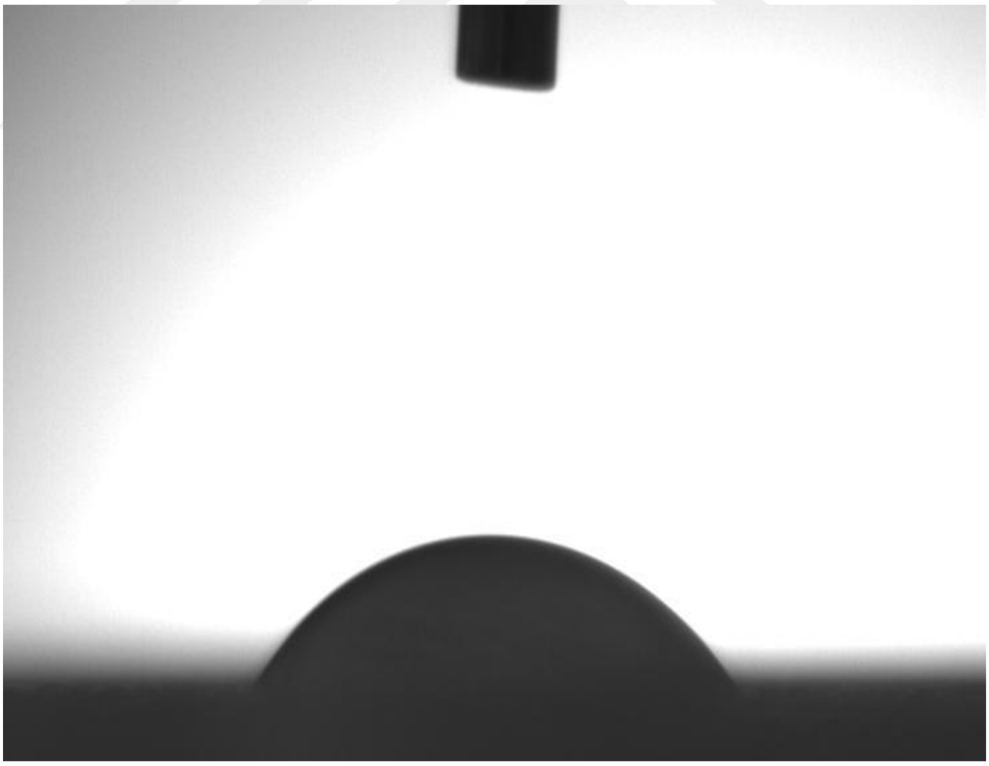

Figure 4.80. Contact angle measurement of plasma samples

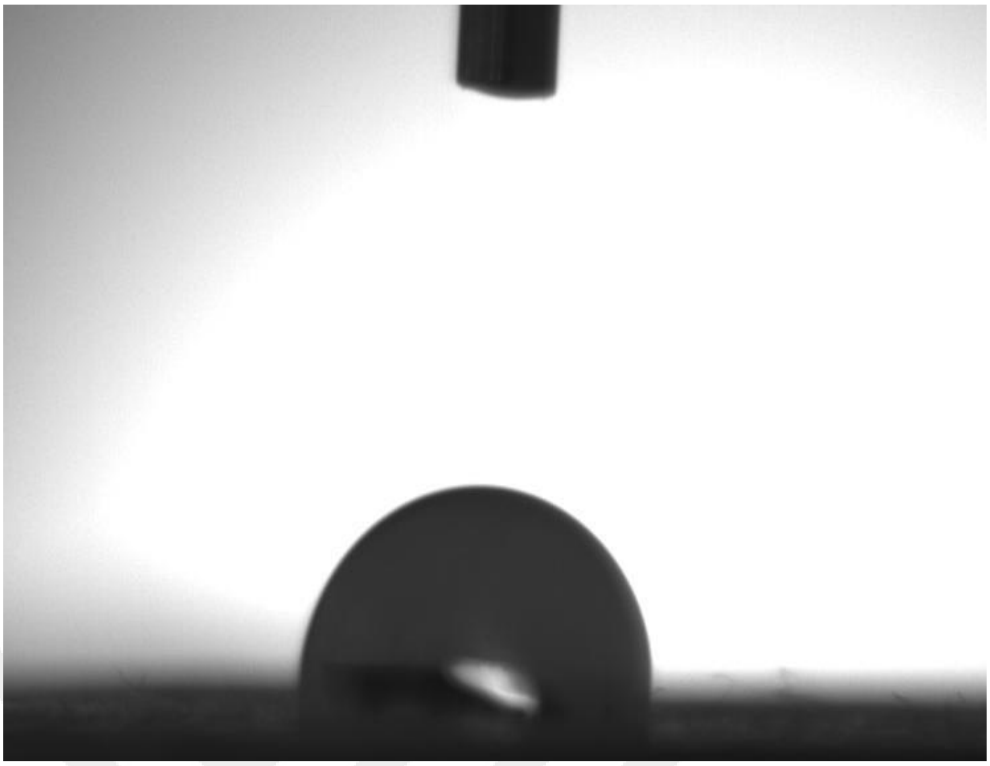

Figure 4.81. Contact angle measurement of Al coated plasma samples

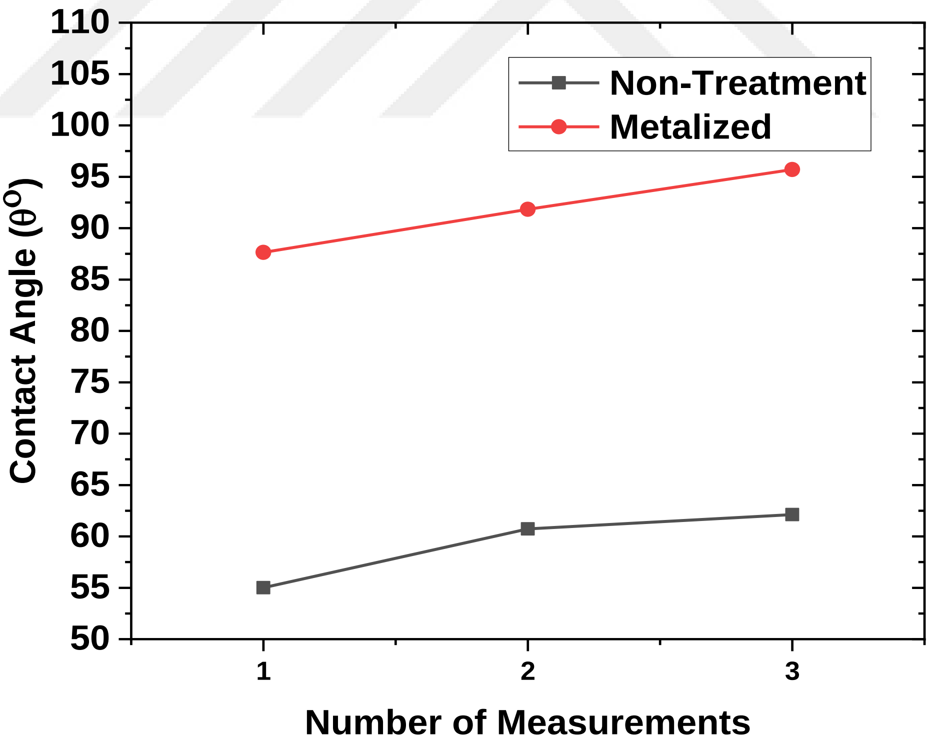

Figure 4.82. Contact angle measurement of plasma and Al coated plasma samples

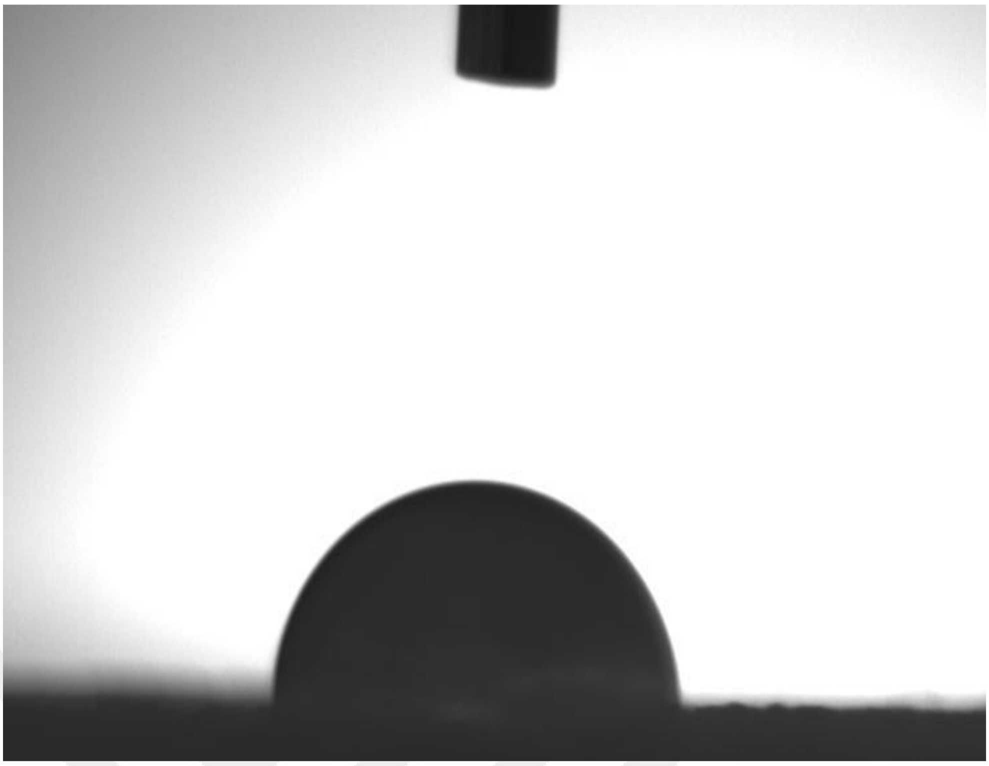

Figure 4.83. Contact angle measurement of abrasion samples

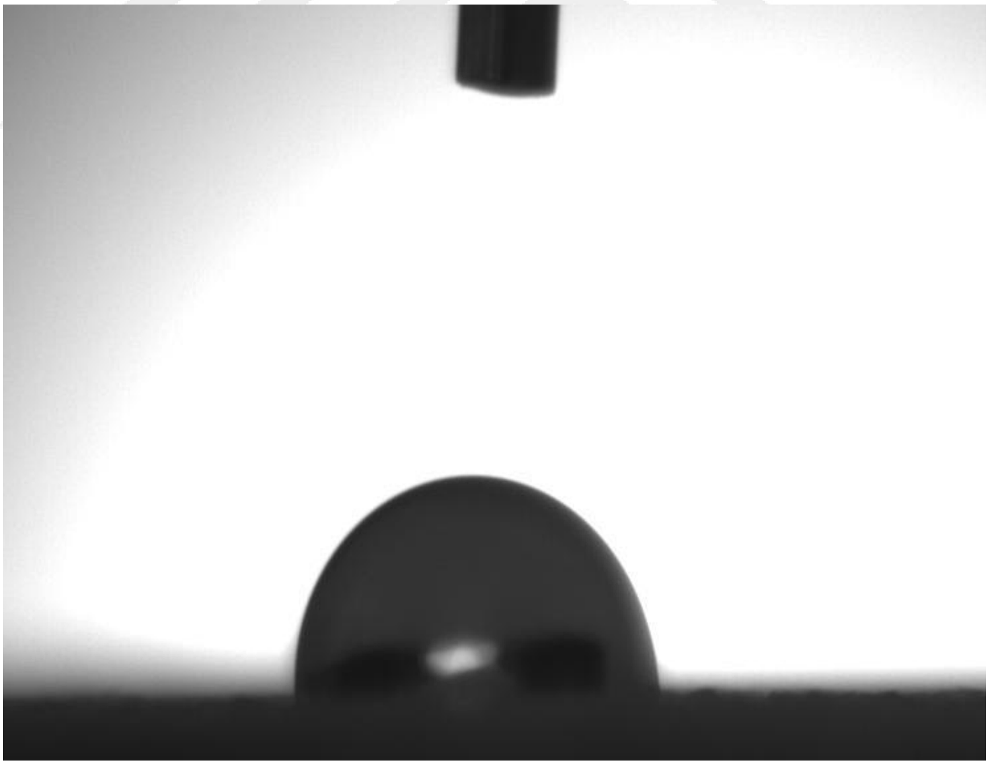

Figure 4.84. Contact angle measurement of Al coated abrasion samples

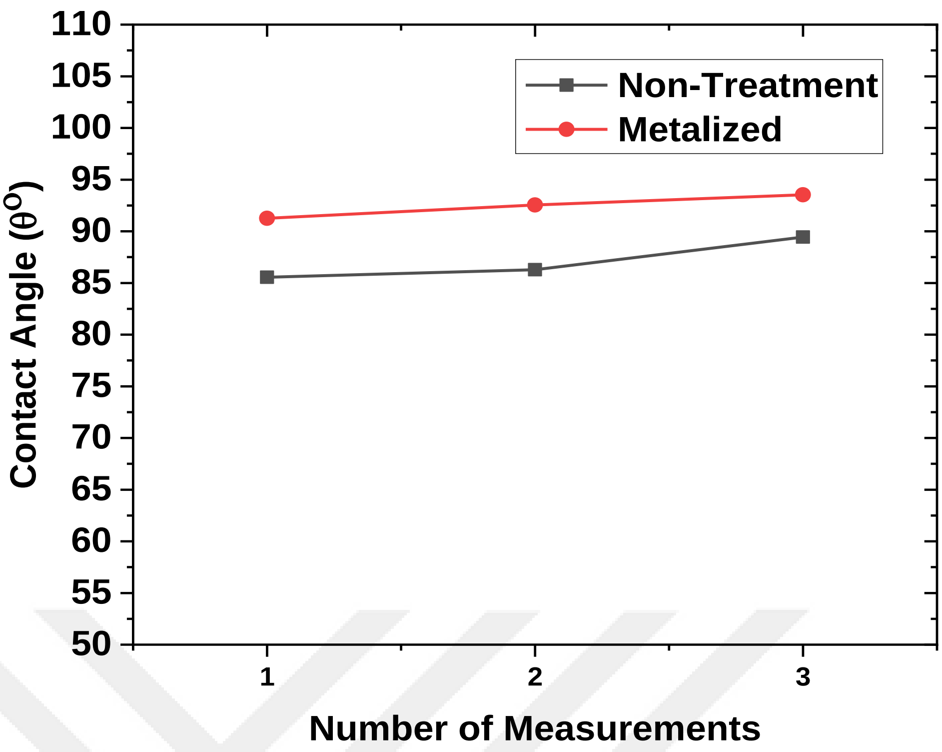

Figure 4.85. Contact angle measurement of abrasion and Al coated abrasion samples

To further investigate changes in surface properties, contact angle measurements were conducted on the surfaces of polymer specimens coated with copper. The contact angle measurement images and measured contact angles before and after copper coating of 3D-printed polymer structures are provided in Figures 4.86-4.100. Contact angle measurement is an effective method for understanding surface interactions between solid-liquid-gas. The terms hydrophilicity and hydrophobicity are used to describe the relative affinity of water molecules to spread on the surface of any substrate. This interaction analysis is referred to as the contact angle (θ), and the obtained value is associated with the surface energy of materials. Generally, a value of $\theta < 90$ degrees is considered to represent a surface with an affinity for the liquid, and a water contact angle less than 90 degrees is normally referred to as hydrophilic. A value of $\theta > 90$ degrees represents the non-wetting property of the surface or its lesser affinity towards the liquid. Surfaces with such characteristics are referred to as hydrophobic (Hebbar et al., 2017). The contact angle measurement results were 78.570°, 80.314°, 75.974°, 88.309°, and 86.914°, respectively. The applied surface treatments have increased the contact angles. Thus, the applied surface treatments tend to lead the polymer structures to have hydrophobic behavior. It is evaluated that the increase in contact angles in the specimen subjected to dichloromethane dipping was due to the pores on the specimen surface. These are likely trapped air pockets within the pores. Therefore, it is evaluated that the surfaces of the produced micro-porous polymer specimens exhibit Cassie-Baxter behavior (Onder et al., 2018). On these surfaces, water droplets typically settle on the protrusions and roll easily across the surface (Zhang et al., 2018). The contact angle of 75.974° in the dichloromethane vapour specimen is believed to result from the incorporation of chloride ions onto the polymer specimen surface (Upadhyay and Bhat, 2003). In cold oxygen plasma surface treatments, it is observed that the chemical structure of PLA changes with O_2 and thus indicating the presence of polar groups on the surface, including hydroxyl, carboxyl, and other oxygen functional groups (Khorasani et al., 2008).

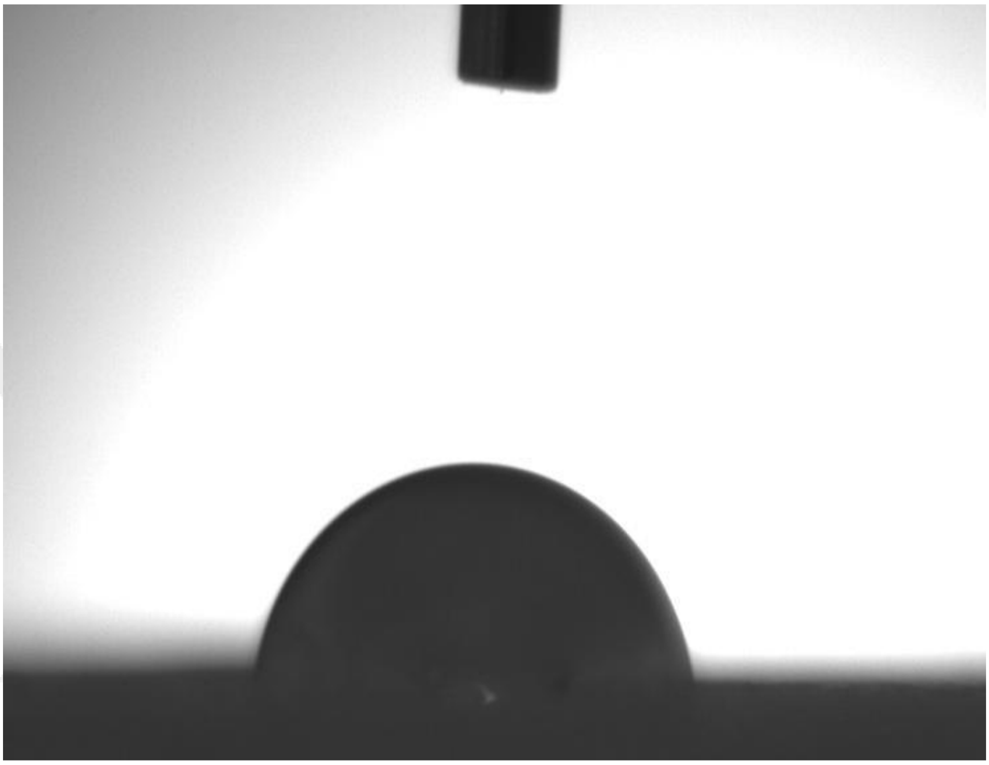

Figure 4.86. Contact angle measurement of as-pinted samples

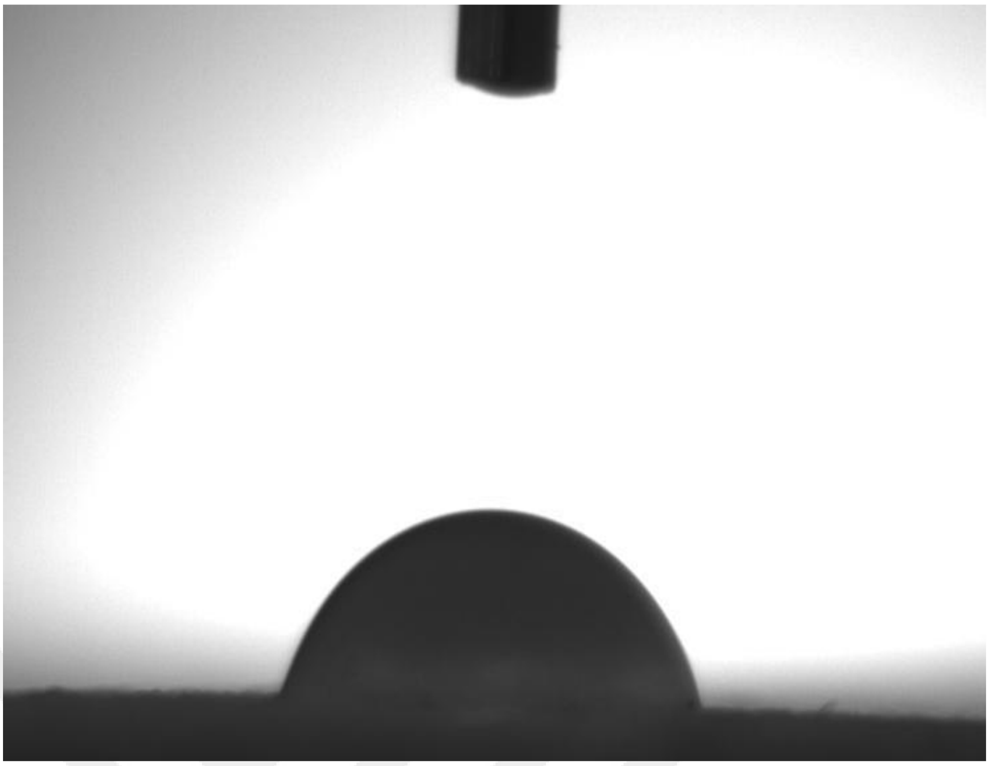

Figure 4.87. Contact angle measurement of Cu coated as-printed samples

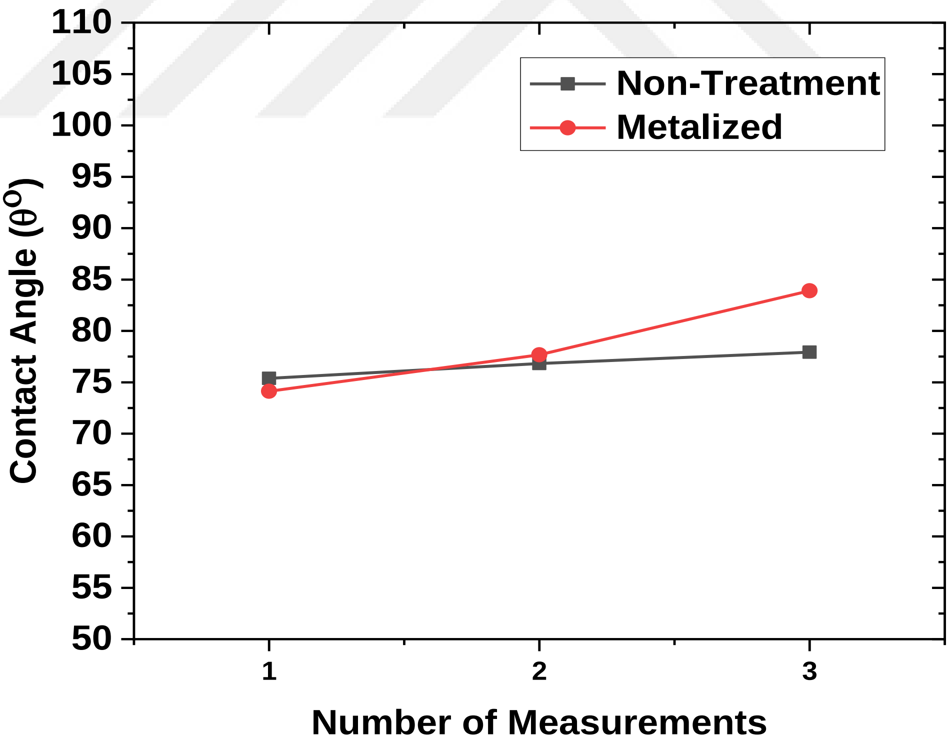

Figure 4.88. Contact angle measurement of as-printed and Cu coated as-printed samples

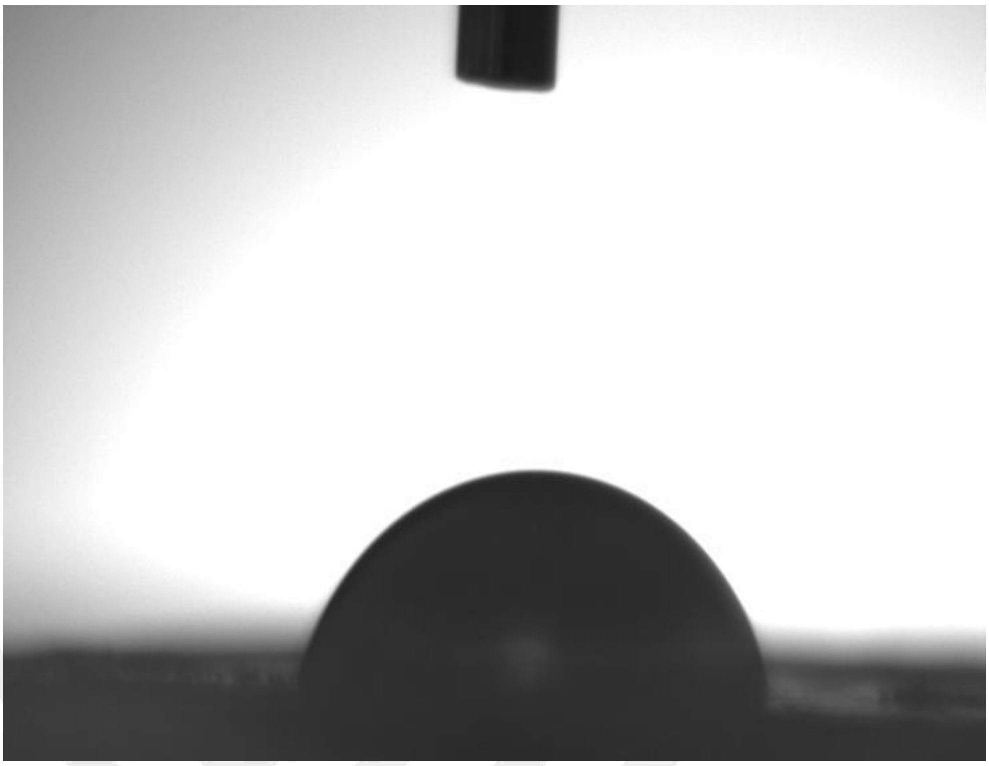

Figure 4.89. Contact angle measurement of dipping samples

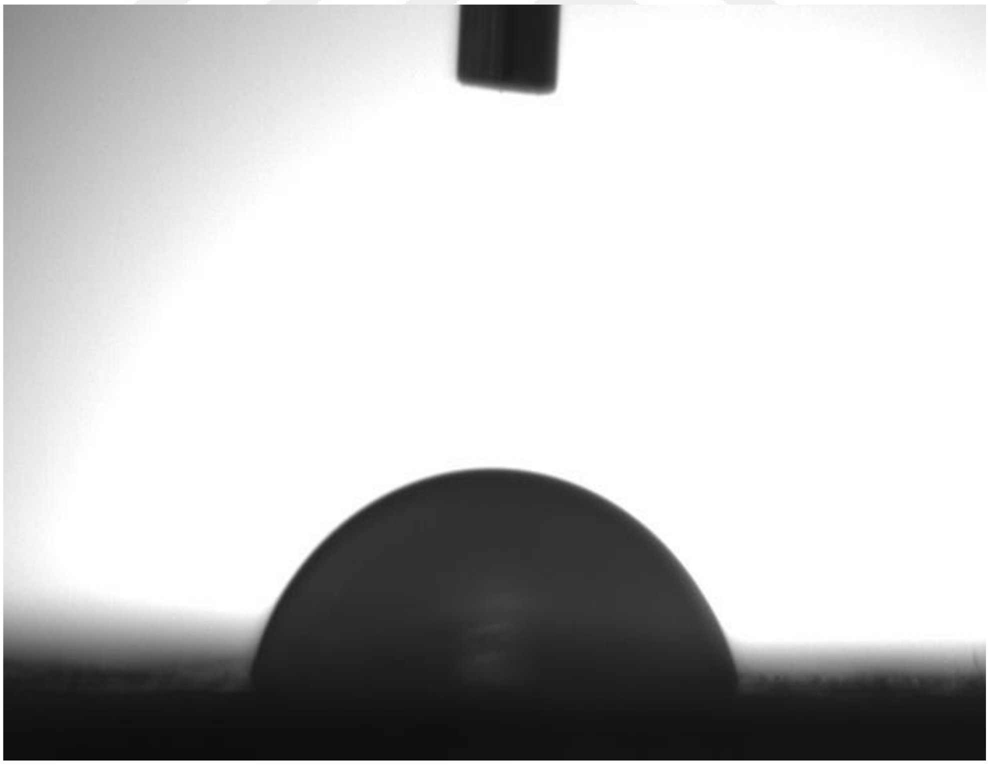

Figure 4.90. Contact angle measurement of Cu coated dipping samples

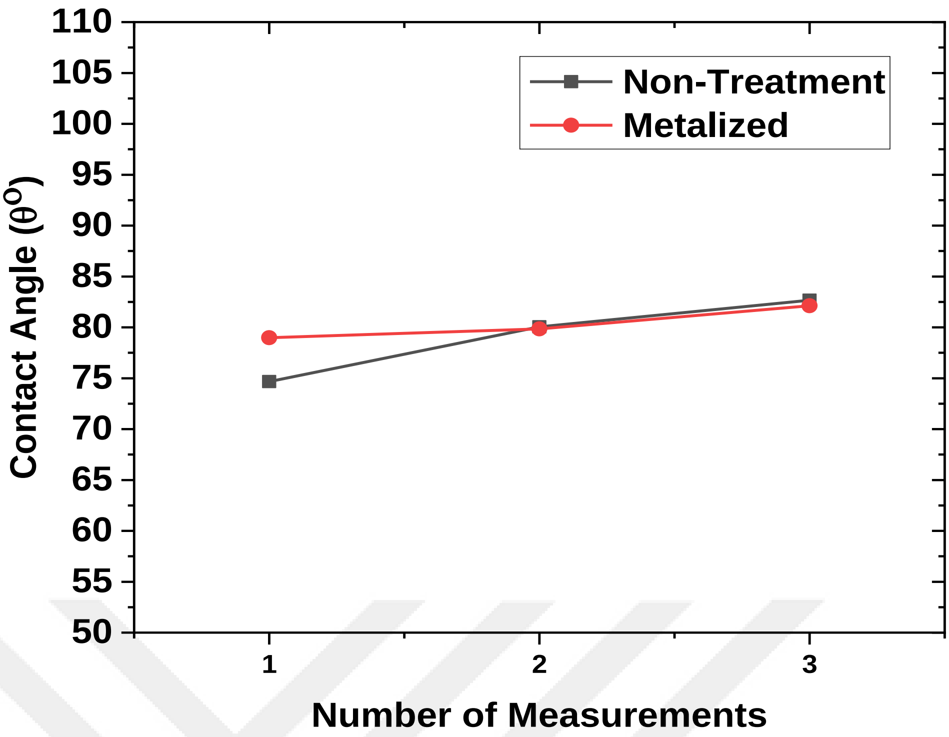

Figure 4.91. Contact angle measurement of dipping and Cu coated dipping samples

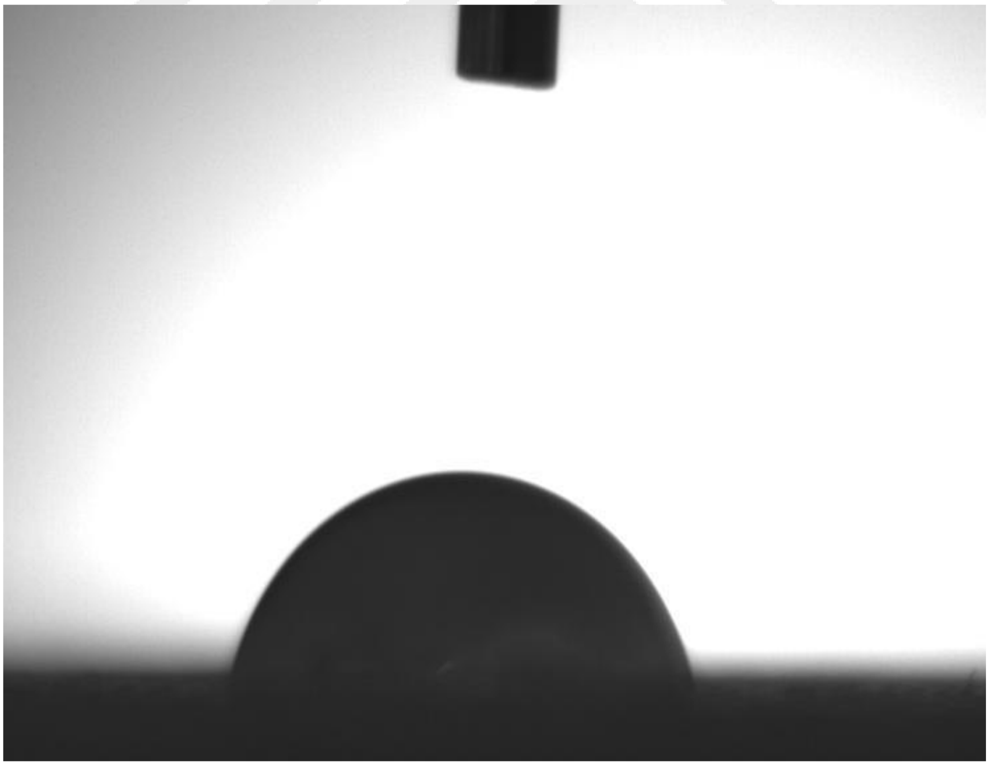
Figure 4.92. Contact angle measurement of vapour samples

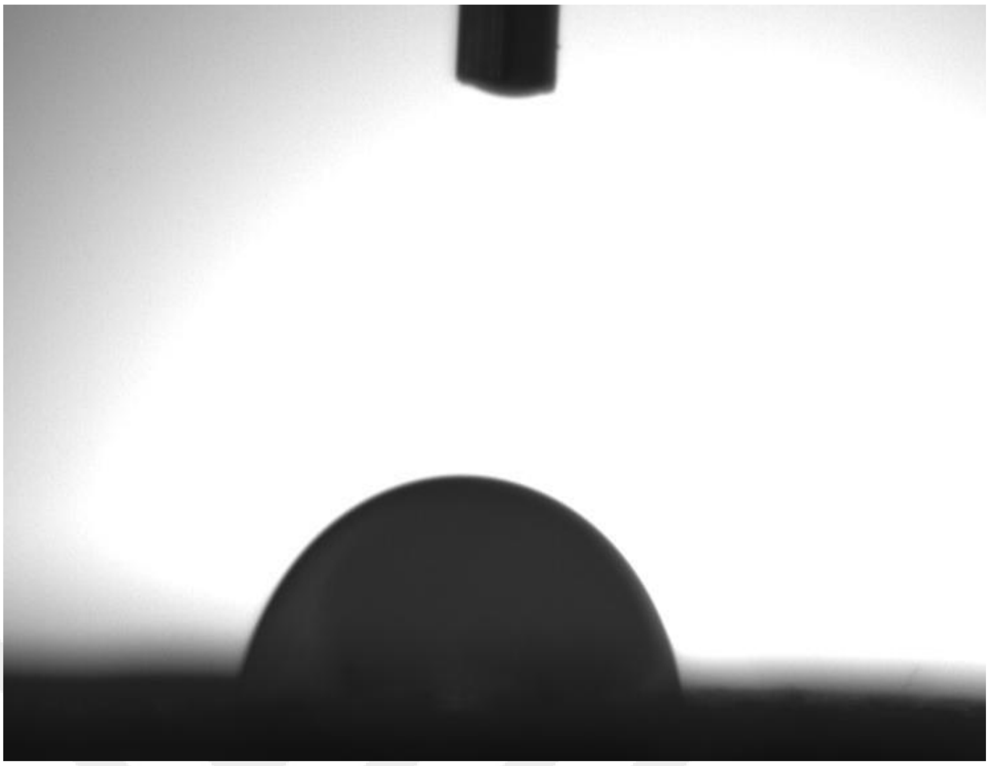

Figure 4.93. Contact angle measurement of Cu coated vapour samples

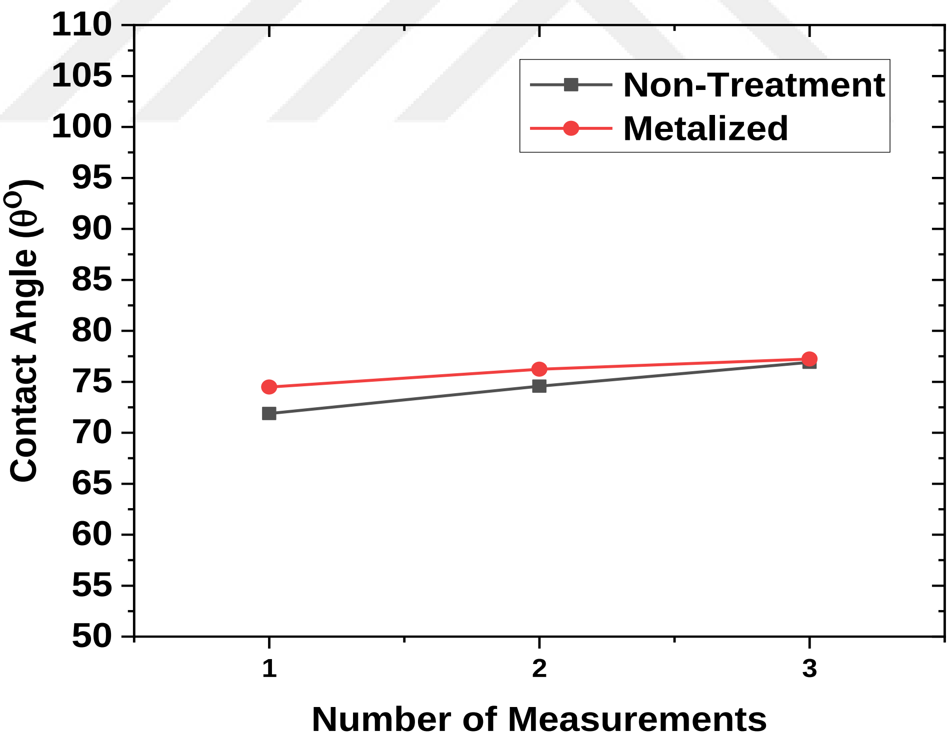

Figure 4.94. Contact angle measurement of vapour and Cu coated vapour samples

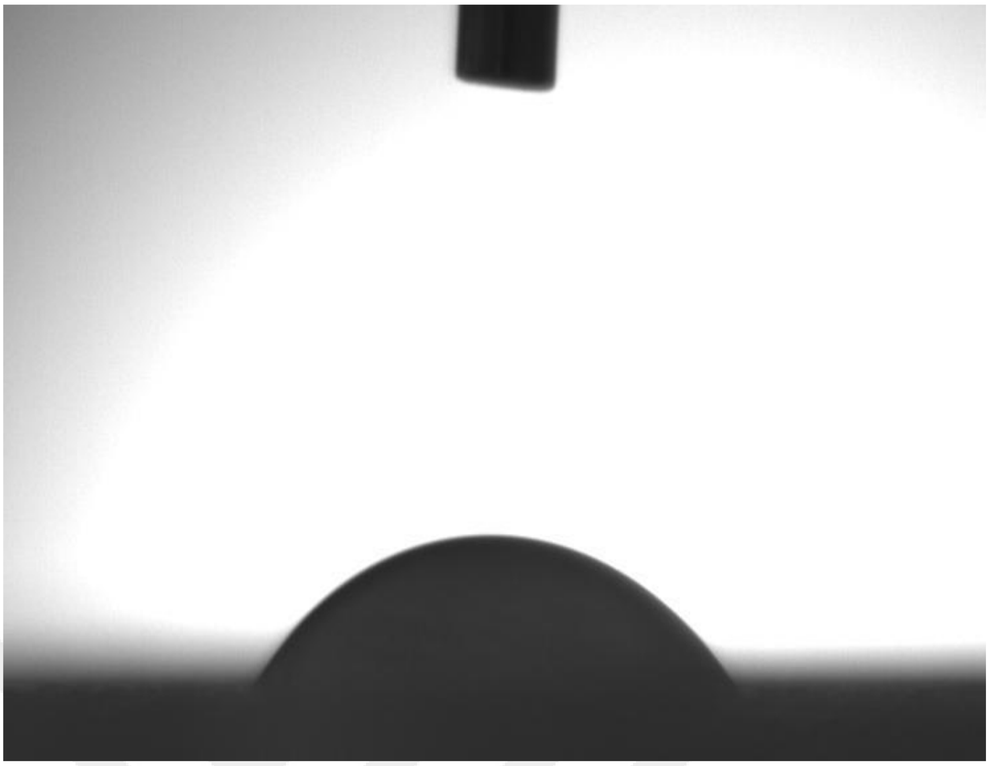

Figure 4.95. Contact angle measurement of plasma samples

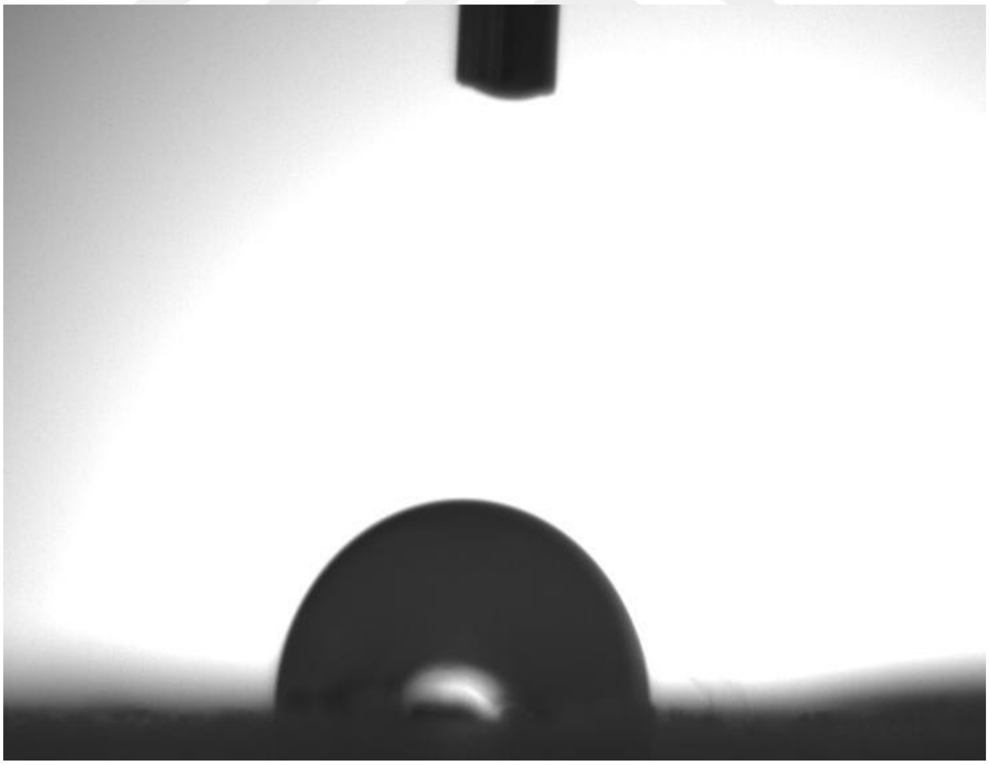

Figure 4.96. Contact angle measurement of Cu coated plasma samples

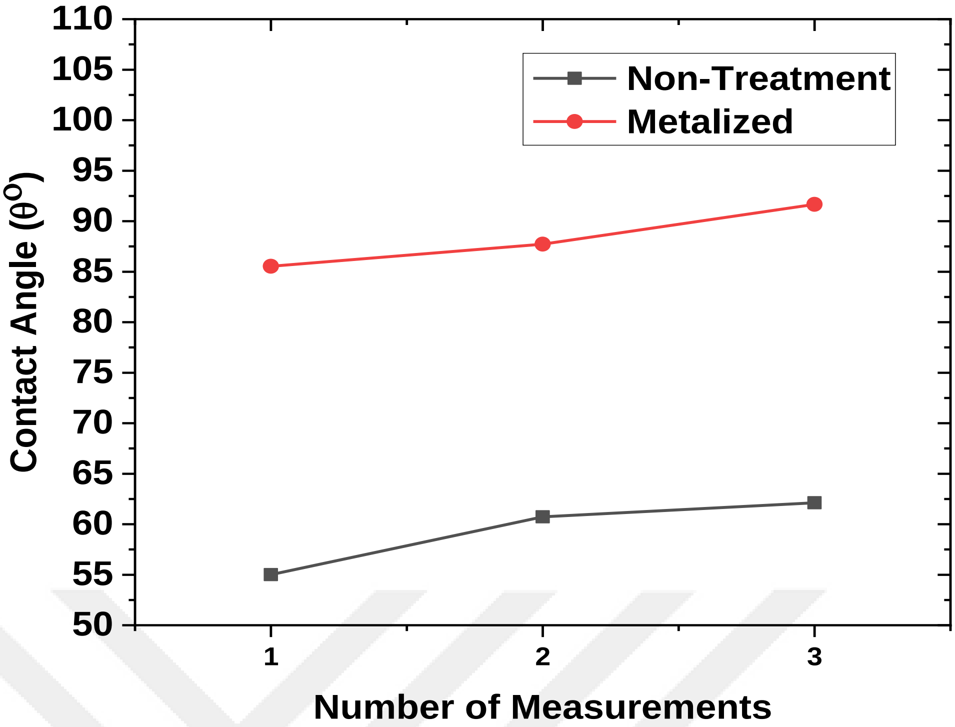

Figure 4.97. Contact angle measurement of plasma and Cu coated plasma samples

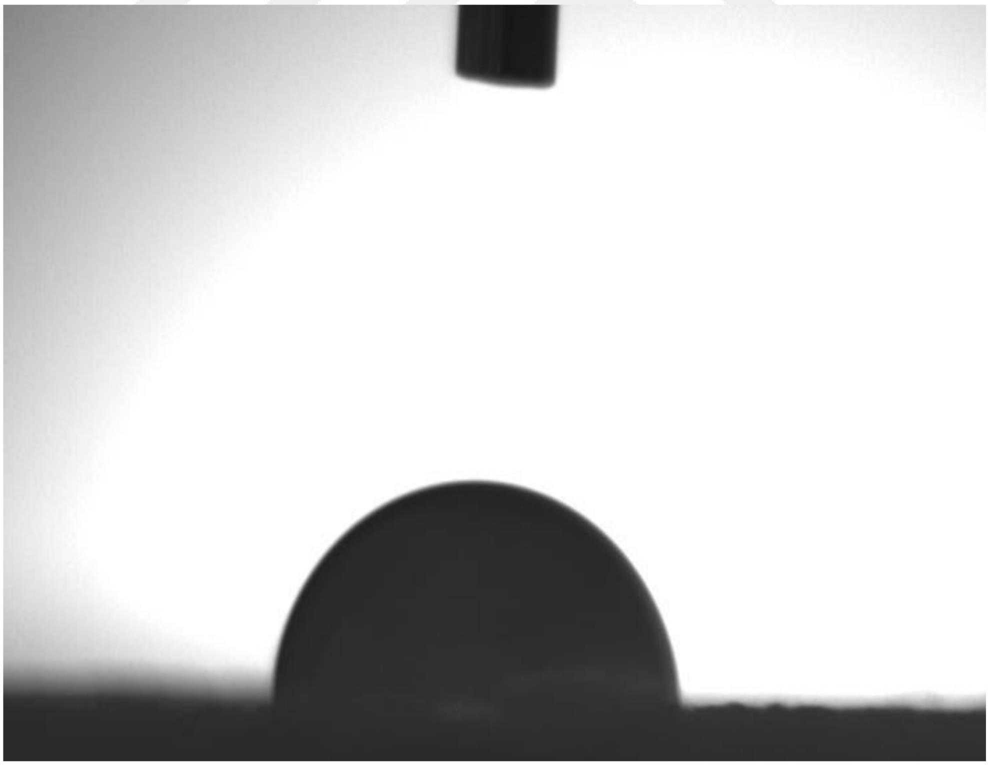

Figure 4.98. Contact angle measurement of abrasion samples

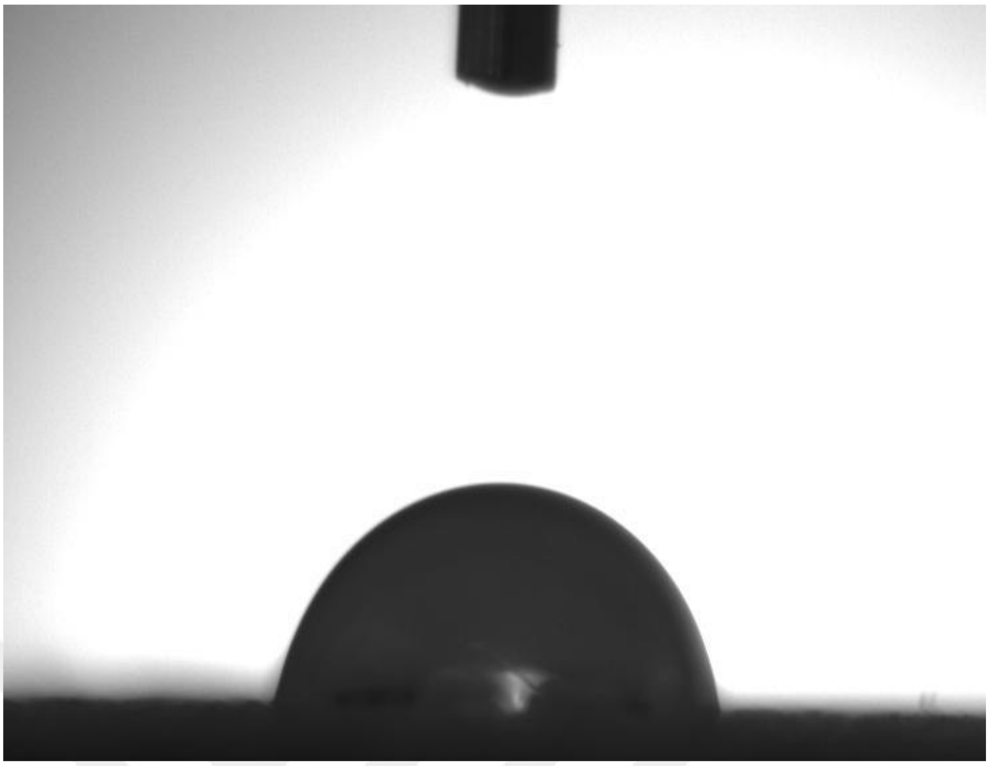

Figure 4.99. Contact angle measurement of Cu coated abrasion samples

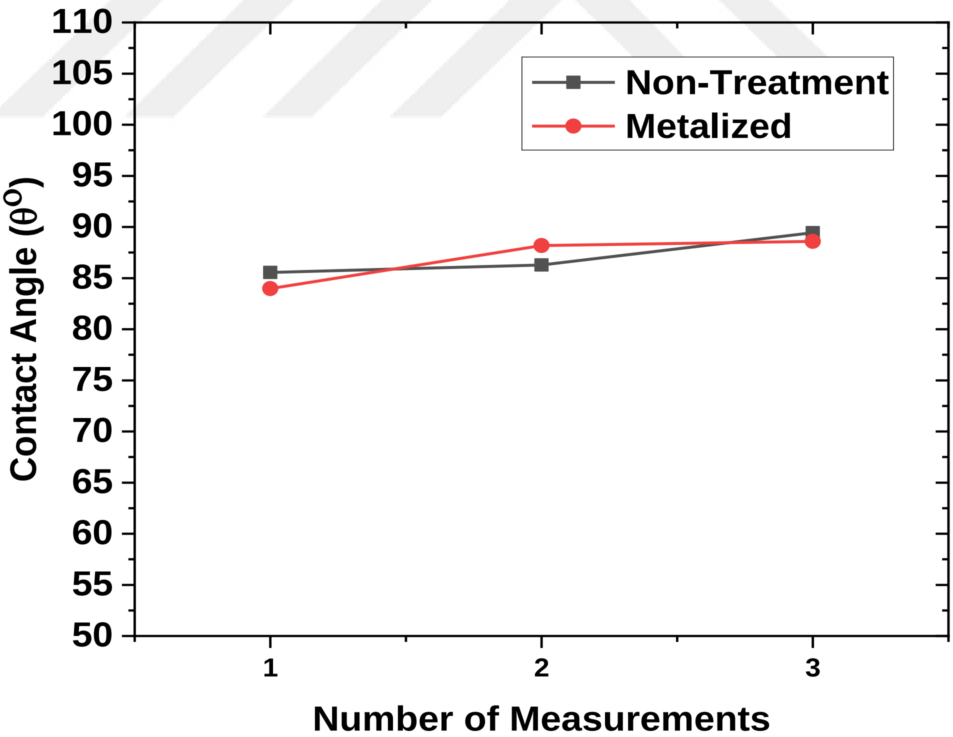

Figure 4.100. Contact angle measurement of abrasion and Cu coated abrasion samples

4.7. Electrical Resistance Measurement

The electrical resistances and calculated conductivities of 3D-printed polymer structures are provided in Figure 4.101 and Table 4.11. Equation 1 was used to calculate the electrical conductivity (σ) values, where ρ is the specific electrical resistance, L is the length, R is the electrical resistance in ohm (Ω), w is the width, and t is the film thickness. Previous studies have indicated that PLA material exhibits conductivity below the range of 10^{-16} S/cm, making it an insulating material. It has been reported to have excellent and superior insulating properties when compared to other petroleum-derived materials at room temperature, demonstrating high electrical resistance.

$$\sigma = \frac{1}{\rho} = \frac{L}{Rwt} \quad (1)$$

Surface coatings' electrical resistance is inversely proportional to electron mobility, therefore, the lower the resistance, the higher the conductivity. The electrical properties of thin aluminium films depend highly on thickness when in the nanometer range (Bragaglia et al., 2022). With the metallization process, the electrical properties of 3D-printed PLA polymer structures have significantly improved depending on the coating thickness. The metallization of 3D-printed polymer structures is a promising method for electrical conductivity compared to traditional polymer metallization methods such as acid etching and material extrusion with conductive filaments (Akin et al., 2023; Quan et al., 2012; Oi et al., 2012).

In physiological environments, the electrical conductivity is affected by the corrosion that occurs in aluminium. In physiological environments, organisms have a tendency to adhere to and grow on the surface of aluminium material. This results in the formation of a biological film or biofilm. Biofilms formed on the surface of almost all structural metals and alloys in liquid environment have the capacity to affect the corrosion of these metals and alloys. This effect arises from the ability of organisms to modify environmental variables such as oxidative power, temperature, speed, and concentration. Corrosion causes non-conductive surfaces that affect the electrical performance of the material. However, there is an advantage to this in aluminium materials. When aluminium comes into contact with oxygen, an oxide layer forms on its surface. The XRD results in our study show the oxide layer formed on the surface. This layer acts as a protective barrier in preventing the material from further corrosion. Thanks to this barrier, it is believed that the coating material will maintain its electrical conductivity by protecting the internal structure even if an oxide layer forms on the surface in the external environment [Davis, 1999].

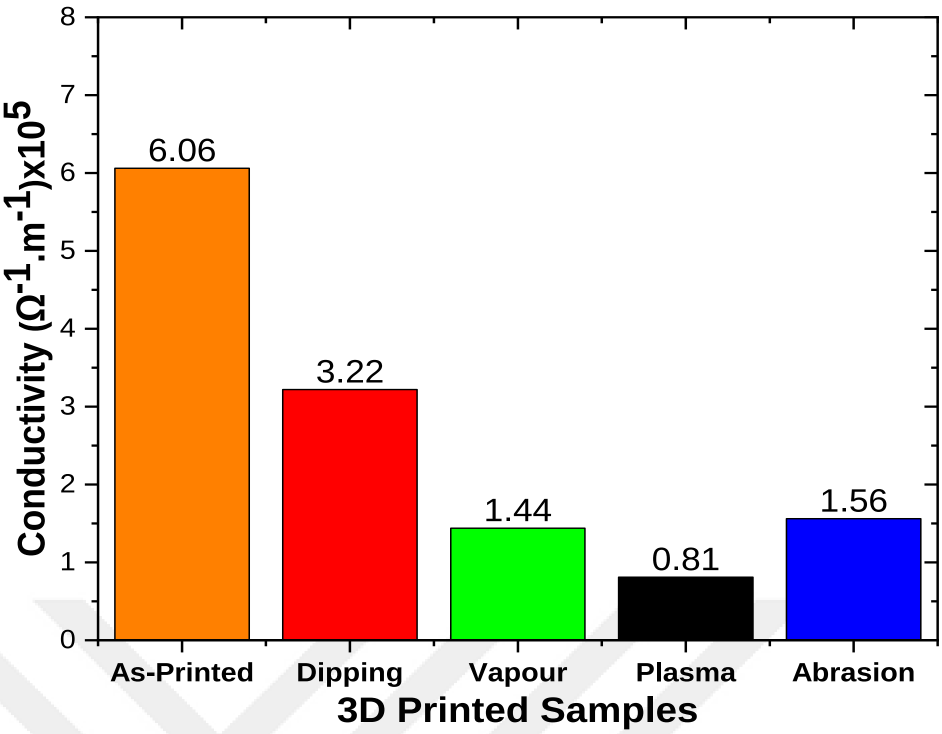

Figure 4.101. Electrical conductivity values of Al coated samples

Table 4.11. Electrical conductivity values of Al coated samples

Specimen	Thickness (m)	Width (m)	Length (m)	Resistance (Ω)	Conductivity $\Omega^{-1}.m^{-1}$
As-Printed	1x10^{-6}	2x10^{-2}	2x10^{-2}	1.65	6.06x10^{5}
Dipping	1x10^{-6}	2x10^{-2}	2x10^{-2}	3.10	3.22x10^{5}
Vapour	1x10^{-6}	2x10^{-2}	2x10^{-2}	6.90	1.44x10^{5}
Plasma	1x10^{-6}	2x10^{-2}	2x10^{-2}	12.20	0.81x10^{5}
Abrasion	1x10^{-6}	2x10^{-2}	2x10^{-2}	6.40	1.56x10^{5}

The electrical resistance measurement results of the polymer structures after copper coating are presented in Figure 4.102 and Table 4.12. Equation 1 was used to calculate the electrical resistance values, where ρ is the specific electrical resistance, L is the length (m), R is the electrical resistance (Ω), w is the width (m), and t is the film thickness (Xie et al., 2024). When looking at the electrical conductivity values, approximately a 50% increase was observed in the specimens treated with dichloromethane vapour surface treatment. Electrical resistance of PLA is 1×10^{12} Ω/m². The electrical conductivity of PLA structures alone is quite low. The copper film coatings applied demonstrate that, due to copper's excellent electrical conductivity, they can facilitate the formation of conductive pathways, thus promoting charge distribution on the polymer structure's surface

(Yang et al., 2019). Additionally, this improvement in conductivity levels is believed to stem from the dense and continuously extending microstructures such as micro-porous observed in SEM images. The varying levels of conductivity in different surface treatments may be attributed to incomplete coverage of the coatings on the coated polymer structures. During coating, the growth of copper films leads to a more compact grain packing. This reduces the electron transfer barrier (Zhang et al., 2019; Liao and Kao, 2012; Zabetakis et al., 2009].

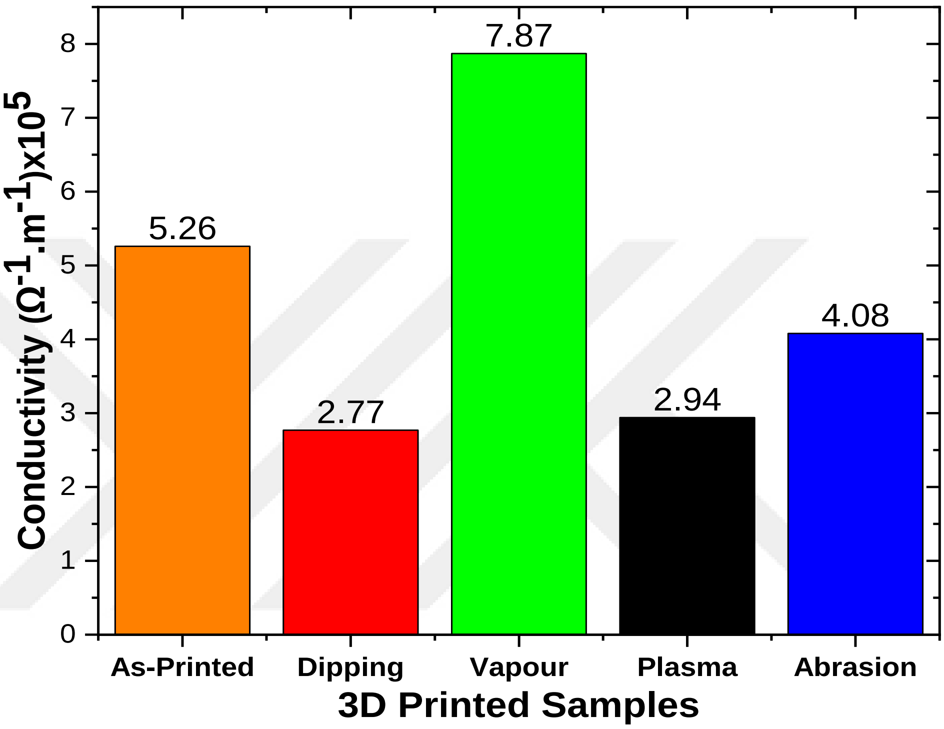

Figure 4.102. Electrical conductivity values of Cu coated samples

Table 4.12. Electrical conductivity values of Cu coated samples

Specimen	Thickness (m)	Width (m)	Length (m)	Resistance (Ω)	Conductivity $\Omega^{-1}.m^{-1}$
As-Printed	$1x10^{-6}$	$2x10^{-2}$	$2x10^{-2}$	1.90	$5.26x10^{5}$
Dipping	$1x10^{-6}$	$2x10^{-2}$	$2x10^{-2}$	3.60	$2.77x10^{5}$
Vapour	$1x10^{-6}$	$2x10^{-2}$	$2x10^{-2}$	1.27	$7.87x10^{5}$
Plasma	$1x10^{-6}$	$2x10^{-2}$	$2x10^{-2}$	3.40	$2.94x10^{5}$
Abrasion	$1x10^{-6}$	$2x10^{-2}$	$2x10^{-2}$	2.45	$4.08x10^{5}$

4.8. Ellipsometry Analysis

The change of refraction index and extinction coefficient of the Al coated specimens were given in Figure 4.103 and 4.104. The sensitivity of noise in emerging optical constants is believed to be associated. There is a strong correlation between optical constants and surface processes. This correlation can be demonstrated by repeating the -nk match with different surface processes. Increasing film thickness is thought to carry the features caused by thickness to longer wavelengths. Thicker films have more maxima and minima points compared to thin films. A resonant combination can occur between film thickness and wavelength in thick surface films. Aluminium film coatings are crucial for the semiconductor industry and are widely used (Hilfiker et al., 2017; Tompkins and Hilfiker, 2015; Tompkins and McGahan, 1999).

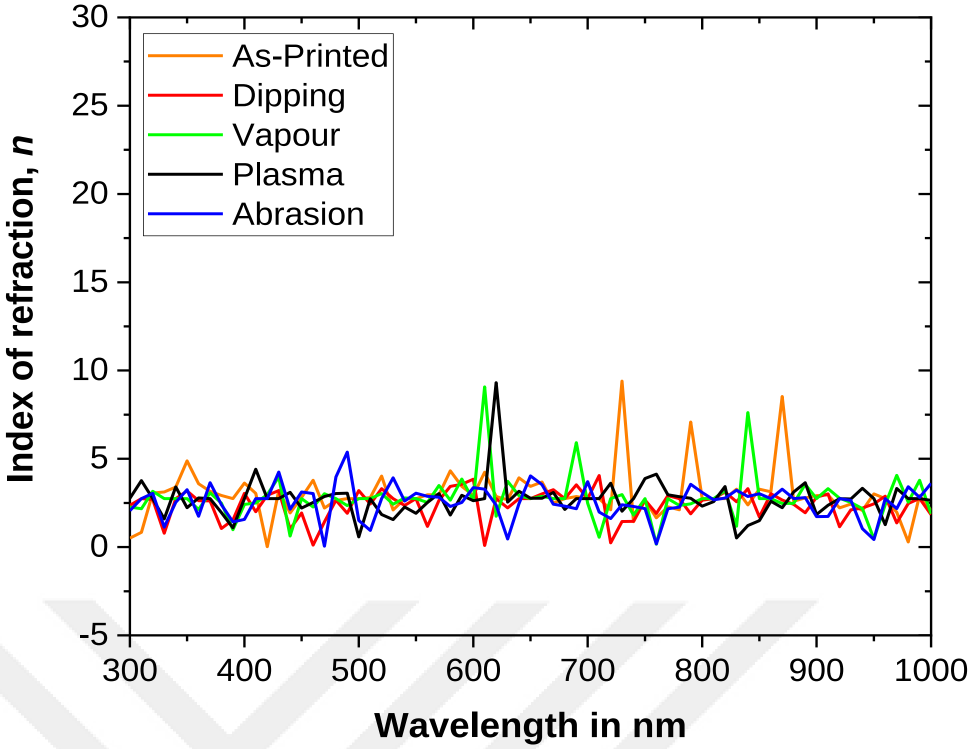

Figure 4.103. Refraction index of Al coated samples

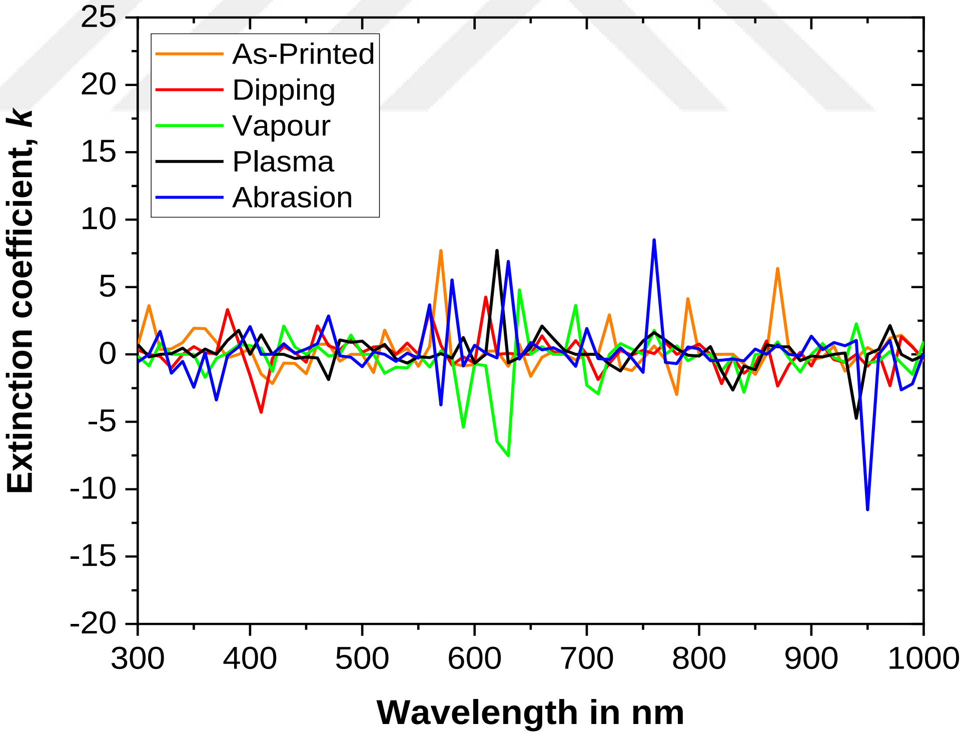

Figure 4.104. Extinction coefficient of Al coated samples

The ellipsometer analysis results of the polymer structures after Cu coating are presented in Figure 4.105 and Figure 4.106. Ellipsometer analysis has been applied as a standard technique in microelectronics since the 1960s for determining film thicknesses and optical constants.

Ellipsometer analysis is recommended as a suitable and powerful inspection technique for copper layers. It is known to be highly sensitive and non-destructive to the surface (Haidu et al., 2012). Ellipsometer analysis can be highly effective in predicting the plasmonic properties of metallic thin films, and specially designed films can be created for various applications such as plasmonic chips, solar cells, optical limiters, and surface-enhanced Raman scattering (SERS) substrates (Kesarwani and Khare, 2019). The refractive index n is related to the phase velocity. At an interface between two materials, the difference in refractive index determines both the direction of transmitted light and the division of light amplitudes between reflection and transmission. The extinction coefficient k is related to the absorption of light as it passes through a material (Fujiwara and Collins, 2018). It is assumed that the measured deviations are due to surface roughness effects of 3D printed polymer structures and some variations in film thickness (Schmiedova et al., 2015). Rapid fluctuations in the values of the refraction index and extinction coefficient are thought to originate from the thickness of the copper film (Hu et al., 2000). Additionally, reaching micron-level thicknesses with copper films may lead to the coating behaving like a substrate material (Srivatsa and Ygartua, 1999). Moreover, the surface roughness of the coated polymer structures also contributes to these fluctuations. This is because surface roughness causes non-specular reflection of incoming light. Additionally, the surface roughness of the sample leads to depolarization of the reflected light beam (Tompkins and McGahan, 1999). These fluctuations do not pose a problem for practical applications. This is because it is well known that surface roughness improves the adhesion between the coating and the substrate material. The coatings applied at the micron level allow also the material to achieve high performance and an aesthetically pleasing appearance (White et al., 2018).

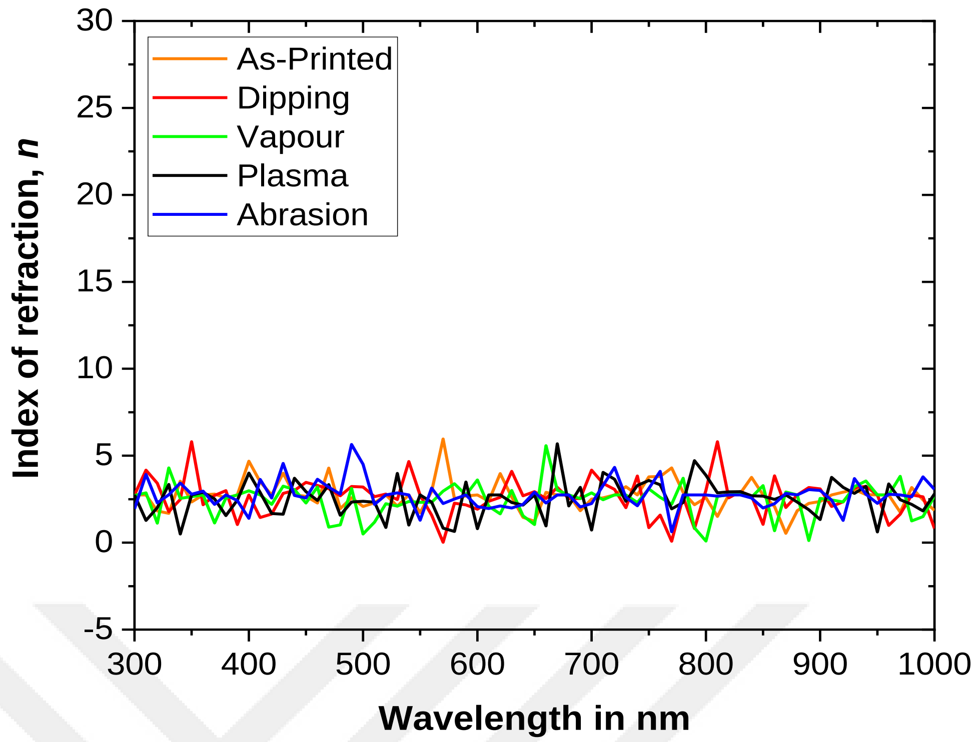

Figure 4.105. Refraction index of Cu coated samples

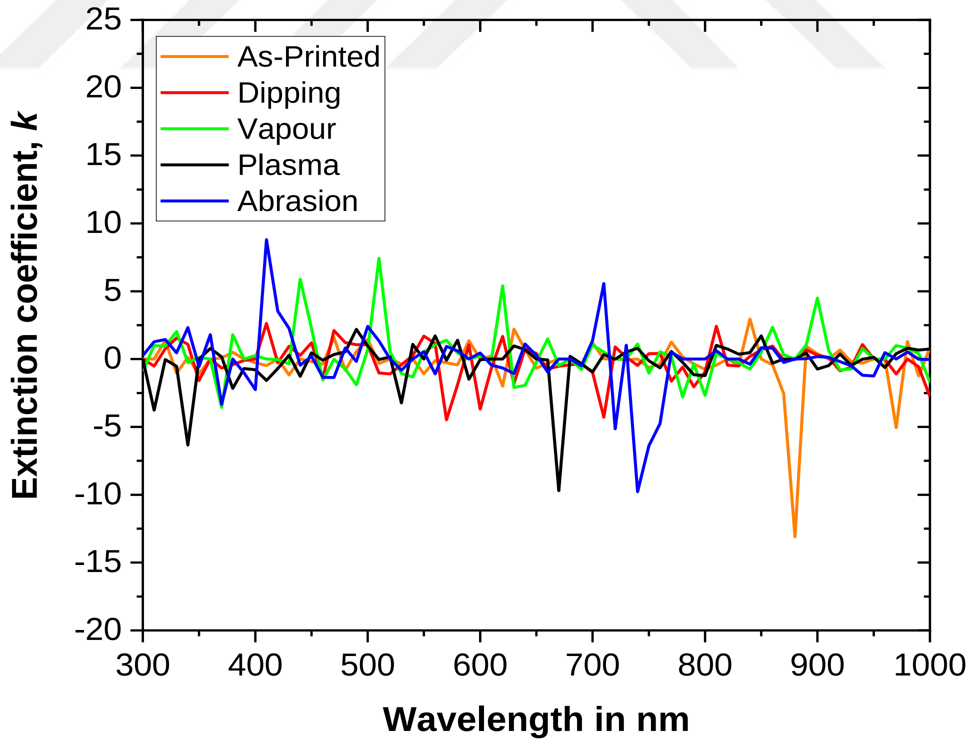

Figure 4.106. Extinction coefficient of Cu coated samples

5. CONCLUSIONS

The aim of this thesis is to enhance the morphological, structural, optical and electrical attributes of polymer structures produced using additive manufacturing, also known as 3D printing technology. In order to achieve this, an investigation was conducted into the process of coating the surfaces of polymer structures with aluminium and copper metallic thin films, i.e. metallization of polymers. FDM technology and PLA as filament material were selected for the production of 3D polymer structures. In order to ensure optimum surface quality and to enhance the functionality of the post-coating metallised samples for a range of structural applications, five different surface treatments were applied to the surfaces of the polymer structures prior to metallization. These included as-printed, dipping, vapour, plasma, and abrasion. Subsequently, aluminium and copper thin film coatings with a film thickness of 1000 nm were formed on the surfaces of the polymer structures via the physical vapour deposition technique of sputter deposition. The morphological, structural, optical, and electrical properties of the metallised 3D polymer structures were investigated by a comprehensive range of analytical techniques, including scanning electron microscopy (SEM), energy dispersive spectrum (EDS) analysis, atomic force microscopy (AFM), X-ray diffraction (XRD) analysis, Fourier transform infrared spectroscopy (FT-IR) analysis, ultraviolet-visible light and near infrared (UV-VIS-NIR) analysis, contact angle measurement, ellipsometry analysis, and electrical resistivity measurement.

Upon examination of the SEM images, it became evident that the layer lines resulting from the layer-by-layer production of polymer structures were no longer discernible in the samples that underwent dipping and vapour surface treatment prior to metallization. Furthermore, it was noted that the surface roughness exhibited a notable improvement in these surface treatments. Following the aluminium coating, a ripple-like surface morphology was identified in the samples treated with steam surface treatment. This was attributed to the considerable disparity in the coefficient of thermal expansion between aluminium and PLA. It was noted that the surface morphology of the samples subjected to vapour surface treatment after copper coating was predominantly smooth, and delamination caused by cohesive forces between the polymer substrate material and the coating material was observed. The EDS analysis confirms the presence of localised polymer regions in all metallised samples, with the presence of significant amounts of carbon elements. Furthermore, the EDS analysis results demonstrate the presence of aluminium and copper elements on the polymer surface. AFM images revealed the presence of a needled surface structure in the samples that had undergone plasma surface treatment prior to metallization. Following the application of an aluminium coating, the formation of surface wrinkles, resulting from the stress relief mechanism, was observed in all samples. In the case of the coated copper samples, the plasma surface treatment of the polymer structures gave rise to a surface topography that resulted in the degradation of a greater quantity of polymer products, which combined to form irregularly shaped large droplets, dependent on the power and duration of the plasma. Upon examination of the XRD analysis results for aluminium coatings, the dominant characteristic diffraction peak was observed to occur at 38.380°, 44.162°, 64.928°, 78.014°, and 82.204°. These peaks can be attributed to the crystal planes (111), (200), (220), (311), and (222), respectively. The dominant characteristic diffraction peak of the copper coatings is located at 43.14°, 50.09°, 73.93°, and 89.50°. These peaks can be attributed to the crystal planes (111), (200), (220), and (311), respectively. Prior to metallization, FT-IR analysis revealed the presence of four principal peaks within the polymer structures. The peak with a wavelength of approximately 1750 cm-1 is attributed to the C = O bond, while the peak with a wavelength of around 1078-1180 cm-1 is associated with the C - O bond. The peak with a wavelength of 1450-1380 cm-1 corresponds to the C - O - H bond, while the peak with a wavelength of about 3000 cm-1 corresponds to the C - H bond. Following metallization, although the substrate material is identical across all samples, the FT-IR spectra demonstrate variations due to chemical alterations on the surface of the polymer samples. Prior to metallization, the contact angles of the polymer structures were observed to be 76.710°, 79.133°, 77.775°, 59.282°, and 87.098° for the samples that had undergone surface treatments by the methods of as-printed, dipping, vapour, plasma, and abrasion, respectively. Following the application of the same surface treatments, the contact angles after aluminium coating were observed to be 87.263°, 68.716°, 78.679°, 91.728°, and 92.446°. Subsequently, the contact angles after copper coating were 78.570°, 80.314°, 75.974°, 88.309°, and 86.914°, respectively. At a thickness of 1000 nm, the electrical conductivity values for aluminium and copper thin films were $6.6x10^5$ S/m and $7.87x10^5$ S/m, respectively. The results of the ellipsometry analysis suggest that the rapid fluctuations in refractive index and extinction coefficient values are attributed to the thickness and surface roughness of the thin metallic film.

The metallization of 3D-printed polymer structures has the potential to provide solutions for a multitude of applications across various sectors, including aerospace, space, electrical, and electronics, automotive, medical, military, marine, and art. To illustrate, copper coatings can be employed in the fabrication of space research equipment and electromagnetic shielding in the aerospace industry, circuit boards, antennas, and electrochemical sensors in electronics, and control units, contact elements, door handles, emblems, and front grilles in automotive applications. Examples of applications where aluminium coatings are already used include the coating of steels for solar concentrating technology in the electricity sector, corrosion protection in marine applications and energy absorbing structures in the energy field. The metallization process thus combines the unique advantages of polymer, metal and additive manufacturing technology.

It is believed that this thesis study will provide researchers with insights for many future studies. Considering the results obtained, it is possible to combine different material properties in the final product by applying different metal, polymer, and ceramic coatings to polymer, metal, ceramic, and composite structures produced by additive manufacturing technologies. The metallization process can be applied to 3D polymer structures produced using commonly used polymer filaments such as ABS, PC, PA, ULTEM, PS, PE, PPSF, PP, PEI, TPU, PVA, and PEEK and compatible combinations of these filaments. In addition to metal coatings, ceramic coatings on the surfaces of polymer structures have become the focus of interest for many researchers in recent years due to the properties of ceramics such as high wear and corrosion resistance, high hardness, high melting point, and low thermal conductivity. In addition to the use of 3D printed polymer substrates, 3D printed metal substrates can also be considered for coating studies due to the advantages of metals. Currently, materials such as 316L, AlSi10Mg, Inconel 718, Ti6Al4V, and CuSn10 are widely used to successfully produce metallic structures using additive manufacturing techniques. By coating these structures with different polymers and ceramics, different materials can be developed for the required applications. Finally, studies of ceramic materials such as Al_2O_3, ZrO_2, and SiO_2 can be intensified. This is because additive manufacturing technology has made it possible to produce ceramic structures in complex shapes.

REFERENCES

Abdulkareem, A., Kasak, P., Nassr, M. G., Mahmoud, A. A., Al-Ruweidi, M. K. A., Mohamoud, K. J., Hussein, M. K., & Popelka, A. (2021). Surface modification of poly (lactic acid) film via cold plasma assisted grafting of fumaric and ascorbic acid. *Polymers*, *13*(21), 3717.

Afshar, A., & Mihut, D. (2020). Enhancing durability of 3D printed polymer structures by metallization. *Journal of Materials Science & Technology*, *53*, 185-191.

Afshar, A., Mihut, D., Baqersad, J., & Hill, S. (2019). Study of metallic thin films on epoxy matrix as protective barrier to ultraviolet radiation. *Surface and Coatings Technology*, *367*, 41-48.

Akin, S., Nath, C., & Jun, M. B. G. (2023). Selective Surface Metallization of 3D-Printed Polymers by Cold-Spray-Assisted Electroless Deposition. *ACS Applied Electronic Materials*, *5*(9), 5164-5175.

Alami, A. H., Allagui, A., & Alawadhi, H. (2014). Microstructural and optical studies of CuO thin films prepared by chemical ageing of copper substrate in alkaline ammonia solution. *Journal of alloys and compounds*, *617*, 542-546.

Amirshaqaqi, N., Salami-Kalajahi, M., & Mahdavian, M. (2014). Investigation of corrosion behavior of aluminum flakes coated by polymeric nanolayer: Effect of polymer type. *Corrosion Science*, *87*, 392-396.

Arias, N., & Jaramillo, F. (2020). Highly reflective aluminum films on polycarbonate substrates by physical vapor deposition. *Applied Surface Science*, *505*, 144596.

Bachiller, C., Nova, V., Ferrer, Á., Martínez, A., Sandoval, N., Marín, M. L., & Ponce-González, L. N. (2023). Additive manufacturing and metallization of high-frequency communication devices. *Progress in Additive Manufacturing*, *8*(1), 3-8.

Baligidad, S. M., Kumar, G. C., Maharudresh, A. C., & Elangovan, K. (2021). Experimental investigations on metallization in laser-sintered PA12 part using RF sputtering. *Applied Physics A*, *127*(7), 510.

Baligidad, S. M., Lakshmi, I. C., Kumar, G. C., Maharudresh, A. C., Pillai, R., & Elangovan, K. (2021). Study on the Morphological and Flexural Properties of RF Sputtered Copper Thin Film for PA12 Part. *Journal of The Institution of Engineers (India): Series C*, *102*(4), 1059-1071.

Baptista, A., Silva, F., Porteiro, J., Míguez, J., & Pinto, G. (2018). Sputtering physical vapour deposition (PVD) coatings: A critical review on process improvement and market trend demands. *Coatings*, *8*(11), 402.

Behera, A., Aich, S., & Theivasanthi, T. (2022). Magnetron sputtering for development of nanostructured materials. In *Design, Fabrication, and Characterization of Multifunctional Nanomaterials* (pp. 177-199). Elsevier.

Bhuiyan, M. E. H., Behroozfar, A., Daryadel, S., Moreno, S., Morsali, S., & Minary-Jolandan, M. (2019). A hybrid process for printing pure and high conductivity nanocrystalline copper and nickel on flexible polymeric substrates. *Scientific reports*, *9*(1), 19032.

Bikas, H., Stavropoulos, P., & Chryssolouris, G. (2016). Additive manufacturing methods and modelling approaches: a critical review. *The International Journal of Advanced Manufacturing Technology*, *83*, 389-405.

Blakey-Milner, B., Gradl, P., Snedden, G., Brooks, M., Pitot, J., Lopez, E., Leary, M., Berto, F., & Du Plessis, A. (2021). Metal additive manufacturing in aerospace: A review. *Materials & Design*, *209*, 110008.

Boparai, K. S., Singh, R., & Singh, H. (2016). Development of rapid tooling using fused deposition modeling: a review. *Rapid Prototyping Journal*, *22*(2), 281-299.

Bragaglia, M., Pascale, V., Rinaldi, M., & Nanni, F. (2022). Silver electroless plating on 3D printed resins via stereolithography: A sustainable solution. *Thin Solid Films*, *757*, 139417.

Chen, D., & Kang, Z. (2017). ABS plastic metallization through UV covalent grafting and layer-by-layer deposition. *Surface and Coatings Technology*, *328*, 63-69.

Chen, Y., Liang, S., He, W., Wang, S., Wang, C., Du, Z., Du, Y., Yang, W., Liu, B., & Hong, Y. (2023). UV-induced graft polymerization of polyamide-6 for electroless copper deposition. *Applied Surface Science*, *639*, 158178.

Cheng, C., Liye, Z., & Zhan, R. J. (2006). Surface modification of polymer fibre by the new atmospheric pressure cold plasma jet. *Surface and Coatings Technology*, *200*(24), 6659-6665.

Credi, C., Bernasconi, R., Levi, M., & Magagnin, L. (2023). Self-activating metal-polymer composites for the straightforward selective metallization of 3D printed parts by stereolithography. *journal of materials research and technology*, *22*, 1855-1867.

Cucchi, I., Boschi, A., Arosio, C., Bertini, F., Freddi, G., & Catellani, M. (2009). Bio-based conductive composites: Preparation and properties of polypyrrole (PPy)-coated silk fabrics. *Synthetic metals*, *159*(3-4), 246-253.

Davis, J. R. (Ed.). (1999). *Corrosion of aluminum and aluminum alloys*. Asm International.

Deng, Y., Chen, W., Li, B., Wang, C., Kuang, T., & Li, Y. (2020). Physical vapor deposition technology for coated cutting tools: A review. *Ceramics International*, *46*(11), 18373-18390.

Dhinakaran, V., Kumar, K. M., Ram, P. B., Ravichandran, M., & Vinayagamoorthy, M. (2020). A review on recent advancements in fused deposition modeling. *Materials today: proceedings*, *27*, 752-756.

Dixit, N. K., Srivastava, R., & Narain, R. (2017). Electroless metallic coating on plastic parts produced by rapid prototyping technique. *Materials Today: Proceedings*, *4*(8), 7643-7653.

Equbal, A., & Sood, A. K. (2015). Investigations on metallization in FDM build ABS part using electroless deposition method. *Journal of Manufacturing Processes*, *19*, 22-31.

Farahmandjou, M., & Golabiyan, N. (2015). New pore structure of nano-alumina (Al2O3) prepared by sol gel method. *Journal of Ceramic Processing Research*, *16*(2), 1-4.

Fontanot, T., Audenaert, J., Hanselaer, P., Pecorari, I., Lughi, V., Vesselli, E., Paroni, S., & Leloup, F. B. (2020). BRDF characterization of Al-coated thermoplastic polymer surfaces. *Journal of Coatings Technology and Research*, *17*, 1195-1205.

Frazier, W. E. (2014). Metal additive manufacturing: a review. *Journal of Materials Engineering and performance*, *23*, 1917-1928.

Fujiwara, H., & Collins, R. W. (Eds.). (2018). *Spectroscopic ellipsometry for photovoltaics* (Vol. 1). Cham: Springer.

Ge, J., Turunen, M. P. K., & Kivilahti, J. K. (2003). Surface modification of a liquid-crystalline polymer for copper metallization. *Journal of Polymer Science Part B: Polymer Physics*, *41*(6), 623-636.

Guanhong, S., Xiaodong, H., Jiuxing, J., & Yue, S. (2011). Parametric study of Al and Al2O3 ceramic coatings deposited by air plasma spray onto polymer substrate. *Applied Surface Science*, *257*(17), 7864-7870.

Guo, R. H., Jiang, S. Q., Yuen, C. W. M., & Ng, M. C. F. (2009). An alternative process for electroless copper plating on polyester fabric. *Journal of Materials Science: Materials in Electronics*, *20*, 33-38.

Haidu, F., Gordan, O. D., & Zahn, D. R. (2012). In situ ellipsometric study of copper growth on silicon. *Thin Solid Films*, *520*(13), 4410-4417.

Hebbar, R. S., Isloor, A. M., & Ismail, A. F. (2017). Contact angle measurements. In *Membrane characterization* (pp. 219-255). Elsevier.

Hilfiker, J. N., Stadermann, M., Sun, J., Tiwald, T., Hale, J. S., Miller, P. E., & Aracne-Ruddle, C. (2017). Determining thickness and refractive index from free-standing ultra-thin polymer films with spectroscopic ellipsometry. *Applied Surface Science*, *421*, 508-512.

Hu, Y. Z., Sharangpani, R., & Tay, S. P. (2000). Kinetic investigation of copper film oxidation by spectroscopic ellipsometry and reflectometry. *Journal of Vacuum Science & Technology A: Vacuum, Surfaces, and Films*, *18*(5), 2527-2532.

Huang, S. H., Liu, P., Mokasdar, A., & Hou, L. (2013). Additive manufacturing and its societal impact: a literature review. *The International journal of advanced manufacturing technology*, *67*, 1191-1203.

Jachowicz, M. (2021). Properties of thin coatings deposited by physical vapour deposition on safety helmets. *International journal of occupational safety and ergonomics*, *27*(1), 55-62.

Jaidev, L. R., & Chatterjee, K. (2019). Surface functionalization of 3D printed polymer scaffolds to augment stem cell response. *Materials & Design*, *161*, 44-54.

Jayakumar, N., Arumugam, H., & Albert Selvaraj, A. D. (2024). Mechanical behaviour of the post processed 3D printed PLA parts using polar and non-polar solvents. *Polymer Bulletin*, *81*(5), 4257-4274.

Ji, E. S., Cha, H. G., Kim, C. W., & Kang, Y. S. (2008). Copper metallization on the surface-modified polyimide films by electroless plating method. *Molecular Crystals and Liquid Crystals*, *492*(1), 275-639.

Jiang, P., Ji, Z., Yan, C., Wang, X., & Zhou, F. (2018). High compressive strength metallic architectures prepared via polyelectrolyte-brush assisted metal deposition on 3D printed lattices. *Nano-Structures & Nano-Objects*, *16*, 420-427.

Jin, Y., Wan, Y., & Liu, Z. (2017). Surface polish of PLA parts in FDM using dichloromethane vapour. In *MATEC Web of Conferences* (Vol. 95, p. 05001). EDP Sciences.

Jin, Y., Wan, Y., Zhang, B., & Liu, Z. (2017). Modeling of the chemical finishing process for polylactic acid parts in fused deposition modeling and investigation of its tensile properties. *Journal of Materials Processing Technology*, *240*, 233-239.

Johansson, B. L., Larsson, A., Ocklind, A., & Öhrlund, Å. (2002). Characterization of air plasma-treated polymer surfaces by ESCA and contact angle measurements for optimization of surface stability and cell growth. *Journal of applied polymer science*, *86*(10), 2618-2625.

Jordá-Vilaplana, A., Fombuena, V., García-García, D., Samper, M. D., & Sánchez-Nácher, L. (2014). Surface modification of polylactic acid (PLA) by air atmospheric plasma treatment. *European polymer journal*, *58*, 23-33.

Joseph, T. M., Kallingal, A., Suresh, A. M., Mahapatra, D. K., Hasanin, M. S., Haponiuk, J., & Thomas, S. (2023). 3D printing of polylactic acid: recent advances and opportunities. *The International Journal of Advanced Manufacturing Technology*, *125*(3), 1015-1035.

Juarez, T., Schroer, A., Schwaiger, R., & Hodge, A. M. (2018). Evaluating sputter deposited metal coatings on 3D printed polymer micro-truss structures. *Materials & Design*, *140*, 442-450.

Junkar, I., Vesel, A., Cvelbar, U., Mozetič, M., & Strnad, S. (2009). Influence of oxygen and nitrogen plasma treatment on polyethylene terephthalate (PET) polymers. *Vacuum*, *84*(1), 83-85.

Juřík, P., Michaljaničová, I., Slepička, P., Kolskáa, Z., & Švorčík, V. (2017, November). Surface changes of poly-L-lactic acid due to annealing. In *Journal of Physics: Conference Series* (Vol. 917, No. 9, p. 092007). IOP Publishing.

Kariž, M., Tomec, D. K., Dahle, S., Kuzman, M. K., Šernek, M., & Žigon, J. (2021). Effect of sanding and plasma treatment of 3D-printed parts on bonding to wood with PVAc adhesive. *Polymers*, *13*(8), 1211.

Károly, Z., Kalácska, G., Zsidai, L., Mohai, M., & Klébert, S. (2018). Improvement of adhesion properties of polyamide 6 and polyoxymethylene-copolymer by atmospheric cold plasma treatment. *Polymers*, *10*(12), 1380.

Kesarwani, R., & Khare, A. (2019). Assessment of interfacial layer thickness of pulsed laser deposited plasmonic copper thin films via spectroscopic ellipsometer. *Optical Materials*, *93*, 98-102.

Khan, M. S., Mishra, S. B., Kumar, M. A., & Banerjee, D. (2018). Optimizing surface texture and coating thickness of nickel coated ABS-3D parts. *Materials Today: Proceedings*, *5*(9), 19011-19018.

Khorasani, M. T., Mirzadeh, H., & Irani, S. (2008). Plasma surface modification of poly (l-lactic acid) and poly (lactic-co-glycolic acid) films for improvement of nerve cells adhesion. *Radiation Physics and Chemistry*, *77*(3), 280-287.

Kołczyk, K., Zborowski, W., Kutyła, D., Kwiecińska, A., Kowalik, R., & Żabiński, P. (2018). Investigation of two-step metallization process of plastic 3D prints fabricated by SLA method. *Archives of Metallurgy and Materials*, *63*.

Lackner, J. M., Waldhauser, W., Ganser, C., Teichert, C., Kot, M., & Major, L. (2014). Mechanisms of topography formation of magnetron-sputtered chromium-based coatings on epoxy polymer composites. *Surface and Coatings Technology*, *241,* 80-85.

Lavecchia, F., Guerra, M. G., & Galantucci, L. M. (2022). Chemical vapor treatment to improve surface finish of 3D printed polylactic acid (PLA) parts realized by fused filament fabrication. *Progress in Additive Manufacturing*, 1-11.

Lee, S. H., Park, I. S., Seo, B. H., Seo, J. H., Choe, H., Jeon, J. H., Lee, Y. U., & Hong, M. (2011). Effect of sputtering parameters on the adhesion force of copper/molybdenum metal on polymer substrate. *Current Applied Physics*, *11*(5), S12-S15.

Liao, Y. C., & Kao, Z. K. (2012). Direct writing patterns for electroless plated copper thin film on plastic substrates. *ACS applied materials & interfaces*, *4*(10), 5109-5113.

Lin, Y. S., Liu, H. M., & Tsai, C. W. (2005). Nitrogen plasma modification on polyimide films for copper metallization on microelectronic flex substrates. *Journal of Polymer Science Part B: Polymer Physics*, *43*(15), 2023-2038.

Liu, F., Xie, D., Jiao, C., Bai, D., Wu, H., Shen, L., Tian, Z., & Zhao, J. (2022). Selective metallization on additive manufactured polymer for fabrication of integrated device. *Journal of Materials Science*, *57*(2), 1506-1515.

Liu, J., He, L., Wang, L., Man, Y., Huang, L., Xu, Z., Ge, D., Li, J., Liu C., & Wang, L. (2016). Significant enhancement of the adhesion between metal films and polymer substrates by UV–ozone surface modification in nanoscale. *ACS Applied Materials & Interfaces*, *8*(44), 30576-30582.

Maciąg, T., Wieczorek, J., & Kałsa, W. (2019). Surface analysis of ABS 3d prints subjected to copper plating. *Archives of Metallurgy and Materials*, *64*(2).

Małachowska, A., Winnicki, M., Konat, Ł., Piwowarczyk, T., Pawłowski, L., Ambroziak, A., & Stachowicz, M. (2017). Possibility of spraying of copper coatings on polyamide 6 with low pressure cold spray method. *Surface and Coatings Technology*, *318*, 82-89.

Mandal, P., Singh, U. P., & Roy, S. (2021, July). A Review on the effects of PVD RF sputtering parameters on rare earth oxide thin films and their applications. In *IOP Conference Series: Materials Science and Engineering* (Vol. 1166, No. 1, p. 012022). IOP Publishing.

Mehran, Q. M., Fazal, M. A., Bushroa, A. R., & Rubaiee, S. (2018). A critical review on physical vapor deposition coatings applied on different engine components. *Critical Reviews in Solid State and Materials Sciences*, *43*(2), 158-175.

Melentiev, R., Yudhanto, A., Tao, R., Vuchkov, T., & Lubineau, G. (2022). Metallization of polymers and composites: State-of-the-art approaches. *Materials & Design*, *221*, 110958.

Melentiev, R., Yu, N., & Lubineau, G. (2021). Polymer metallization via cold spray additive manufacturing: A review of process control, coating qualities, and prospective applications. *Additive manufacturing*, *48*, 102459.

Midander, K., Cronholm, P., Karlsson, H. L., Elihn, K., Möller, L., Leygraf, C., & Wallinder, I. O. (2009). Surface characteristics, copper release, and toxicity of nano-and micrometer-sized copper and copper (II) oxide particles: a cross-disciplinary study. *Small*, *5*(3), 389-399.

Mihut, D. M., Lozano, K., Tidrow, S. C., & Garcia, H. (2012). Electromagnetic interference shielding effectiveness of nanoreinforced polymer composites deposited with conductive metallic thin films. *Thin Solid Films*, *520*(21), 6547-6550.

Mohamed, O. A., Masood, S. H., & Bhowmik, J. L. (2015). Optimization of fused deposition modeling process parameters: a review of current research and future prospects. *Advances in manufacturing*, *3*, 42-53.

Momeni, M. M., Mirhosseini, M., Nazari, Z., Kazempour, A., & Hakimiyan, M. (2016). Antibacterial and photocatalytic activity of CuO nanostructure films with different morphology. *Journal of Materials Science: Materials in Electronics*, *27*, 8131-8137.

Moraczewski, K., Rytlewski, P., Malinowski, R., Tracz, A., & Żenkiewicz, M. (2015). Influence of DC plasma modification on the selected properties and the geometrical surface structure of polylactide prior to autocatalytic metallization. *Materials Chemistry and Physics*, *153*, 135-144.

Mwema, F. M., Oladijo, O. P., Akinlabi, S. A., & Akinlabi, E. T. (2018). Properties of physically deposited thin aluminium film coatings: A review. *Journal of alloys and compounds*, *747*, 306-323.

Negi, S., Dhiman, S., & Sharma, R. K. (2013). Basics, applications and future of additive manufacturing technologies: A review. *Journal of Manufacturing Technology Research*, *5*(1/2), 75.

Nigam, S., Mahapatra, S. S., & Patel, S. K. (2018). Study of various aspects of copper coating on ABS plastic by electric arc spraying. *Materials Today: Proceedings*, *5*(2), 8446-8453.

Nilsson, A. M., Jonsson, J. C., & Roos, A. (2014). Spectrophotometric measurements and ray tracing simulations of mirror light pipes to evaluate the color of the transmitted light. *Solar Energy Materials and Solar Cells*, *124*, 172-179.

Ngo, T. D., Kashani, A., Imbalzano, G., Nguyen, K. T., & Hui, D. (2018). Additive manufacturing (3D printing): A review of materials, methods, applications and challenges. *Composites Part B: Engineering*, *143*, 172-196.

Oi, T., Shinyama, K., & Fujita, S. (2012). Electrical properties of heat-treated polylactic acid. *Electrical Engineering in Japan*, *180*(1), 1-8.

Onder, O. C., Nazeer, M. A., Yilgör, E., & Yilgör, I. (2018). Spontaneous formation of microporous poly (lactic acid) coatings. *Progress in Organic Coatings*, *125*, 249-256.

Pana, I., Parau, A. C., Dinu, M., Kiss, A. E., Constantin, L. R., & Vitelaru, C. (2022). Optical properties and stability of copper thin films for transparent thermal heat reflectors. *Metals*, *12*(2), 262.

Panda, S. S., Chabra, R., Kapil, S., & Patel, V. (2020). Chemical vapour treatment for enhancing the surface finish of PLA object produced by fused deposition method using the Taguchi optimization method. *SN Applied Sciences*, *2*(5), 916.

Pedroni, M., Vassallo, E., Aloisio, M., Brasca, M., Chen, H., Firpo, G., Ghezzi, F., Morandi, S., Pietralunga, S. M., Silvetti, T., & Virgili, T. (2021). Plasma sputtered tungsten oxide thin film on poly (lactic acid) for food packaging applications. *Coatings*, *11*(11), 1281.

Pedrosa, P., Rodrigues, M. S., Neto, M. A., Oliveira, F. J., Silva, R. F., Borges, J., ... & Vaz, F. (2018). Properties of CrN thin films deposited in plasma-activated ABS by reactive magnetron sputtering. *Surface and Coatings Technology*, *349*, 858-866.

Prakash, K. S., Nancharaih, T., & Rao, V. S. (2018). Additive manufacturing techniques in manufacturing-an overview. *Materials Today: Proceedings*, *5*(2), 3873-3882.

Prasanth, D., Sibin, K. P., & Barshilia, H. C. (2019). Optical properties of sputter deposited nanocrystalline CuO thin films. *Thin Solid Films*, *673*, 78-85.

Puerta, A. P. V., Fernandez-Vidal, S. R., Batista, M., & Girot, F. (2019). Fused deposition modelling interfacial and interlayer bonding in PLA post-processed parts. *Rapid Prototyping Journal*, *26*(3), 585-592.

Qadir, M., Li, Y., & Wen, C. (2019). Ion-substituted calcium phosphate coatings by physical vapor deposition magnetron sputtering for biomedical applications: A review. *Acta biomaterialia*, *89*, 14-32.

Quan, H., Zhang, S. J., Qiao, J. L., & Zhang, L. Y. (2012). The electrical properties and crystallization of stereocomplex poly (lactic acid) filled with carbon nanotubes. *Polymer*, *53*(20), 4547-4552.

Rahmatollahpur, S., Tohidi, T., & Jamshidi-Ghaleh, K. (2010). Investigation of aluminium thin layer microstructure on BOPP polymer substrate. *Journal of materials science*, *45*, 1937-1941.

Rajan, K., Samykano, M., Kadirgama, K., Harun, W. S. W., & Rahman, M. M. (2022). Fused deposition modeling: process, materials, parameters, properties, and applications. *The International Journal of Advanced Manufacturing Technology*, *120*(3), 1531-1570.

Rani, K. V., Sarma, B., & Sarma, A. (2017). Plasma sputtering process of copper on polyester/silk blended fabrics for preparation of multifunctional properties. *Vacuum*, *146*, 206-215.

Rats, D., Hajek, V., & Martinu, L. (1999). Micro-scratch analysis and mechanical properties of plasma-deposited silicon-based coatings on polymer substrates. *Thin Solid Films*, *340*(1-2), 33-39.

Ren, Y., Xu, L., Wang, C., Wang, X., Ding, Z., & Chen, Y. (2017). Effect of dielectric barrier discharge treatment on surface nanostructure and wettability of polylactic acid (PLA) nonwoven fabrics. *Applied Surface Science*, *426*, 612-621.

Rezzoug, A., Abdi, S., Bouhelal, N., & Daoud, I. (2016). Metallic coating for carbon fiber reinforced polymer matrix composite substrate. *International Journal of Materials and Metallurgical Engineering*, *10*(1), 59-64.

Rodriguez-Hernandez, J. (2015). Wrinkled interfaces: Taking advantage of surface instabilities to pattern polymer surfaces. *Progress in Polymer Science*, *42,* 1-41.

Romani, A., Mantelli, A., Tralli, P., Turri, S., Levi, M., & Suriano, R. (2021). Metallization of thermoplastic polymers and composites 3D printed by fused filament fabrication. *Technologies*, *9*(3), 49.

Rytlewski, P., Bahners, T., Polewski, F., Gebert, B., Gutmann, J. S., Hartmann, N., Hagemann, U., & Moraczewski, K. (2017). Laser-induced surface activation of biocomposites for electroless metallization. *Surface and Coatings Technology*, *311*, 104-112.

Rytlewski, P., & Żenkiewicz, M. (2013). Applications of lasers in metallization of thermoplastic and thermosetting polymers. *Journal of Achievements in Materials and Manufacturing Engineering*, *57*(2), 59-67.

Safi, I. (2000). Recent aspects concerning DC reactive magnetron sputtering of thin films: a review. *Surface and Coatings Technology*, *127*(2-3), 203-218.

Schmiedova, V., Heinrichova, P., Zmeskal, O., & Weiter, M. (2015). Characterization of polymeric thin films for photovoltaic applications by spectroscopic ellipsometry. *Applied Surface Science*, *349*, 582-588.

Schweikart, A., & Fery, A. (2009). Controlled wrinkling as a novel method for the fabrication of patterned surfaces. *Microchimica Acta*, *165*, 249-263

Schweitzer, J., Schrodj, G., Florentin, A., Denys, E., Vidal, L., David, T., Rouillard, F., Bally, F., Spano, F., Roucoules, V., & Vonna, L. (2023). Morphology of ultrathin gold and copper coatings thermally evaporated on polydimethylsiloxane elastomers: From isolated nanoparticles to continuous coatings. *Thin Solid Films*, *781*, 139972.

Shahidi, S., Moazzenchi, B., & Ghoranneviss, M. (2015). A review-application of physical vapor deposition (PVD) and related methods in the textile industry. *The European Physical Journal Applied Physics*, *71*(3), 31302.

Siddikali, P., & Sreekanth, P. R. (2022). Performance evaluation of CNT reinforcement on electroless plating on solid free-form-fabricated PETG specimens for prosthetic limb application. *Polymers*, *14*(16), 3366.

Singh, S., Ramakrishna, S., & Singh, R. (2017). Material issues in additive manufacturing: A review. *Journal of Manufacturing Processes*, *25*, 185-200.

Slepička, P., Fidler, T., Vasina, A., & Švorčík, V. (2012). Ripple-like structure on PLLA induced by gold deposition and thermal treatment. *Materials Letters*, *79*, 4-6.

Song, A. Y., Oh, Y. A., Roh, S. H., Kim, J. H., & Min, S. C. (2016). Cold oxygen plasma treatments for the improvement of the physicochemical and biodegradable properties of polylactic acid films for food packaging. *Journal of food science*, *81*(1), E86-E96.

Spacek, A. D., Neto, J. M., Biléssimo, L. D., Ando Junior, O. H., Santana, M. V. F. D., & Malfatti, C. D. F. (2018). Proposal of the tubular daylight system using acrylonitrile butadiene styrene (abs) metalized with aluminum for reflective tube structure. *Energies*, *11*(1), 199.

Srivastava, S. K., Gupta, M. K., Gupta, G. K., Joshi, T. C., Shrivastava, V., & Mondal, D. P. (2023). Fluidized spray driven polymer mediated ultra stable Aluminum metal coating with enhanced dielectric properties. *Materials Science and Engineering: B*, *294*, 116490.

Srivatsa, A. R., & Ygartua, C. L. (1999). Analysis of low dielectric constant and Cu-based single- and multilayered films using spectroscopic ellipsometry. *Optical Metrology: A Critical Review*, *10294*, 249-265.

Sugavaneswaran, M., Prince, M. T., & Azad, A. (2019). Effect of Electroplating on Surface Roughness and Dimension of FDM parts at Various build orientations. *FME Transactions*, *47*(4).

Sun, C., Wang, Y., McMurtrey, M. D., Jerred, N. D., Liou, F., & Li, J. (2021). Additive manufacturing for energy: A review. *Applied Energy*, *282*, 116041.

Sun, W. J., Li, J., Mele, G., Zhang, Z. Q., & Zhang, F. X. (2013). Enhanced photocatalytic degradation of rhodamine B by surface modification of ZnO with copper (II) porphyrin under both UV–vis and visible light irradiation. *Journal of Molecular Catalysis A: Chemical*, *366*, 84-91.

Tengsuthiwat, J., Yorseng, K., Siengchin, S., & Parameswaranpillai, J. (2019). Thermomechanical, water absorption, ultraviolet resistance and laser-assisted electroless plating behavior of Cu2O and melamine–formaldehyde-coated sisal fiber-modified poly (lactic acid) composites. *Polymer Composites*, *40*(8), 3264-3274.

Tompkins, H. G., & Hilfiker, J. N. (2015). *Spectroscopic ellipsometry: practical application to thin film characterization*. Momentum Press.

Tompkins, H. G., & McGahan, W. A. (1999). Spectroscopic ellipsometry and reflectometry: a user's guide. *(No Title)*.

Upadhyay, D. J., & Bhat, N. V. (2003). Surface modification and characterization of dichloromethane plasma treated polypropylene film. *Plasmas and polymers*, *8*, 237-257.

Vaněčková, E., Bouša, M., Sokolová, R., Moreno-García, P., Broekmann, P., Shestivska, V., ... & Kolivoška, V. (2020). Copper electroplating of 3D printed composite electrodes. *Journal of Electroanalytical Chemistry*, *858*, 113763.

Vasconcelos, B., Vediappan, K., Oliveira, J. C., & Fonseca, C. (2018). Mechanically robust silver coatings prepared by electroless plating on thermoplastic polyurethane. *Applied Surface Science*, *443*, 39-47.

Vásquez-Peralvo, J. A., Tamayo-Domínguez, A., Pérez-Palomino, G., Fernández-González, J. M., & Wong, T. (2022). 3D Inductive Frequency Selective Structures Using Additive Manufacturing and Low-Cost Metallization. *Sensors*, *22*(2), 552.

Velicu, I. L., Tiron, V., Rusu, B. G., & Popa, G. (2017). Copper thin films deposited under different power delivery modes and magnetron configurations: A comparative study. *Surface and Coatings Technology*, *327*, 192-199.

Wang, M., Favi, P., Cheng, X., Golshan, N. H., Ziemer, K. S., Keidar, M., & Webster, T. J. (2016). Cold atmospheric plasma (CAP) surface nanomodified 3D printed polylactic acid (PLA) scaffolds for bone regeneration. *Acta biomaterialia*, *46*, 256-265.

Wang, P., Li, J., Wang, G., He, L., Yang, J., Zhang, C., Han, Z., & Yan, Y. (2023). Hybrid additive manufacturing based on vat photopolymerization and laser-activated selective metallization for three-dimensional conformal electronics. *Additive Manufacturing*, *63*, 103388.

White, J., Tenore, C., Pavich, A., Scherzer, R., & Stagon, S. (2018). Environmentally benign metallization of material extrusion technology 3D printed acrylonitrile butadiene styrene parts using physical vapor deposition. *Additive Manufacturing*, *22*, 279-285.

Woskowicz, E., Łożyńska, M., Kowalik-Klimczak, A., Kacprzyńska-Gołacka, J., Osuch-Słomka, E., Piasek, A., & Gradoń, L. (2020). Plasma deposition of antimicrobial coatings based on silver and copper on polypropylene. *Polimery*, *65*(1), 33-43.

Xia, L., Lu, L., Liang, Y., & Cheng, B. (2019). Fabrication of centrifugally spun prepared poly (lactic acid)/gelatin/ciprofloxacin nanofibers for antimicrobial wound dressing. *RSC advances*, *9*(61), 35328-35335.

Xiang, H., Nie, J., Zhou, Z., Yang, Y., Yu, Z., & Liu, J. (2023). Selective metallization on ordinary polymer substrates by laser direct activation of copper phosphate or nickel phosphate. *Langmuir*, *39*(5), 2063-2072.

Xiao, R., Feng, X., Fan, R., Chen, S., Song, J., Gao, L., & Lu, Y. (2020). 3D printing of titanium-coated gradient composite lattices for lightweight mandibular prosthesis. *Composites Part B: Engineering*, *193*, 108057.

Xiao, X., Miao, L., Xu, G., Lu, L., Su, Z., Wang, N., & Tanemura, S. (2011). A facile process to prepare copper oxide thin films as solar selective absorbers. *Applied Surface Science*, *257*(24), 10729-10736.

Xie, D., Wu, W., Huang, J., Wang, X., Zhang, Y., Wang, Z., Jiang, P., Tang, L., Wu, F., & Wang, Q. (2024). Effect of electrodeposited Cu interlayer thickness on characterizations and adhesion force of Ni/Cu/Ni coatings on polyetherimide composite substrates. *International Journal of Adhesion and Adhesives*, *129*, 103580.

Yang, L., Li, S., Zhou, X., Liu, J., Li, Y., Yang, M., ... & Zhang, W. (2019). Effects of carbon nanotube on the thermal, mechanical, and electrical properties of PLA/CNT printed parts in the FDM process. *Synthetic Metals*, *253*, 122-130.

You, X., Chen, Y., Huang, Y., Wang, C., Zhou, G., He, W., Wang, S., Tang, Y., Zhang, W., Li, Z., & Tang, P. (2020). Surface coarsening of carbon fiber/cyanate ester composite for adhesion improvement of electroless copper plating as conductive patterns. *Materials Chemistry and Physics*, *255*, 123597.

Yu, S., Sun, Y., Ni, Y., Zhang, X., & Zhou, H. (2016). Controlled formation of surface patterns in metal films deposited on elasticity-gradient PDMS substrates. *ACS applied materials & interfaces*, *8*(8), 5706-5714.

Zabetakis, D., Loschialpo, P., Smith, D., Dinderman, M. A., & Dressick, W. J. (2009). Direct-write patterning palladium colloids as a catalyst for electroless metallization for microwave composites. *Langmuir*, *25*(3), 1785-1789.

Zerankeshi, M. M., Sayedain, S. S., Tavangarifard, M., & Alizadeh, R. (2022). Developing a novel technique for the fabrication of PLA-graphite composite filaments using FDM 3D printing process. *Ceramics International*, *48*(21), 31850-31858.

Zhang, J., Feng, J., Jia, L., Zhang, H., Zhang, G., Sun, S., & Zhou, T. (2019). Laser-induced selective metallization on polymer substrates using organocopper for portable electronics. *ACS applied materials & interfaces*, *11*(14), 13714-13723.

Zhang, J., Zhou, T., Wen, L., & Zhang, A. (2016). Fabricating metallic circuit patterns on polymer substrates through laser and selective metallization. *ACS applied materials & interfaces*, *8*(49), 33999-34007.

Zhang, X., Ding, B., Bian, Y., Jiang, D., & Parkin, I. P. (2018). Synthesis of superhydrophobic surfaces with Wenzel and Cassie–Baxter state: experimental evidence and theoretical insight. *Nanotechnology*, *29*(48), 485601.

Zhang, X., Miao, D., Ning, X., Cai, M., Tian, Y., Zhao, H., & Jiang, S. (2019). The stability study of copper sputtered polyester fabrics in synthetic perspiration. *Vacuum*, *164*, 205-211.

Zhao, X., Wang, T., Li, Y., Huang, L., & Handschuh-Wang, S. (2019). Polydimethylsiloxane/nanodiamond composite sponge for enhanced mechanical or wettability performance. *Polymers*, *11*(6), 948.

Zhu, H., Chen, Z., Sheng, Y., & Thi, T. T. L. (2010). Flaky polyacrylic acid/aluminium composite particles prepared using in-situ polymerization. *Dyes and Pigments*, *86*(2), 155-160.

CURRICULUM VITAE

İsmail AKTİTİZ, completed his high school education at Ali Akkanat Anatolian High School in 2010. He graduated from Sakarya University Metallurgical and Materials Engineering Department in 2014. In 2019, he completed his Master's degree at Süleyman Demirel University, Department of Mechanical Engineering. He started his PhD education at Çukurova University, Department of Mechanical Engineering in 2019. He has been working as a research assistant at Adana Alparslan Türkeş Science and Technology University, Department of Mechanical Engineering.

APPENDICES

A.1. PUBLISHED ARTICLES

1. Aktitiz, İ., Darıcık, F., Aydın, A. and Aydın, K., 2024. Metallization of 3D Printed Polylactic Acid Polymer Structures via RF Sputtering, *Journal of Materials Engineering and Performance*, https://doi.org/10.1007/s11665-024-10387-9.
2. Aktitiz, İ., Darıcık, F., Aydın, A. and Aydın, K., 2024. Experimental Investigations on Metallization in The Surface Modified Additively Manufactured Plastic Substrates Using DC Sputtering, *Proceedings of the Institution of Mechanical Engineers, Part E: Journal of Process Mechanical Engineering,* https://doi.org/10.1177/095440892412959.
3. Korkut, V., Darıcık, F., Aktitiz, İ. and Aydın, K., 2023. Failure of Surface Modification 3D Printed Polymer Materials by UV/Ozone Irradiation. *Engineering Failure Analysis,* https://doi.org/10.1016/j.engfailanal.2023.107466.
4. Aktitiz, İ., Aydın, K., Darıcık, F. and Topcu, A., 2022. Production of Different Metal Oxide Nanoparticle Embedded Polymer Matrix Composite Structures by The Additive Manufacturing Technology and Investigation of Their Properties. *Polymer Composites*, 43(11), 7826. https://doi.org/10.1002/pc.26894.
5. Aktitiz, İ., Aydın, K. and Topcu, A., 2021. Characterization of TiO2 Nanoparticle–Reinforced Polymer Nanocomposite Materials Printed by Stereolithography Method. *Journal of Materials Engineering and Performance,* 30:4975-4980. https://doi.org/10.1007/s11665-021-05574-x.
6. Aktitiz, İ., Delibaş, H., Topcu, A., and Aydın, K. 2021. Morphological, Mechanical, Magnetic, and Thermal Properties of 3D Printed Functional Polymeric Structures Modified With Fe2O3 Nanoparticles, *Polymer Composites*, 42(12), 6839. https://doi.org/10.1002/pc.26344.
7. Aktitiz, İ., Aydın, K. and Topcu, A., 2020. Stereolitografi (SLA) Tekniği ile Basılan 3 Boyutlu Polimer Yapılarda İkincil Kürleme Süresinin Mekanik Özelliklere Etkisi, *Çukurova Üniversitesi Mühendislik-Mimarlık Fakültesi Dergisi,* 35(4), 949-958. https://doi.org/10.21605/cukurovaummfd.868895.